Metformin as a potential therapy for malignant astrocytoma

Lawrence Eagles, MSc

A thesis submitted in fulfilment of the requirements of the University of Wolverhampton for the degree of

Doctor of Philosophy

Brain Tumour Research Centre Research Institute in Healthcare Sciences Faculty of Science and Engineering

University of Wolverhampton

January 2018

Authors Declaration

This work or any part thereof has not previously been presented in any form to the University or to any other body whether for the purposes of assessment, publication or for any other purpose (unless otherwise indicated). Save for any express acknowledgments, references and/or bibliographies cited in the work, I confirm that the intellectual content of the work is the result of my own efforts and of no other person.

Lawrence Eagles

Date

Abstract

Background

Glioblastoma Multiforme (GBM) is the most commonly occurring tumour of the central nervous system (CNS). Currently GBM is considered an incurable malignancy with patients experiencing abysmal life expectancies. Lack of progress in the discovery of novel treatments has led to the repurposing of existing licenced medication as a possible alternative option. Metformin is from the biguanide family of drugs and is the most common medication used in the treatment of type 2 diabetes. Clinical studies have reported that, in type 2 diabetic patients, metformin might reduce cancer incidence and severity. Currently, metformin is being assessed in clinical trials as a treatment for a range of cancer types including GBM. The antineoplastic mechanisms utilized by metformin and other biguanides have not been fully elucidated.

Methods

The effects of metformin were evaluated, alone and in combination with other agents, on a panel of GBM cell cultures. Functional analysis of metformin mechanism of action was assessed through measurement of apoptosis, depolarisation of the mitochondria membrane, caspase pathway activation, cell cycle progression and the expression levels of micoRNAs.

Results

Analysis of fourteen GBM cell cultures showed a cytotoxic response to metformin that was significantly linked to the *P53* status ($p=0.0024$). In combination drug testing, one of the four drugs showed a synergistic pairing with metformin. The kinase inhibitor sorafenib, showed synergism ($CI \leq 1$) in eight GBM cell cultures. Flow cytometry of metformin treated GBM cells showed no significant increase ($p>0.005$) in apoptotic cell populations. Caspase 3/7 levels showed no significant increase post metformin treatment ($p>0.005$). Metformin caused depolarisation of the mitochondrial membrane in six GBM cell cultures. Four microRNAs were shown to have expression levels changes post-metformin treatment. Upregulation of expression was identified in miR-140, miR-192, let-7c. Downregulation was identified in miR-222.

Conclusions

Metformin was shown to have cytotoxic effect on a GBM cell cultures and has potential as GBM therapeutic agent and possible treatment synergy with sorafenib. The significance of *P53* status to metformin sensitivity may suggest that its use should be directed to a sub-set of GBM patients. Mechanism for cell death by metformin was shown not to rely on apoptotic pathways but caspase 3/7 independent depolarization of mitochondrial cell membranes and cell cycle arrest. Investigations into autophagy may help to further define the pathways metformin is utilising to promote cell death. The impact of metformin on the expression profile of miR-222, miR-192 and let-7c is in line with clinical studies of other cancer types. This shows possible insight into the cancer independent actions of metformin. The interplay recorded between glucose availability and cell death indicates a possible key factor in the utilisation of metformin as a therapeutic agent. This finding may warrant the addition of dietary control regimes in clinical trials to maximise metformin efficacy. This work highlights the strong potential for biguanides in the development of new drug treatments and in expanding our knowledge of cancer metabolism.

Contents

List of tables

List of figures

Abbreviations

AIC	4-Amino-5-imidazole-carboxamide
AKT	Protein Kinase B
AMPK	AMP-activated protein Kinase (AMPK)
ATRX	TP-dependent helicase ATRX
BBB	Blood brain barrier
BBTB	Blood brain tumour barrier
BRAF	Proto-oncogene B-Raf
CDK	Cyclin dependent kinase
cDNA	Complementary DNA
CNS	Central nervous system
CO_2	Carbon dioxide
CRUK	Cancer research UK
CSC	Cancer stem cell
CSF	Colony stimulating factor
DISC	Death-inducing signalling complex
DMEM	Dulbecco's modified Eagles Medium
DMSO	Dimethyl sulphoxide
DNA	Deoxyribonucleic acid

DS	Disulfiram
DDx	Differential diagnosis
EGFR	Epidermal growth factor receptor gene
FASN	Fatty acid synthase
FBS	Foetal bovine serum
FGFR	Fibroblast growth factor receptor
FITC	Fluorescien isothiocyante
GBM	Glioblastoma multiforme
G-CIMP	Glioma-CpG island methylator phenotype
HEPES	4-(2-hydroxyethyl)-1-piperazineethanesulphonic acid
HIF	Induces hypoxia-inducible factor
IDH1	Isocitrate dehydrogenase 1
JC-1	5,5',6,6'-tetrachloro-1,1',3,3'-tetraethylbenzimidazolcarbocyanine iodide
LAD	Lactic acidosis
LDH	Lactate dehydrogenase
MDR	Multiple Drug resistance
MGMT	O^6-Methylguanine-DNA methyltransferase
miRNA	Micro-RNA

mTOR	Mammalian target of rapamycin
mM	Milli Molar
MTIC	Methytriazine
MTT	3-(4, 5-Dimethylthiazol-2-yl)-2, 5-diphenyltetrazolium
NADPH	Nicotinamide adenine dinucleotide phosphate
NF1	Neurofibromatosis type 1
NHA	Normal human astrocytes
NOS	Not otherwise specified
OS	Overall survival
OSCC	Oesophageal squamous cell carcinoma
PCR	Polymerase chain reaction
PFS	Progression free survival
PHGDH	Phosphoglycerate dehydrogenase
P13K	Phosphoinositide 3-kinase
PI	Propidium iodide
Pri-miRNA	Primary-miRNA
PTEN	Phosphatase and tensin homolog
REDD1	Regulated in development and DNA damage response 1
RIPK	Receptor-interacting protein kinases

RLU	Relative light units
RNA	Ribonucleic Acid
RT	Radiotherapy
RT-PCR	Reverse transcription polymerase chain reaction
SMI	Small-molecule inhibitors
TACC	Transforming acidic coiled-coil
TCA	Trichloro-acetic acid
TCGA	The Cancer Genome Atlas
TJ	Tight junction
TTFields	Tumour treating fields
TMZ	Temozolomide
TP53	Tumour protein 53
μM	Micro Molar
VEGF	Vascular endothelial growth factor
VHL	Von Hippel-Lindau tumour suppressor
WHO	World Health Operation
ΔΨ	Mitochondrial membrane potential
1p/19Q	Deletion of the short arm of chromosome 1 and the long arm chromosome 19

Acknowledgements

Firstly, I would like to thank my supervisor, Prof. Tracy Warr for providing me with the immense privilege to be able to complete this PhD project and thesis. Her support has shaped the scientist and person I am today.

I am very grateful to my co-supervisor Farzana Rowther. Forever she has been a constant source of encouragement and an invaluable friend over the years. I also have great appreciation to Prof. John Darling and Prof. Weiguang Wang for all their valuable support.

My deepest gratitude goes to Dr Mark Morris for allowing me to work under him during my MSc project. It was this work that opened my eyes to science research and put me on the path I am on today.

I would to thank the members of my research group, Dr Katherine Karakoula, Dr Prasanna Channathodiyl and Daniel Blakeway for the pleasure of working alongside them. There are too many colleagues at the university I would wish to thank, but I do want to note my key appreciation of Dr Angel Armesilla, Dr Vinodh Kannappan and Dr Sathishkumar Kurusamy for being such true people that I aspire to emulate.

I am grateful to the technical staff at the University of Wolverhampton for all the support over my time here. I especially want to thank the efforts of Dr Angie Williams and Henrik Townsend.

I am grateful to my friend, and fellow Tenno, Drew Masci for his eternal aid. Forever will I be indebted to everyone at Digital Extremes for providing much needed respite on my journey, as they progress on their own.

I would like to thank the University of Wolverhampton for its philosophy, without which I would not have been able to achieve this qualification.

Lastly, I would like to thank my family. Throughout my many years of ups and downs they have always been there; unwaveringly behind me, always pushing me onward and upward to greater things.

Dedication

To my family

CHAPTER 1

Introduction

1 Introduction

1.1 Cancer

Cancer is one of the leading causes of morbidity and mortality in the world (Siegel *et al.*, 2016). It is a disease that affects all ages and all populations. The data published in 2014 by the WHOs international Agency for Research on Cancer (IARC) estimated, that at current rates, approximately 14 million new cases of malignant tumours would be reported, and 6.2 million people will die of cancer annually (McGuire, 2016). The figures have increased in recent years however this can be partially attributed to the development of newer, more reliable methods of cancer detection (Christopher *et al.*, 2014; Torre *et al.*, 2015; Siegel *et al.*, 2016; Philips *et al.*, 2018).

1.2 Brain tumours

Tumours of the brain and the CNS constitute some of the rarest cancer types, in 2015 CNS tumours represented 1.4% of all new cancer diagnosis, however they were also the cause of 2.6% of cancer related mortalities (Howlader *et al.*, 2016). Recent studies indicate a sustained and significant rise in GBM prevalence across all ages that cannot be attributed to any one risk factor, and which also suggests the cause maybe with widespread environmental and/or lifestyle factors (Philips *et al.*, 2018). Cancer mortality is especially important in relation to children, which account for 30% of cancer deaths (McNeill *et al.*, 2016). For adolescents in the USA (aged birth-19 years) from 2016 onwards, brain tumours surpassed leukaemia as the leading cause of cancer death (Rebecca *et al.*, 2016).

Glioma are CNS tumours that originate from glial cells and categorized with grades I through IV based on the severity. Grades I-III are "low grade"

gliomas and are characterized by slower growth rates. Grade IV are high grade tumours that are aggressive and malignant commonly described as glioblastoma multiforme (GBM) (Eckel-Passow *et al.*, 2015).

1.2.1 GBM

Though the diagnosis of a GBM is rare, it is the most common type of brain tumour (69%) with poor patient outcomes (Ohgaki and Kleihues, 2007; Howlader *et al.*, 2016). Acquisition of a GBM is universally and rapidly fatal. The expected median survival for a GBM patient is around 15 months, with 2 years survival less than 35% (Bleeker *et al.*, 2012). GBM cells show a high amount of morphological variation. The cell silhouette can vary from spindle-shaped to polygonal with an overly pigmented chromatin (Schultz *et al.*, 2005. Nuceli are distinct but have irregular membranes and are typically elongated. Binucleated and multinucleated cells can also be found within a GBM tumour (Schultz *et al.*, 2005). A main pathological feature that separates GBM from lower grade astrocytoma are necrotic foci normally with peripheral pseudo-palisading cellular areas (Kleihues and Sobin, 2000; Brat and Van Meir, 2004).

1.2.2 GBM subtyping

Historic methods of classification relied primarily on pathologists staining and identifying histological appearance from a surgical dissection, the techniques date back almost 100 years (Bailey and Cushing, 1925). Modern classification of CNS tumours follows WHO guidelines, the first edition of which was released in 1979. An update to the fourth edition guidelines was released in May 2016. This update relied more on molecular subtyping to characterise different sub groups (Arevalo *et al.*, 2017). The methodology of this categorization is

demonstrated in figure 1.1. The key attribute for determination within the GBM sub-group is now based on molecular analysis, focusing on tumours IDH mutation status. The majority of GBM (>90%) present as primary tumours in adults (Ohgaki and Kleihues, 2007). GBM are labelled as primary or secondary based on the source of origination. Primary GBM are tumours that develop de novo, without any sign of developing from a prior tumour. Secondary GBM are generated through development of a lower grade astrocytoma.

However, GBM tumours are highly heterogeneous entities with a range of possible mutations and molecular markers. Isocitrate dehydrogenase (*IDH*) catalyses the oxidative decarboxylation of isocitrate and is one of the major modern determinants in glioma stratification and identification. *IDH* mutations are primarily found in secondary GBM and rarely in primary (Hai *et al.*, 2009; Korshunov *et al.*, 2017). Identification of the mutation is a good prognostic marker but not an overall predictive marker for patient survival (van den Bent *et al.*, 2010). Tumour protein (*TP53*) is a 53-kilodalton tumour suppressor protein. It is primary function is regulation of DNA binding proteins that prevent the acquisition of mutations (Kandoth *et al.*, 2013). *TP53* is further discussed in 1.3.3. Phosphatase and tensin homolog (*PTEN*) is a tumour suppressor protein that regulates the *AKT* pathway controlling cell growth, survival and cell cycle progression. In GBM *PTEN* deficiency has been linked to promoting malignant growth through macrophage recruitment, and therapeutic resistance through histone regulation (Benitez *et al.*, 2017; Chen *et al.*, 2018). Epidermal growth factor receptor (*EGFR*) is a transmembrane protein that is often found to be mutated in GBM, leading to the promotion of

more aggressive phenotypes and uncontrolled cell division (Monga *et al.*, 2017; Xu *et al.*, 2017). 1p/19Q co-deletion is referring to the loss of the short arm on chromosome 1 and the long arm of chromosome 19. It is a genetic hallmark of oligodendrogliomas, but the loss of these regions has also been proven prognostically favourable for GBM patients (Hill *et al.*, 2003). O^6-methylguanine–DNA methyltransferase (*MGMT*), further discussed in 1.3.2.1, is an important predictive marker in clinical settings that is linked to the effectiveness of the key GBM, treatment temozolomide (TMZ) (Molenaar *et al.*, 2014).

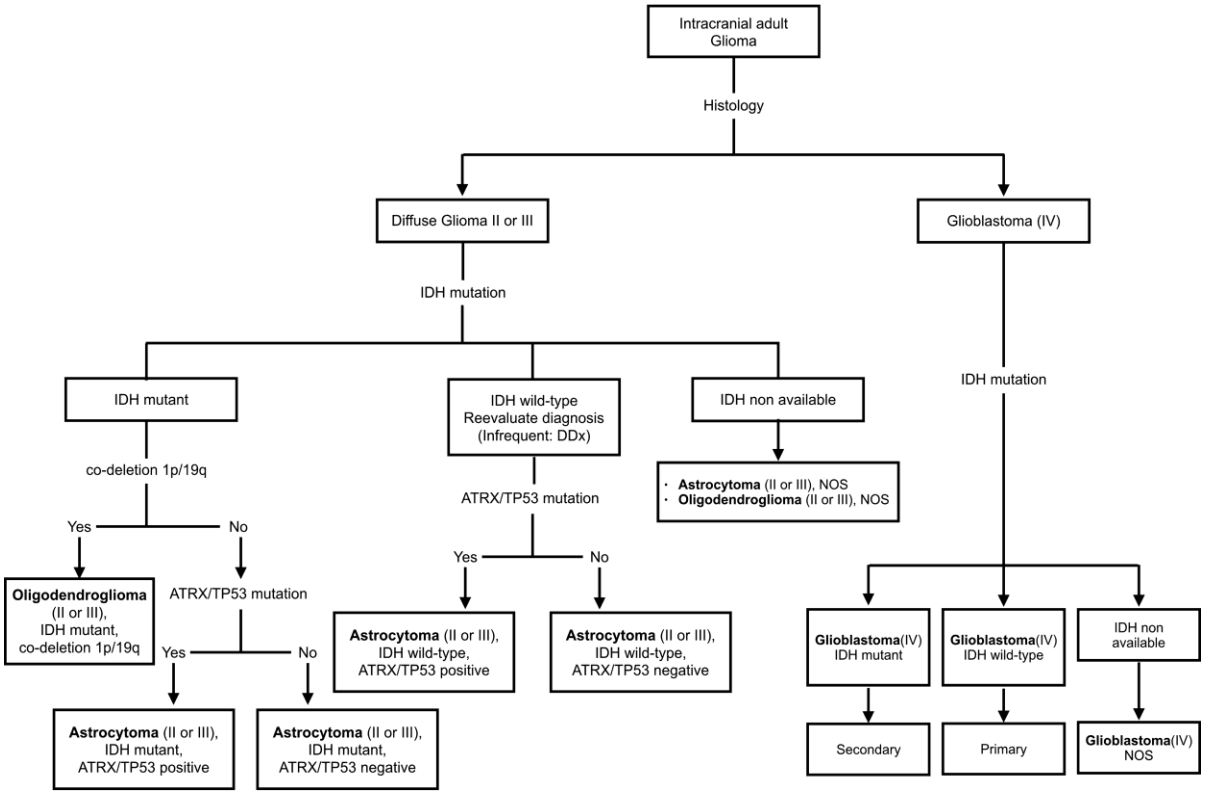

Figure 1.1 WHO methodology for the classification of adult gliomas. New WHO classification flow chart for the intracranial adult gliomas. Primary stratification based on histological separation followed by *IDH* mutation status. Diffuse glioma then segregated based off co-deletion present on chromosome 1p/19q or the mutation of *ATRX/TP53*.

Oligoastrocytomas were omitted due to rarity.

DDx, Differential diagnosis; IDH, Isocitrate dehydrogenase; *ATRX*, TP-dependent helicase ATRX; *TP53*, Tumour protein *p53*; NOS, not otherwise specified (Arevalo *et al.*, 2017).

1.3 Treatment of GBM

1.3.1 Treatment methods

Primary treatment method for GBM is a multi-modal response including surgical resection, whole brain radiation therapies (60Gy as standard) and chemotherapy (Stupp *et al.*, 2015). The main chemotherapeutic agent used in the treatment is TMZ, an alkylating agent. First introduced in 2005 as part of the STUPP protocol; TMZ when combined with standard radiotherapy increased 2-year-survival from 10.4% to 26.5% in GBM patients (Stupp *et al.*, 2005). In addition to TMZ, other actively used chemotherapy agents include platinum compounds; irinotecan and etoposide, nitrosureas: carmustine (BCNU) and lomustine (CCNU) and vincristine, part of the PCV regimen (Alifieris *et al.*, 2015). Many of the treatments are commonly linked to strong side effects that impair patient wellbeing including nausea and vomiting (Aapro and Alberts, 1981; Goldberg *et al.*, 2004; Jordan *et al.*, 2005; Hesketh, 2008).

1.3.2 Mechanisms of resistance in GBM

GBM are characterized as having high genetic heterogeneity that normally leads them to have many intratumoral phenotypes (Meyer *et al.*,2015). Due to this non-homologous make up of GBM, the tumours are highly resistant to chemotherapy agents and have many mechanisms that act against successful treatment.

1.3.2.1 DNA repair through *MGMT* methylation

The DNA management and repair gene *MGMT* has been heavily linked with GBM cell survival (Bell *et al.*, 2018). *MGMT* functions by removing the O6 position of guanine, this can limit the effectiveness of alkylating agents for

example TMZ (Esteller *et al.*, 2000). Methylation of *MGMT* is common in GBM (approximately 45%) and this is linked with more favourable patient survival (Hegi *et al.*, 2005). The methylation and silencing of *MGMT* has been long proposed as a prognostic marker. However, the accuracy of this as the independent predictive factor for GBM has often been debated (Fietkau *et al.*, 2013). Recent methods combing Isocitrate dehydrogenase 1 (IDH1) data with *MGMT*s has shown improvements in predictive accuracy (Remco *et al.*, 2014).

1.3.2.2 Angiogenesis

As with most tumour cells, GBM cells are very resource intensive, requiring large amounts of energy to maintain a functional metabolism (Zhao *et al.,* 2011). The primary resource for tumour cells is glucose, used as fuel for glycolysis and leads to an over production of lactate (Goodwin *et al.,* 2015). This is part of a reprogramming of cellular metabolism to produce a system defined as the Warburg effect (Poteet *et al.*, 2013). To maintain high rates of tumour growth, increased blood supply though vascularisation is needed. GBM are one of the most vascularised tumour types and so large amounts of VEGF is produced to induce angiogenesis in the surrounding tissue (Soda *et al.*, 2013). Bevacizumab is an anti-angiogenesis drug that has had success in reducing tumour growth and increasing progression-free survival (Narita, 2015). However, patients go on to develop resistance to the drug after several treatments and so the impact on overall patient survival is minimal (Lu and Bergers, 2013). Anti-angiogenesis drugs are expected to play a role as part of combination therapies and are currently being combined with other treatments in future clinical trials (Schiff *et al.*, 2018).

1.3.2.3 Blood brain barrier

The blood brain barrier (BBB) is a key defence mechanism within the body designed to protect the flow of potentially hazardous agents from reaching the brain, but it is also often a hindrance to the ability to deliver drugs to a target tumour (Oberoi *et al.*, 2015). Structurally the BBB is made up of several layers of cells, the core of which is capillary endothelial cells lined by basal lamina (Feustel *et al.*, 2012). The specialised capillary cells possess multi-molecule complex structures built up of transmembrane and membrane associated proteins. The tight junctions (TJ) are built between adjacent cells, the complexes tightly control transport and signalling out of the capillary (Luissint *et al.*, 2012). Supplementing the endothelial cells are astrocytes and pericytes. The end-feet of astrocyte cells sheath the BBB but do not act as barrier, instead they function by supporting the endothelial cells and TJs (Praveen *et al.*, 2004; Hong *et al.*, 2015). Pericytes are intricately linked into brain capillary endothelium and are vitally important in regulation of endothelial cell expression and polarisation of astrocyte end-feet (Lai *et al.*, 2005; Armulik *et al.*, 2010). As one complete structure the BBB possess several transport mechanisms to move required molecules into the brain tissue, a list of mechanism is given in figure 1.3 (Wong *et al.*, 2013).

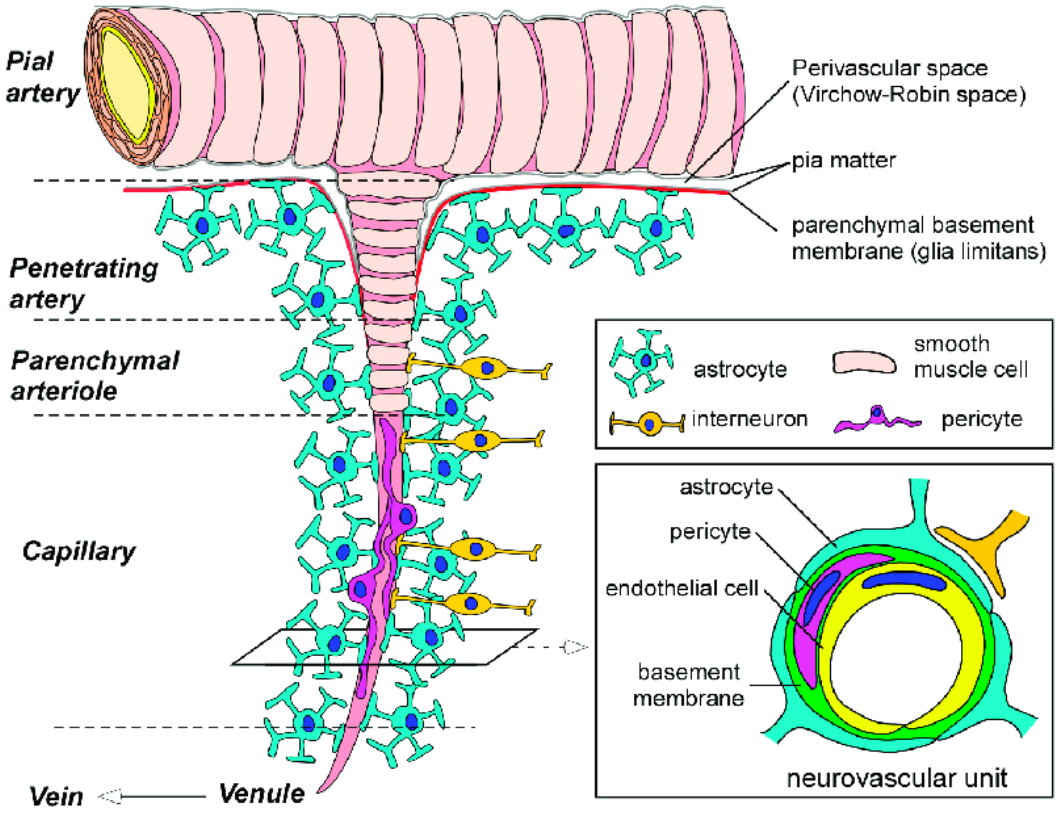

Figure 1.2 Composition and structure of the BBB. The BBB is a multi-layered barrier, regulating all signalling and transport of molecules into brain tissue. All material exchange happens at the endothelial cells in capillaries which are protected by complex structures called tight junctions. Interspersed among the endothelial cells are pericytes that help regulate the expression levels of near-by endothelial and astrocytic cells. They also has a role in renewing the BBB. The BBB is then wrapped in the feet of astrocyte cells, the astrocytes regulate and maintain the BBB. (Yamazaki *et al.*, 2017)

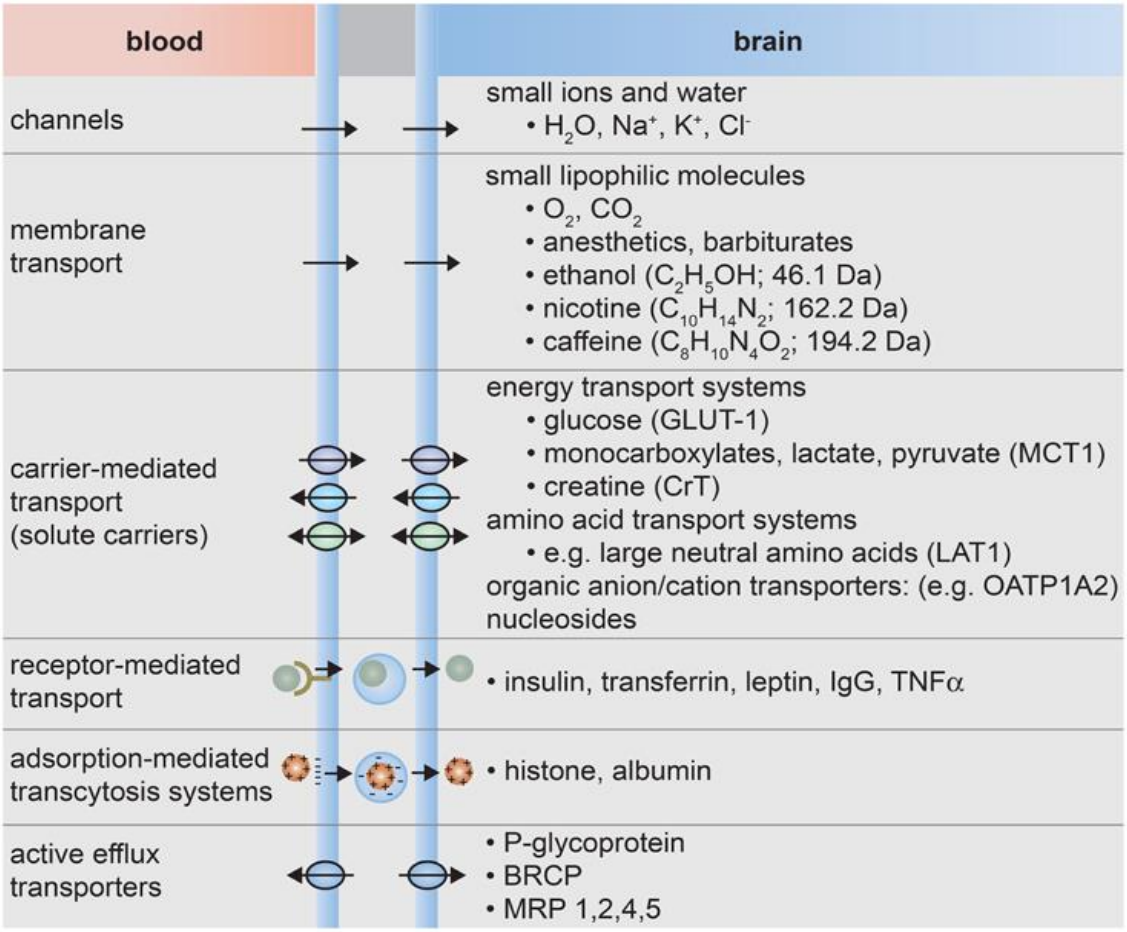

Figure 1.3 Transport mechanisms across the blood brain barrier. The BBB possess several mechanisms to help the exchange of required molecules into the brain tissue. Small ions and water can cross the barrier through use of ion channels. Small lipid soluble molecules can cross through the phospholipid membranes of the BBB cells. All other molecules requiring transport in and out of the brain tissue require support from transport proteins and solute carrier systems. (Wong *et al.*, 2013)

The development of a tumour in CNS can have an adverse effect of the structure and integrity of the BBB. At the blood brain tumour barrier (BBTB) the blood vessels become "leaky" due to abnormal growth and potentially produce easier vascular access to the tumour site (Kemper *et al.*, 2006). This is achieved by glioma cells invading perivascular space and displacing astrocytic end feet from the BBB (Watkins *et al.*, 2014). As the barrier

degrades, pericyte numbers reduce, increasing permeability of the BBB to water and molecules by endothelial transcytosis (Armulik *et al.*, 2010). This damage should be a boon to tumour drug delivery, but the invasive potential of GBM leads to cells migrating away from the BBTB. This forces cells into areas where protection from drugs is afforded by still functional sections of the BBB (Van Tellingen, 2015). Gliomas also show up-regulation and expression of multidrug resistance protein-1 (MDR-1), part of the ATP-binding cassette transporter superfamily. The increased expression of this protein allows cancer cells to remove many chemotherapeutic agents from the cell (Munoz *et al.*, 2014; Alifieris and Trafalis, 2015).

1.3.3 Tumour genetics

Tumours operate through a range of genetic mutations. The identification of tumour promoting genes and tumour suppressors has been and key in understanding the multifaceted impacts and progression of diffuse glioma.

1.3.3.1 GBM Genome project

GBM, like all human cancer cells, possesses multiple chromosomal abnormalities, nucleotide substitutions and divergent epigenetic alterations (Cancer Genome Atlas Research Network, 2008). Long term research projects have been established with the goal of using large scale multi-dimensional analysis to understand and map the variations. The Cancer Genome Atlas (TCGA) is a public resource that collates and catalogues genetic data from human tumours (Kim *et al.*, 2018). As part of the initial pilot study, the first tumour type analysed through TCGA was GBM (Tomczak *et al.*, 2015). From this initial data analysis, key GBM features were determined. Deregulation of

several pathways including *p53*, retinoblastoma protein (RB) and RTK/RAS/PI3K. A summary of this data is shown in figure 1.4. Further analysis has highlighted alterations in the epidermal growth factor receptor (EGFR), neurofibromatosis type 1 gene (NF1) and isocitrate dehydrogenase 1 (IDH1) (Verhaak *et al.*, 2010). Analysis of DNA methylation levels in GBM data has caused the creation of the glioma-CpG island methylator phenotype (G-CIMP). Promoter regions of genes can be rich in cytosine and guanine paired bases, referred to as 5'—C—phosphate—G—3' (CpG) islands and hyper methylation of them leads to gene silencing. G-CIMP was identified in a subgroup of gliomas with a specific DNA methylation status (Noushmehr *et al.*, 2010).

The analysis of the database has also identified other smaller subsets of GBM. Less than four percent of tumours displayed chromosomal translocation of tyrosine kinase domains of fibroblast growth factor receptor (FGFR) genes into coding domains of the transforming acidic coiled-coil (TACC) gene. This led to the creation of FGFR-TACC oncogenic fusion protein that localised to mitotic spindle of astrocytes causing aneuploidy (Singh *et al.*, 2012).

TCGA data has also identified microRNAs that regulate and control GBM development. Two miRNAs, miR-148a and miR-31 have been identified to promote tumour growth and regulate angiogenesis through meditation of hypoxia-inducible factor 1-alpha (Wong *et al.*, 2015).

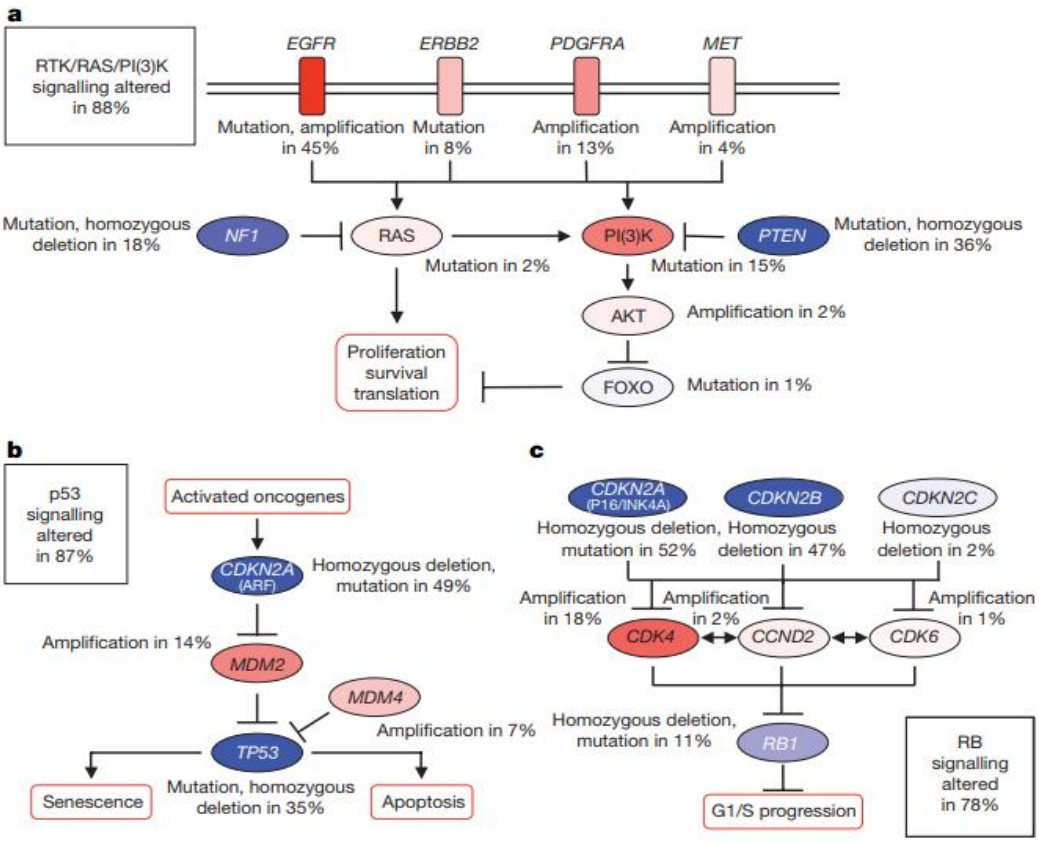

Figure 1.4 Key GBM signalling pathway dysregulation. Data on the genetic alteration in signalling pathways analysed by the TCGA. Three pathways were identified as having frequent aberration and signalling changes, (a) *RTK/RAS/PI3K*, (b) *p53* and (c) *CDKN2A.* Red coloured objects signifies activating genetic alterations and blue signifies inactivating alterations. The darker the shade of the object, the high the frequency/percentage that the object was shown to be altered. Percentage chance of each section being altered is described alongside it. Each pathway shown has a box describing the overall percentage chance that pathway signalling was affected. (Cancer Genome Atlas Research Network, 2008).

1.3.3.2 Genetic mutations

Tumour protein 53 (*P53*) was originally labelled as a proto-oncogene, this was until correct identification of the wild-type form (Finlay *et al.*, 1989). Now *P53* is known as the most common mutation to be found in all human cancers (Kandoth *et al.*, 2013). The gene is an important tumour regulator and suppressor. It functions through a range of mechanisms that include detection of DNA damage, G1/S cell cycle arrest and ultimately apoptosis. *P53* upregulation and activation occurs in the presence of DNA damage where *P53* will bind to DNA (Basu and Murphy, 2016). Mutations of *P53* can cause reductions in expression and prevent it binding to DNA (Muller and Vousden, 2013). This then leads to a large gain of function for the tumour cell. The benefits can be cancer specific but are known to include increases in invasion, migration, proliferation, progression of cell cycle, drug resistance, colony formation, angiogenesis and overall cell survival (Muller and Vousden, 2014). In GBM, *P53* is mutated 25-30% in primary tumours and 60-70% in secondary tumours but studies have yet to show an association with overall GBM prognosis (England *et al.*, 2013). In addition to tumour suppression roles, in GBM *P53* has been shown to be a regulator of the mevalonate metabolic pathway (Laezza et al, 2015). In a variety of cancers phosphatase and tensin homolog (PTEN) is a commonly mutated oncogene. In glioma, loss of PTEN is associated with immune-resistance and, alongside mutations in *P53*, it can have an impact on glioma cell survival and tumorigenesis (Parsa *et al.*, 2007; Zheng *et al.*, 2008). EGFR is a transmembrane protein that has key role in starting a signalling cascade that controls cell division (Delgado-Lopez and Corrales-Garcia, 2016). It is known to be amplified in 40% of GBM this leads

to increases in cellular proliferation and resistance to radiotherapy (Barker *et al.*, 2001; William *et al.*, 2017).

1.4 Development of new treatments

1.4.1 Clinical trials and drug development

TMZ was first licensed for the treatment of GBM in 1999 and became a frontline treatment for GBM in 2005 where it remains to this day (Sansom, 2009; Stupp *et al.*, 2005). Currently novel drugs have to proceed through numerous clinical trials to prove safety and efficacy (Piantadosi, 2017). Only on completion of this can it be considered for mass deployment as an accepted treatment. Clinical trials and approval can take years and there is no guarantee a drug will gain successful approval. Clinical trial design and execution in neuro-oncology has many challenging issues (Van Meir *et al.*, 2010; Patrick *et al.*, 2017). For GBM treatment there have been many clinical trial for a range of therapies, but none have achieved the levels of use and acceptance as TMZ. This issue may also have been compounded by the problem that in the last few decades, research and development productivity in drug discovery has been falling (Kola *et al.*, 2004; Paul *et al.*, 2010; Herper., 2012) This can be attributed partly to reductions in investment for high risk and low return drug development (Pammolli, *et al.*, 2011). Though modern invention of next generation sequencing the landscape of cancer trials has begun to change. Historically cancer has been solely categorized histologically by the site of origin, now the role of biomarkers relevant to different subtypes are being recognised and tumours are being acknowledged as heterogeneous entities requiring tailored treatments (Duffy *et al.*, 2014; Korpanty *et al.*, 2014; Tefferi *et al.*, 2015).

1.4.2 Novel treatment methodologies

New techniques are being developed to work alongside and augment existing treatments. The techniques have a variety of strategies to influence tumours ranging from utilizing electromagnetic energy fields to developing personalised patient treatments (Carlsson *et al.*, 2014).

1.4.2.1 Immunotherapy

Immunotherapy models attempt to reprogram the patients innate immune system to enable it to target and combat the tumour. Due to the complex nature of immune responses, many potential effectors can be targeted. This includes cellular targets; adoptive and engineered T cell transfers, vaccination using both specific and non-specific antigens, and immunomodulation through pathway inhibitors (Reardon *et al.*, 2014). DCVax-L is an example of an immunotherapy treatment methodology that is currently undergoing clinical trials. This a labour-intensive technique requires individual samples from a patient and involves presenting tumour biopsy to differentiated dendritic cells before returning them to the patient to induce T-Cell aggression (Prins *et al.*, 2011).

1.4.2.2 Monoclonal antibodies

The aim with monoclonal antibodies is to disrupt receptor signalling through targeting cell surface receptors and ligands. Inevitably this will prevent downstream pathway activation and further cellular signalling (Melstrom and sentovich, 2017). Avastin (Bevacizumab) is a monoclonal antibody that is designed to target VEGF and reduce angiogenesis at tumour sites. This strategy would produce a technique which would act independent of cancer type and cell profiling. Recent studies found however that adding avastin

added no benefit over the standard treatment regimen (Gilbert *et al.*, 2014). In addition, the nutritional depletion caused by reduction of VEGF may trigger a tumour escape response and increase the number of invasive cells (de Groot *et al.*, 2010).

1.4.2.3 Small-molecule inhibitors

Small-molecule inhibitors (SMI) are small structures designed to bind to or inhibit specific cellular pathways or act as epigenetic regulators. Several SMIs have been generated including caspase activating NSC-154829, Wnt Pathway inhibitor SEN461 and apoptotic inducer vacquionol-1 (Trembath *et al.*, 2007; De Robertis *et al.*, 2013; Kitambi *et al.*, 2014). Due to expense and difficulty in construction, very few small-molecule inhibitors have made it to clinical trials and this limits further development on the molecules. However, the production and use of the materials was considered completely intractable twenty years ago. As technologies improve the development of new small-molecule inhibitors may produce new treatment options (Arkin *et al.*, 2014).

1.4.2.4 Mechanical solutions

In addition to traditional medical drug developments future alternative therapies for brain tumours are being developed. The Novocure Optune system is a wearable device that generates tumour treating fields (TTFields) within the patient's brain. Tumour cells kept under high exposure to the anti-mitotic electrical fields have a reduction in tumour cell division (Chaudhry *et al.*, 2015). In GBM clinical trials TTFields have shown proven efficacy in management of tumours and the technology is now being developed for other tumour types (Burri *et al.*, 2017). Thermotherapy utilises ferromagnetic

magnetic nanoparticles injected into a tumour to cause damage to surrounding cells. After injection into the patient, the nanoparticles are exposed to an alternating magnetic field that causes the production of heat at the tumour site (Jordan and Maier-Hauff, 2007). However, the future of this technology is unclear as the use of iron oxide nanoparticles is becoming increasingly controlled by regulating agencies to safeguard the use of the materials (Gobbo *et al.*, 2015). Novel methods show possible new potential for GBM treatment however further testing and rigorous assessment is still required before it will be accepted as useable treatments by governing authorities.

1.4.3 Repurposing existing medication

The generation and approval of a new drug can take approximately $1-2 billion and take over 10 years to gain approval (Hong *et al.*, 2011; Massey and Robertson, 2018). Due to the length time that is required to complete rigours clinical trials for the approval of new medications, an alternative option is repurposing of existing licenced medication. The fact that a licenced medication is already deemed safe for human consumption and use the clinical trial process can be shortened. Repurposing of existing licenced drugs for the treatment of GBM is an alternative that could lead to faster implementation of new treatments (Abbruzzese *et al.*, 2017). Two examples of approved repurposed medications include: sildenafil designed to treat angina but repurposed for erectile dysfunction and minoxidil a blood pressure medication now used to treat hair loss (Blume-Peytavi *et al.*, 2016; Goldstein *et al.*, 2016). For the treatment of GBM there are several candidates for potential

repurposing, including ritanserin, disulfiram and metformin (Liu *et al.*, 2012; Brenneman *et al.*, 2016; Chae *et al.*, 2016).

1.5 Metformin

Metformin, 1,1-dimethylbiguanide hydrochloride, is a biguanide drug that is used as the first-line medication in the treatment of type 2 diabetes (Maruthur *et al.*, 2016). Currently metformin is the most commonly used oral antihyperglycemic agent in the US (Abdul-Ghani and Defronzo, 2017). Since 2002, the WHO began listing metformin as an essential medication highlighting its efficiency and effectiveness (World Health Organization, 2002).

1.5.1 History of metformin

The origin of metformin lies in the chemical guanidine extracted from the plant *Galega officinalis* (Goats rue/French lilac). Historically it has been recorded that *Galega officinalis* was utilized to treat the symptoms of diabetes since 1772 (Clifford, 2017). The guanidine extract was subsequently synthesised into a new chemical form called biguanide in the 1870s (Watanabe, 1918; Bailey and Clifford, 2004).

The first synthesis of metformin from biguanide was in 1922 and experiments on animals occurred in 1929, where it was shown to reduce blood glucose levels of dogs and rabbits (Werner and James, 1922; Slotta and Tschesche, 1929). Metformin was later used for the treatment of diabetes in the United Kingdom from the 1950s (Hadden, 2005). Figure 1.2 displays the various biguanide molecular structures. It did not gain world-wide acceptance until the approval for clinical use in the USA in 1995. (Nattrass and Alberti, 1978; DeFronzo *et al.*, 1995; Bailey and Turner, 1996). One of the delays for the

USA acceptance of biguanides was the risk of lactic acidosis, this was lessened only after phenformin and buformin became de-classified and removed from clinical use as diabetes medications in most countries (DeFronzo *et al.*, 1995). The structures of the biguanide and similar compounds is shown in figure 1.5. To this day metformin is the only remaining legal biguanide for the treatment of type 2 diabetes worldwide that is also listed as a WHO essential medication (World Health Organization, 2017). In 2005, a study examining statistical data identified a possible link between type 2 diabetics using metformin and a reduced risk of cancer (Evans *et al.*, 2005). In the following years, this link has been expanded to encompass a variety of tumour types (Pollak, 2012; Kasznicki *et al.*, 2014). Currently, metformin is being tested in a range of clinical trials to assess its anti-cancer potential (Heckman-Stoddard *et al.*, 2017). This has led to the testing of metformin as a potential candidate to be repurposed for use in cancer treatment (Chae *et al.*, 2016).

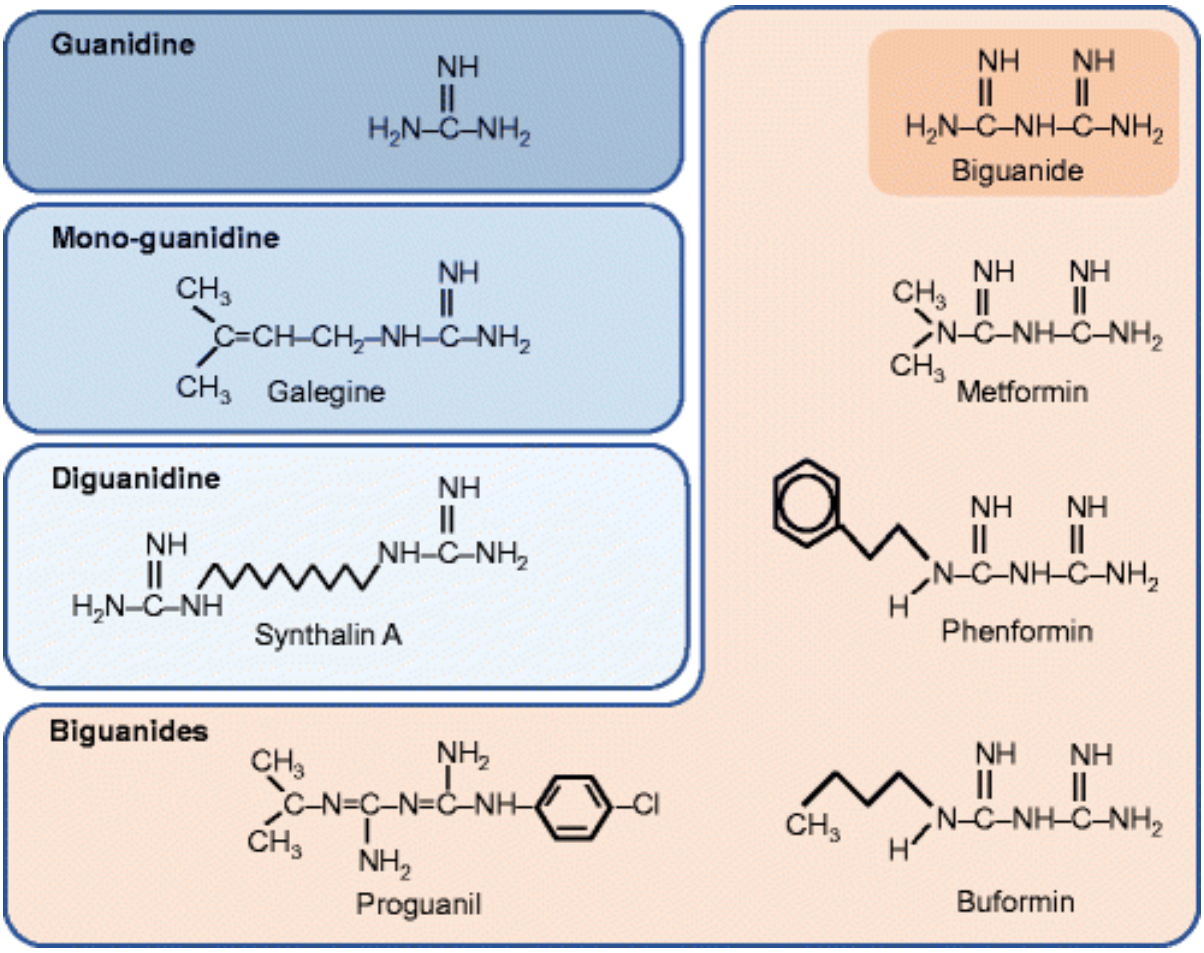

Figure 1.5 Structure of biguanides and similar classes of chemicals. Biguanide is the precursor molecule used in the development of all further biguanides that was originally made from the fusion of two guanidine. Guanidine was the original chemical extracted from plant *Galega officinali*, Mono-guanidine and diguanidien are other derivatives of guanidine that were also used as potential diabetic treatments. Phenformin and Buformin have been banned for use in most countries. Proguanil is used as a treatment of malaria and metformin is used primarily to treat type 2 diabetes. (Bailey, 2017)

1.5.2 Safety and metformin

1.5.2.1 Patient risks

Metformin has had a long history of use and is used by millions on a daily basis (Bailey, 2017). However, metformin does have side effects and risks involved with its application. The primary risk that has been established is lactic acidosis (DeFronzo *et al.*, 2016). This was more prevalent in the two other clinically used biguanides phenformin and buformin (Ching *et al.*, 2008, Bailey, 2017). Comparatively, the risk of lactic acidosis following metformin treatment was the lowest of the three chemicals. Current measurements put cases of lactic acidosis caused by metformin at <10 per 100,00 patient-years (DeFronzo *et al.*, 2016). The use of metformin is not advised for patients with even moderate renal impairment. Given the increased likelihood of excessive plasma metformin accumulation that could potentially trigger metformin induced lactic acidosis (DeFronzo *et al.*, 2016). However, it has been noted the metformin-associated lactic acidosis may be inappropriate. The measurements of lactic acidosis and metformin blood concentration are not normally carried out immediately on patient admission and so the delay of the measurements resulting in a change of the patient's metabolic status causing a potential bias on reporting actual numbers (Lalau and Kajbaf, 2014).

1.5.2.2 Ecological impacts

Metformin passes through and is excreted from the human body without being metabolised (Hassan and Carlton, 2018). The drug then enters the water supply still in the same form of which it was generated. The KWR research institute in Germany conducted a review on the prevalence of metformin in the surface water and found in rivers and lakes concentrations exceeding

1µg/L (Ter Laak and Baken, 2014). Metformin readily dissolves in water and sewage treatment plants are not currently set up to remove metformin. After passing through them it has been shown that microbial agents degrade metformin into guanylurea as shown in Figure 1.6 (Ter Laak and Baken, 2014). Kosma *et al.,* (2015) reported levels of metformin were present in Greek waste waters but that levels of guanylurea were the higher ecological risk. The presence of both chemicals has been detected in the lakes, rivers and surrounding sea of Germany at ng/L doses (Trautwein et al 2014). Measurable concentrations of the levels indicate there is no natural process to degrade the elements further in the environment. Without treatment plants removing waste metformin from water supplies further could see metformin naturally enter food chains and become unknowingly consumed (Eggen and Lillo, 2012). The long-term risk of exposure to humans is minimal however varying effects have been seen in other species. *Brassica napus cv. Sheik* and *Brassica rapa cv. Valo* have shown a high affinity for metformin uptake in seeds (Eggen and Lillo, 2012). Carrots grown in soil concentrations of 6-10mg/kg dw saw negative effects on growth and development. Niemuth and Klapper (2015) showed that exposing fathead minnows to metformin concentrations in line to current post waste treatment effluents caused an increase in the generation of intersex organisms. Hanisch *et al.*, 2004 also evaluated the risk to the aquatic environment using the PEC/PNEC ratio and got a value above 1, indicating metformin as a low concern but potential risk compound for the environment. Currently there is no consensus as to the possible ecological ramification of metformin exposure to the environment. Data on acute and

chronic guanylurea toxicity are very limited (Laak and Baken, 2014) and so further research will be needed before an overall conclusion can be gained.

Metformin (N,N-Dimethylimidodicarbonimidic diamide)	Guanylurea (1-carbamimidoylurea)
Elemental composition = $C_4H_{11}N_5$ Average mass = 129.1659 Da (Average mass of metformin hydrochloride = 165.6268 Da) Aqueous solubility (25˚C) = 1000 g/L Charge at neutral pH = 2+	Elemental composition = $C_2H_6N_4O$ Average mass: 102.096 Da Aqueous solubility (25˚C) = 1000 g/L Charge at neutral pH = 2+
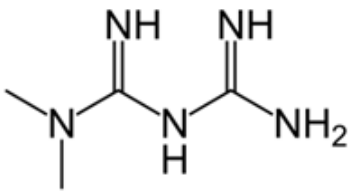 Cas# 657-24-9	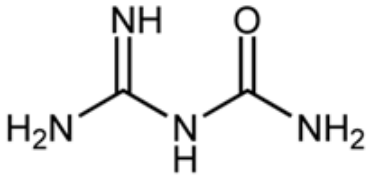 Cas# 28-36-9

Figure 1.6 Breakdown of the chemical structure and attributes of metformin and guanylurea. Metformin is not metabolised within the human body. Guanylurea is generated in the environment by the breakdown of metformin. (Thomas *et al.*, 2010; Sheurer *et al.*, 2012; Laak and Baken, 2014; Christina *et al.*, 2015).

1.5.3 Advantages of repurposing metformin

Metformin presents a low risk drug as a repurposed medication. It can be taken orally daily and will cause very little disruption to patients. The primary side effects of metformin use include: diarrhoea, nausea, vomiting, and flatulence, but are ameliorated through dose control and delivery mechanism (Legro, 2017). The BBB presents a major obstacle for the development of new anti-cancer drugs. Metformin has been shown to readily cross the blood brain barrier and reach brain tissue (Łabuzek *et al.*, 2010). In addition, metformin may have a protective effect for the brain, as it has been shown to upregulate the functions of the BBB, in rat studies. This demonstrated through activation

of AMP-activated protein Kinase (AMPK) metformin increased barrier tightness and reduced overall permeability. (Takata *et al.*, 2013). Metformin in a medicinal form is readily available world-wide. The essential medication labelling from the WHO has meant that metformin availability even in less developed countries is still high (World Health Organization, 2017). This wide spread access and low cost has led to metformin being purposed as a potential adjunct to thrombolysis treatment for low to mid income economies (Bromage, and Yellon, 2015). Metformin has also already been successfully repurposed as a second line treatment for polycystic ovary syndrome (Velazquez *et al.*, 1994). POS is characterised by anovulation and irregular menstrual cycles leading to infertility (Lord *et al.*, 2003). Metformin treatment has been demonstrated to increase ovulation and improves menstrual frequency (Legro, 2017).

1.5.4 Metformin cancer clinical trials

Repurposing metformin as a cancer treatment is already being tested in a range of clinical trials for a variety of cancers. The results of these have shown a variety of outcomes.

A phase II trial of stage IIc/III/IV ovarian, fallopian tube and primary peritoneal cancer, tested metformin alongside chemotherapy and debulking surgery on thirty-two patients. This translational study reported positive outcomes for patients receiving metformin and supported metformin in phase-III trials (Buckanovich *et al.*, 2017).

A phase III trial of 3256 women, who had completed standard therapy for early stage breast cancer, was conducted using metformin (Dowling *et al.*, 2018). The study focused on levels of the cancer antigen 15-3, an important biomarker for breast cancer progression and metastasis (Geng *et al.*, 2014). The trial concluded that metformin significantly lowered cancer antigen 15-3 levels (Dowling *et al.*, 2018).

A phase 0 clinical trial on 41 non-diabetic breast cancer patients focused on changes in metabolic markers and gene expression caused by doses of metformin up to 1500mg. The outcome was that metformin affected breast cancer metabolism at the clinical doses. Metformin inhibited fatty acid oxidation and mitochondrial gene expression in cancer tissue but not normal patient cells (Lord *et al.*, 2016).

I-SPY 2 is a phase II trial evaluating ganitumab and metformin alongside standard neoadjuvant therapies for high-risk breast cancer patients. It used a Bayesian predictive model with a ≥85% threshold for success. Two hundred and thirty-four patients took part in the trial. None of the treatment sub-types achieved the threshold level for success and were deemed not to show an impact in reducing patient's tumour burden (Yee *et al.*, 2017).

Chae 2016 studied ongoing and completed, cancer based, metformin clinical trials. In several trials metformin was shown to reduce levels of tumour survival bio markers, but overall, it concluded that data on survival outcomes for patients was still lacking. There were only two studies with complete data, two phase II late stage pancreatic cancer clinical trials. Both trials saw no

improvement from adding metformin to the treatment regimen (Kordes *et al.*, 2015; Reni *et al.*, 2015). From the available data it is speculated that metformin maybe more suitable for earlier stages of cancer. However, more mature study data and survival rate assessments are required to ascertain metformin use as a therapeutic cancer treatment (Chae *et al.,* 2016).

1.6 Metformin mechanism of action

The mechanisms of metformin anti-neoplastic activity are not fully understood (Rena *et al.*, 2017). It is believed to operate indirectly through lowering insulin levels in patients with hyperinsulinemia and directly through inhibition of respiratory complex I of the electron transport chain in mitochondria (Pollak, 2012).

1.6.1 AMPK and mTOR

Inhibition of mitochondrial complex I leads to activation of AMPK (Han *et al.*, 2015). This protein has been demonstrated to act as both tumour suppressor, through inhibition of mammalian target of rapamycin (mTOR), an oncogene facilitating cell division and has a role in aiding metabolic reprogramming (Jeon *et al.*, 2012; Liu *et al.*, 2013).

mTOR functions as a kinase that regulates several downstream processes including protein synthesis, lipid synthesis cell survival, cell motility, autophagy and transcription (Hay *et al.*, 2004). Control of downstream pathways is maintained by the creation of two different protein signalling complexes, mTOR complex (mTORC) 1 and 2 (Lipton *et al.*, 2014; Saxton *et al.*, 2017). The two complexes have variations in the proteins used but both utilize mTOR

as the core component (Kim *et al.*, 2015). Figure 1.7 shows the full mTOR signalling network and pathways.

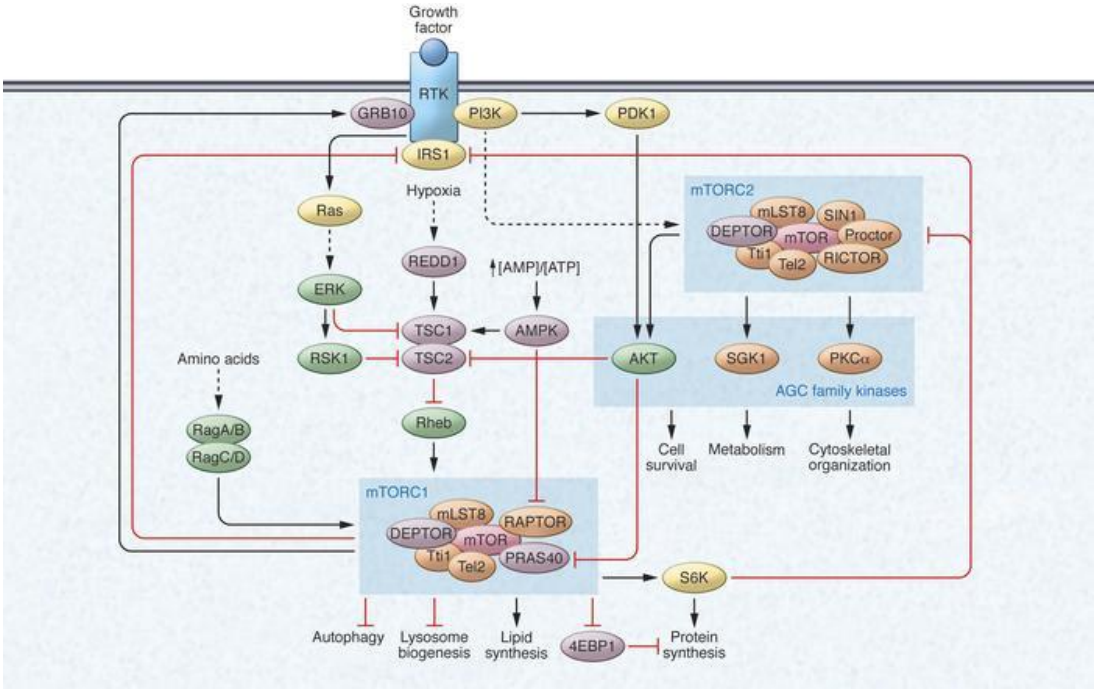

Figure 1.7 mTOR signalling complex and pathway. mTOR forms two separate complexes mTORC1 and mTORC2 to regulate multiple downstream effectors. mTORC1 affects anabolic and catabolic pathways. mTORC2 affects cellular proliferation pathways including cell survival, metabolism and cytoskeletal organisation. mTORC1 is primarily inhibited by AMPK phosphorylation of RAPTOR and the AKT substrate PRAS40. mTORC1 can also inhibit mTORC2 through the downstream effector S6K. (Kim *et al.*, 2015)

Metformin control and inhibition of mTORC has been reported through several pathways. In prostate cancer metformin increases expression of the regulated in development and DNA damage response 1 (REDD1) protein in a *p53*-dependent manner (Sahra *et al.*, 2011). REDD1 is an endogenous negative regulator of mTORC1 that can be activated through metabolic stress (McGhee *et al.*, 2009; Tiwarekar *et al.*, 2018).

In pancreatic cancer, metformin downregulates the transcription factors of specificity proteins 1, 3 and 4 leading to inhibition of downstream mTOR signalling (Nair *et al.*, 2014).

AMPK suppression of mTOR can also be achieved through phosphorylation of TSC2 and RAPTOR (Inoki *et al.*, 2003; Gwinn *et al.*, 2008). This inhibition impacts fatty acid synthesis and causes reduction in tumour proliferation and growth (Dowling *et al.*, 2007). In GBM, AMPK is constitutively activated and upregulated (Liu *et al.*, 2013). Inhibition of the mTOR pathway by metformin has also been shown to be independent of AMPK activation (Kalender *et al.*, 2010). Metformin acts through increasing affinity of the protein kinase B (AKT) substrate PRAS40 binding to RAPTOR and negatively regulates mTOR complex 1 (Liu *et al.*,2013).

1.6.2 Micro RNA

1.6.2.1 Overview

Micro RNAs (miRNA) are short non-coding regions of RNA no longer than approximately 30 base pairs. Originally thought to be fragment translated products of non-coding "junk" DNA regions. However, now it is known that miRNA play a critically important role in post-transcriptional regulation and silencing of other RNAs. (Santa-Maria *et al.*, 2015). Primarily miRNAs act within the cell but the extracellular effects of miRNAs have been well documented and the detection of circulating miRNAs in blood plasma as a biomarker is being developed for clinical applications (Pirola *et al.*, 2015). The result of

miRNA regulation on cells can affect a range of biological process such as cell proliferation, differentiation, survival and motility (Christopher *et al.*, 2016).

1.6.2.2 Generation and function of miRNAs

The formation of miRNAs occurs within the nucleus. RNA polymerase II (Pol II), this enzyme responsible for transcribing most miRNA. The resulting product is referred to as a primary-miRNA (pri-miRNA) and possess good self-complimentary sequences that aid in self binding to form a hairpin stem-loop. Other features of pri-miRNA are poly A tails on the 3' end. This structure makes the pri-miRNA detectable by the proteins DGCR8 and Drosha, which together form a microprocessor complex (Gregory *et al.*, 2004). This complex function is to remove the miRNA still connected at the hairpin loop of the pir-miRNA and produce a double stranded sequence with a short nucleotide overhang on the 3' end, now referred to as pre-miRNA (Denli *et al.*, 2004). There is a small sub-group of pre-miRNAs that are generated through Drosha-independent means, that bypass the microprocessor complex and are spliced out of introns (Berezikov *et al.*, 2007). Originally the mi-RNA variants were not believed to be present within mammalian organisms, however recently studies have identified the presence in human genomes. Variations in the expression profiles have also been linked to cancer and tumour cells, giving them a potential use as a diagnostic tool (Butkytė *et al.*, 2016). Export out of the nucleus to the cytoplasm is handled by nuclear transmembrane protein exportin-5 (Wu *et al.*, 2018). This protein is able to identify pre-miRNA due to the nucleotide overhand that was left post Drosha cleavage (Wilson *et al.*, 2013). Once in the cystol the pre-miRNA is cleaved by the RNasa III enzyme

Dicer. This removes the hairpin loop from one end of the pre-miRNA leaving a double strand RNA fragment that will eventually denature leaving the complete miRNA free. Though there are two complete nucleotide strands, referred, to as 5' and 3', both are not always used as functional miRNA to become incorporated in a miRNA-induced silencing complex (miRISC) (Eulalio *et al.*, 2008, Fabian and Sonenburg, 2012). Any non-functional strands are degraded after separating from the other miRNA, post Dicer modification (Kawamata *et al.*, 2015). Figure 1.8 shows an overview of this process from gene to miRISC. The complete mIRISC is able to identify and bind to mRNA sequences in the cytoplasm by using the miRNA component as a template (Sheu-Gruttadauria *et al.*, 2018). Once bound the mRNA is unable to be translated by ribosomes and is effectively silenced (Islam *et al.*, 2017). This post transcriptional method of silencing then leads to the degradation of the mRNA and is shown in figure 1.9.

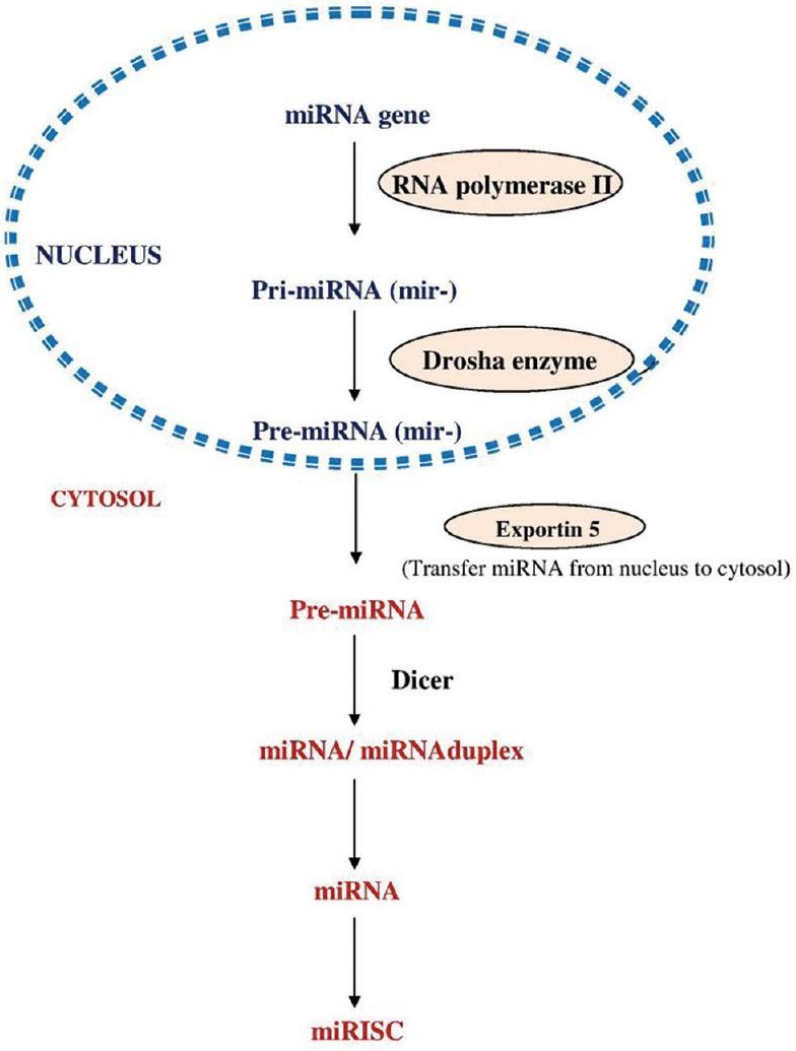

Figure 1.8 Schematic overview of miRNA biogenesis. Occurring within the nucleus miRNA are formed from both miRNA genes and from non-functional introns. Transcription of miRNA is moderated by Pol II. Within the nucleus miRNA take on structural changes due to modification by Drosha enzyme. The changes allow it to pass through the nuclear membrane through exportin 5 and enter the cytoplasm. Further changes and cleavage occur due to the Dicer protein leaving a miRNA duplex. One or both strands join into a completed protein complex (mIRISC) to enact mRNA transcriptional regulation. (Christopher *et al.*, 2016)

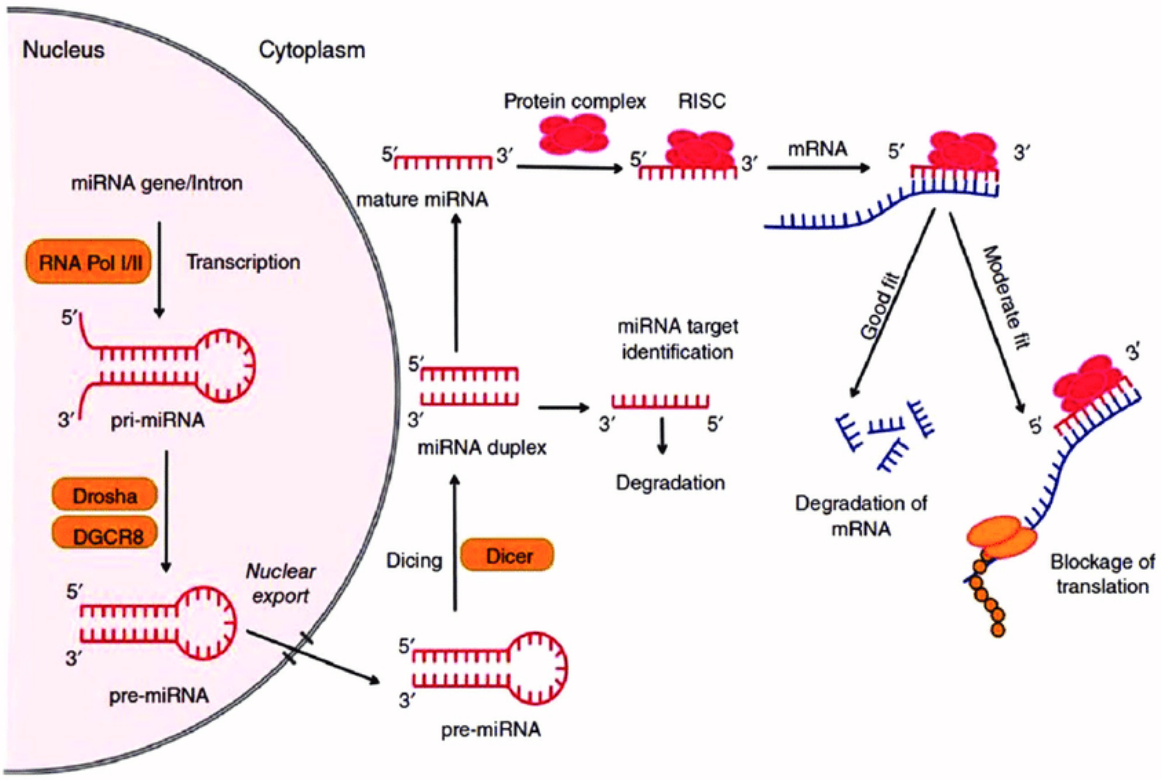

Figure 1.9 Generation and function of miRNA. miRNA are generated in the nucleus and, post restructuring and modification, are released through the nuclear membrane as pre-miRNA. In the cytoplasm the miRNA is further modified by cleavage of the hairpin loop to produce miRNA duplexes. One strand is degraded and the other becomes mature miRNA. In this final state the miRNA can combine with proteins to form a RNA-induced silencing complex (RISC). One the complex is fully formed; the miRNA component allows the RISC to bind to complimentary bases of mRNA in the cytoplasm. Depending on how complimentary the sequence between the miRNA and then mRNA determines the overall fate of the mRNA. Near or exact complimentary base sequences will allow the mRNA to become degraded. Non-specific binding allows the miRNA to bind to mRNA and block the translation of the mRNA sequence (Islam *et al.*, 2017).

1.6.2.3 MiRNAs role in cancer

As a cell progresses towards a cancerous state, the ability to control and regulate the expression of RNA, including miRNA, is often damaged or lost (Lin *et al.*, 2015). This dysregulation in miRNA expression impacts a range of cellular process involved in preventing further tumour development, including cell cycle arrest, differentiation and apoptosis (Hata and Lieberman, 2015). The role each miRNA has in the progression of tumours varies, an individual miRNA can take on oncogenic or tumour suppressive affect. Distinguishing what effect an individual miRNA has on a cell is context dependent. An example of a strong oncogenic miRNA is miR-21. In most human cancers miR-21 is found to be over expressed and acts as an oncogene by targeting and decreasing the expression of FBX011 tumour suppressor gene (Yang *et al.*, 2015). This oncogenic role is also in GBM, where miR-21 has an impact on *P53*, TGF-β and mitochondrial apoptosis tumour-suppression pathways (Chan *et al.*, 2005; Papagiannakopoulos *et al.*, 2008; Maachani *et al.*, 2016). miR-466 acts as a tumour suppressor in prostate cancer where it has a negative effect on cell proliferation and prevents metastasis by targeting bone-related transcription factor RUNX2 (Colden *et al.*, 2017). Cancer type dependent variation have also been identified. MiR-222 is frequently upregulated in cancers, including GBM where it reduces apoptosis and aids in cell survival (Zhang *et al.*, 2010). However, the inverse of this is demonstrated in prostate cancer where miR-222 acts as a tumour suppressor (Fuse *et al.*, 2012)

1.6.2.4 Impact of metformin on micro-RNA expression

There is growing evidence that metformin has an impact on the expression and modulation of a range of miRNAs. The changes have been linked to a range of metformin effects including anti-cancer properties. A review by Pulito *et al.* (2014) identified nine main miRNAs that were impacted by metformin treatment across a range of cancers (miR-26a, miR-33a, miR-140, miR-142, miR-192, miR-200, miR-205 miR-222 and let-7c). Metformin has been shown to induce apoptosis through increasing expression in miR-708-5p causing it to suppression expression of the endoplasmic reticulum membrane protein neuronatin in prostate cancer (Yang *et al.*, 2015). It also induces mitochondrial-dependent cellular apoptosis in KB human oral cancer cells through increased expression of miR26a (Wang *et al.*, 2016). Cell cycle arrest has also reported in a range of tumour types. In renal cancer cells metformin induces G0/G1 arrest and delayed entry into S phase through up regulation of miRNA34a. In pancreatic cancer cells a similar G1-phase arrest is seen from metformin treatment, but this is induced through down regulation of miR-221 (Tanaka *et al.*, 2015).

1.6.3 Cell Death

1.6.3.1 Role of apoptosis

Apoptosis, or programmed cell death, is an important cellular mechanism that functions to enable the destruction and removal of cells in a controlled manner. This mechanism utilizes a host of intracellular machinery to perform a range of functions within an organism including; embryonic development, structural development, immune response, hormone dependant atrophy and chemical-induced cell death (Elmore, 2007). Once apoptosis has begun it is irreversible and ultimately ends in the breakdown of all cellular function. Many cellular pathways are involved in the activation and execution of the process. The main two mechanisms observed are the extrinsic pathway and intrinsic pathway (Budihardjo *et al.*, 1999). Both pathways act through the function of various caspase proteins but are activated and regulated through different means. The pathways shown for both intrinsic and extrinsic apoptosis are shown in Figure 1.10. The extrinsic pathway is mediated by cell surface death receptors that respond to death ligands normally presented by immune-effector cells (Lowe *et al.*, 2000). This leads to the formation of a death-inducing signalling complex (DISC) that activates the cascade of caspase pathways within the cell. The intrinsic pathway centres around various functions of the mitochondria that can include activation of the caspase pathway and activation of APAF1 through release of cytochrome C (Fulda and Debtain, 2006).

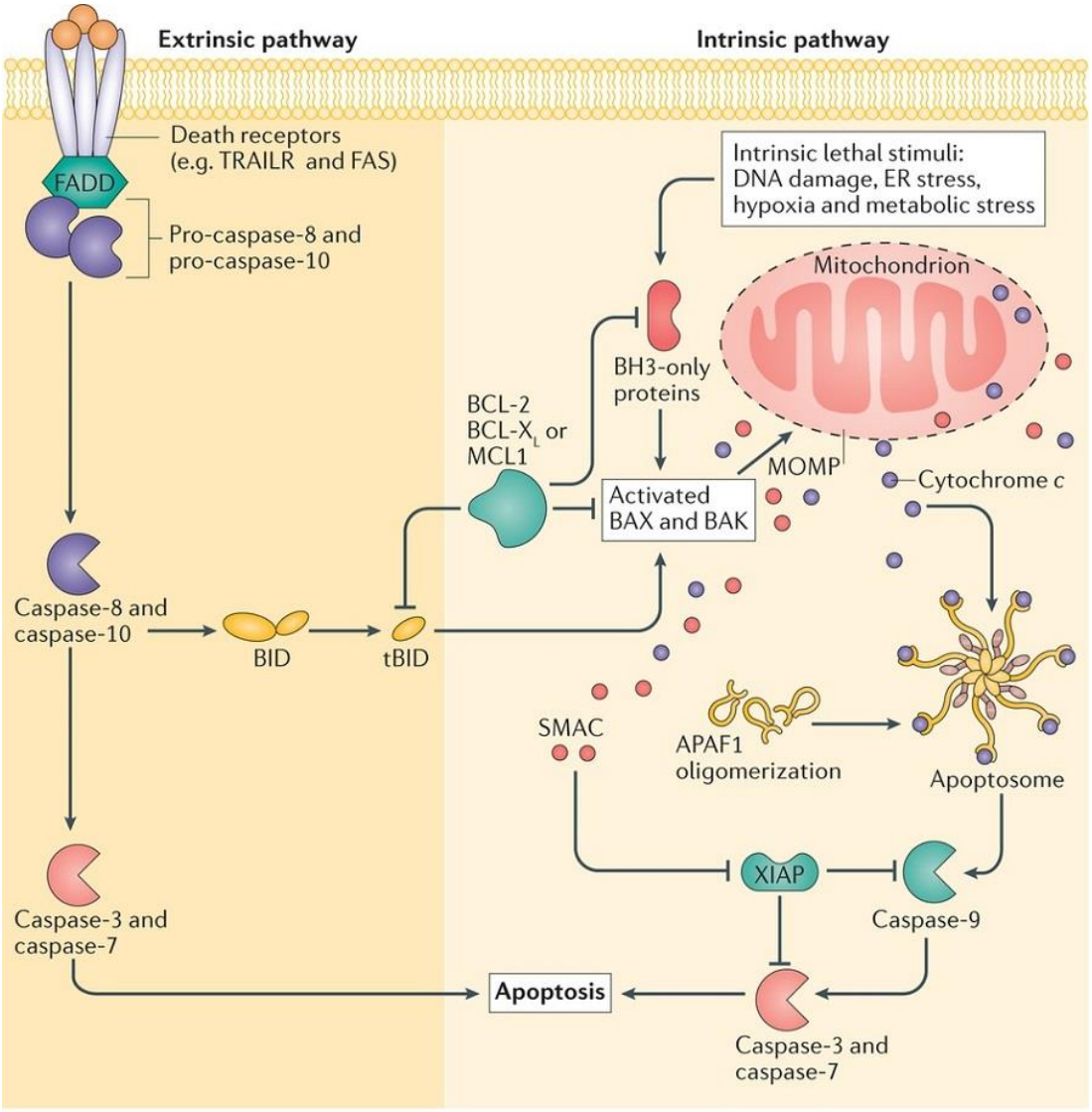

Figure 1.10. Extrinsic and intrinsic apoptotic pathways. Apoptosis is a cellular process that utilises a range of signalling pathways. The two version of apoptosis vary based on the initial signalling trigger. Extrinsic apoptosis cascades down from an extra cellular signal that generates the creation of a DISC. Intrinsic apoptosis has several triggers relating to metabolic activity, DNA damage and cellular stress. Intrinsic and extrinsic pathways both utilise several caspase family proteins that eventually end in the activation of the execution effector caspases 3 and 7. (Lowe *et al.*, 2000; Hunt, 2002).

Mitochondria have an important role in the intrinsic apoptotic pathway and regulate downstream caspase effectors through release of cytochrome C (Hunt, 2002). A key component of mitochondrial action is the mitochondrial membrane potential (Δψ) that powers the tricarboxylic acid cycle (Martínez-Reyes *et al.*, 2016). In some cells the depolarisation of the transmembrane potential, loss of oxidative phosphorylation and the release of apoptogenic factors by the mitochondria are key to intrinsic apoptotic progression. However, there is also data to show that the factors are not effectors of apoptosis and occur later in progression, as an end result of other components of the apoptotic-signalling pathway (Ly *et al.*, 2003). Though the complete mechanisms are unknown, metformin has been shown to affect mitochondria through multiple pathways which could induce mitochondrial stress leading to apoptosis. Biguanides can inhibit complex 1 of the mitochondrial respiratory chain and inhibit mitochondrial ATP synthase through accumulation within the mitochondria matrix (Owen *et al.*, 2000, Bridges *et al.*, 2014). Metformin can also lead to the inhibition of mitochondrial glycerophosphate, a redox shuttle enzyme, causing a reduction in lactate to glucose conversion and decreasing hepatic gluconeogenesis (Madiraju *et al.*, 2014). In addition, metformin has been shown to reduce mitochondrial fragmentation and suppress mitochondrial fission by reducing dynamin-related protein 1 (Wang *et al.,* 2017). In prostate, lung and melanoma cancer cells, metformin has been shown to cause an increase in mitochondrial uptake of calcium through the mitochondrial calcium uniporter, causing mitochondria to swell. However, it simultaneously also inhibited the opening of the mitochondrial permeability

transition pore and increased mitochondrial biogenesis, both protective measures against apoptosis (Loubiere *et al.*, 2017).

1.6.3.2 Disruption of apoptosis in cancer

Cancer cells have evolved many ways to prevent and block cell death from apoptotic pathways. Extrinsic pathways can be blocked through increasing the concentration of anti-apoptotic molecules, blocking key activation receptors or by mutations that impair the function of pro-apoptotic genes. An example is mutations that cause loss or damage to cell surface receptors CD95 or TRAIL (Fulda and Debatin 2006). Loss of TRAIL has been found in head, neck, osteosarcoma (Pai et al, 1998; Dechant *et al.*, 2004). The ability to control the activation of apoptosis is an important goal in the development of some treatments. However there has been limited progress in developing the extrinsic caspase pathway for clinical benefit. Due to the less specific nature of activating extracellular receptors of cells, non-specific binding has caused toxicity issues with treatments. The attempts include utilising tumour necrosis factor alpha (TNF-α) and targeting first apoptosis signal receptor CD95 (FAS) with antibodies (Ashkenazi, 2015). Clinical trials of TRAIL receptor agonists have had poor outcomes (Merchant *et al.*, 2012, von Pawel *et al.*, 2014). Recent novel information, understanding cancer cells resistance to TRAIL and potential mechanisms to counter the pro-tumorigenic effects of endogenous TRAIL, highlight that TRAIL based treatment methodologies could still be utilised effectively (von Karstedt *et al.*, 2017).

Mitochondria are key organelles that have a role in cell survival and proliferation through production of metabolites and ATP. Metformin has been

shown to induce apoptosis in multiple tumour types including, but not limited to: ovarian, prostate, gastric, lung, leukaemia and breast cancer cells (Han *et al.*, 2015; Li *et al.*, 2015; Moon *et al.*, 2015; Rodríguez-Lirio *et al.*, 2015;; Yang *et al.*, 2015 Zhang., 2016).

1.6.3.3 Autophagy

Autophagy is an alternative method of cell destruction. It functions through use of autophagosomes. These are double membrane cytosolic vesicles that, once active, move around a cell absorbing macromolecules and organelles. Once material has been collected, the autophagosomes combine with lysosomes and become autolysosomes. The fused complex then breaks down all the absorbed phagosomes contents (Ramirez *et al.*,2013). Trigger of autophagy in GBM has been identified as a potential therapeutic target (Palumbo *et al.* 2012).

Self-degradation of cells can also occur through autophagy, a controlled cellular process in which the cells own lysosomes deconstruct other internal cellular structures (Xie *et al.*, 2007). This process is used for a variety of roles including removal of damaged organelles, regulation of metabolism, cellular survival and as a method of programmed cell death (Parzych *et al.*, 2014; Kobayashi, 2015). An overview of the stages of autophagy are outlined in Figure 1.11. Autophagy is controlled by several upstream regular pathways, primarily through regulation of mTOR supplemented with regulatory signalling from Phosphoinositide 3-kinase (P13K) and AKT (Heras-Sandoval *et al.*, 2014). The relationship of the upstream elements is shown in Figure 1.12.

Metformin can induce autophagy through inducing cellular stress and decreasing mitochondrial ATP (Lindqvist *et al.*, 2018). For hepatocellular carcinoma, metformin induces autophagy through upregulation of tumour suppression protein CEBPD (Tsai, 2017). In colon cancer cells metformin induced autophagy in a *P53* dependent manner, with wild type *P53* displaying activation of autophagy due to metformin treatment (Buzzai *et al.*, 2007). In lymphoma, metformin can induce autophagy in conjunction with the anti-cancer drug doxorubicin leading to a reduction in cell growth (Shi *et al.*, 2012).

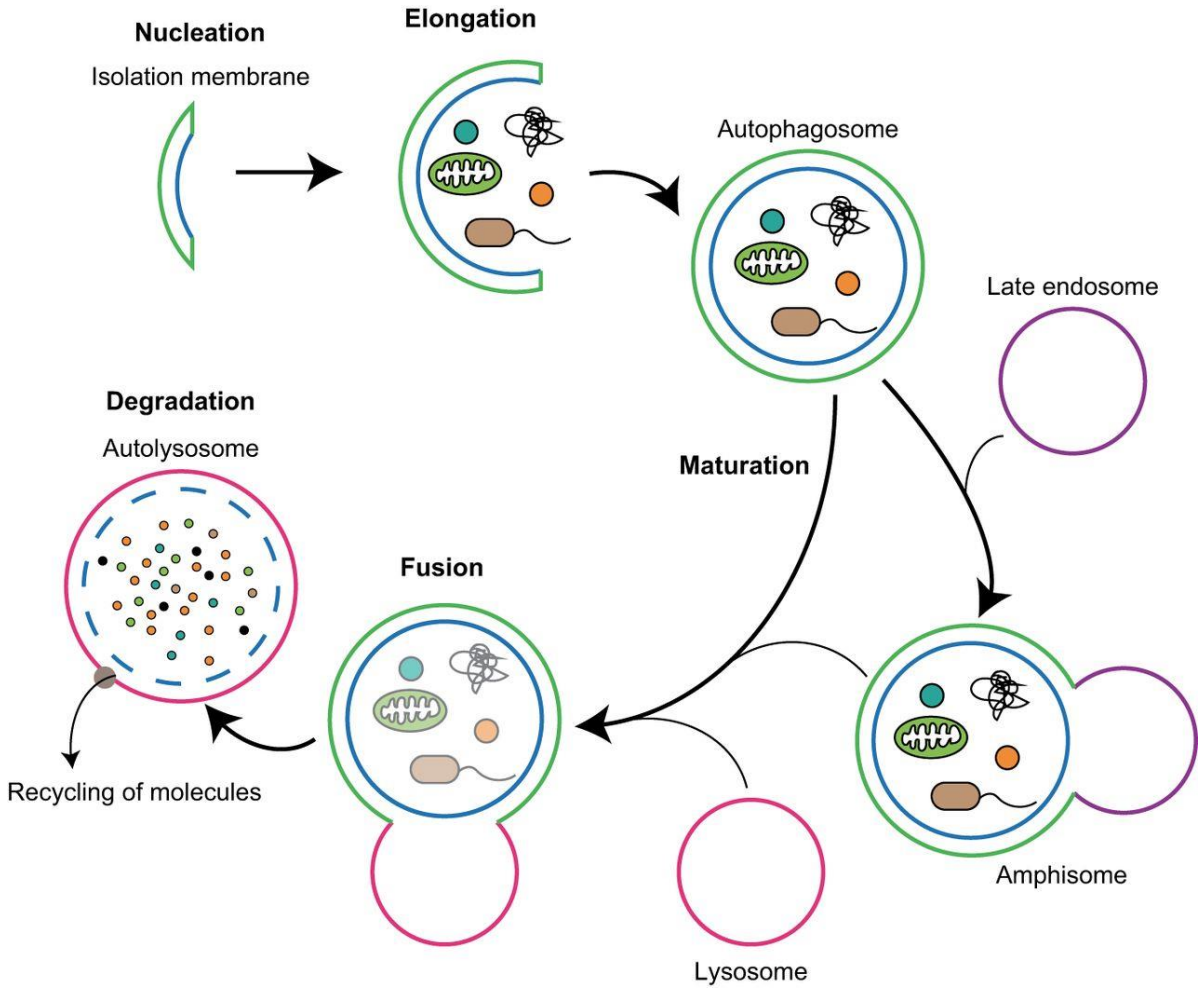

Figure 1.11 Outline of autophagy. Autophagy begins with a double membraned structure gathering proteins, organelles and other cellular materials found with the cytoplasm. This leads to the formation of the autophagosome. This compact structure continues to fuse with a lysosome and occasionally, depending on the membrane bound cargo, an endosome. Once fusion of the membranes has completed the completed autolysosome degrades all contained materials to be recycled as molecules for other cellular processes. (Nakamura *et al.*, 2017)

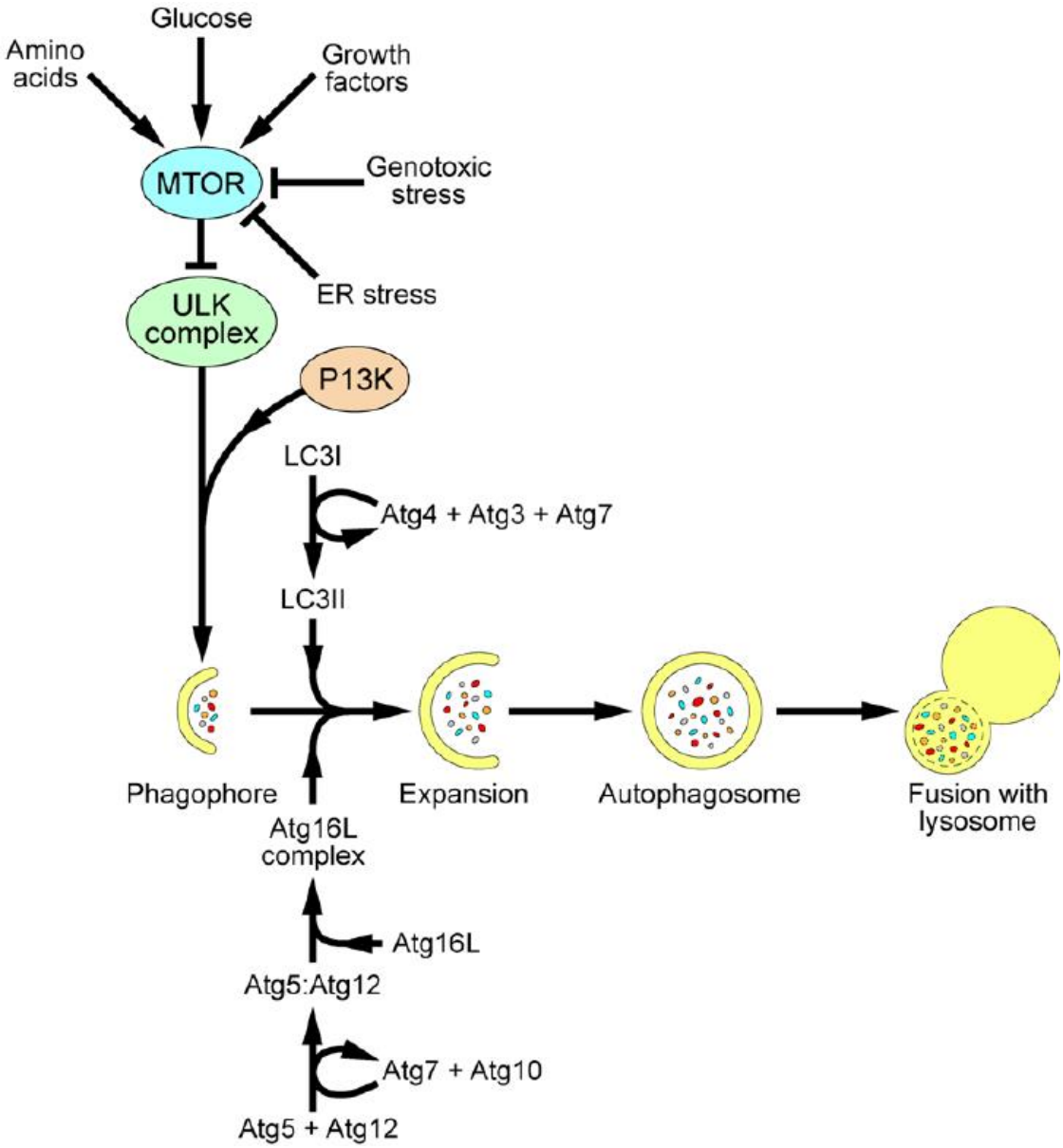

Figure 1.12 Autophagy regulation pathway. The primary mechanism controlling autophagy is mTOR. Inactivation of mTOR can occur from a range of cellular signalling relating to cellular stress, growth factors, glucose and amino acid levels. This leads to substrates produced by P13K complexes and the ULK Complex to move to be transported to the nascent phagophore. Further protein complexes are then recruited to create the complete autophagosome. (Maier *et al.*, 2012)

The suppression of autophagy is commonly associated with tumorigenic cell transformations, inferring that autophagy has an important role in tumour suppression (Gozuacik *et al.*, 2004; Fulda *et al.*, 2015). Metformin has also been seen to act through induction of autophagy in a range of tumours such as oesophageal squamous cell carcinoma, thyroid and endometrial cancer cells (Feng *et al.*, 2014; Song *et al.*, 2016; Gu *et al.*, 2017). For GBM cell lines it has been shown that metformin, when used in combination with arsenic trioxide, can induce both apoptosis and autophagy (Carmignani *et al.*, 2014). Primarily acting through concomitant activation of AMPK, REDD1 and inhibition of the mTOR pathway (Sesen *et al.*, 2015).

1.6.4 Cell cycle

Cell cycle and its regulation is critical to the maintenance of existing cell populations and the generation of new cells. Dysregulation of the cell cycle, leading to unchecked proliferation, is a common feature in cancer cell development (Evan and Vousden, 2001). Progression through the cell cycle is heavily controlled and regulated. To prevent the cellular process happening incorrectly there are several checkpoints in the cell cycle that must be passed before proceeding (Vermeulen *et al.*, 2003). The checkpoints occur at key stages in cell division and are a failsafe to prevent DNA damage and aberrant cell behaviour. If checkpoint specific pre-requisites are not met at the checkpoint, then the cycle arrests and division is prevented (Bertoli *et al.*, 2014). The main two groups of molecules responsible for controlled progression through the check points are cyclins and cyclin-dependent kinases (CDK). CDK bind to form protein complexes that allow the cell to advance to

each subsequent step and inevitably complete cell division (Spoerri *et al.*, 2015). Table 1.1 contains a list of checkpoints and the linked cyclin Cdk complexes. A full summary of the cell cycle developmental checkpoints can be found in figure 1.13.

Table 1.1 – Required cyclin CDK combination for cell cycle checkpoint progression

Checkpoint	Cyclin[1]	Cdk
G1 phase checkpoint	Cyclin D	Cdk4
		Cdk6
S phase checkpoint	Cyclin E	Cdk2
G2 phase checkpoint	Cyclin A	Cdk2
		Cdk1
Spindle checkpoint	Cyclin B	Cdk1

[1]Cyclin required for cell cycle checkpoint progression. For G1 and G2 phase checkpoints cyclins must form relevant complex's with both listed Cdk to enable progression through the checkpoint. (Spoerri *et al.*, 2015)

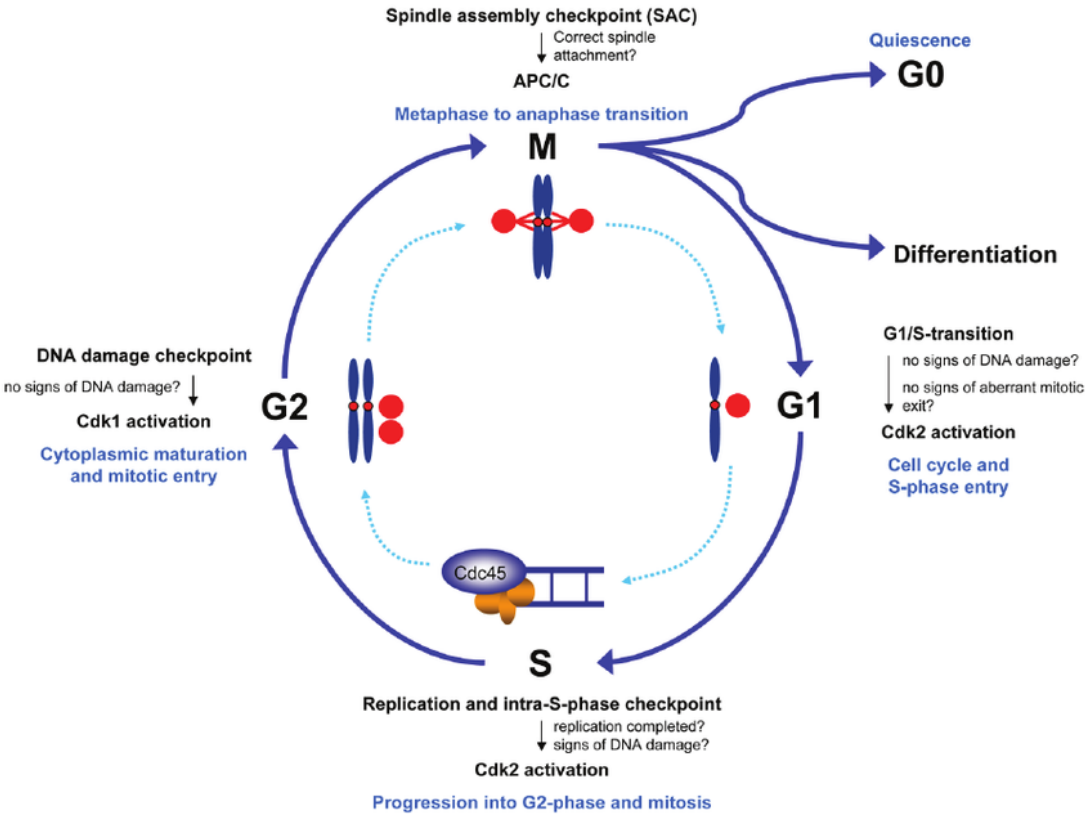

Figure 1.13 Cell cycle developmental progression checkpoints. There are four main stages to cell cycle progression: G1, S, G2 and M phase. Controlling the cells movement through the phases are four main check points, G1 to S phase transition, S phase checkpoint, G2 phase checkpoint and the spindle assembly checkpoint. Each check point ensures that the cell has not suffered damage and that correct prerequisite stages have been completed. G1/S, S phase and G2 phase all check for DNA damage that would lead to mutation and errors post division. The three phases also possess an additional unique checkpoint assessment; G1/S asses that previous mitosis was completed correctly, S phase checks for duplication of genetic material and G2 assess the cell mitotic preparation. The spindle check point assesses correct establishment of mitotic spindle for correct allocation of chromosomes. Each stage is controlled by the creation of a specific cyclin Cdk protein complex (Schnerch *et al.*, 2012).

Metformin has been shown to induce cell cycle arrest in a cancer specific manner through a range of mechanisms. In lung cancer cells metformin has been shown to induce G1 cell cycle arrest through suppression of the atypical repressor E2F8. Expression of E2F8 has been linked with poor patient survival (Jin *et al.*, 2017). G1 and G2/M cell cycle arrest was seen in separate prostate cells treated with metformin in separate experiments (Babcook *et al.*, 2014; Gonnissen *et al.*, 2017). In GBM cell lines LN18 and LN229 metformin has been shown to increase radio sensitivity and induce G2/M cell cycle arrest in conjunction with TMZ (Adeberg *et al.*, 2017). In drug resistant leukaemia metformin arrests cells in S and G2/M phases through downregulation of cyclin A, cyclin B1 and cdc2 (Rodríguez-Lirio *et al.*, 2015). Breast cancer cell respond to metformin by upregulating cyclin G2, cyclin G2 is a key regulator of the G2/M checkpoint through inhibition of CycB1-Cdc2 (Zimmermann *et al.*, 2012, Zimmermann *et al.*, 2016).

1.6.5 Necrosis and Oncosis

Necrosis is a cellular process that sometimes is associated with cell death. It is considered by some that necrosis should not be a true mechanism of cell death as it is merely the fate of a cell that has accidentally died. Instead the term oncosis leading to necrosis is the correct terminology (Elmore, 2007). However, necrosis is a similar but less regulated mechanism compared to apoptosis, in that the breakdown of the cell still happens but focuses on the breakdown of intracellular membranes. The materials released enter the extracellular milieu and cause the cells to promote response from nearby immune cells (Zong *et al.*, 2004). Metformin is not normally associated with

cell death through necrosis. However, one study has shown that in prostate cancer cells the combination of simvastatin metformin is able to induce Ripk1- and Ripk3- dependent necrosis (Babcook *et al.*, 2014).

1.6.6 Other mechanisms

The high mutation rate of cancerous cells leads to alterations in metabolism pathways (Lindgvist *et al.*, 2018). In contrast to normal cells, that produce energy through oxidative phosphorylation, cancer cells primarily utilize glycolysis and lactic acid fermentation as energy sources (Vander Heiden *et al.*, 2009). This behaviour is referred to as oxidative phosphorylation or the Warburg effect (Goodwin *et al.*, 2015). This change in metabolism is driven by mutations and dysregulation in normal cellular pathways. The embryonic isoform of pyruvate kinase, M2, is exclusively expressed in tumour cells instead of normal pyruvate kinase M1 (Christofk *et al.*, 2008). This is a key driver in the Warburg effect and aids in promoting mTORC1, boosting cell proliferation (Ye *et al.*, 2012). Overexpression of phosphoglycerate dehydrogenase (PHGDH) blocks glucose metabolites becoming pyruvate to end the Krebs cycle and instead redirects them to produce serine (Locasale *et al.*, 2011). Over expression has also been linked to glioma cell proliferation and invasion (Liu *et al.*, 2013). Von Hippel-Lindau (VHL) tumour suppressor that can be suppressed in tumours, this cause redirection glucose away from the Krebs cycle to generate lactate (Lee *et al.*, 2016). Degradation of VHL has also been shown to promote glioma genesis (Zhu *et al.*, 2017). IDH1 allows tumour cells to generate lipids from citrate and is linked with aggression in GBM (Sun & Denko, 2014; Miroshnikova *et al.*,

2016). Fumate-hydratase (FH) deficient cells accumulate fumarate that induces hypoxia-inducible factors (HIFs) that have been shown to aid in the regulation of GBM (Frezza *et al.*, 2011; Yang *et al.*, 2012). The interaction of cancer alteration to metabolic pathways is given in figure 1.14.

There are suggestions that the mechanism of action of metformin is cancer type independent and acts through inhibiting mitochondrial complex 1 (NADH dehydrogenase) of cancer cells (Wheaton *et al.*, 2014). Metformin has also been shown to be an inhibitor of hexokinase 2 blocking the first step in glycolysis (Salani *et al.*, 2014) The reprogrammed metabolism of cancer cells is a potential vulnerability that could be exploited to treat tumours while leaving normal cells unharmed (Würth *et al.*, 2013, Weinburg *et al.*, 2015).

Regarding cancer stem cells (CSC), metformin has been shown to have a cytotoxic effect because of its ability to targets glioma CSCs (Mouhieddine *et al.*, 2015). This possible mechanism will deprive the tumour cell population of its stem/progenitor cells preventing regrowth and possible resurgence.

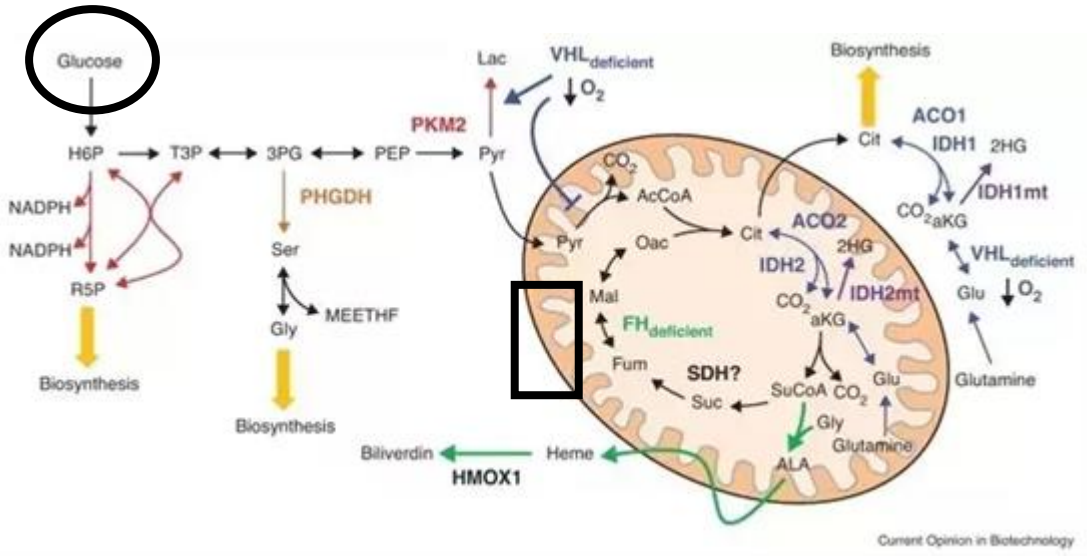

Figure 1.14 Mutations and metabolism alterations in cancer. Metabolism pathways utilised by cancer cells. Colour coding indicates areas of effects from different mutations. Red – Embryonic pyruvate Kinase M2 is over expressed and drive the Warburg effect. Orange – PHGDH enables the generation of serine from glucose metabolites and promotes glioma proliferation. Blue – VHL deficiencies enables increased generation of lactate from glucose metabolites and promotes the generation of glioma cells. Purple – IDH1 enable tumour cells to generate lipids from citrate and promotes glioma aggression. Green – Deficiency in FH leads to a build-up of fumarate that promote HIFs.

Additions to the diagram show the target areas that metformin can impact. Black circle – Metformin inhibits hexokinase 2, an enzyme utilised at the start of glycolysis (Salani *et al.*, 2014). Black rectangle – Metformin can inhibit mitochondrial complex 1 (Wheaton *et al.*, 2014).

PKM2, M2 isoform of pyruvate kinase; PHGDH, phosphoglycerate dehydrogenase; PDH, pyruvate dehydrogenase complex; PDK, pyruvate dehydrogenase kinase; ACO, aconitase; IDH, isocitrate dehydrogenase; SDH, succinate dehydrogenase complex (mitochondrial Complex II); FH, fumarate hydratase; HMOX, heme oxygenase. (Hiller *et al.*, 2013).

1.6.7 Overview

The mechanisms through which metformin induces anti-tumour effects remains unclear and varies based on cancer type and environment. Defining an outline to the actions of metformin is hindered by its ability to induce multiples forms of cell death. Studies in both melanoma and endometrial cells have identified that metformin can induce cell cycle arrest (in one or more phases), autophagy and apoptosis in the same cell population (Tomic *et al.*, 2011; Takahashi *et al.*, 2014). The large variation in reported findings may highlight that metformin mechanism does not directly induce pathways of cell death and therefore all the observed result are potential side effects. Hence, it is probable that the mechanism of action for metformin is dependent on tumour type.

1.7 Drug synergy

1.7.1 Metformin

The testing of metformin as a therapy for GBM comes with very little risk. The drug is readily available and is relatively stable. The drug is not metabolized by human cells and is normally excreted in the same form it is ingested in, indicating it is hydrophillic (Bailey, 2017). The drug does not bioaccumulate in human tissue unless renal function is impaired (Viollet *et al.*, 2012). This makes an ideal candidate to test through *In vitro* and *In vivo* models. It can readily dissolve in water and DMSO so will be deliverable to cells in the culture media (Block *et al.*, 2009; Sankar *et al.*, 2013). Lactic acidosis (LAD) is the primary side effect of any risk however this is of a low incidence in patients and normally linked to an impairment in renal function (Salpeter *et al.*, 2010).

Studying metformin in cell culture will help identify its mechanism of action and if it might have suitability to be repurposed as an anti-cancer agent.

1.7.2 Combination treatments

Metformin would never be used as a mono drug therapy for cancer treatment. Instead metformin would be used as part of a treatment regime involving several different drugs to increase overall efficacy. Identifying potential synergistic partners for metformin would further the possibility of use in treatment for GBM patients. Disulfiram and Sorafenib have already been identified as potential candidates to work synergistically with metformin for cancer treatments (Aldea *et al.*, 2014, Jivan, *et al.*, 2015).

1.7.2.1 Temozolomide

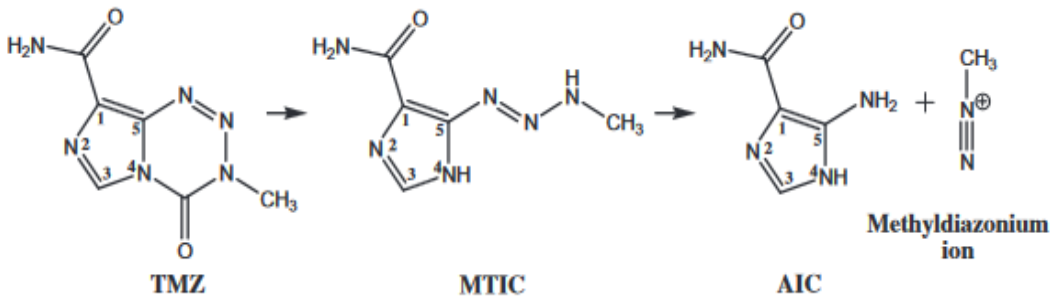

Figure 1.15 Structure and hydrolysis of TMZ. TMZ must become hydrolysed into its reactive component form of a methydiazonium ion and an inactive AIC. The activation of hydrolysis is regulated by a pH greater than 7. (Lopes, et al 2013) Formula: $C_6H_6N_6O_2$

TMZ is part of the STUPP protocol and is the mainstay in standard treatment of GBM. The drug functions as an alkylating agent that damages DNA to trigger cell death (Lee *et al.*, 2018). The drug is administered orally and absorbed in

gastrointestinal tract. As soon as the drug is exposed to a pH>7 it will spontaneously hydrolyse into methytriazine (MTIC) (Lopes, et al 2013). This process is heavily mediated by pH and gives TMZ an *in vitro* half-life in serum of approximately 30 min (Andrasi *et al.*, 2011). MTIC has an *in vitro* half-life of approximately 25 min before degrading to drugs final form of an inactive 4-Amino-5-imidazole-carboxamide (5-AIC) and an active methydiazonium ion. AIC is a stable molecule in water at pH approximately 7 (Andrasi, *et al.*, 2010).

1.7.2.2 Sodium Oxamate

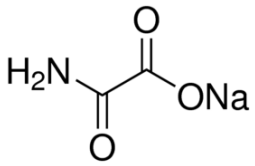

Figure 1.16 – Structure of sodium oxamate. Formula: NH2COCOONa Molecular mass 111.03 g/mol

Sodium oxamate is a glycolysis inhibitor reducing the conversion of pyruvate to lactate in cystol through direct effect on lactate dehydrogenase (LDH). This results in a net reduction of the build-up of lactic acid and prevents the onset of lactic acidosis (LAD) in cells. The presence of LAD in cancer cells is linked to cancer proliferation and metastasis (Walenta, *et al.*, 2004). Oxamate has been identified to have synergy with the metformin analogue phenformin (Miskimins, *et al.* 2014).

1.7.2.3 Disulfiram

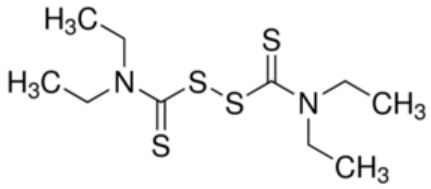

Figure 1.17 – Structure of the anti-alcohol-dependency drug disulfiram. The primary target of disulfiram is the enzyme acetaldehyde dehydrogenase. Formula: C10H20N2S4. Molecular mass 296.539 g/mol

Disulfiram (DSF) has been used as an anti-alcohol-dependency drug for over 60 years (Johanson, *et al.*, 1992). In recent years DSF when combined with copper has been assessed for it potential repurposing as an anti-tumour agent (Cvek *et al.*, 2011). It impacts tumour cells primarily through inhibition of the ALDH and NF-kB pathway (Liu *et al.*, 2012, Liu *et al.*, 2014). A study has also shown that DSF efficacy can be enhanced by metformin in oesophageal squamous cell carcinoma (OSCC) (Jivan, *et al.*, 2015). The mechanism of disulfiram action requires the presence of copper chloride to work at optimum levels and GBM cell lines DSF combined with copper has been shown to have cytotoxic effect (Liu *et al.*, 2012).

1.7.2.4 Sorafenib

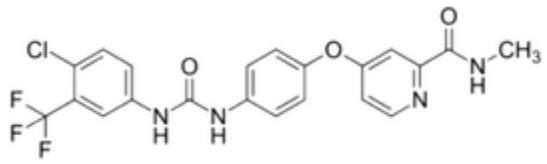

Fig. 1.18 – Structure of sorafenib. Sorafenib is a kinase inhibitor drug primarily used in the treatment of kidney, liver and thyroid cancer. The drug functions by inactivating B-Raf protein through binding to its kinase domain. Formula: C21H16ClF3N4O3. Molecular mass 464.825 g/mol.

Sorafenib is a multi-kinase inhibitor currently used for the treatment of renal cell carcinoma that primarily acts by blocking receptor tyrosine kinase signalling in VEGFR, PDGFR, C-Kit and RET (Wilhelm *et al.*, 2006). The net downstream effect is reduction in tumour proliferation, anti-angiogenic and an increase in apoptotic effects. Since the drugs approval in 2007, the prospective range of therapeutic targets has been expanded to include liver and thyroid cancer (Escudier *et al.*, 2007; Llovet *et al.*, 2008; Brose *et al.*, 2013). Sorafenib has shown potential as a repurposed therapeutic agent against the tropical disease *Schistosoma mansoni* (Keiser, *et al.*, 2015) and the Rift Valley fever virus (Kehn-Hall, *et al.*, 2017). Sorafenib use on GBM is still not fully explored, though it has been seen to work synergistically with TMZ for *in vitro* studies (Robert B *et al.*, 2013). However, the drug efficacy at improving radio-sensitivity seems disputed (Sherman *et al.*, 2014) (Riedel *et al.*, 2016). It has been in at least one cell line that metformin acts synergistically with sorafenib (Aldea *et al.*, 2014). Sorafenib is also being tested as part of GBM clinical trials as an anti-angiogenesis VEGFR-2 inhibitor (Schiff *et al.*, 2018).

1.8 Cell culture models

1.8.1 Tissue culturing and micro-environment

In vitro cancer study is primarily carried out using tissue culturing methods to generate suitable micro environments for growing cells. However, tissue culturing produces only a facsimile of a cells natural environment and can lead to genetic and phenotypic changes over time (Bara *et al.*, 2014, Nestor *et al.*, 2015). EGFR amplification is common in GBM but upon transfer to cell culture this amplification is rapidly lost (William *et al.*, 2017). Cell culturing micro environments can create false reproductions of the original growing conditions for the cultured cells, for example the availability of glucose. The average healthy, non-diabetic, adult has circulating glucose levels around 5-6mmol/l and an adult diabetic has blood glucose levels around 7 mmol/L to 10mmol/L (Menendez *et al.*, 2012). The average tissue culture media uses glucoses concentration in the 10-25 mmol/l range. The three most common cell culture media are DMEM (25mM glucose), RPMI 1650 (11.11mM glucose) and DME/F-12 (17.50mM glucose). Alternative media formulation can better represent normal tumour growing conditions. Hams F-10 is a media originally designed for the culturing of Chinese hamster ovary cells (Ham, 1963). This media utilises 6mM glucose and is closer to resting circulating blood glucose of the human body. The overabundance of glucose in growth media has been demonstrated to reduce metformin efficacy in both breast and ovarian cancer. (Menendez *et al.*, 2012; Wahdan-Alaswad, *et al.*, 2013; Litchfield, *et al.*, 2015).

1.8.2 Culture models

All tumours consist of a large heterogenous collection of cells (Reya *et al.*, 2001). Experimenting on the cells has always been a difficult process. Only a small amount of material from biopsy is available for use and then not all of the remaining tissue is viable for tissue culturing and investigation. Exclusively working solely on such finite samples makes consistent longevity of such work a logistical problem. The main alternative method is the creation of *in vitro* cell cultures.

The act of culturing cells for experimentation has become an important model for modern molecular biology, but most modern culturing techniques have origins from plant culture systems modernised during the 1940s (Thorpe, 2007). Culturing animal and cancer cells is a more complex process. The first successfully created immortalized human cancer cell line was generated from cervical cancer in 1951, now referred to as Hela cells (Lucey, *et al.*, 2009). Since then many GBM cell lines have also been derived from human tumours, including U251MG, U87MG and U373MG (Ponten *et al.*, 1968, Westermark *et al.*, 1973; Ponten *et al.*, 1978). All these cultures are readily available worldwide. However, since the initial production, the introduction and use of these cell lines has caused several problems. In 1999, a cross contamination of U251 and U373 has occurred. Though the full extent of the mix up will probably never be fully ascertained, a great deal of work will have been completed and published under incorrect assumptions (Torsvik *et al.* 2014).

The use of cell cultures has been a mainstay as a biological system since its inception, however now under more modern assessment techniques, its

reliability and use are being scrutinized. When compared to its original progenitor sample, U251MG cell cultures no longer retain genotypic and phenotypical features that were present 60 years ago. Comparison of high and low passage U251MG showed that, over time, the cell line loses its typical GBM signature while also gaining many genetic deletions and duplications (Torsvik *et al.*, 2014). This highlights the need for embracing more relevant biological models of cell culture. A middle ground between experimenting directly on biopsy material and using immortal cell lines are short term cell cultures. Short term cell cultures are cells processed in the same manner to a regular cell line but are not used above a fixed passage (Speirs *et al.*, 1998; Roberts *et al.*, 2017). The use of cells in this manner should prevent the culture from, phenotypically and genetically, deviating to heavily from its original source. This allows the cultures to remain a good representative model of the original tumour, that it was generated from, while at the same time also providing an ample supply of cellular material to serve as a functional system.

1.9 Summary

GBM possess a genetically variable phenotype and currently has limited treatment options with positive outcomes. Developing new treatment solutions for sub-sets of GBM could generate targeted treatment possibilities. Metformin has potential as an anti-tumour therapy and can potentially synergistically work with other treatments. Research and clinical trials are already investigating metformin use in several tumour types. Investigations into the use of metformin on GBM are limited and the mechanisms of action through which metformin can act are not understood. The mechanism, inducing cell death, effects on tumour metabolism and regulation of miRNA, are all areas where further knowledge is needed before metformin can be assessed as a GBM treatment option and utilized for clinical trials. The limitations of immortal cell lines combined with the inherent genetic variability of GBM do not make the cultures a suitable assessment model. Understanding the effect metformin has on a diverse range of GBM short term cell cultures will generate a unique response profile and identify potential target sub-groups.

1.10 Aim and objectives

Metformin has been identified as a possible candidate for repurposing as a cancer therapeutic. The underlying anti-tumour mechanisms of metformin are not well understood. This study hypothesises that metformin can be demonstrated to act as an anti-GBM agent *in vitro*. The aim of this study was to utilise characterised patient derived short term cell cultures to investigate the potential of metformin as repurposed GBM treatment. The objectives of this study were:

- To investigate the efficacy of biguanides to inhibit proliferation of GBM cells *in vitro* under a range of physiological conditions.
- To determine whether metformin acts synergistically with other drugs including disulfiram, TMZ, sodium oxamate and sorafenib.
- To analyse the effect of glucose availability on metformin sensitivity and levels of induced cell death
- To understand the role of metformin in inducing cell death in GBM cultures. Identifying the mechanism of action and potential pathways utilised including apoptosis, caspase analysis and mitochondrial membrane potential.
- To identify and evaluate candidate miRNAs with expression changes affected by metformin.

CHAPTER 2

Materials and methods

Chapter 2 Materials and methods

This study was conducted under ethical approval granted by the Life Science Ethics Committee, University of Wolverhampton, LSEC/22/0909

2.1 Cell culture

2.1.1 Cell Cultures

All patient-derived short-term cell cultures had been previously established from fresh GBM biopsy material obtained during surgical resection at the National Hospital for Neurology and Neurosurgery between 1980 and 2008 (Professor John Darling). All tumour tissues were classified according to WHO criteria (Louis *et al.*, 2007). Tumour samples used for cell culture were surplus to diagnostic requirements and were anonymised at source. Cultures were established as described by Lewandowicz *et al.* (2000) and stored in liquid nitrogen until required.

Thirteen GBM short-term cell cultures were utilised up to passage 20. The established GBM cell line, U251MG, passage 78-86, was provided by Dr Darrell Bigner, Duke University, USA (Bigner *et al.*, 1981). A normal human astrocyte culture (NHA)(Lonza), passage 2-10, was used as a non-cancerous control. Details of cultures are provided in Table 2.1.

2.1.2 Maintenance of cell cultures

All cell culture work was completed within Biomat 2 sterile class II Laminar flow hood using Sarstedt tissue culture consumables. Culture vials were removed from liquid nitrogen and immediately placed into a 37^{o}C water bath for 1 minute. The contents of the vial were transferred to a fresh 25ml universal tube and 2ml of 37^{o}C media was add drop by drop to the tube. The tube was then centrifuged for 5 minutes at 1200xg. After confirming a visible

pellet had gathered the supernatant was aspirated. Fresh growth media was added to gently resuspend the pellet and then was transferred into a T25 growth flask and placed in a Panasonic MCO-170AIC-PE IncuSafe carbon dioxide (CO_2) Incubator at 37ºC (Panasonic UK). Fresh media was provided to growing cultures every 36 hours. Cells were passaged when confluent by washing with PBS (Life Technologies) followed by treatment with 3 ml trypsin (Sigma Aldrich, UK) for 5 min at 37 ºC to detach the adhered cells. Trypsin was inactivated by the addition of 10 ml culture media. After removing from the flask, the cell suspension was centrifuged at 1200xg for 5 min and cells resuspended in fresh media and sub-cultured into new tissue culture flasks using a split ratio of 1:3.

For long-term storage of cells in liquid nitrogen, $1x10^6$ cells were re-suspended in a 1ml mixture of 10% DMSO (Sigma Aldrich, MERCK, UK) and 90% FCS. The 1 ml solutions were transferred to cryovials and left overnight at -80ºC in a NALGENE® Mr. Frosty (Thermo Scientific, UK). After 12 hours, the cryovials were moved to liquid nitrogen for indefinite storage.

2.1.3 Growth media

NHA cultures were grown in ABM Basal Medium supplemented with AGM SingleQuot Kit Suppl. and Growth Factors (Lonza, UK). This proprietary cell growth medium solution contains 4.80% gentamicin sulphate to prevent microbial growth. NHA cultures were grown in vented flasks at 5% CO_2 and stored in a standard pressure sealed incubator at 37ºC.

All other cultures were grown in HAMs F-10 supplemented with Australian 10% FCS (Gibco, UK) without antibiotics or anti-microbial agents. Cultures were

grown in non-vented flasks in a standard growth incubator under normoxic conditions. The F-10 media contained HEPES to maintain the optimum pH and removing the need to use a CO_2 incubation unit.

For experiments in which cells were grown in varying glucose levels, glucose-free HAMs F-10 (PAN Biotech) supplemented with 10% FCS, HEPES and glucose to the desired levels (Sigma, UK). Appendix I contains a breakdown of the F-10 media formulations used for all experiments.

2.1.4 Growth proliferation curves

$1x10^5$ cells were seeded into 8 x T25 flasks and proliferation was measured over a 10-day time course. Readings were taken at 1, 2, 3, 5, 7, 9 and 11 days. For time point, cells were trypsinised, collected and re-suspended in growth media before being counted using a version 1 Countess Cell counter (Thermo Fisher). Live cells were stained with trypan blue growth media mix (1:1) and then counted. The reading was the average of two separate readings and each completed growth curve was the average of three repeats.

Sample[1]	Sex[2]	Age at diagnosis[3]	Location[4]	*TP-53* status[5]	*TP53 deletion*	*MGMT* status[6]	*EGFR over representation*
IN859	F	72	R frontal	Deletion	Yes	Methylated	chr 7p
IN1265	F	70	R occipital	exon 5 codon 160-162 DEL GGCCAT	-	Unmethylated	chr 7p
IN1461	F	44	L Parietal	Wild type	-	Unmethylated	chr 7p
IN1472	F	46	Unknown	exon 9 codon 319 AAG>TAG, LYS> STOP	Yes	Unmethylated	-
IN1528	M	61	R temporo-parietal	exon 8 codon 272 GTG>GAG, VAL>GLU	Yes	Methylated	chr 7p
IN1612	M	53	R post-temporal	Aberrant	Yes	Unmethylated	chr 7p
IN1682	F	48	R parietal	Wild type	-	-	chr 7p
IN1752	M	45	Unknown	Wild type	-	-	-
IN1760	F	56	L temporal	Wild type	-	Partial methylation	chr 7p
IN1951	M	30	R parietal	Wild type	-	Unmethylated	-
IN1979	M	46	L temporo-parietal	exon 8 codon 267 CGG>CCT, ARG>PRO	Yes	Unmethylated	-
IN2045	M	25	L frontal	exon 6 codon 215 AGT>GGT, SER>GLY, exon 7 codon 248 CGG>TGG, ARG>TRP	-	Partial methylation	-
IN2093	M	55	R frontal	Wild type	-	Unmethylated	-
U251MG	-	-	-	exon 8 codon 273 CGT>CAT, ARG>HIS	-	Partial methylation	chr 7p
NHA	N/A	N/A	N/A	Wild type	-	Unmethylated	-

Table. 2.1 Details and characterisations for all cell cultures. [1]IN-Institute of Neurology; [2]M = Male, F = Female; [3]Age listed in years at diagnosis; [4]L = Left, R = Right; [5]The mutation status of the tumour protein gene *P-53* characterised through sequencing (Potter *et al.*, 2018); [6]*MGMT* status identified by methylation specific PCR (Licchesi et al, 2009).

2.2 Growth Inhibition Assays

2.2.1 Drugs

Metformin, phenformin, sodium oxamate, camptothecin and temozolomide were purchased from Sigma Aldrich. Sorafenib was purchased from Cambridge Bioscience, UK.

2.2.2 Determination of ID_{50} growth inhibition and drug synergy

Cells were seeded into a 96 well plate at 4000 cells per well (CPW) in 200µl growth media and incubated until exponential growth phase has been reached. Drugs were prepared to required concentrations and serial diluted with growth media in a separate 96 well plate. The media was aspirated and replaced with media containing appropriate concentrations of drugs before being returned to the incubator for 72 or 96 hours. Media was aspirated, and the cells fixed to the plate using 150µl TCA and placed at 4^{o}C. After 1 hour, the plate was washed twice in water removing excess TCA. Viability of cells was then assessed using the sulforhodamine B (SRB) colorimetric assay (Vichai, 2006). Staining of the cells was completed by adding 100µl of 0.4% SRB (Sigma, Merck) suspended in 2% acetic acid (Sigma, Merck) to each well. The plate was left for 1 hour at room temperature before being washed twice with water. Plates were dried at 37^{o}C for 1 hour before being analysed. Two hundred µl of 10mM Tris solution (Sigma, Merck) was added to each well and gently mixed for 5 minutes till all the SRB dye had re-entered suspension. Plates were read for absorbance in a GloMax®-Multi Microplate Reader (Promega) at a wavelength of 560nm. Each plate used eight concentrations of drug and two negative controls grouped in batches of 3 replicates. From the replicates, outliers could be removed, and average data generated.

2.2.3 Calculation of ID_{50} values

Data points were analysed using GraphPad PRISM software using a log(inhibitor) vs. Response or a four-parameter logistic curve (4PL) algorithm. This method utilises all the data points against log molar dosages and assumes a, non-standard, variable slope as outlined in Fig. 2.1. From this ID_{50}s value are output for each drug tested on the cultures. Groupings of data were analysed for significant difference of the means using an un-paired students t-test.

Model

Y= Bottom + (Top-Bottom) / (1+10^((LogID50-X)*Hillslope))

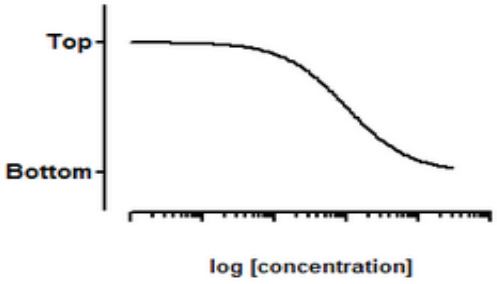

Figure 2.1 – Mathematical model used for all analysis on graph pad prism. The method allows for variable analysis of the drug response yielding more accurate ID_{50}s than seen on a standard curve model.

2.2.4 ID_{50} flask setups for experiments

All setups that utilised the ID_{50} setups seeded cells at the same concentration as tested on the 96 well plates. T25 flasks were seeded with 5ml at 20,000 cells per ml and T75 flasks were seeded with 15 ml of cells at 100,000 cells per ml.

2.2.5 Drug Synergy Assays

For synergy analysis, cultures were treated with single or paired drug combinations. ID_{50} values calculated using cytotoxic SRB assay outlined in 2.3.2. Doses for metformin were in the mM range. Figure 2.2 illustrates the layout of a combination SRB 96 well plate. The concentrations used in the combined drug wells were equimolar to the equivalent wells of the mono-drug treatment. ID_{50} values for each combination of the experiment were analysed using graph pad prism software. Drug synergy was determined by calculating a combination index (CI) using the Chou-Talay method (Chou., 2010). The full equation of this method is given in Figure 2.3. CI values < 1 and > 1 were considered to be synergistic and antagonistic, respectively. Values of 1 were defined as having an additive effect when used in combination. The further the CI deviated, in both directions, from 1 the stronger the net effect. Each synergy plate contained two replicates per combination and each plate was repeated three times.

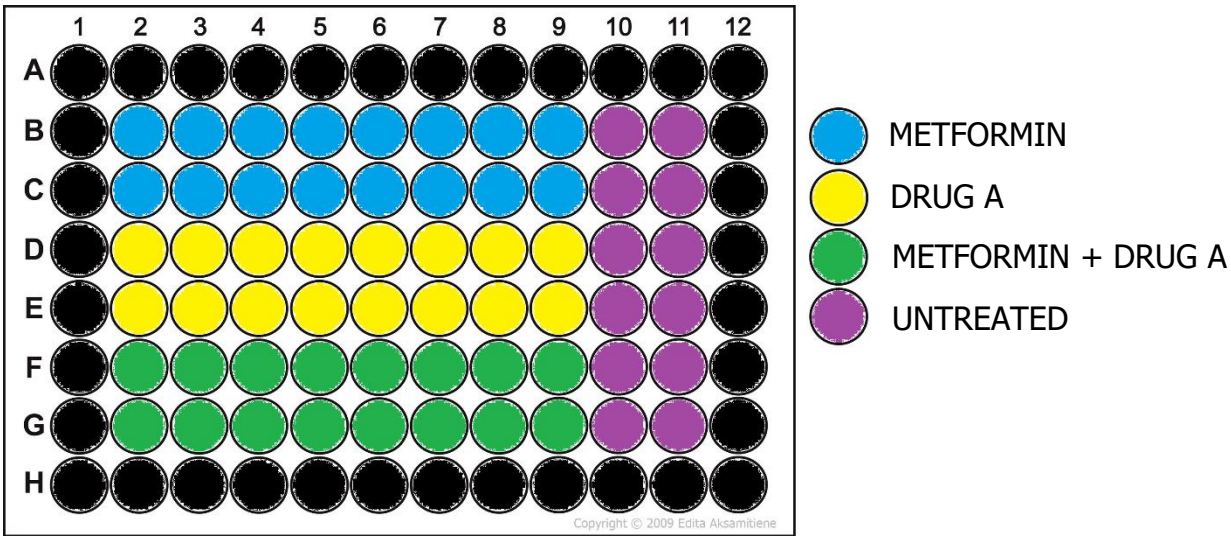

Figure 2.2 – Layout of 96 well plate for Chou Talay synergy assays. Each drug was assessed with two replicate data sets. Drugs were serially diluted along each row. Highest concentration was in column 2 and lowest in column 9. Columns 10 and 11 were used as control wells for untreated growth comparison. Metformin wells (Blue) dose ranged from 80mM to 0.625mM. Drug concentrations used for each drug tested were selected based on the pre-assessed ID_{50} values for GBM cultures. Concentration used for the drug combination rows were kept in equimolar dosage with the mono treatment counterparts.

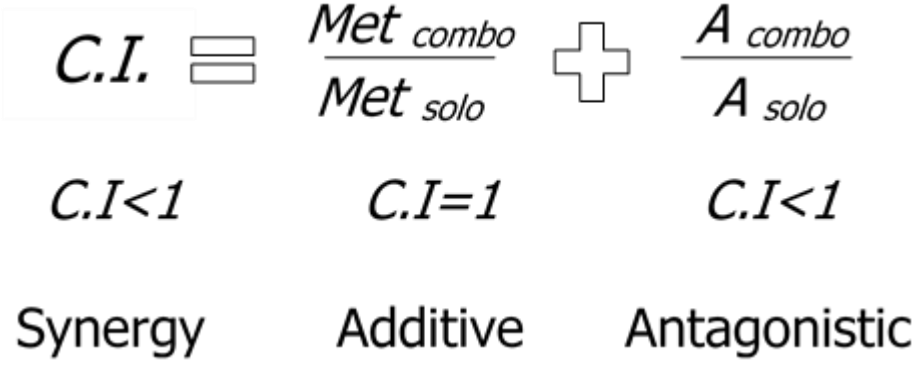

Figure 2.3 – Chou Talay synergy equation. The equation for working out the CI of each drug assessed with the Chou Talay synergy assay (Chou., 2010). Met Solo and A solo represent the ID_{50} values for metformin and the assessed drug when used as individual treatments. The ID_{50} values represent the sensitivity of the cell to that individual drug. Met combo and A combo represent the ID_{50} of the drugs when used together in an equimolar combination. The ID_{50} values represent the sensitivity to the drugs when used in combination. The equation divides the combination ID_{50} value by its individual treatment counterpart. The CI index is then generated from the values for each drugs response. The drugs must average a contribution to the total CI index of less than 0.5 each to be determined as achieving a synergistic response. A resulting CI index of less than 1 implies the combination of the drug produces a response greater than sum of the individual treatments.

2.3 Assessment of glucose

The concentrations of glucose in media was determined using by using a OneTouch Ultra diabetic glucose meter (OneTouch) and disposable measurement sticks. The accuracy of the device was assessed using reference standards created using glucose added to PBS and growth media. To assess the cellular use and uptake of glucose, cultures were grown in T25 flasks in 5 ml of the desired media formulation. Every 24 hours 25µL of media was removed and added to a measurement stick. This was repeated till the time course was finished at 96 hours

2.4 Flow cytometry

All flow cytometry analysis was carried out using a BD Accuri C6 Plus cell analyser (BD Biosciences UK). All protocols were set to record 20,000 counts from the required gating. Cells were always run at a slow flow rate speed (14µl/min flow rate, 10µm samples core). This kept core stream size to a minimum, reduced the spread of the results and reduce the number of coincident events. Initial gating was set for each experiment using U251MG cells with and without camptothecin to induce apoptosis. Camptothecin was used at 100µM over a 72-hour period to induce a positive apoptotic control.

2.4.1 Detection of apoptosis

The BD Pharmingen Annexin V FITC Apoptosis Detection Kit I was used to assess early apoptosis and its progression over time. For each experiment, cells were measured every 24 hours over a 96-hour period. For each time point, 5 $x10^3$ cells were seeded into a T25 flask. To analyse the total cell population all media was collected from each flask to include any floating cells and any adherent cells were detached with trypsin. Harvested cells were then

washed twice with cold PBS before being resuspended in 1x Binding buffer at a concentration of $1x10^6$ cells/ml. 100µl of this solution ($1x10^5$ cells) was transferred to a sterile 25 ml universal tube and 5µl of FITC Annexin V and 5µl of PI were added. The tube was gently vortexed and placed in the dark for 30 minutes at room temperature. Finally, 400µl of 1X Binding Buffer was added to the tube. The cells were gently mixed and then placed into the flow cytometer. The setup and gating used for analysis was adapted from templated provided by BD Biosciences. The gating for the readings was aligned against the untreated control of each culture.

2.4.2 Mitochondrial membrane potential

BD MitoScreen (JC-1) Kit was used to assess the potential of the mitochondrial membrane (ΔΨ). Cells were grown in T25 flasks till the exponential growth phase was reached. Cells were then treated for 72 hours with drug or vehicle control, after which the growth media was collected, and trypsin was used to remove any remaining adherent cells from the flask. Cells were centrifuged at 1200xg and supernatant aspirated. 5ml PBS was used to wash the cells before being centrifuged at 1200xg. The cells were resuspended in 500 µl of JC-1 working solution and incubated for 15 min in a 37°C CO_2 incubator. The cells were centrifuged at 1200xg and washed with 1x assay buffer before being analysed in a flow cytometer. The setup and gating used for analysis was adapted from templated provided by BD Biosciences. The gating for the readings was aligned against the untreated control of each culture. Camptothecin was used at 100µM over a 72-hour period to induce a positive apoptotic control.

2.4.3 Cell cycle

Analysis of cell cycle was completed with propidium iodide stained ethanol fixed cells. Cells were grown in T25 flask and treated with metformin at 96-hour ID_{50} values. After 96 hours of incubation the cells were trypsinised (approximately $1x10^6$ cells) and placed in a 10ml sterile universal. Cells were centrifuged at 1200xg and supernatant aspirate out. Cells were the washed with 5ml PBS. After discarding the supernatant, the pellet was resuspended in 200µl PBS. While being vortexed, 2 ml of 100% ice cold ethanol was added slowly in drops to the solution. This was to prevent clumping of the cells. Cells were then left overnight at -20^{o}C. To the 10ml universal, 8ml of PBS was added and the tube was then centrifuged at 1600xg for 5 min. Ethanol fixed cells are more buoyant and required higher speeds to successfully pellet them. This cell pellet was then washed again with PBS removing any remaining ethanol. To the washed pellet 300µl of a PI mix (100µg/ml RNASE A, Propidium Iodide 50µg/ml in PBS) was added to the cells. Cells were then incubated at room temperature for 15 minutes before being ran through the flow cytometer.

Doublet cells, two cells in G1-phase being record as one event by the flow cytometer, were prevented from causing false G2/M positives by plotting FL2-A versus FL2-H. This allowed for discrimination between G1 doublets and G2/M single cells and generation of suitable gating to remove them (Rafael, 2001). Gating groups were defined to separate out the stages of cell division (G0/G1, S, and G2/M) as given in Figure 2.7. A sub-G1 population was also created to analyse the level of DNA fragmentation and concentration of late apoptotic

cells. (Darzynkiewicz and Zhao, 2014). Camptothecin was used at 100μM over a 72-hour period to induce an apoptotic control.

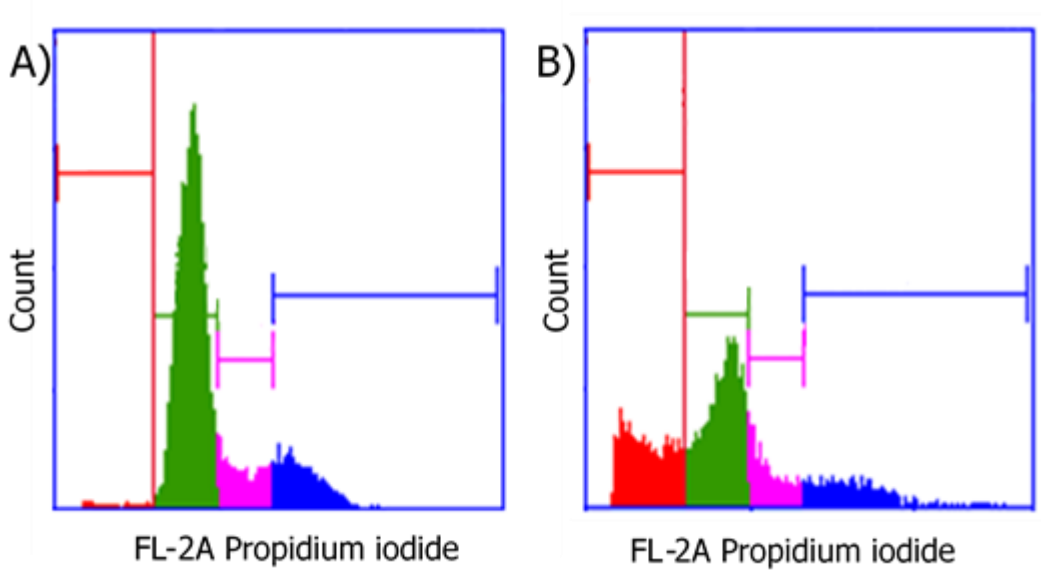

Figure 2.4 Examples of flow cytometry cell cycle analysis. Diagrams represent cell cycle analysis results. The amount of propidium iodide staining detected on the FL-2A channel represents quantity of DNA present with the cell. Cells in G0/G1, green region, are cells in resting state with normal levels (n=2) of genetic material. As cells enter S-phase, pink region, DNA starts to replicate and FL-2A reading increases. Upon reaching G2/M phase, blue region, the cell possesses double the quantity of DNA (n=4). Upon dividing flow cytometer will detect the daughter cells as separate G0/G1 cells. An increase in the population of a phase may be indicative of cells arresting in cell cycle at that progression check point. A) A standard pattern for cell cycle analysis from a flow cytometer. The different regions are as follows: G0/G1 – Green, S – Pink, G2/M – Blue, Sub-G0/G1 – Red. The red horizontal line indicates the apoptotic cell cut off (sub-G0/G1, n<2). B) An example of apoptosis cells induced by camptothecin. Cells undergoing apoptosis have fragmented DNA. This is detected as low reading in the FL-2A channel and allows for the separation of apoptotic populations.

2.5 Caspase pathway analysis

Caspase values were assessed using promega Caspase-Glo (Promega) assay. This assay cleaves the caspase-3/7 releasing a substrate for luciferase (amino luciferin). This leads on to a luciferase reaction which as a by-product will produce light that can be detected in a plate reader. The complete experiment is summarised as a flow diagram in Figure 2.8.

Cells were grown simultaneously on two 96 well growth plates. One plate was fixed, stained and analysed using the SRB assay outlined in 2.3.1. Simultaneously, the second plate was exposed to 200 µl of Caspase-Glo mixed reagent. The plate was then put on a plate mixer for ten minutes followed by being incubated at room temperature in the dark for twenty minutes. The ensuing cell solution was transferred to a white walled 96 well plate and then luminesce was recorded on a Promega Glomax plate reader. Each measured value from the Caspase-Glo sample was then normalised against its respective sample from the SRB plate. This normalisation allows for a better representation of caspase 3/7 activity per cell. Camptothecin was used at 100µM over a 72-hour period to induce a positive apoptotic control.

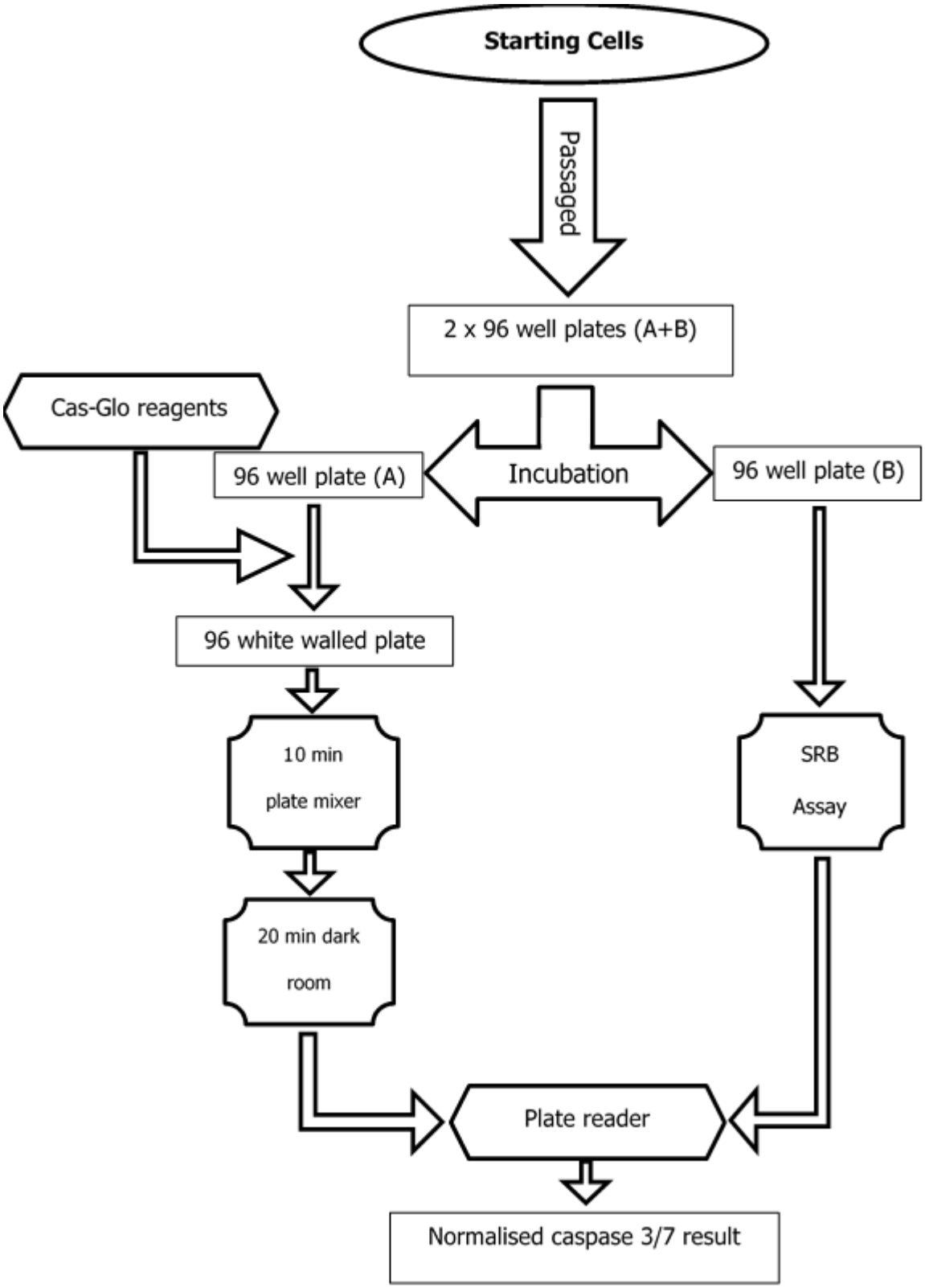

Figure 2.5 Flow diagram of Caspase-glo assay with normalisation. Standard caspase glo assay was augment with an SRB assay run alongside under identical treatment conditions. The addition of this extra simultaneous assay allowed for the normalisation of the luminesce from the caspase assay based on the number of viable cells.

2.6 miRNA analysis

2.6.1 Database analysis

Microarray expression and isoform data from the TCGA was downloaded and individual miRNAs were compared across a range of tumour types using MS Excel. Data was normalised against miR-17 used as a normal endogenous control (Davoren *et al.*, 2008).

2.6.2 Extraction of RNA

Cells for miRNA extraction were seeded at of $4.8x10^4$ cells per ml and grown in T75 flasks until the exponential growth phase was reached. Cells were then treated at the relative ID_{50} concentrations for metformin at 37^oC for 96 hours before harvesting them for RNA extraction using a miRVANA RNA extraction kit according to the manufacturer's instructions. Cell pellets were washed with PBS and transferred to a 1.5ml Eppendorf. After centrifugation and removal of supernatant, 450µl of Lysis/binding solution was added and the resulting solution was vortexed. To the homogenous lysate 45µl of miRNA homogenate Additive was added and the lysate was left on ice for 10 min. After this 450µl of Acid-Phenol: Chloroform and the tube was vortexed for sixty seconds to mix. The tube was then centrifuged for five minutes at ten thousand G at room temperature. The upper phase (aqueous) was transferred to a fresh tube with x1.25 the recovered total volume of 100% ethanol. The total lysate/ethanol mixture was placed into a filter cartridge tube, centrifuged for 15 seconds and the flow through discarded. 700µl of miRNA Wash solution 1 was added to the filter cartridge and centrifuges for 10 seconds. The flow through was discarded and this step was then repeated twice with 500µl of Wash solution 2/3. After the second wash step, the filter cartridge was spun for one minute at

maximum speed to remove any residual fluid. The filter cartridge was moved to a new collection tube and 100µL of pre-heated 100^{o}C water was added. Collection tube with filter cartridge was then spun at maximum speed for 30 seconds. Water in collection tube now contained total RNA from extraction. Filter cartridge was then discarded and the total RNA in collection tube was stored at -80^{o}C until required.

2.6.3. Assessment of total RNA

Assessment of the quantity and quality of extracted genetic material was carried out on a NanoDrop 2000 spectrophotometer (Thermo Scientific, UK). This outputted the concentration of nucleic acids as ng/µl. This was equated using a modified Beer-Lambert, $c = (A*\epsilon)/b$, it utilizes the concentration (c)(ng/µl), the absorbance (A) in Au (260 nm), the wavelength dependent extinction coefficient (ϵ) (ng-cm/µl) and pair length (b) (cm). The ratio between the genetic material (260nm) against precipitated proteins (280nm) and organic compounds/chaotropic salts (230nm) was used to assess quality of each sample. A260/280 ratios above 2 and 2.0-2.2 for A260/230 were deemed pure and useable for miRNA experiments. Quantification from Nanodrop was used to equalise all RNA samples used to a concentration of 20ng/µl.

2.6.4 Stem Loop PCR

Assessment of miRNA levels was carried out using specific stem loop primers as outlined by Chen *et al.* (2005).

2.6.4.1 Stem loop primer design

Information required for the design of stem loop primers was acquired from MiRBASE (http://www.mirbase.org) for use with the miRNA primer designer tool. This tool was developed by Fuliang Xie for the East Carolina University (Xie, 2015). Output from this tool would give the three primers required for each PCR (stem-loop RT, forward and reverse primers) and were purchased as custom DNA oligos from Sigma UK.

2.6.4.2 Stem loop reverse transcription and PCR

Reverse transcription of the miRNA was completed using a TaqMan MiRNA Reverse Transcription Kit (Thermo Fisher, UK), following manufacturer's instructions. Stem loop cDNA was generated from the kit using a reaction volume of 20µl with 40ng of extracted total RNA and 10µM of Stem loop PCR primers (Sigma, UK). PCR of the miRNA samples was amplified for 30 cycles using specific primers in a reaction volume of 40µl contain 2mM dNTP (Sigma UK), 2.5 mM MgCl2 (Qiagen UK), 20µM of each forward and reverse miRNA primer (Sigma UK) and 1 unit of HotStarTaq DNA polymerase (Qiagen UK).

2.6.4.3 Gel Electrophoresis

Amplification products were separated on a 2% agarose electrophoresis gel (Themo fisher) in 1x TBE buffer (Geneflow), visualised with ethidium bromide (SIGMA, MERCK) and compared with a 50bp DNA ladder (Thermo Scientific). Gels were scanned using Gel DocTM EZ imager and analysed with Syngene Gel software.

2.6.5 Quantitative Real time PCR

Q- PCR was carried out using TaqMan assays (Fisher Life Technologies UK) using an Applied Biosystems 7500 Fast Real-Time PCR system. The creation of the cDNA from total RNA was completed using TaqMan MiRNA Reverse Transcription Kit (Thermo Fisher, UK) as listed in 2.7.7 with the replacement of using 3µl of Taqman RT primer (Fisher Life Technologies UK). Data from PCR was used to work out expression fold change (2^-ΔΔCt) for all samples. Analysis For the normalisation of the results the snRNA U6 (RNU6B) was used as an endogenous housekeeping control. Selection of an endogenous control for miRNA analysis is not straightforward. There is a fair amount of conflicting research as to suitability of all choices (Occhipinti *et al.*, 2016). Applied Biosystems recommend the use of U6 as a candidate control gene for use in miRNA data analysis (Applied Biosystems, 2011). However, Xiang *et al.* (2014) showed that in nasopharyngeal carcinoma samples that U6 showed variation between samples and that it was susceptible to decay after repeated freeze thaw cycles. In liver carcinoma, it has also been shown that there can be variation between the expression in normal tissue and carcinoma cells (Lou *et al.*, 2015). Despite this though U6 has previously been used for miRNA normalisation in tumour analysis (Gee *et al.*, 2011) and is still used in as a common choice for qRT-PCR normalisation (Chang *et al.*, 2018; Lin *et al.*,2018; Manzine *et al.*, 2018; Zhou *et al.*, 2018)

2.7 Statistical tests and data processing

For most experiments, a minimum of three biological repeats were created to allow for statistical analysis. This allowed for standard deviations on all data to be equated and t-tests to be carried on identifying the significance of the data. T-tests were carried out using graph pad web tool QuickCalcs. All graphs were created using Microsoft Excel Open office version 1701 (Build 7766.2096). Error bars for all graphs display the standard error of the mean for each sample based on its replicates. Graph pad prism version 7.03 was used for all the calculations of ID_{50} values on all samples. Linear regression analysis was carried out using the data analysis module for Microsoft Excel.

CHAPTER 3

Results

3.1 Growth characteristics and biguanide growth inhibition in GBM *in vitro*

Metformin has been identified to have anti-tumour potential in cancer prevention and reduction of cancer severity (Heckman-Stoddard *et al.*, 2017). Initial experiments identified if this was identifiable in GBM. The experimental panel of 13 short term GBM cell cultures, 1 immortalised cell line (U251MG) and NHA were assessed initially for biguanide drug cytotoxicity. However, to provide optimal drug treatment during exponential growth of each culture, the doubling time of the entire panel had to be evaluated. This then allowed cytotoxic experiments to proceed to generate ID_{50} values for the culture panel.

3.1.1 Growth curves

All cultures grew successful under relevant conditions as detailed in section 2.1.4. Figure 3.1 shows growth curves for all cultures used. The doubling times of each culture measured from the highest gradient of the exponential phase, are listed in table 3.1. The doubling times for the GBM cells ranged from 24 hours (U251MG) to 70 hours (IN2093). with a mean doubling time of 40 hours and a median of 42 hours. NHA, the normal cell control, had the second slowest observed doubling times.

Table 3.1. Doubling time of culture panel

Culture[1]	Doubling time[2] (Hours)
U251MG	24
IN859	24
IN1612	28
IN1528	32
IN1979	35
IN2045	36
IN1760^{+}	40
IN1752^{+}	44
IN1472	45
IN1682^{+}	50
IN1265	50
IN1951^{+}	55
IN1461^{+}	60
NHA^{+}	63
IN2093^{+}	70

Cultures ordered highest to lowest based off the doubling time. [1]All cultures marked with a $^{+}$ indicate *P53* wild type. [2] Doubling time of the cultures taken in hours from initial seeding of culture flasks. All samples are averaged from three replicate time courses with two counts at every sample read. Doubling times worked out from the highest gradient of plotted growth curve during exponential growth phase. *P53* wild type cultures possess relatively higher doubling times compared to those cells possessing mutations.

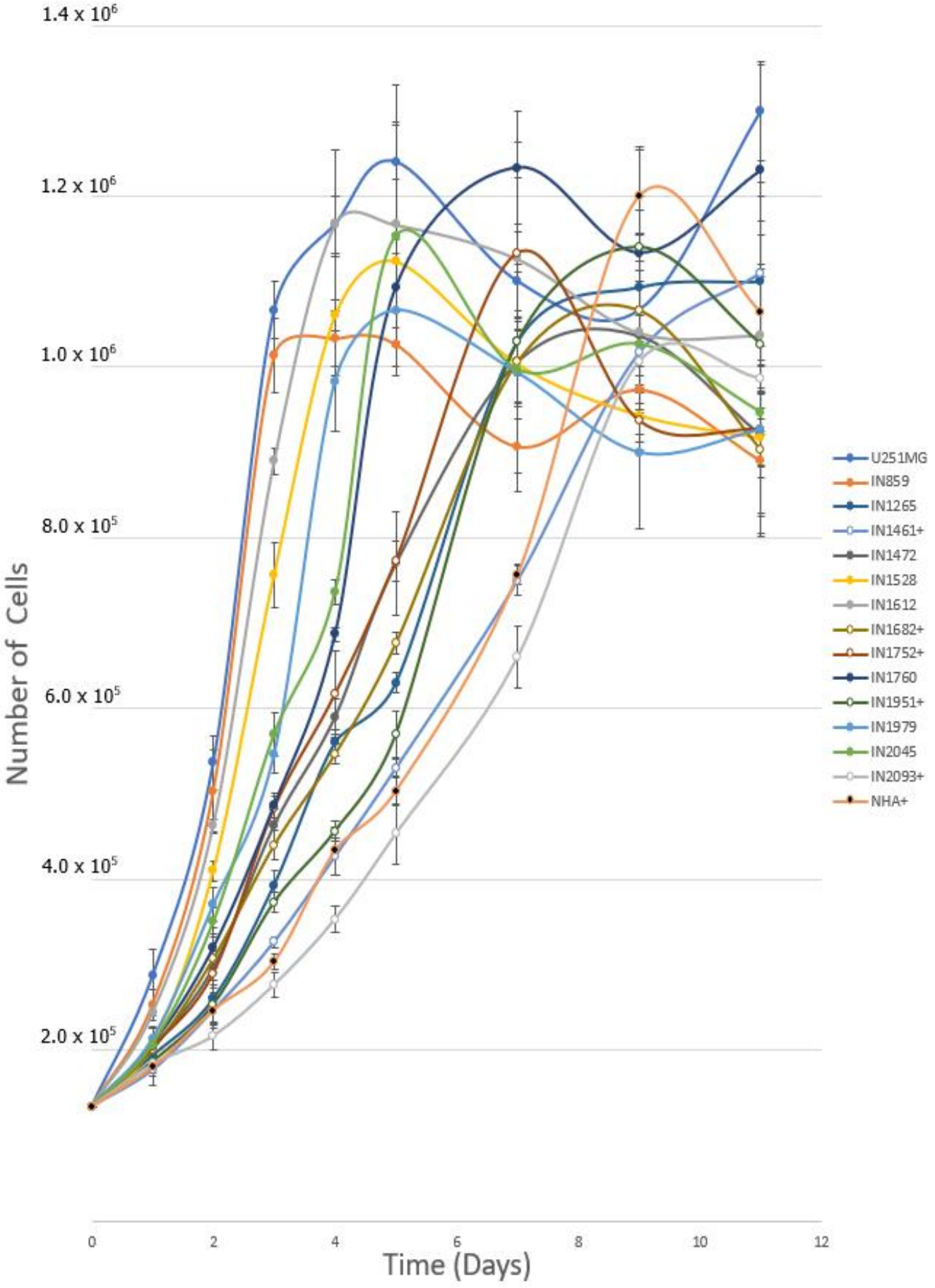

Fig 3.1 Graph displaying the growth curve data for all GBM cultures tested alongside NHA. Cultures seeded at day zero with $2x10^5$ cells. Cultures were collected at eight-time points along time course. Data shown is averaged from three replicate time courses. Doubling times for cultures generated from the highest gradient on each time course during its exponential growth phase.

GBM cultures possessing a *P53* mutation or deletion versus had significantly shorter doubling times compared to the *P53* wild type cultures (P=0.0046).

3.1.2 Growth inhibition

3.1.2.1 Metformin

All GBM cultures treated with metformin showed a cytotoxic response after more than three days of exposure. Table 3.2 lists the ID_{50} values for metformin treated cultures for 72h and 96h. ID_{50} values for cultures tested fell within a milli-molar scale (1-100mM). Following both 72h and 96h exposure, there was a very significant difference (P=0.0006, P=0.0024) in response to metformin based on *P53* status. Cultures with *P53* wild type were less sensitive to metformin and generally had higher ID_{50} values that *P53* aberrant cultures. All *P53* aberrant cultures, and two of the *P53* wild type cultures, showed a significant reduction ($p<0.05$) in ID_{50} values after an additional 24 hours of drug treatment. At both time points, IN859 was the most sensitive culture with ID_{50} values below 10mM. NHA had a high tolerance of metformin; the ID_{50} was the highest in all cultures tested at both 72 and 96 hours as expected for a non-tumour control. The percentage reduction in ID_{50} at 96 hours exposure compared to 72 hours varied between cultures with the lowest being IN1461(-7%) and the highest being IN1528 (-59%). Figures 3.2a and 3.2b display the averaged results from the SRB growth inhibition assay. Complete SRB toxicity data for 72 and 96 hours metformin drug treatment can be found in Appendices 1 and 2 respectively.

Table 3.2 – ID50 values for all cultures treated with metformin.

Culture reference[1]	*P53* Status	Metformin ID_{50} 72 hours (mM)[2]	Metformin ID_{50} 96 hours (mM)[2]	Reduction in ID_{50} 72hr v. 96hr metformin treatment[3]	P-value[4]
IN859	Aberrant/Deletion	6.38 (±1.78)	4.52 (±0.6)	-29%	0.0209*
U251 MG	Aberrant	11.44 (±2.35)	4.83 (±2.11)	-58%	0.0223*
IN1472	Aberrant	11.75 (±3.38)	5.38 (±0.26)	-54%	0.0315*
IN2045	Aberrant	12.11 (±4.38)	6.41 (±3.50)	-47%	0.0405*
IN1528	Aberrant	26.20 (±1.11)	10.78 (±0.42)	-59%	0.0001***
IN1612	Aberrant	18.28 (±3.93)	10.82 (±3.73)	-41%	0.0291*
IN1265	Aberrant	20.22 (±3.74)	11.13 (±2.05)	-45%	0.0209*
IN1979	Aberrant	30.01 (±1.6)	25.66 (±3.84)	-14%	0.0142*
IN1760^{+}	Wild Type	22.90 (±1.6)	11.59 (±5.05)	-49%	0.0211*
IN1682^{+}	Wild Type	36.22 (±6.45)	24.87 (±5.41)	-31%	0.0796
IN1752^{+}	Wild Type	48.93 (±9.83)	29.19 (±5.62)	-40%	0.0393*
IN1461^{+}	Wild Type	61.13 (±4.7)	56.59 (±6.89)	-7%	0.4001
IN1951^{+}	Wild Type	69.52 (±8.9)	57.33 (±4.26)	-18%	0.0993
IN2093^{+}	Wild Type	69.29 (±14.57)	63.7 (±7.17)	-8%	0.5829
NHA^{+}	Wild Type	90.95 (±14.39)	84.3 (±8.50)	-7%	0.5285

[1] All cultures marked with a $^{+}$ indicate *P53* wild type. [2] Metformin ID50 concentration. Standard deviation for each average is listed after each result (±). *P53* sub groups are ordered lowest to highest based on the 96-hour metformin ID50. [3] Percentage reduction in the ID50 value of the culture going between the 72 and 96-hour time point. [4] P-value for the statistical difference between the means of the 72 and 96-hour metformin ID50 values. Level of significance is denoted with *.

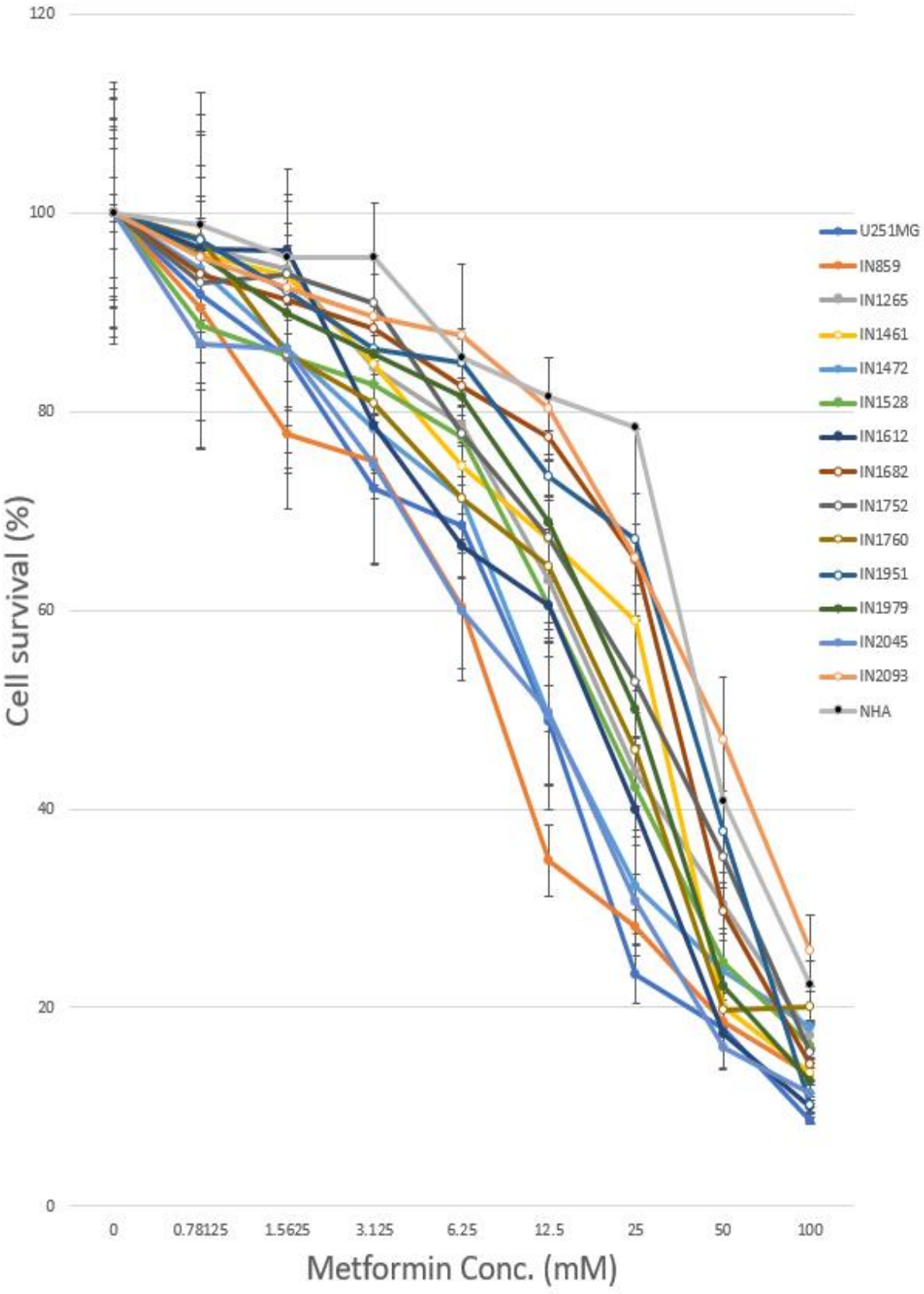

Figure 3.2a – Graph showing SRB cytotoxicity assay results for culture panel at 72 hours metformin treatment. Percentage cell survival is measured by comparing each OD value against averaged OD value at control well (0mM metformin). Error bars display standard deviation averaged from 3 replicates. Serial dilution drug concentrations ranged from 100mM at highest to 0.78mM at lowest achieved through serial dilution. *P53* wild type data points coloured white, NHA data points coloured black

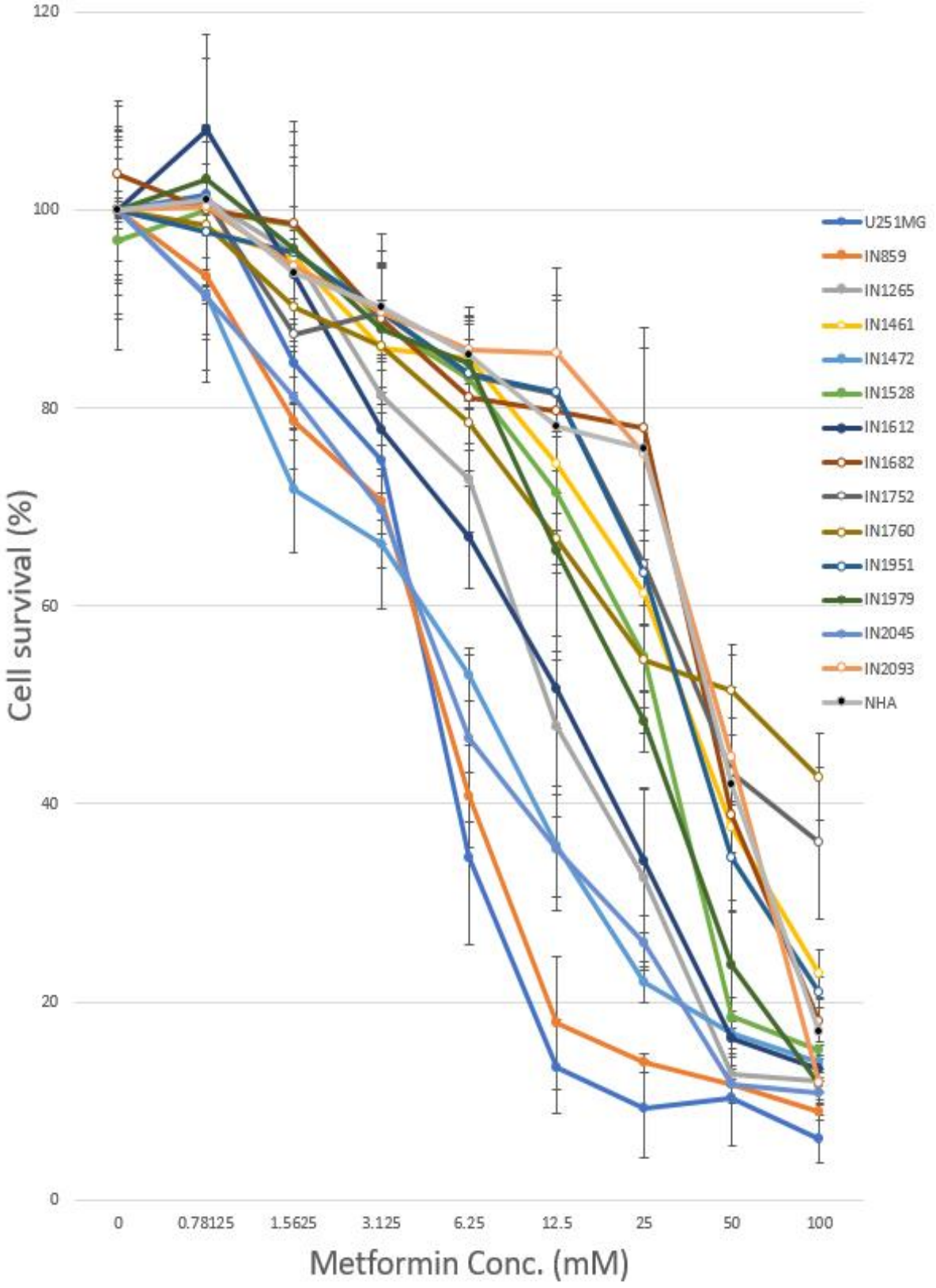

Figure 3.2b – Graph showing SRB cytotoxicity assay results for culture panel at 96 hours metformin treatment. Percentage cell survival is measured by comparing each OD value against averaged OD value at control well (0mM metformin). Error bars display standard deviation averaged from 3 replicates. Serial dilution drug concentrations ranged from 100mM at highest to 0.78mM at lowest achieved through serial dilution. *P53* wild type data points coloured white, NHA data points coloured black

3.1.2.2 Retreatment of metformin

Metformin is not metabolised in the human body and not known to accumulate in normal tissue (Bailey, 2017). However, to assess the features in GBM cells four GBM cultures were assessed for differences in ID_{50} values following 96-hours exposure to metformin with daily replacement of growth media and drug compared to a single treatment at the start of the assay (Table 3.3). The four cultures utilized were the most sensitive to metformin treatment and with the lowest ID_{50} values of the panel. All four cultures showed a significant increase in ID_{50} value after daily retreatment with metformin. U251-MG exhibited the highest change in ID_{50} value with daily metformin dosage showing an increase of over 200% compared to single treatment. IN859 and IN1472 showed a highly statistically significant change in ID_{50} value with p values of 0.0051 and 0.0026 respectively. Figures 3.3 shows the results of the retreatment experiments. U251MG and IN859 showed the largest increase in ID_{50} values. The two cultures also showed the lowest doubling time of the panel in Table 3.1.

Table 3.3 – ID50 values for all cultures treated with metformin.

Culture reference	*P53* Status	Metformin ID_{50} 96 hours (mM)[3]	Metformin ID_{50} daily retreatment (mM)[1]	% Change in ID_{50} single vs multiple treatments at 96 hr[2]	P-value[3]
U251MG	Aberrant/Deletion	3.77(±1.5)	11.43(±2.08)	+204%	0.0418*
IN859	Aberrant	3.4(±1.48)	15.2(±5.3)	+342%	0.0051**
IN1472	Aberrant	4.77(±1.24)	12.2(±1.47)	+155%	0.0026**
IN2045	Aberrant	4.9(1.21±)	14.3(±4.47)	+192%	0.00246*

All values are the average of three repeats that all are within the mM dose range. Standard deviation for each average is listed after each result (±).[2]Percentage change in theID50 value of the culture when compared against single dose time course. [3]P-value for the statistical difference between the means of the ID50 single vs multiple treatments at 96 hr. Level of significance is denoted with *.

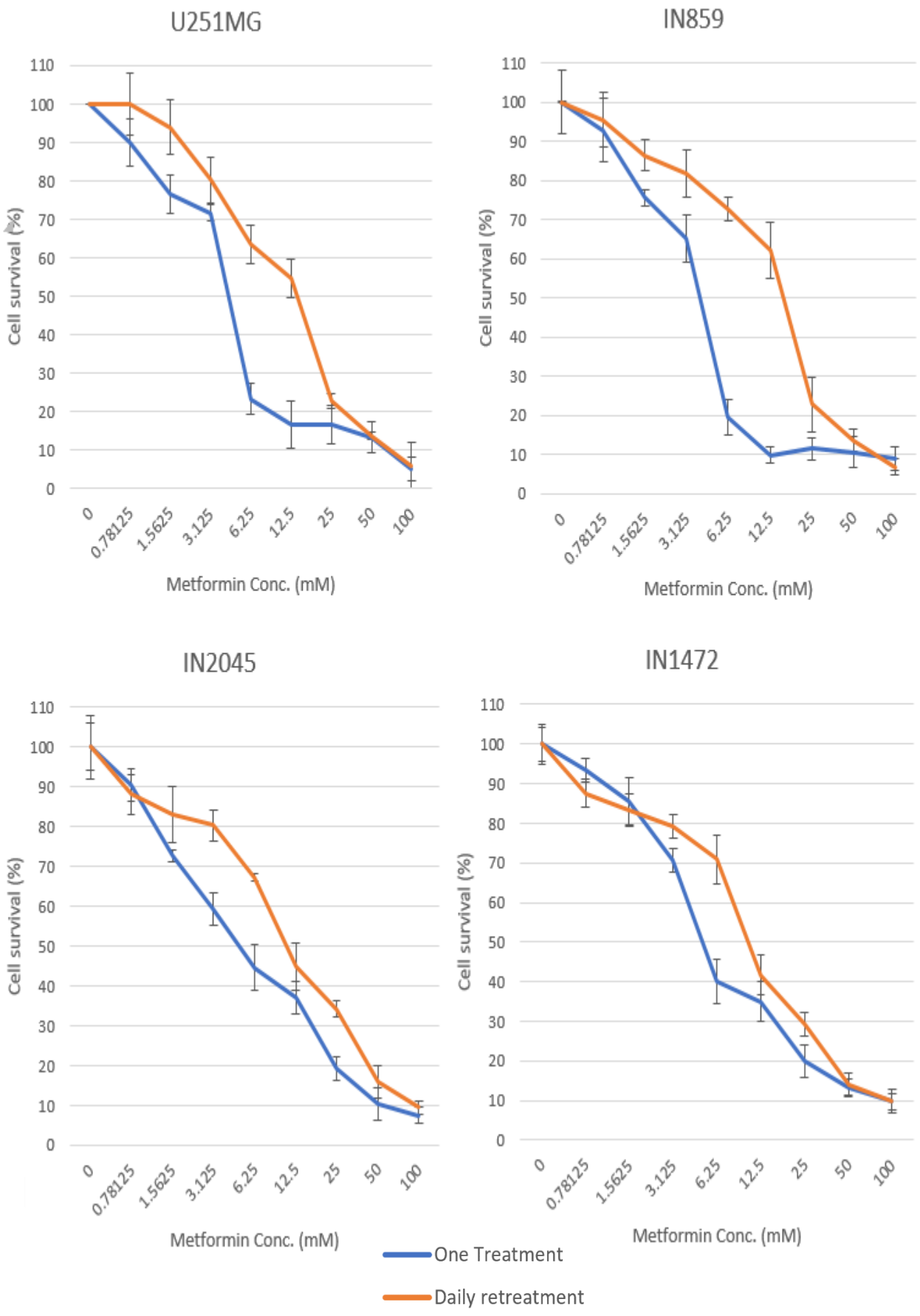

Figure 3.3 – Graphs of 96-hour daily retreatment of metformin compared with solo treatment. All cultures demonstrated a significant increase ($p>0.05$) in metformin ID values when retreated with metformin. All cultures tested were *P53*aberrant cultures that had demonstrated sensitivity to metformin in 96-hour ID50 values as shown in table 3.2. One treatment cultures were dosed with metformin at the start of the 96-hour time course and incubated. Multiple treatment cultures has growth media and metformin replaced every 24hrs.

3.1.2.3 Phenformin

In addition to testing metformin, other biguanides have anti-cancer potential (Jiang *et al.*, 2016). The biguanide phenformin has been discontinued for use as a treatment for type 2 diabetes but could still be repurposed to treat tumours if shown to be more effective than metformin (Pryor and Cabreiro, 2015).

All GBM cultures treated with phenformin showed a cytotoxic response after 3 days of exposure. Table 3.4 lists the ID_{50} values for cultures treated with phenformin for 72 hours. The ID_{50} values for phenformin range of 5.74mM between 0.29mM (IN859) to 6.03mM (IN1760) at 6.03mM. There is no significant association between *P53* status and response to phenformin (P=0.569). In addition, there is no clear relationship between ID_{50} values for metformin and phenformin after 72 hours treatment. Several of the cultures with relatively high metformin ID_{50} values, have relatively low phenformin ID_{50} values, as illustrated in Figure 3.4. All phenformin ID_{50} values are a magnitude smaller than metformin ID_{50} values but still fall within the mM dose range. Due to time constraints and lack of availability of cells, NHA as a normal cell control was not able to be completed for the phenformin data set.

Table 3.4 – ID50 values for all cultures treated with phenformin.

Culture reference	*P53* Status	Phenformin ID_{50} 72 hours (mM)[1]
IN859	Aberrant	0.29(±0.06)
IN2045	Aberrant	0.61(±0.19)
IN1979	Aberrant	0.74(±0.13)
IN1528	Aberrant	0.78(±0.35)
U251	Aberrant	0.87(±0.41)
IN1612	Aberrant	1.71(±1.73)
IN1472	Aberrant	2.40(±0.45)
IN1265	Aberrant	3.87(±3.32)
IN1682+	Wild Type	0.82(±0.59)
IN2093+	Wild Type	2.08(±0.65)
IN1951+	Wild Type	2.43(±0.89)
IN1461+	Wild Type	3.31(±1.61)
IN1752+	Wild Type	3.83(±1.90)
IN1760+	Wild Type	6.03(±0.51)

[1]Phenformin ID50 value of cultures. All values are the average of three repeats that all are within the mM dose range. Standard deviation for each average is listed after each result (±). *P53* sub groups are ordered lowest to highest based on the 96-hour phenformin ID50. All cultures marked with a + indicate *P53* wild type. [2]*P53* status of each culture was to group cultures together. Phenformin cytotoxicity graphs for all cultures can be found in Appendix 3.

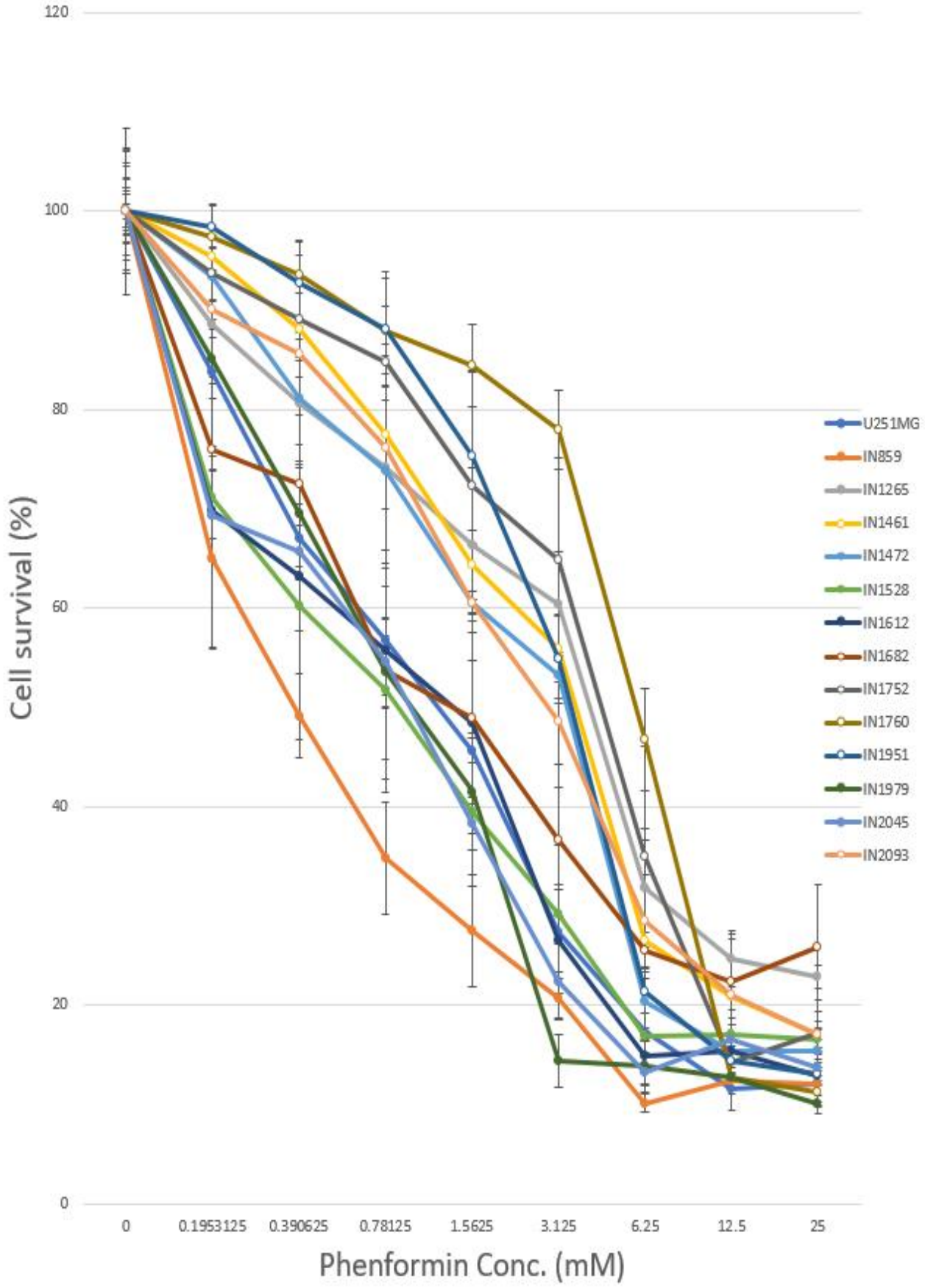

Figure 3.4 – Graph showing SRB cytotoxicity assay results for culture panel at 96 hours phenformin treatment. Percentage cell survival is measured by comparing each OD value against averaged OD value at control well (0mM metformin). Error bars display standard deviation averaged from 3 replicates. Serial dilution drug concentrations ranged from 25mM at highest to 0.19mM at lowest.

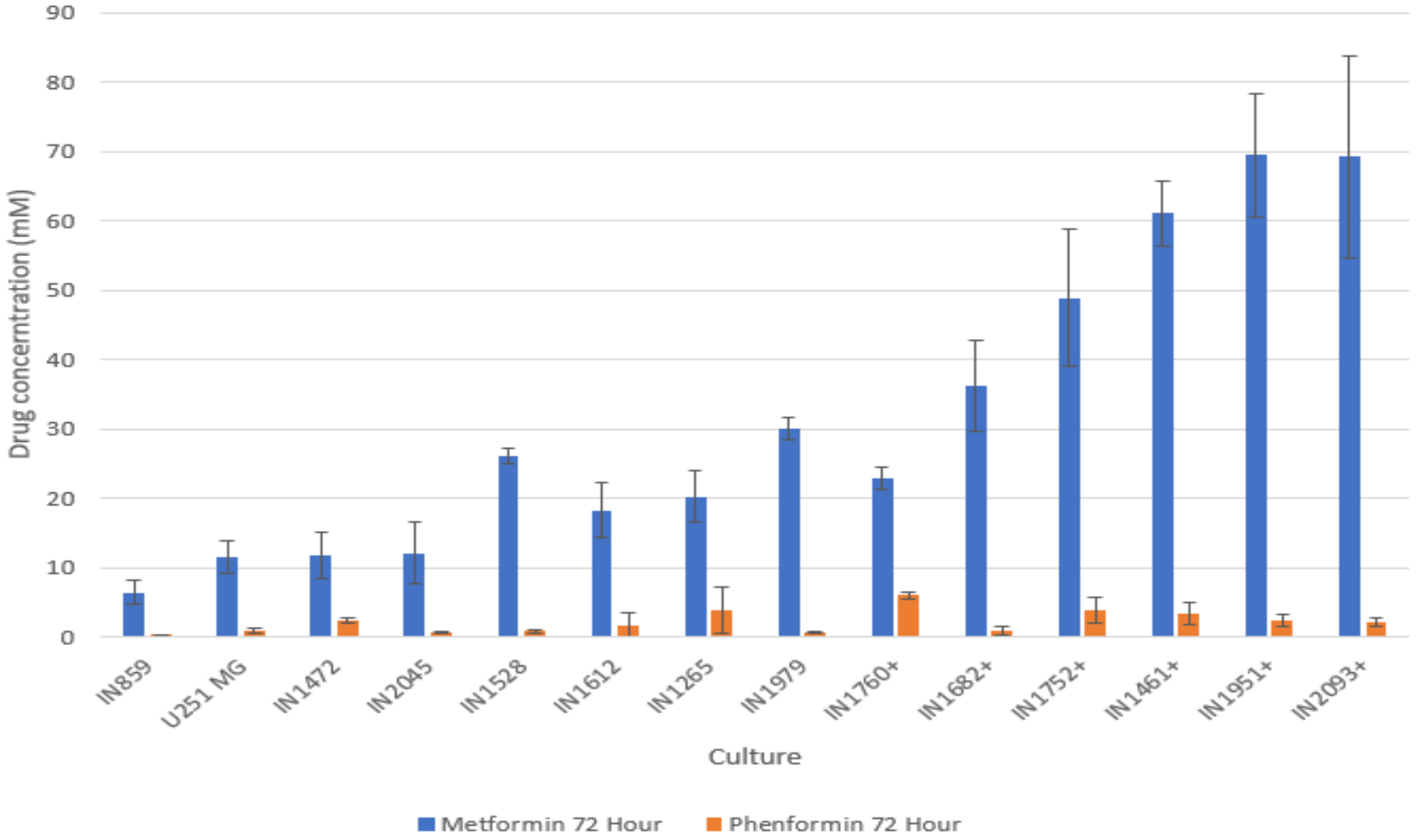

Figure 3.5 – Comparison of the ID50 values for both metformin and phenformin at the 72-hour time point. Cultures are ordered lowest to highest based on the metformin ID50 value. Cultures marked with a $^{+}$ are *P53* wild type cultures. Drug concentration for both drugs was in the mM range. No clear relationship can be defined between the ID50 values of the two drugs.

3.1.2.4 Overview of response of GBM cultures to metformin

ID_{50} values were generated for all GBM cultures for both metformin and phenformin. A summary of ID_{50} values at the 72-hour time point for both drugs is given in Table 3.5. Phenformin ID_{50} values were lower than metformin ID_{50} values in all GBM cultures. The average ID_{50} values were lower in *P53* aberrant GBM cultures for both metformin and phenformin, but only metformin values showed a significant difference between cultures grouped by *P53* status.

Table 3.5 – Overview of metformin and phenformin ID50 values

	Average metformin 72-hour ID_{50} value (mM)	Average phenformin 72-hour ID_{50} value (mM)	% change in drug ID_{50} value
All cultures	33.31 (±22.05)	2.22 (±1.68)	-93%
P53 Aberrant	17.86 (±8.41)	1.48 (±1.28)	-92%
P53 Wild type cultures.	51.33 (±18.93)	3.08 (±1.78)	-94%

Metformin and phenformin ID50 values were within the mM dose range. *P53* status is a significant indicator of metformin sensitivity with GBM cultures. *P53* wild type cultures have a lower sensitivity to the cytotoxic effect of metformin. Phenformin ID50 values are on average an order of magnitude smaller than metformin ID50 *values* but show no relationship with metformin or *P53* status.

3.1.3 Summary

3.1.3.1 Growth curves

Results on culture growth curves showed that *P53* was a significant factor influencing cell doubling time. *P53* is a tumour suppressor gene and activation of it has a negative impact on cell proliferation (Kaiser and Attardi, 2018). GBM cultures possessing an aberrant *P53* would be expected to show higher rates of growth. The two cultures with the lowest doubling time are IN859 and U251MG (24 hours). A short term low passage culture would not usually be expected to grow as fast as a high passage, established, immortalised cell line and is indicative of the high heterogeneity present with GBM. IN2093 was the slowest growing culture with a doubling time of 70 hours, slower rate of proliferation than the NHA normal control with a doubling time of 60 hours. It would be expected that, NHA as a normal cell control, would be slower than all tumour cells.

3.1.3.2 Metformin growth inhibition

An inhibitory growth response to metformin was observed in all GBM cultures. A large range in ID_{50} values was observed in the GBM panel and this variance in metformin sensitivity in GBM was associated with cell-specific factors. *P53* was identified as a significant factor in metformin sensitivity of the GBM cultures. The role of *P53* in response to metformin treatment varies in different types of cancer (Sun *et al.*, 2016; Shimazu *et al*, 2017; Lee *et al.*, 2018). The results obtained in GBM cultures in the current study are similar to previously published data in colon cancer, in which *P53* -/- xenografts showed higher susceptibility than *P53*+/+ to metformin treatment (Buzzai, 2007). The authors hypothesise that metformin treatment is forcing a metabolic

conversion that *P53*-/- are unable to withstand. Conversely in prostate and breast cancer, metformin has been to induce *P53*-dependent apoptosis (Sahra *et al.*, 2010; Li *et al.*, 2015; Tran *et al.*, 2017).

NHA showed the least growth inhibition after treatment with metformin and the highest ID_{50} value at both 72 (90.95mM ±14.39) and 96-hour (84.3mM ±8.50) time points. The GBM cell culture with the most similar level of sensitivity was IN2093; however, the ID_{50} value at 96-hours was >20mM lower than that of NHA. The large difference in the cytotoxic sensitivity of normal cells compared to GBM cells indicates that metformin mechanism of action is related to cancer specific changes, possibly alterations in metabolism changes and the Warburg effect (Wahl and Venneti, 2018).

Metformin dosages required to induce cell death were all in the mM range. This dosage is much higher than metformin levels detected in circulating plasma *in vivo*. Metformin levels reaching mM concentrations have been detected in health gut tissue (Bailey et al, 2008; Proctor et al, 2008)

Daily reapplications of metformin were shown to decrease sensitivity to metformin in GBM cultures. The results given in Table 3.3 show an overall increase in the ID_{50} values of the four cultures tested. Due to fact that metformin is not metabolised (Hassan and Carlton, 2018), the reapplication of fresh drug daily made no impact on maintain metformin concentration and it is unlikely that metformin is accumulating in GBM cells. However, the increase in growth can be attributed to the cells receiving fresh nutrients daily, thus removing this potentially limiting factor on growth in the wells. In addition,

when considering the rate at which the glucose would be expended by the cells (as shown in Figure 3.20), the reapplication of fresh media would normalise the concentration of glucose around 6mM/L. Wahdan-Alaswad *et al.* (2017), demonstrated that in breast cancer cells an increase in glucose media concentration reduced the efficacy of metformin. Glucose concentration and the availability of resources are important factors that impact of cytotoxic effects by metformin.

3.1.3.3 Phenformin growth inhibition

Phenformin also induced cytotoxicity in GBM cultures. When compared to ID_{50} values of metformin, phenformin ID_{50} values were an order of magnitude lower at near μM concentrations and this may be linked to the increased lipid solubility of phenformin (Schafer, 1983). This potentially would allow the drug to more readily cross cell and mitochondria membranes to affect mitochondria complex I (Wheaton, *et al.* 2014). The observed difference between metformin and phenformin highlights the need for further investigation into other drugs in the biguanide class as potential therapeutic agents. However, due to a high incidence of lactic acidosis phenformin is no longer a widely-used drug though it is still available in China, Brazil and Italy (Ching, 2008; Fimognari *et al.*, 2008). To consider phenformin for repurposing as GBM therapy would require additional clinical trials and tests. Metformin is a licenced drug and is already being considered and tested in prostate cancer clinical trial as a repurposed therapeutic agent (Pryor and Cabreiro, 2015; Heckman-Stoddard *et al.*, 2018). New investigations into novel biguanides and derivates could produce new

formulation that have improved cellular response (Markowicz-Piasecka *et al.*, 2018).

3.2 Assessing drug synergy in GBM cultures

Metformin would not be used as a monotherapy and the identification of other drugs it can work additively with will increase its likelihood of use in clinical trials (Aldea *et al.*, 2014). Potential synergistic drug partners were assessed with metformin using the SRB assay to assess the combined treatment effect. Four drugs were assessed for combination therapy treatments. The culture panel utilised for 3.2 was reduced, due to the resource and time cost of maintaining active culture flasks for the entire panel. The reduced panel still contained variation in *p53* status and cell doubling time.

3.2.1 Synergy culture panel

Eight cultures were utilized to assess the potential synergy of four drugs with metformin. The four drugs were disulfiram, TMZ, sodium oxamate and sorafenib. Drugs were chosen based on the pre-existing use for GBM or the promising potentials as GBM therapeutic agents. TMZ is the front-line treatment for GBM (Messaoudi *et al.*, 2015). Disulfiram and sorafenib have shown cytotoxic effects in GBM cell lines (Liu *et al.*, 2012; Aldea *et al.*, 2014). Sodium oxamate has been shown to synergise with phenformin in GBM (Miskimins, *et al.* 2014). The panel of cultures comprised six *P53* mutant cultures and two *P53* wild type cultures. Setup and analysis of the experiment was carried out as detailed in 2.3.5. Table 3.6 shows the comparative drug combinations used in relation to metformin.

Table 3.6 – Drug concentrations used in synergy analysis with metformin.

Drug[1]	Units	Drug concentration[3]								
		Highest							Lowest	Control[4]
Metformin	mM	80	40	20	10	5	2.5	1.25	0.63	0
Disulfiram[4]	nM	1000	500	250	125	62.5	31.25	15.63	7.81	0
Temozolomide	µM	500	250	125	62.5	31.25	15.62	7.81	3.9	0
Sodium Oxamate	µM	160	80	40	20	10	5	2.5	1.25	0
Sorafenib	µM	80	40	20	10	5	2.5	1.25	0.63	0

All drugs were utilized both individually and in equimolar doses with metformin. [1]Drugs tested for synergy. All drugs tested for synergy analysis were dissolved in water. Drugs are ordered based on the concentration used in experiments. All experiments compared ID_{50} independently and combined with metformin. [2]Drug concentration values used in the serial dilution to produce an 8-point concentration range for each drug. [3] Control values taken as an average of two wells per replicate. [4]All disulfiram wells were supplemented with 10µM copper Chloride.

3.2.2 Synergy analysis using the Chou-Talay theorem

Paired drug treatment for synergy analysis were assessed using the Cho-talay theorem (Chou., 2010). This generates a combination index relative to the effectiveness of each drug when used as a mono therapy and when you in conjunction with the other. The complete equation is given in figure 3.2.

3.2.2.1 Disulfiram

Disulfiram was shown to have a cytotoxic effect on all cultures tested over a 96-hour treatment period. In all treatments, disulfiram was supplemented with 10μM copper chloride to enable the drug to function at maximum efficacy (Liu *et al.*, 2014). Table 3.7 summarizes the ID_{50} values generated from combination analysis of disulfiram. The ID_{50} value for U251MG concurs with previously published results (Liu *et al.*, 2012) and was the most sensitive of all the cultures to disulfiram. There was no significant association between *P53* status and response to disulfiram (p=0.0908).

Table 3.7 – ID50 values for disulfiram in GBM cultures

Culture reference	***P53* Status**	**Disulfiram ID_{50} 96 hours (nM)[1]**
U251MG	Aberrant	164.53 (±14.31)
IN859	Aberrant	195.3 (±48.59)
IN1265	Aberrant	210 (±68.06)
IN2045	Aberrant	227.2 (±20.77)
IN1528	Aberrant	240.63 (±71.31)
IN1979	Aberrant	276.13 (±65.87)
IN1760^{+}	Wild Type	260.4 (±61.4)
IN1682^{+}	Wild Type	298.6 (±18.04)

[1]ID50 values for disulfiram at 96 hours when supplemented with 10μM copper chloride. Cultures ordered lowest ID50 to highest. No significant distinction due to *P53* status was present in the panel. All cultures marked with a $^{+}$ indicate *P53* wild type. *P53* status of each culture used to group cultures together.

The concentration of disulfiram ranged from 7.81nM to 1000nM and was used both separately and in equimolar concentrations with metformin. Separate SRB assay data for the three treatments is given in Figure 3.6. Combination data for disulfiram and metformin is shown in Table 3.8. All cultures demonstrated a strong antagonistic result from the combination of disulfiram with metformin. The lowest of the average combination index was 1.31, observed in IN2045. Only IN1760 showed a synergistic response in one of its replicates, a CI index of 0.81. This is a strong synergistic value; however, this culture was also one with the highest standard deviation in its results.

Table 3.8 – Drug synergy analysis for disulfiram supplemented when combined in equimolar dosage

Culture reference	***P53* Status**	**Combination Index[1]**			**Average**	**Result[2]**
		A	**B**	**C**		
U251MG	Aberrant	1.26	1.27	1.40	1.40(±0.07)	Antagonism
IN859	Aberrant	1.55	1.32	1.55	1.47(±0.13)	Antagonism
IN1265	Aberrant	1.63	2.18	2.03	1.95(±0.28)	Antagonism
IN1528	Aberrant	1.49	1.25	1.74	1.49(±0.24)	Antagonism
IN1979	Aberrant	2.01	1.73	1.84	1.86(±0.14)	Antagonism
IN2045	Aberrant	1.30	1.19	1.43	1.31(±0.12)	Antagonism
IN1682[+]	Wild Type	1.87	2.01	1.62	1.83(±0.20)	Antagonism
IN1760[+]	Wild Type	1.52	0.81	1.95	1.42(±0.57)	Antagonism

All cultures marked with a [+] indicate *P53* wild type. *P53* status of each culture used to group cultures together. [1]Combination index result as a measure of synergy comparing each drug individually to an equimolar combination. Due to intragroup comparisons required each result shown separately [2]Overall result from synergy analysis based on average combination index result. All samples showed an antagonistic response to the drug combination.

CI Index >1 – Antagonism (Red), CI Index = 1 – Additive (Orange), CI Index <1 = Synergy (Green).

All graphs in figure 3.6 display a lower dose response curve with metformin compared to disulfiram. The combination dose response curves show similar trends to the metformin curve. Chou-talay analysis requires a reduction in the combination treatment over one individual drug and the lack of this difference explains the antagonist results detailed in table 3.8. Additional graphs representing this drug synergy analysis for disulfiram with metformin can be found in appendix D. From this result, it is clear there is no increase in cytotoxicity in GBM cells from the addition of disulfiram to metformin.

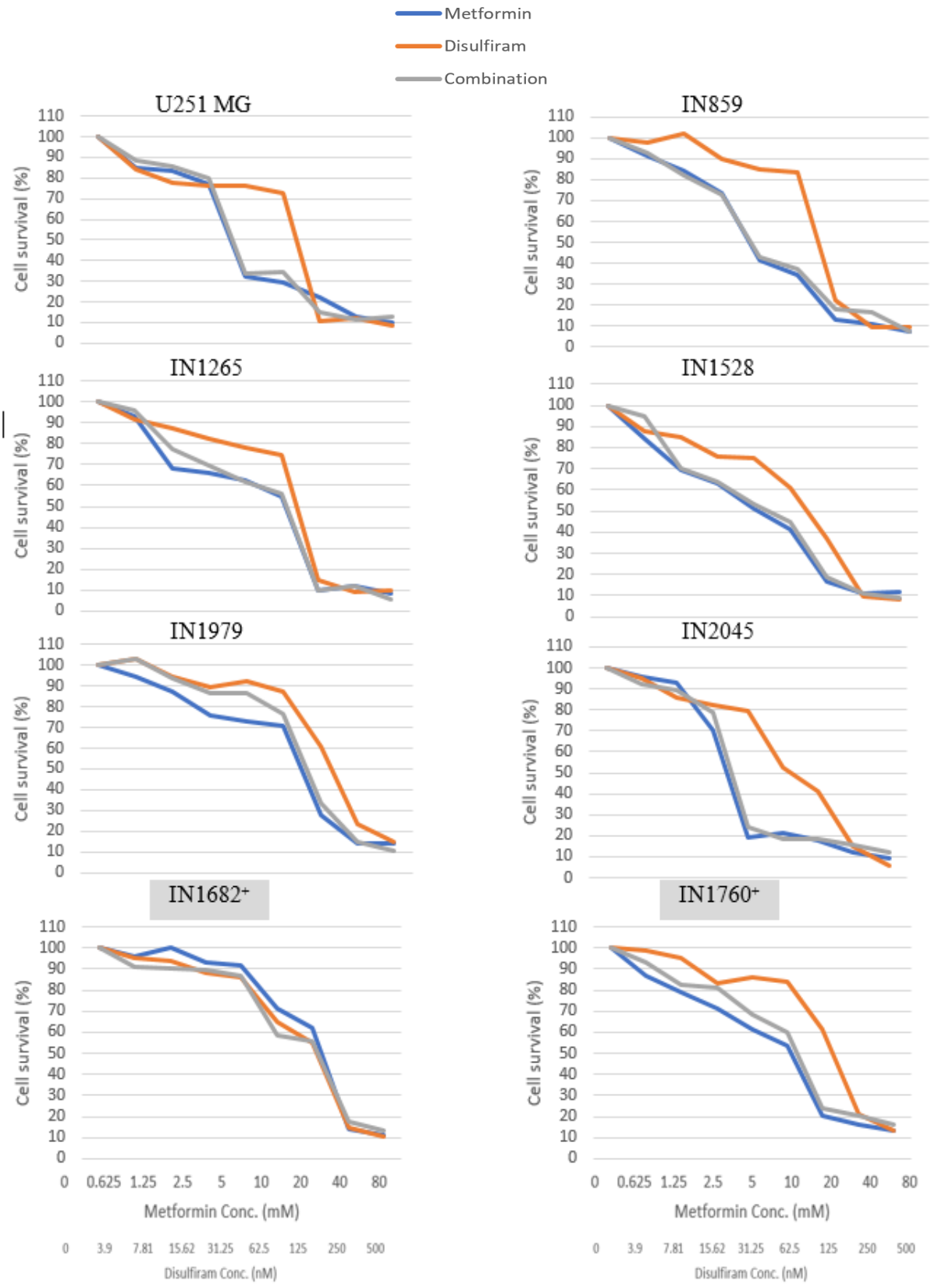

Figure 3.6 – Graphs representing the combination synergy experiments of metformin alongside disulfiram. All culture tested in solo and combination treatment in equimolar dosages in a 96-hour period. Cultures that showed synergy marked with a †. Disulfiram results show higher ID50 curves than metformin. Combination curves of most graphs are similar to metformin treatment leading to antagonist results. All cultures marked with a + indicate *P53* wild type.

3.2.2.2 Temozolomide

Temozolomide was shown to have a cytotoxic effect on all cultures tested over a 96-hour treatment period. TMZ is stable in acid pH but has a half-life of approximately 2 hours at pH7 (Brian *et al.*, 1994; Patel *et al.*, 2003). To account for the short half-life of temozolomide additional temozolomide was supplemented into the growth media daily. The media was not changed, and additional glucose was not provided to the cells. This was to prevent the increase in cell growth and reduced sensitivity of metformin that was shown in 3.1.3. *MGMT* status has been known to be a factor on the sensitivity of GBM in respect to the overall efficacy of temozolomide (Franceschi *et al.*, 2018). Cultures with methylated *MGMT* genes should have an increased sensitivity to temozolomide (Tosoni *et al.*, 2017; Bell *et al.*, 2018). Table 3.9 summarizes the ID_{50} values generated from synergy analysis of temozolomide. When comparing the response to *MGMT* status there was no clear pattern to the ID_{50} values for temozolomide. U251MG was the most sensitive to the temozolomide treatment with an ID_{50} of 116μM. *P53* status of the culture showed no significant effect (P=0.1516).

Table 3.9 – ID50 values for TMZ in GBM cultures

Culture reference	*P53* Status	*MGMT* status[1]	Temozolomide ID_{50} 96 hours (μM)
U251MG	Aberrant	Methylated	116 (±0.63)
IN1528	Aberrant	Methylated	163.81 (±64.60)
IN1265	Aberrant	Unmethylated	240.89 (±86.24)
IN1979	Aberrant	Unmethylated	257.3 (±24.16)
IN859	Aberrant	Methylated	274.07 (±69.85)
IN2045	Aberrant	Methylated	353.33 (±34.77)
IN1760+	Wild Type	Methylated	336.8 (±38.97)
IN1682+	Wild Type	ND	337.33 (±54.73)

[1] *MGMT* methylation status of the culture. ID50 values for temozolomide at 96 hours. Cultures ordered lowest ID50 to highest. No significant distinction due to *P53* status was present in the panel. All cultures marked with a + indicate *P53* wild type. ND – Not determined. [1]The methylation of the *MGMT* gene is a known factor in the sensitivity of tumour response to temozolomide

Combination data for temozolomide and metformin treatment was shown in Table 3.10. Three cultures showed a synergistic response to the drug combination (CI<1); U251MG, IN2045 and IN1760, all of which were *MGMT* methylated. No relationship was apparent between *P53* status and TMZ synergy with metformin. *MGMT* status did not affect the synergism between TMZ and metformin. This result fits with the TMZ ID_{50} values not showing any significant relationship.

Table 3.10 – Drug synergy analysis for temozolomide when combined in equimolar dosage with metformin.

Culture reference	*P53* Status	*MGMT* status[1]	Combination Index[2]			Average	Result[5]
			A	B	C		
U251MG	Aberrant	Methylated	0.85	0.96	0.88	0.89(±0.05)	Synergism
IN859	Aberrant	Methylated	1.7	1.55	1.57	1.61(±0.08)	Antagonism
IN1265	Aberrant	Unmethylated	0.89	1.18	1.25	1.11(±0.19)	Antagonism
IN1528	Aberrant	Methylated	1.41	1.38	1.04	1.28(±0.21)	Antagonism
IN1979	Aberrant	Unmethylated	1.45	1.44	1.22	1.38(±0.13)	Antagonism
IN2045	Aberrant	Methylated	0.95	1.05	0.77	0.93(±0.14)	Synergism
IN1682^{+}	Wild Type	ND	1.30	1.51	1.20	1.33(±0.15)	Antagonism
IN1760^{+}	Wild Type	Methylated	0.95	0.94	0.87	0.92(±0.04)	Synergism

All cultures marked with a $^{+}$ indicate *P53* wild type. *P53* status of each culture was used to group cultures together. [1]*MGMT* methylation status of the culture. The methylation of the *MGMT* gene is a known factor in the sensitivity of tumour response to temozolomide [2]Combination index result as a measure of synergy comparing each drug individually to an equimolar combination. Due to intragroup comparisons required each result shown separately [5]Overall result from synergy analysis based on average combination index result. Three cultures showed a synergistic response and 5 showed an antagonistic response. CI Index >1 – Antagonism (Red), CI Index = 1 – Additive (Orange), CI Index <1 = Synergy (Green). ND – Not determined.

The concentration of TMZ ranged from 3.9μM to 500μM and was used both separately and in equimolar concentrations with metformin. Separate SRB assay data for the three treatments is given in Figure 3.7. In cultures IN859 and IN1265, the metformin dose response curve was below the combination treatment demonstrating an antagonist reaction increasing the ID_{50} value when used in combination. Additional graphs representing this drug synergy analysis for temozolomide with metformin can be found in Appendix E. The result here showed that there is possible synergy between metformin and temozolomide.

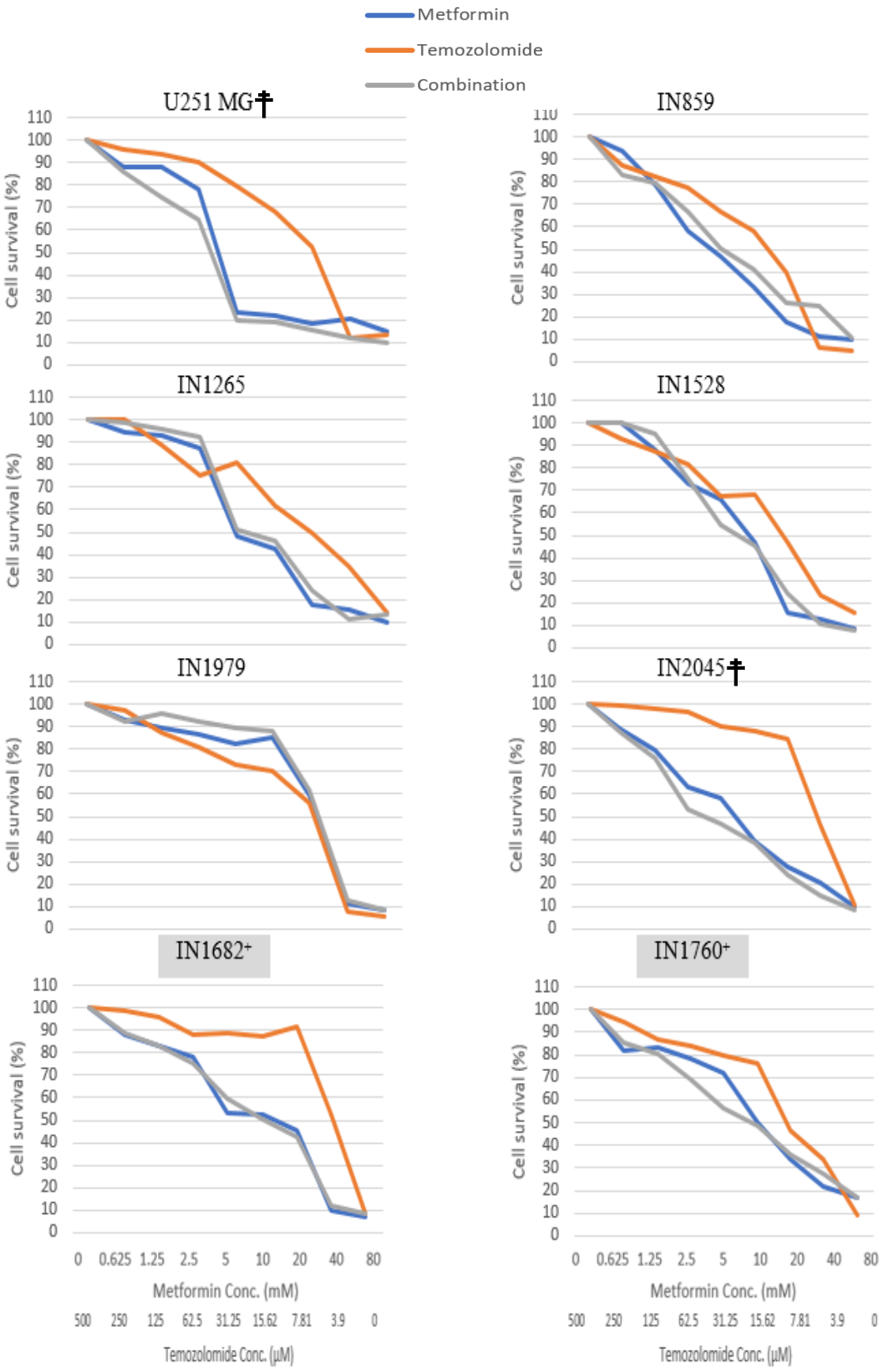

Figure 3.7 – Graphs representing the combination synergy experiments of metformin alongside temozolomide supplemented with copper chloride. All cultures tested in solo and combination treatment in equimolar dosages in a 96-hour period. Cultures that showed synergy marked with a †. Temozolomide results show lower ID_{50} values than metformin. Combination curves of most graphs are similar to metformin treatment. All cultures marked with a + indicate *P53* wild type.

3.2.2.3 Sodium Oxamate

Sodium oxamate was shown to have a cytotoxic effect on all cultures tested over a 96-hour treatment period. The ID_{50} values ranged from 57.18μM (IN2045) to 95.94μM (IN1760) and five out of the eight (5 of 8) ID_{50} values of the cultures tested were between the highest two concentration points. IN2045 was the most sensitive to sodium oxamate treatment with an ID_{50} of 57.18μM There was no clear relationship between *P53* status and sodium oxamate ID_{50} value (p=0.1816). ID_{50} sodium oxamate is listed in table 3.11.

Table 3.11 – ID50 values for sodium oxamate in GBM cultures

Culture reference	***P53* Status**	**Sodium Oxamate ID_{50} 96 hours (μM)[1]**
IN2045	Aberrant	57.18 (±25.99)
IN859	Aberrant	63.27 (±14.04)
IN1265	Aberrant	66.87 (±27.81)
IN1528	Aberrant	81.68 (±14.49)
U251MG	Aberrant	85.27 (±18.88)
IN1979	Aberrant	91.81(±27.88)
IN1682^{+}	Wild Type	84.81 (±33.5)
IN1760^{+}	Wild Type	95.94 (±27.76)

All cultures marked with a $^{+}$ indicate *P53* wild type. *P53* status of each culture used to group cultures together.

[1]ID50 values for sodium oxamate at 96 hours. Cultures ordered lowest ID50 to highest. No significant distinction due to *P53* status was present in the panel.

Combination data for sodium oxamate and metformin treatment is shown in Table 3.12. Only one culture showed a synergistic response with the drug combination of sodium oxamate and metformin, U251MG. All the short-term GBM cultures showed an overall antagonistic response. There was a synergistic response in one replicate of IN1979 treatment (CI=0.93) but the averaged data produced a CI of 1.18. This was the lowest result in all the short-term cultures. The concentration of sodium oxamate ranged from 1.25μmM to 160μM and was used both separately and in equimolar

concentrations with metformin. Separate SRB assay data for the three treatments is given in Figure 3.8.

Table 3.12 – Drug synergy analysis for sodium oxamate when combined in equimolar dosage

Culture reference	*P53* Status	Combination Index[1]			Average	Result[2]
		A	B	C		
U251MG	Aberrant	0.64	0.76	0.79	0.73(±0.08)	Synergism
IN859	Aberrant	1.29	1.24	1.86	1.46(±0.34)	Antagonism
IN1265	Aberrant	1.86	1.69	1.66	1.73(±0.11)	Antagonism
IN1528	Aberrant	1.54	1.11	1.37	1.34(±0.22)	Antagonism
IN1979	Aberrant	1.40	0.93	1.20	1.18(±0.24)	Antagonism
IN2045	Aberrant	1.68	1.49	0.96	1.38(±0.37)	Antagonism
IN1682+	Wild Type	1.95	1.33	1.08	1.45(±0.45)	Antagonism
IN1760+	Wild Type	1.43	1.10	1.34	1.29(±0.17)	Antagonism

All cultures marked with a + indicate *P53* wild type. *P53* status of each culture used to group cultures together. [1]Combination index result as a measure of synergy comparing each drug individually to an equimolar combination. Due to intragroup comparisons required each result shown separately [2]Overall result from synergy analysis based on average combination index result. One culture, U251, showed a synergistic response from the drug combination. All short-term cultures showed antagonism.

CI Index >1 – Antagonism (Red), CI Index = 1 – Additive (Orange), CI Index <1 = Synergy (Green).

Additional graphs representing this drug synergy analysis for sodium oxamate with metformin can be found in Appendix F. Apart from the result from U251MG sodium oxamate there seems to be no benefit from the combination of sodium oxamate and metformin. U251MG strong synergy may be indicative of a factor unique to that culture that is not present within short term cultures.

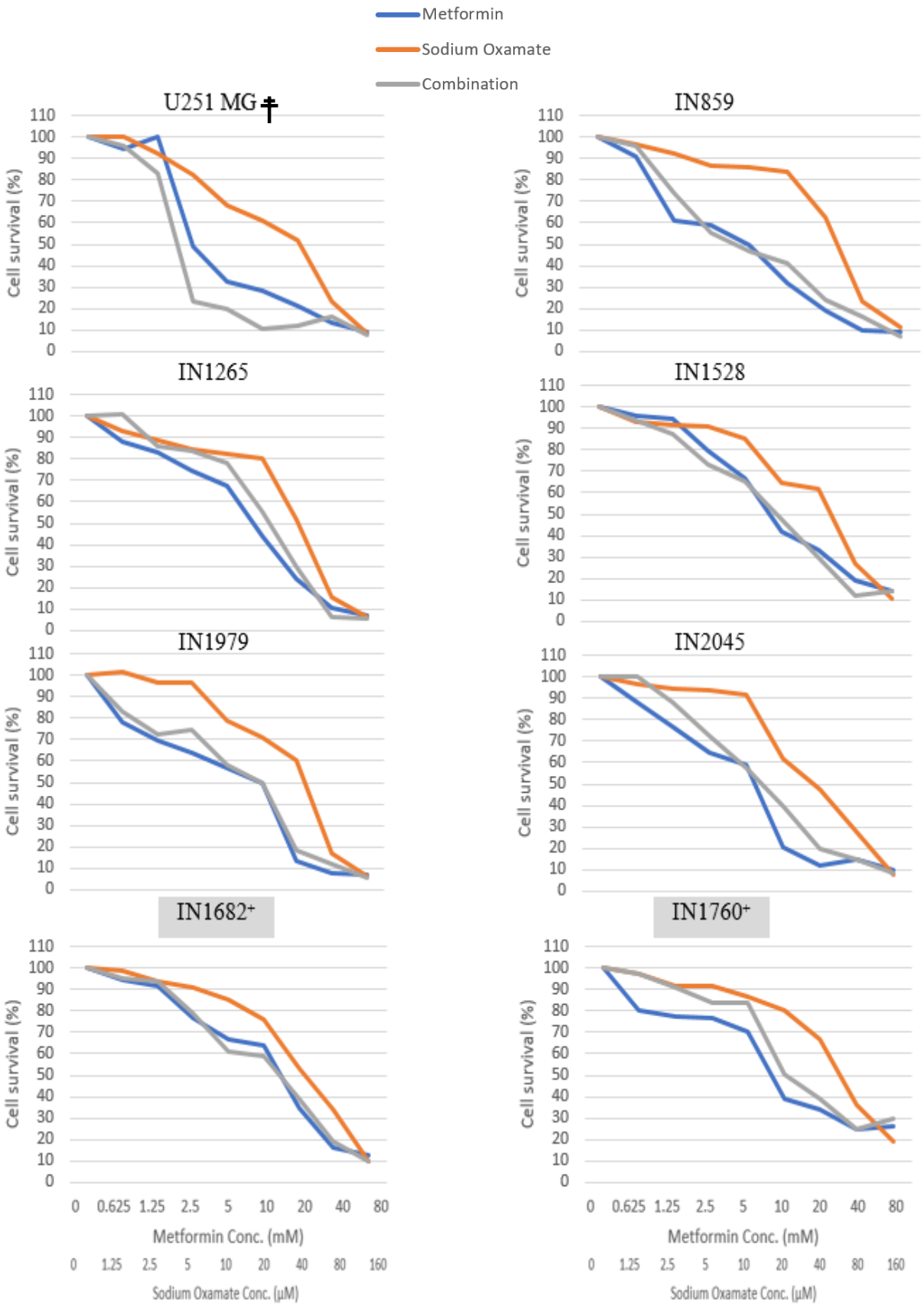

Figure 3.8 – Graphs representing the combination synergy experiments of metformin alongside sodium oxamate. All cultures tested in solo and combination treatment in equimolar dosages in a 96-hour period. Cultures that showed synergy marked with a †. Sodium oxamate showed synergy in U251MG but no other cultures tested. In all other cultures metformin mono treatment had the lowest ID50 values. All cultures marked with a + indicate *P53* wild type.

3.2.2.4 Sorafenib

Sorafenib was shown to have a cytotoxic effect on all cultures tested over a 96-hour treatment period. There was no clear pattern between *P53* status and sorafenib ID_{50} value (P=0.5889). IN1979 was shown to be the most sensitive to sorafenib with an ID_{50} value of 18.47μM. All the ID_{50} for the cultures tested is listed in table 3.13.

Table 3.13 – ID50 values for sorafenib in GBM cultures

Culture reference	***P53* Status**	**Sorafenib ID_{50} 96 hours (μM)[1]**
IN1979	Aberrant	18.47 (±6.67)
IN1528	Aberrant	21.56 (±5.77)
IN2045	Aberrant	26.25 (±19.3)
IN859	Aberrant	33.36 (±7.76)
IN1265	Aberrant	36.06 (±12.87)
U251MG	Aberrant	42.83 (±23.49)
IN1682+	Wild Type	26.01 (±13.86)
IN1760+	Wild Type	28.28 (±2.97)

All cultures marked with a + indicate *P53* wild type. *P53* status of each culture used to group cultures together.

[1]ID50 values for sorafenib at 96 hours. Cultures ordered lowest ID50 to highest. No significant distinction due to *P53* status was present in the panel.

When used in combination, all the cultures tested had a synergistic response. The culture with the lowest CI was IN1265. This result may stem from its sorafenib ID_{50} value, which was the highest of aberrant cultures tested. IN2045 had the highest CI of any culture and this is due to a variation in its replicates. Due to its CI index remaining around 1 it showed a synergistic, additive and antagonistic response to the drug combination. *P53* status did not show a link to the drug combination of sorafenib and metformin. The concentration of sorafenib ranged from 0.63μM to 80μM and was used both separately and in equimolar concentrations with metformin. Separate SRB assay data for the three treatments is given in Figure 3.9.

Table 3.14 – Drug synergy analysis for sorafenib when combined in equimolar dosage with

Culture reference	*P53* Status	Combination Index[1]			Average	Result[2]
		A	B	C		
U251	Aberrant	0.97	0.98	0.90	0.90(±0.4)	Synergism
IN859	Aberrant	0.86	0.87	0.96	0.90(±0.06)	Synergism
IN1265	Aberrant	0.40	0.49		0.45(±0.06)	Synergism
IN1528	Aberrant	0.94	0.85	0.81	0.87(±0.06)	Synergism
IN1979	Aberrant	0.93	0.99	0.94	0.95(±0.03)	Synergism
IN2045	Aberrant	1.0	0.76	1.10	0.96(±0.17)	Synergism
IN1682+	Wild Type	0.91	0.90	0.64	0.82(±0.15)	Synergism
IN1760+	Wild Type	0.69	0.78	0.77	0.75(±0.05)	Synergism

All cultures marked with a + indicate *P53* wild type. *P53* status of each culture used to group cultures together. [1]Combination index result as a measure of synergy comparing each drug individually to an equimolar combination. Due to intragroup comparisons required each result shown separately [2]Overall result from synergy analysis based on average combination index result. CI Index >1 – Antagonism (Red), CI Index = 1 – Additive (Orange), CI Index <1 = Synergy (Green). IN1265 C result was anomalous and removed averaged data.

In all graphs, there is a visible separation of the dose response curves for the combination treatment against the mono drug treatments. Additional graphs representing this drug synergy analysis for sodium oxamate with metformin can be found in appendix G.

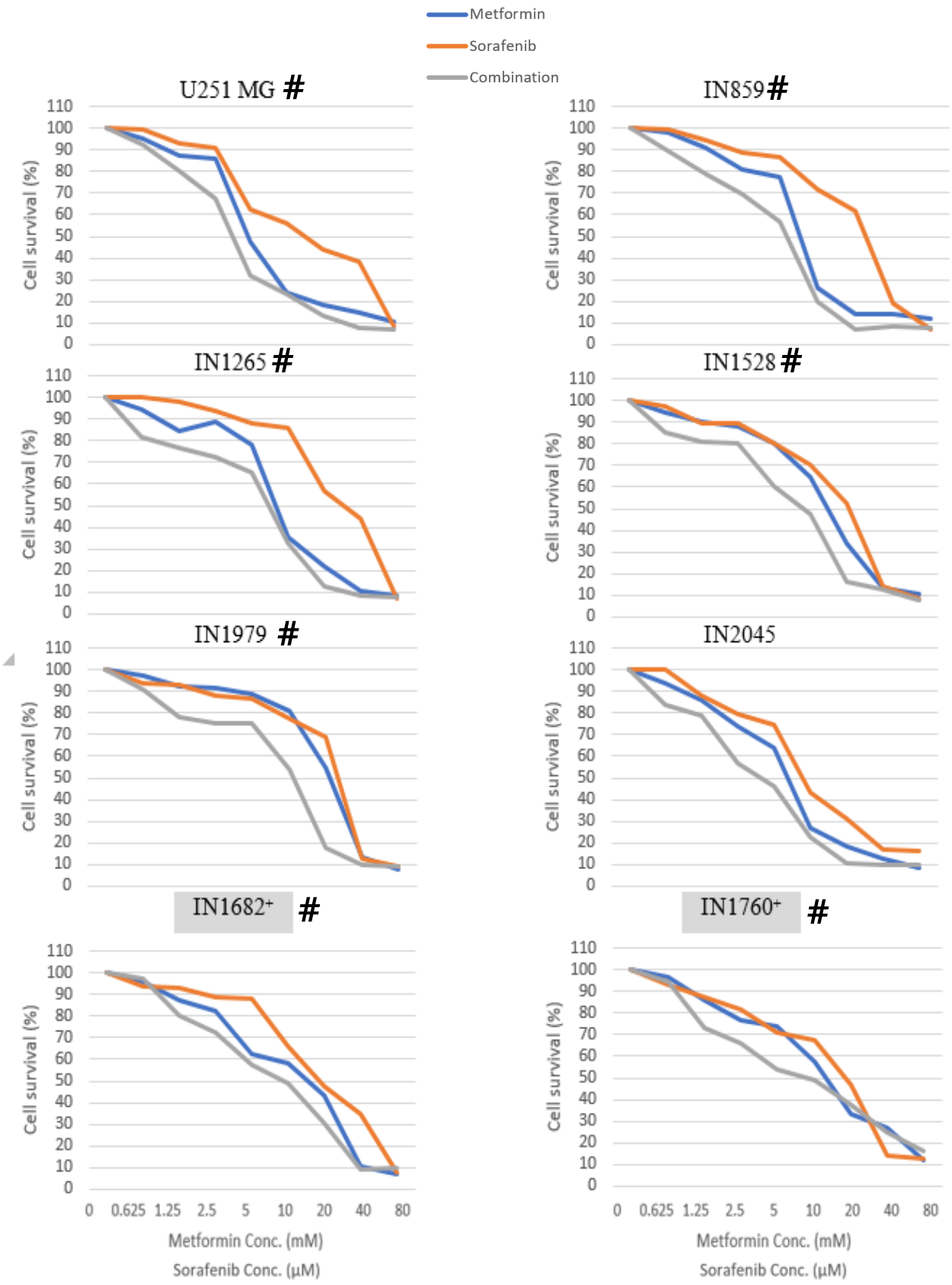

Figure 3.9 – Graphs representing the combination synergy experiments of metformin alongside sorafenib. All culture tested in solo and combination treatment in equimolar dosages in a 96-hour period. Results that showed synergy marked with a #. All cultures showed strong synergy this is identifiable by the separation of the combination dosage response from the mono treatment results. [1]All cultures marked with a + indicate *P53* wild type.

3.2.3 Synergy Time course

Sorafenib was the only drug tested that demonstrated a synergistic response with metformin in all GBM cultures as shown in Table 3.14. To further evaluate this synergy, a time course experiment was conducted using the SRB assay. This allowed for examination of the synergistic effect at fixed concentration combinations over time. A standard dosage of 10mM metformin was used for all cultures across the time course combinations. The cultures chosen were U251MG, IN859, IN1528 and IN2045. All cultures are *P53* mutant or deletions and the cultures have been shown to be sensitive to metformin with ID_{50} values after 96 hours treatment of 4.52mM, 4.83mM, 6.41mM and 10.82mM for (U251MG, IN859, IN2045 and IN1528), respectively. Sorafenib was treated at 10μM and 20μM both in solo and in combination with 10mM metformin. The sorafenib ID_{50} values for the cultures were all above this range 21.56 μM, 26.25 μM, 33.36 μM and 42.83 μM (IN1528, IN2045, IN859 and U251MG). Graphical representations of the experiments can be seen in Figure 3.10a and Figure 3.10b. From the results, the time course responses follow three main groups. In all cultures the strongest response was the combination of metformin and 20μM sorafenib. For U251MG sorafenib at 10μM had a low effect on the cells. IN859 had a similar 96-hour time point for 10μM sorafenib but the drug showed a greater effect across the time course. U251MG, IN859 and IN1528 showed a similar response for sorafenib at 20μM and both metformin combinations. IN2045 showed a stronger a stronger response from sorafenib at 20μM than combination of 10μM sorafenib and metformin.

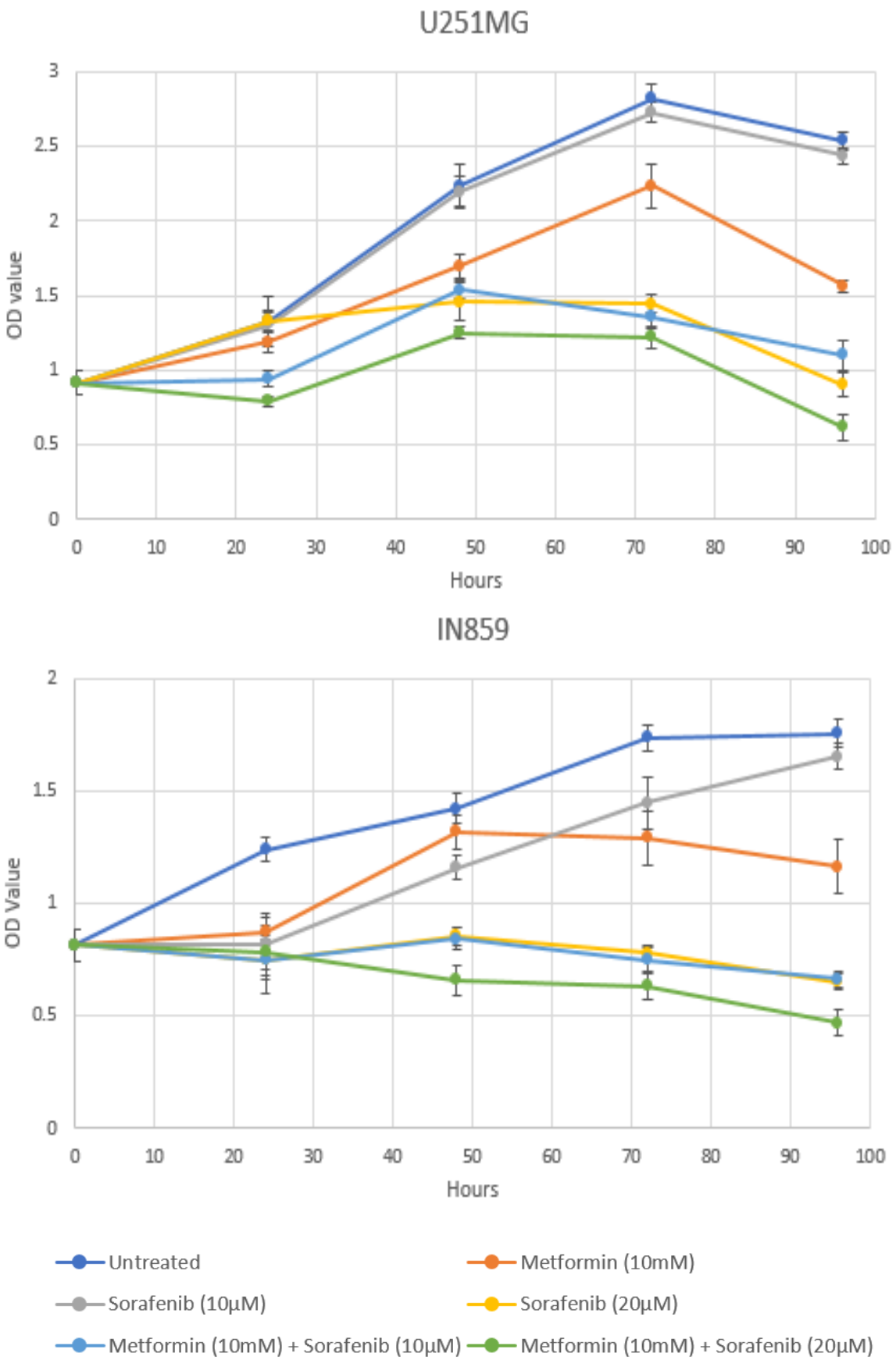

Figure 3.10a – Drug synergy analysis time course of metformin and sorafenib. Metformin and sorafenib were tested in solo and in combination over a 96-hour time course. Figure A shows U251MG and IN859. OD values were obtained every 24 over the time course. Error bars show the standard deviation of the replicate samples used.

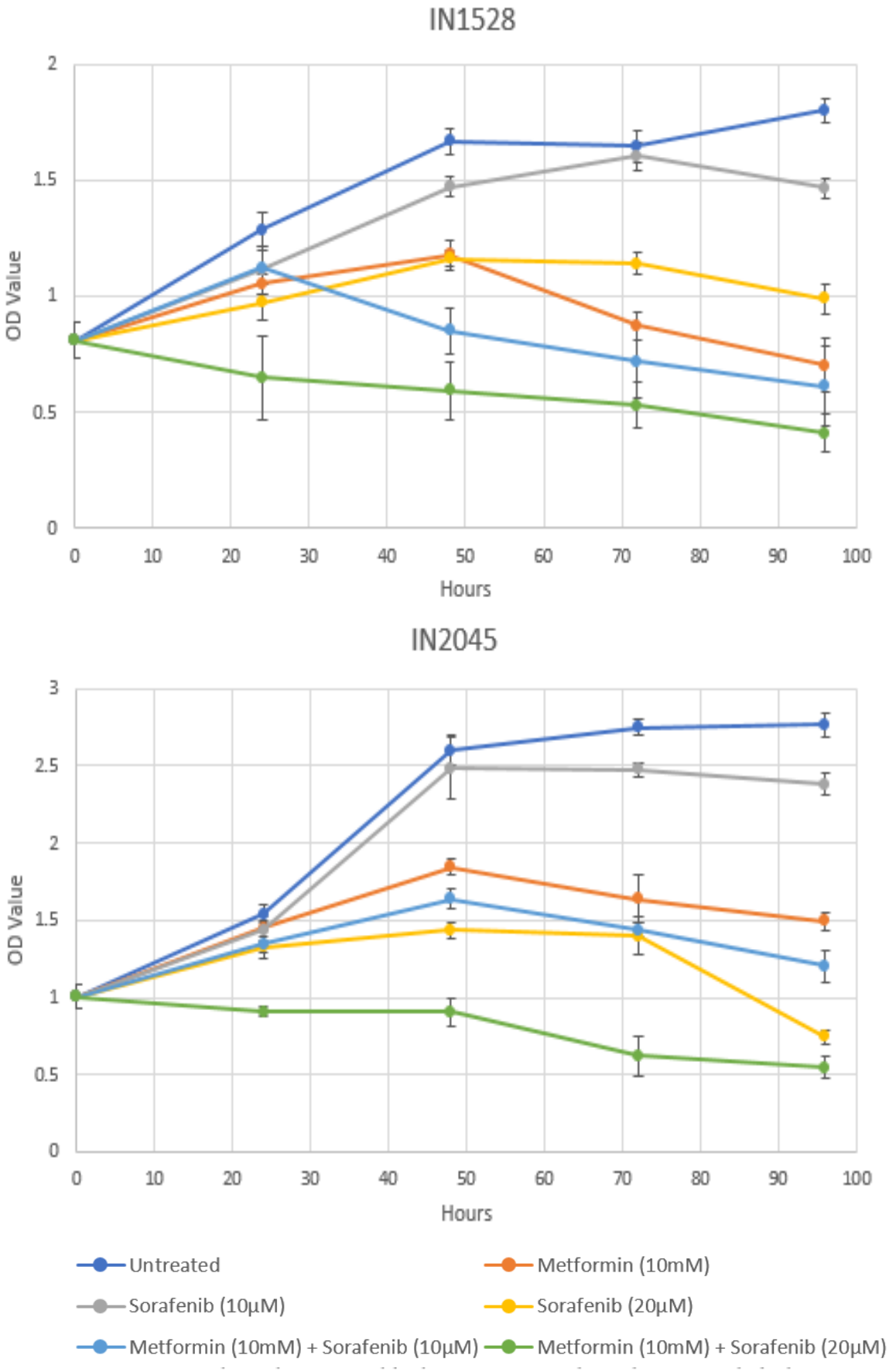

Figure 3.10b – Drug synergy analysis time course of metformin and sorafenib. Metformin and sorafenib were tested in solo and in combination over a 96-hour time course. Figure B shows IN1528 and IN2045. OD values were obtained every 24 over the time course. Error bars show the standard deviation of the replicate samples used.

3.2.4 Summary

3.2.4.1 Drug Synergy

Three of the drugs tested, TMZ, sodium oxamate and disulfiram, showed synergy in at least one culture. Disulfiram showed no synergy in any culture. The most effective combination was a synergistic effect when paired with sorafenib. This is in line with the response glioma stem cells reported by Aldea, et al, 2014. They hypothesized that the synergy was due to the separate target pathways of the two drugs working together to impact overall cell survival. The metformin affecting the cell through AKT/mTOR pathway and the sorafenib through RAF/MAPK, are two important cell signalling cascades with important roles in cell proliferation that have been reported as often dysregulated in GBM (Cheng *et al.*, 2009; Gao *et al.*, 2013). Aldea *et al.* (2014) hypothesised that there is interplay between member proteins of the pathways to act as a redundancy in case of tyrosine kinase inhibition and reduction in MAPK signalling. The failure of sorafenib to provide an advantage in GBM clinical trials was suggest as an example for this (Hainsworth *et al.*, 2010; Peereboom *et al.*, 2013). The strong synergistic response may also be due to the method metformin inhibit the mTOR pathway. Most inhibition of mTOR happens through activation of adenosine monophosphate- AMPK (Ben Sahra *et al.*, 2011). However, metformin is able to directly impact the mTOR pathway through increase mTORs affinity to bind with its regulatory associated protein, RAPTOR (Liu *et al.*, 2014). This increased affinity can be seen in the synergy time courses. Compared with sorafenib as a single treatment the combination of metformin and sorafenib could produce a larger inhibitory response than seen individually.

Sodium oxamate has been shown to synergise with phenformin in Miskimins, *et al.* 2014. This study utilized a range of cultures including breast, colon, lung, prostate, tonsil cancer as well as melanoma. In the GBM cultures tested only U251MG showed synergy, the rest of the culture panel all showed strong antagonism. One common factor between the two studies is the use of established cell lines. The cultures utilised by Miskimins, *et al.* 2014 were purchased from the American Type Culture Collection and there is no mention of the passage range used. It is possible that this response is linked to a change developed within cell lines. Oxamate acts through inhibition of LDH to reduce the conversion of pyruvate and stop the build-up of lactic acid in cell cystol (Zhai *et al.*, 2013). For cancer cells *in vivo*, lactic acidosis is common in the tumour microenvironment (Gatenby and Gillies, 2004). This state has been theorised to be used by the cancer cells to mitigate the immune response by allowing them to modulate the micro-environment pH through lactic acid secretion (Choi, *et al.* 2013). Utilisation of lactic acid in this way may be an attribute lost in the immortal cell lines, as it no longer suffers from the same target immune response as a selection pressure. This may explain the synergistic response only seen in U251MG.

Disulfiram showed no beneficial effect when combined with metformin. All cultures yielded an antagonistic result when the two drugs were used together in the presence of copper. In OSCC cells, the presence of metformin was shown to increase the tumour inhibiting properties of disulfiram and increase the concentration of copper in cytosol (Jivan et al 2015). Disulfiram has also already been shown to be a cytotoxic agent for GBM cell cultures (Liu, *et al.*

2012). Cellular response to metformin has been shown to be tumour-type dependent with variations in mechanisms and path -ways used (Babcook *et al.*, 2014; Adeberg *et al.*, 2017; Lindqvist *et al.*, 2018). The lack of a synergy result shown here could possibly be due to variations between GBM and OSCC.

There was variation in the response of GBM cultures to treatment with temozolomide and metformin. Three of the eight cultures showed a synergistic response, U251MG (CI=0.89), IN2045 (CI=0.93) and IN1760 (CI=0.92). There does not seem any reason why the three cultures showed a synergistic response and the rest strong antagonism. There was no clear factor to identify why the three cultures showed a synergistic response in comparison to the strong antagonism present in the remaining five cultures. When separated as a group the three share no common factor that sets them apart from the rest of the panel. All other cultures showed a strong antagonism in the drug combination (CI>1.1). Of the three cultures that showed synergism the strongest result was in U251MG (CI=0.89), the other two cultures had a combination index less than 0.1 from the separation point. The Chou-Talay method is relatively strict in its identification when separating synergy and antagonism. However additive effects are harder to identity under this method. Though the U251MG result is a synergistic response it could be that the other two cultures are showing an additive effect of the two drugs. Examining the separate ID_{50}s we see that both 1760 and 2045 have TMZ values of greater than 330μM. The Metformin ID_{50}s of the cultures are towards the lower end of the panel range, 11.59mM and 6.41mM. This difference of high TMZ ID_{50} and relatively low metformin ID_{50} could be the reason for the

additive effect seen here. U251 was the highest sensitivity to TMZ and second highest sensitivity to metformin this culture may be behaving differently due to genetic and metabolic differences of being a long-term cell culture (Torsvik, *et al.* 2014). IN1682 also possessed a TMZ ID_{50} in excess of 330μM however its metformin ID_{50} was higher (24.86mM).

The last factor to consider is the structure and half-life of TMZ. Rate of decay of TMZ to its intermediary form MITC is pH dependent and can become stable under acidic conditions (Baker, *et al.* 1999; Lopes, *et al.* 2013). Although fresh TMZ was added to cultures daily, the media was not changed, and acidic conditions may have been produced towards the end of the time course experiment. A variation between the pH of the cell culture media may lead to the difference in response to TMZ identified here. Measurement of pH changes in culture media across the time course would be an important factor to record for future studies

3.3 Glucose

Metformins use as a diabetic therapy reduces blood sugar levels and increases glucose uptake (Bailey, 2017). Results from 3.1.2.2 showed that GBM cultures benefitted from daily supplemental glucose and displayed reduced efficacy for metformin. To assess metformins effect on non-supplemented glucose levels in growth media it was measured over a time course. A reduced culture panel of six GBM and NHA was used due to limited resources and time.

3.3.1 Assessment of glucose in culture media

Assessment of glucose levels in growth media was done through adaptation of a diabetic blood glucose meter. Growth media is not the intended measurement medium for the device. Glucose standards with a range of different concentrations were generated in F10 media supplemented with FCS and PBS (as a comparative control) and assessed with the glucose meter and the results are listed in Table 3.15 and Figure 3.7. In both PBS and F-10, the glucose meter was able to detect the increases in glucose concentration. At higher glucose concentrations (>5.5mM), there was an overestimation of the amount of glucose in the tested sample. However, this was not seen to be significant (P=0.0802) deviation from the expected trend. The device was shown to be limited as it was insufficiently sensitive to detect glucose at concentrations below 1.0mM.

Table 3.15 – Glucose measurements from PBS and F-10

Concentration Glucose added to solution (mM)	Measured glucose quantity in PBS (mM)	Measured glucose quantity in Pan F-10 supplement with FCS (mM)
0.00	ER4	ER4 (±)
1.0	Lo1	Lo (±)
1.5	1.5 (±0.2)	1.6 (±0.2)
2.0	2.2 (±0.4)	2.4 (±0.2)
3.0	3.0 (±0.2)	3.2 (±0.2)
4.0	3.9 (±0.2)	4.4 (±0.2)
5.0	5.4 (±0.7)	5.4 (±0.3)
6.0	6.6 (±0.5)	7.0 (±0.8)
10.0	10.3 (±1.1)	11.1 (±0.6)

Lo relates to the reading on the display when any sample with less than 1.0mM glucose was samples. Any sample with a greater concentration of glucose could be detected and get an output reading from the machine. ER4 was what the machine displayed when given each medium with no supplementary glucose.

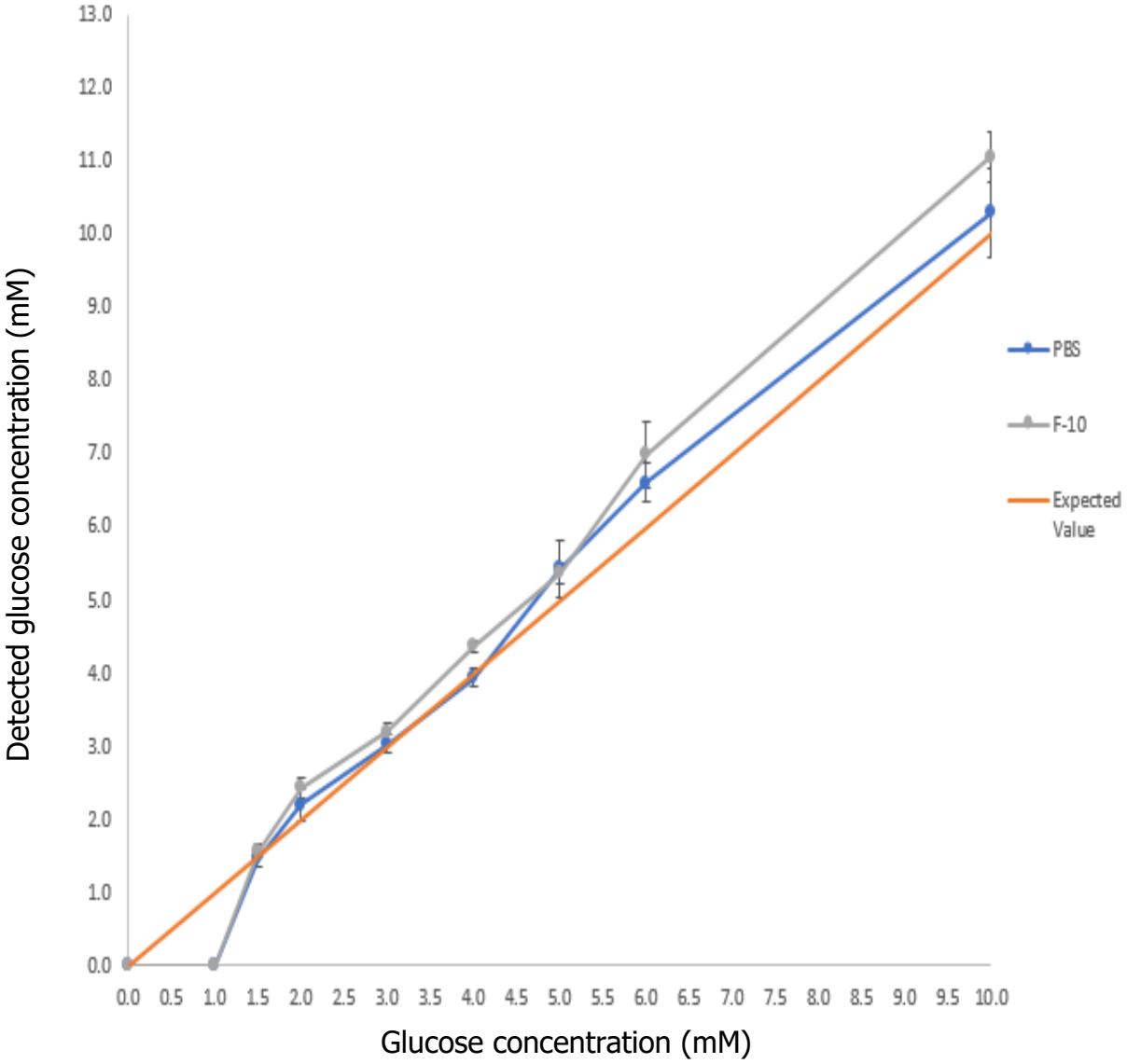

Figure 3.11 – Measured glucose reading from defined control standards. A range of glucose standards diluted in PBS and pans F-10 measured by a diabetic blood glucose meter. Expected value represents the concentration of glucose added to the solution deviations from this line represent inaccuracy in the devices reading.

The results displayed in Table 3.1 showed low standard deviations and indicates the suitability of the glucose meter for accurately measuring glucose values in cell media. It also demonstrates that the limit of detection for measuring glucose was 1.0mM glucose.

3.3.2 Measurement of media glucose over time

To assess the uptake of glucose by cells undergoing metformin treatment and to measure the effect of glucose on metformin sensitivity, GBM cultures were treated with the ID_{50} value of metformin in T25 flasks. Untreated control cells were grown in parallel and measurements of glucose were taken at 24-hour intervals. For this six GBM cell cultures and NHA were used. NHA was used to add a non-cancerous control. Two of the cultures, IN760 and IN1682 are both *P53* wild type cultures sensitive to metformin. Four of the cultures U251MG, IN859, IN1979 and IN2045 are all *P53* aberrant cultures. *P53* wild type cultures showed the greatest sensitivity to metformin the four cultures selected have ID_{50} values that cover the range of observer aberrant cultures. Of the aberrant cultures IN859 has the lowest metformin ID_{50} (4.52mM) and IN1979 has the highest (25.66mM).

The results of all the time course experiments are shown in Figure 3.12. All cultures displayed a similar pattern of glucose depletion over time. Glucose was depleted faster in metformin-treated samples compared to untreated controls, regardless of whether cells were grown in media supplemented with 6mM or 3mM glucose. All cultures tested with 3mM glucose and metformin expended glucoses to unmeasurable levels within 72 hours.

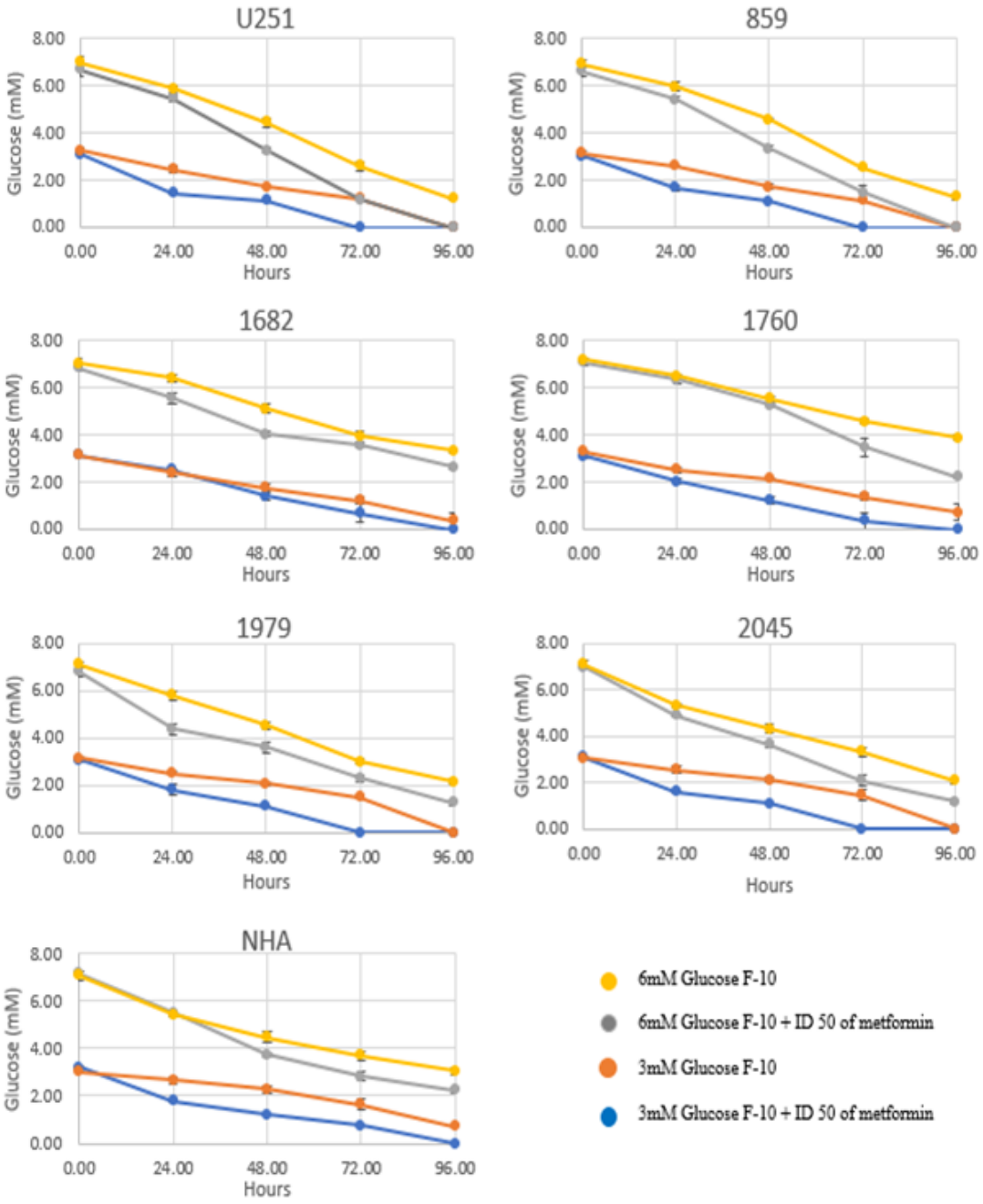

Figure 3.12 – Measurements of availability of glucose in growth media over time. Cultures started at 3mM or 6 mM glucose. Cultures were treated with metformin for 96 hours and compared against a vehicle control. All cultures showed decreasing levels of glucose over the time course.

3.3.3 Effects of low glucose concentrations on response to metformin treatment

Five GBM patient derived short-term cultures were used to investigate the effect of low glucose conditions on the sensitivity of cultures to metformin. This smaller cohort of cultures was representative of the panel containing two *P53* wild type short term cultures (IN1682 and IN1760), three *P53* aberrant short-term cultures (IN859, IN1979 and IN2045), one *P53* aberrant established cell line (U2351MG) and NHA as a normal cell control. The cultures were used for all investigations of potential mechanisms of cell death induced by metformin in Section 3.4. GBM cells were grown in Pan F-10 supplemented with 3mM glucose and treated with metformin for 96 hours. Results were compared against ID_{50} values from standard F-10 growth media (6mM glucose) as described in Table 3.2. To confirm the suitability of the Pan F-10 formulation, the ID_{50} values of metformin in Pan F-10 supplemented with 6 mM glucose was also assessed. This data is summarised in Table 3.16. All GBM cell cultures demonstrated a reduction ID_{50} values when the glucose concentration of the media was lowered to 3mM. Three cultures showed significant reductions in the ID_{50} values, U251MG, IN859 and IN1979. The only remaining *P53* mutant, IN2045, showed the largest reduction in ID_{50} value (-62%) but due to high standard deviation this result was not significant.

Table 3.16 Metformin ID50 values for GBM cells grown in low glucose conditions (3mM)

Culture	ID_{50} values PAN[1] + 3mM	PAN[1] + 6mM Glucose	% Change in ID_{50}[2]	P-value	Gibco (6mM)[3]
U251MG	2.3 (±1.15)	5.2 (±3.65)	-53%	0.0336*	4.83 (±2.11)
IN859	1.8 (±1.09)	4.01 (±4.21)	-61%	0.0189*	4.52(±0.6)
IN1979	18.6(±1.22)	28.51 (±4.9)	-27%	0.0396*	25.66 (±3.84)
IN2045	2.41 (±3.2)	5.23 (±2.64)	-62%	0.1244	6.41 (±3.5)
IN1682	19.3 (±1.5)	26.7 (±2.54)	-22%	0.0396	24.87 (±5.41)
IN1760	8.05(±1.2)	14.8 (±3.97)	-31%	0.1244	11.59 (±5.05)
NHA	78.3(±7.63)		-7%	0.5285	84.3 (±8.50)

[1]Pan F-10 formulation contains no glucose. [2]Changes in ID50 value when comparing Pan+3mM glucose with Gibco F-10 (6mM) [3]Results for standard Gibco F-10growth media found in table 3.2.

3.3.4 Summary

The glucose values detected by the glucose meter in Pan F-10 varied slightly from the expected standard but the difference was not statistically significant (P=0.0802). However, the glucose meter has a limit of detection for measuring low concentrations of glucose (<1mM). Measurements of glucose over the 96-hour time course showed an increase in the depletion rate of glucose when cells were grown in the presence of metformin at ID_{50} concentrations. In U251MG, IN859 and IN1760, at the 72 and 96-hour readings, metformin caused a reduction in glucose concentration to levels 24-hours earlier than glucose readings measured by the untreated sample. The mechanism responsible for this depletion is unclear, although this observation is consistent with the original 1956 name of metformin; glucophage (Bailey, *et al.* 2004). This reduction in media glucose concentration may be due to metformin

increasing the cellular uptake of glucose (Sinnett-Smith *et al.* 2014; Saisho, 2015; Niccoli, *et al.*, 2016).

3.4 Mechanisms of cell death induced by metformin

Metformins mechanism of anti-tumour action are still not fully elucidated (Chae *et al.*, 2016). It has been identified to inhibit complex I on the election transport chain (Jiang *et al.*, 2016). The use of mechanisms has been shown to diverge based on the type cancer; the inhibition of mTOR through AMPK activation has been shown to be a dependency for tumour inhibition in several cancers and independent in other (Liu *et al.*, 2014). Identifying specific mechanism and pathways through which metformin acts on GBM is an important factor to assess its potential use as a cancer therapy. This was assessed through use of flow cytometry and functional assays.

3.4.1 Cell cultures

Five GBM patient-derived short-term cultures were used to investigate mechanisms through which metformin induces cytotoxicity. This cohort was augmented with the GBM cell line U251MG and NHA as a non-cancerous control. A summary of the features of the cultures is given in Table 3.17. This smaller cohort was selected to maintain the range and diversity of the original panel whilst enabling greater depth and focus of the study. IN859 and IN2045 represented mutant *P53* cultures. Cultures IN1682 and IN1760 are both *P53* wild types. U251MG is a *P53* mutant used as a cell line comparative control and NHA was used as a non-cancerous control. The cells are also representative of the larger panel regarding metformin sensitivity and doubling time.

Table 3.17 List of characteristics for tumours selected for flow cytometry analysis

Culture	*P53* Status[1]	*MGMT* status	Doubling time[2]	Metformin ID_{50}[3]
U251MG	Aberrant	Partial methylation	24	4.83 (±2.11)
IN859	Aberrant	Methylation	24	4.52 (±0.6)
IN2045	Aberrant	Partial methylation	36	6.41 (±3.5)
IN1682	Wild type	-	50	24.87 (±5.41)
IN 1760	Wild type	Partial methylation	40	11.59 (±5.05)
NHA	Wild type	Unmethylated	63	84.3 (±8.50)

[1]The mutation status of *P-53*; [2]Doubling time in hours; [3]ID50 of drugs after 96 hours treatment given in mM concentrations

3.4.2 Induction of apoptosis

Apoptosis was assessed by cellular staining with Annexin V and 7-AAD followed by flow cytometric analysis. For this technique, apoptosis was determined by tracking progression of cell populations through three predefined gated quadrants and an example of this progression can be seen in Figure 3.13. Separation by quadrants allows for division of the cell population based upon positive binding of appropriate fluorophores. The lower left quadrant represents live cells with a negative binding for both chemicals. The lower right quadrant indicates positive binding of annexin V to phospholipid phosphatidylserine. This protein, normally held facing the cytosolic (inner) of the cell membrane, is important for extracellular signalling in apoptotic pathways (Segawa and Shigekazu, 2015). The proteins become exposed as an early indicator for cellular apoptosis (Koopman *et al.*, 1994). However, once the cell enters the later stages of cell death, the cell membrane inevitably becomes permeable allowing the annexin V to diffuse into the cystol and reach the internal membrane. The second dye, 7-AAD, is used to distinguish between healthy cells and dead cells. 7AAD is a DNA binding agent that

intercalates between cytosine and guanine bases (Xiucai *et al.*, 1991; Philpott *et al.*, 1996). However, it is unable to normally bypass the cellular membrane. This defines 7-AAD negative cells as possessing a functional membrane and 7-AAD positive cells (upper two quadrants) possessing damaged cellular membranes.

Early apoptosis would then be identified by binding of annexin V, resulting in an increase in the FL2 channel. An increase in FL3 indicates that 7-AAD-A can cross into the cell and that the cellular membrane has been compromised, equivalent to late stage cell death. To confirm apoptosis, the cells must be measured over time a course to detect shifts in the cell populations as shown in Figure 3.13. The technique is unable to define the mechanism of cell death once the cells reach the upper right quadrant. In the later stages of necrosis, autophagy and apoptosis, the membrane has the same permeability and hence, this method is unable to distinguish the different cells. The possible outcomes from flow cytometric analysis are summarised in Table. 3.18

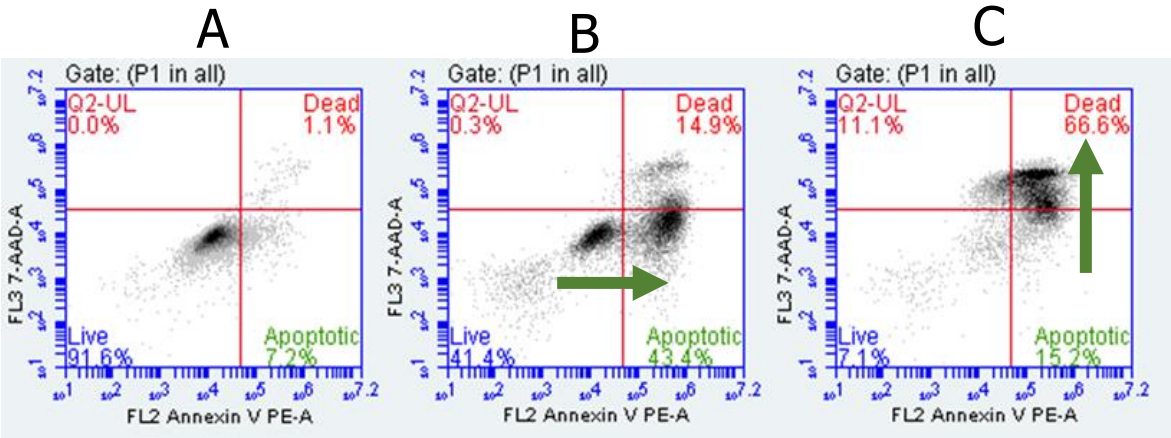

Figure 3.13 Identification of apoptosis across a time course through flow cytometry. A: Untreated samples showing a strong population in the bottom left quadrant. B: Samples treated with camptothecin for 72 hours. A new population in the bottom right apoptotic quadrant indicates binding of annexin V with no damage to permeability of cell membrane. This is a strong positive detection of apoptosis. C: Camptothecin treated cells at 96 hours. Population has shifted into the top right dead quadrant. Cells are confirmed as dead as membrane has become permeable and 7-AAD is able stain DNA.

Table 3.18 Interpretation of binding of the different fluorochromes to measure apoptosis

Quadrant	Label	Annexin V (FL2)	7-AAD (FL1)
Lower left	Live cells	Negative	Negative
Lower right	Apoptotic cells	Positive	Negative
Upper right	Dead cells	Positive	Positive
Upper left	Permeable membrane/Necrotic cells	Negative	Positive

Describes the potential outcomes from flow cytometry analysis of apoptosis

Analysis of cell membranes for apoptotic markers was completed over a 96-hour time course. Readings were taken at intervals of 24 hours for a period of 96 hours for all samples. Cultures were treated at the ID_{50} value for metformin and growth media containing either high (6mM) or low (3mM) concentrations of glucose and compared with an untreated control (using water as a vehicle). For all cultures, 72 hours treatment with 100μM camptothecin was used as a positive control for induction of apoptosis. Figure 3.14 shows a comparison of an apoptotic positive result with an untreated control. Figure 3.15a and 3.15b show an example of a completed apoptotic time course.

A) Untreated

B) Treated

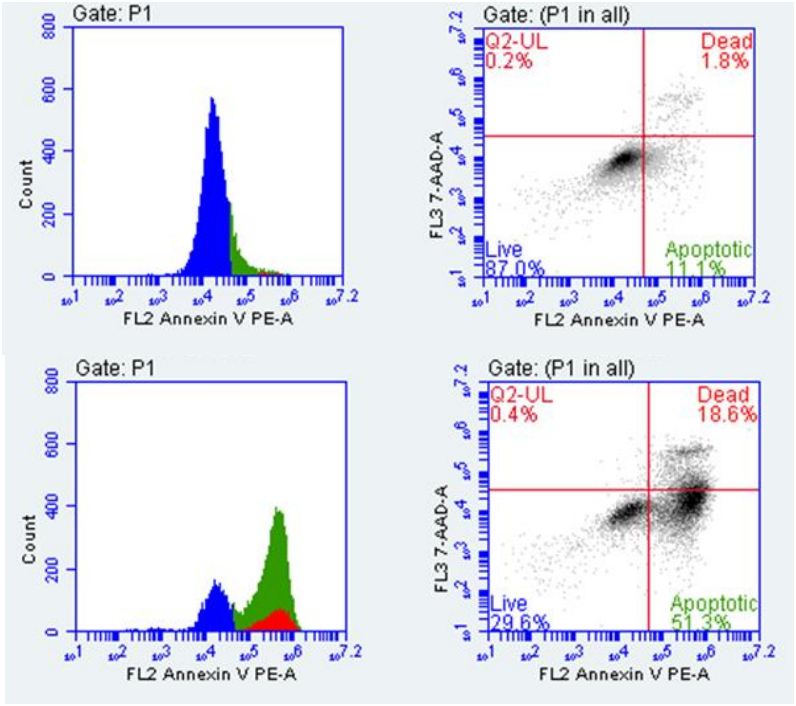

Figure 3.14. Apoptosis was induced in U251MG using 100μM camptothecin over a 96-hour period. A) Untreated control cells. Limited positive binding of annexin V. B) Camptothecin induced apoptosis. Large population in bottom right quadrant. Dead cell population also increased. Coloration in graph indicates quadrant. Blue – Live cells, Green – apoptotic cells, Red – Dead cells.

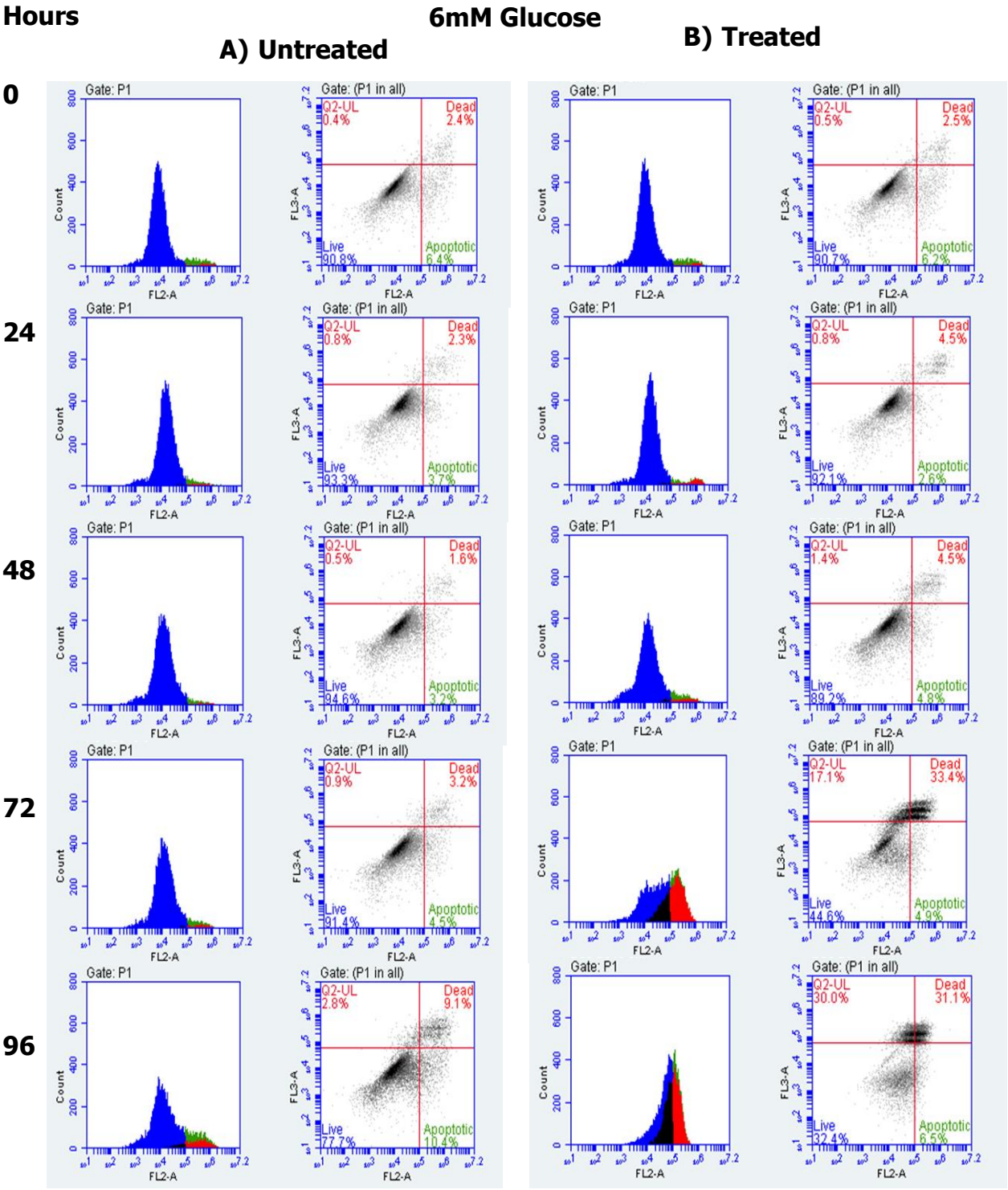

Figure 3.15a 96-hour apoptotic time course of IN2045 treated with metformin in 6mM culture media. A) Untreated samples. Minimal variation in the live cell population over the time course. No increase in apoptosis. B) ID50 metformin treated samples. After 72 hours of metformin treatment dead cell population rises rapidly. No sign of generation of apoptotic population. Coloration in graph indicates quadrant. Blue – Live cells, Green – apoptotic cells, Red – Dead cells.

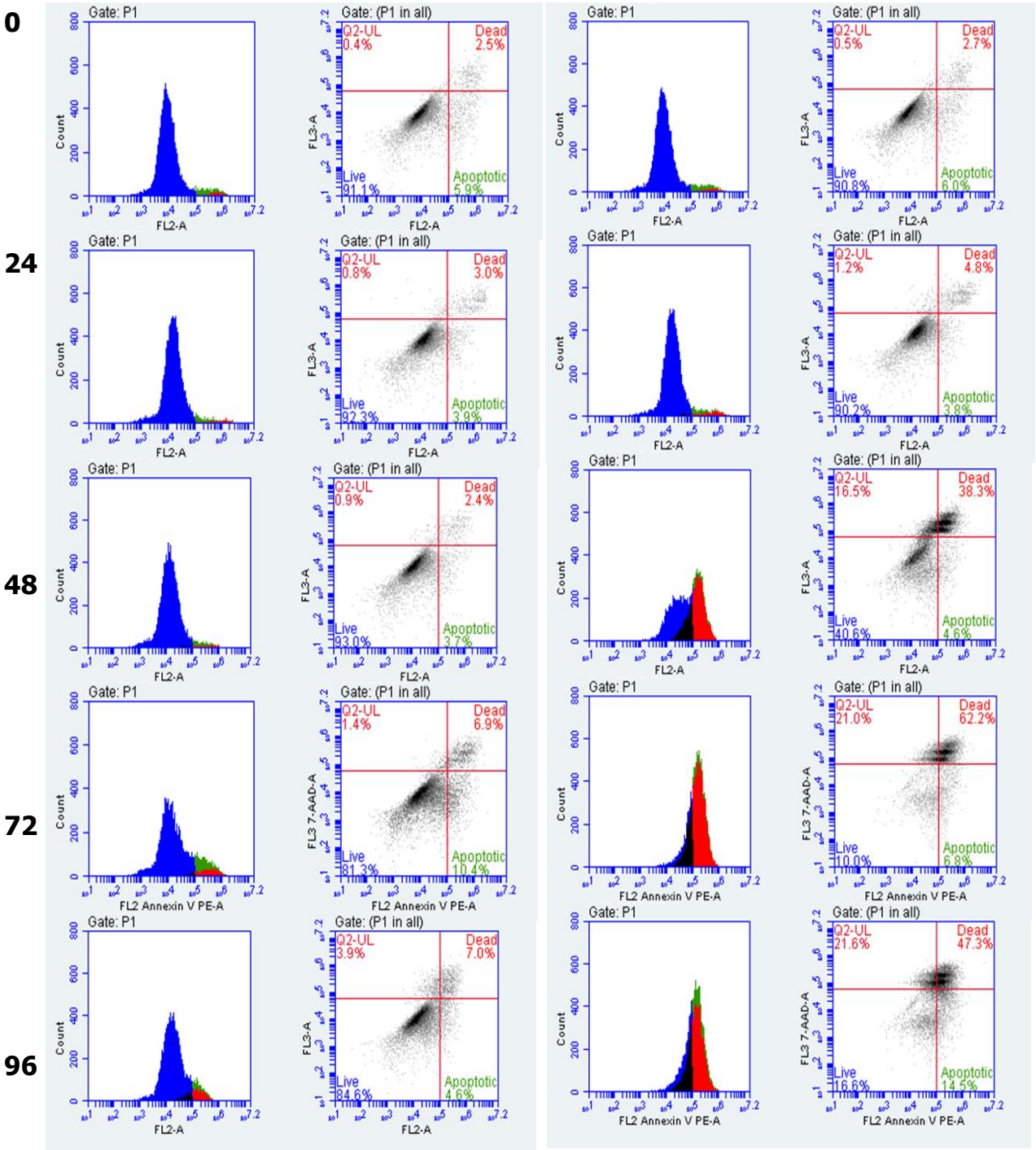

Figure 3.15b 96-hour apoptotic time course of IN2045 treated with metformin in 3mM culture media. A) Untreated samples. Minimal variation in the live cell population over the time course. No increase in apoptosis. B) ID50 metformin treated samples. After 72 hours of metformin treatment dead cell population rises rapidly. No sign of generation of apoptotic population. Coloration in graph indicates quadrant. Blue – Live cells, Green – apoptotic cells, Red – Dead cells.

Figure 3.15a shows that when IN2045 cells are grown in media containing 6mM glucose, metformin induced cell death appears after 72 hours of drug treatment. No apoptotic sub-population is detected across the time course. In the progression from 72 to 96 hours, the dead population increased above 30% although there was no increase in annexin V uptake. At the 96-hour time point a population is present in the upper left region. This quadrant indicates binding of 7-AAD without positive binding of annexin V and is indicative of possible necrotic cell death. Figure 3.15b shows a 96-hour time course of IN2045 grown in media containing 3mM glucose and the ID_{50} concentration of metformin. There was no induction of apoptosis or increase in cell death in untreated cultures. However, in the metformin treated cells, a large dead cell population was evident after 48 hours. Across the time course there was no increase in the apoptotic population but progression of cells from lower left quadrant directly to upper right quadrant. The live cell population was reduced to a minority after 72 hours. In comparison to the camptothecin induced positive control illustrated given in Figure 3.14, the population of cells in Figures 3.15a and 3.15b transition from a live state to death without progressing through the apoptotic quadrant. Figures 3.16, 3.17, 3.18, 3.19, 3.20 and 3.21 show data at different time points for each culture time course with different treatment types. Across all time courses there was no clear progression of cells through the three quadrants (Live cells --> Apoptotic cells --> Dead cells). No significant ($p<0.05$) change in the apoptotic quadrant was observed in any of the treatment conditions. However, all GBM cultures

showed significant population differences in the live and dead cells populations after 96 hours of treatment with metformin. NHA showed significant changes in both 6mM and 3mM live population but not in either dead population. Additional apoptotic time course for all cultures found in Appendix H.

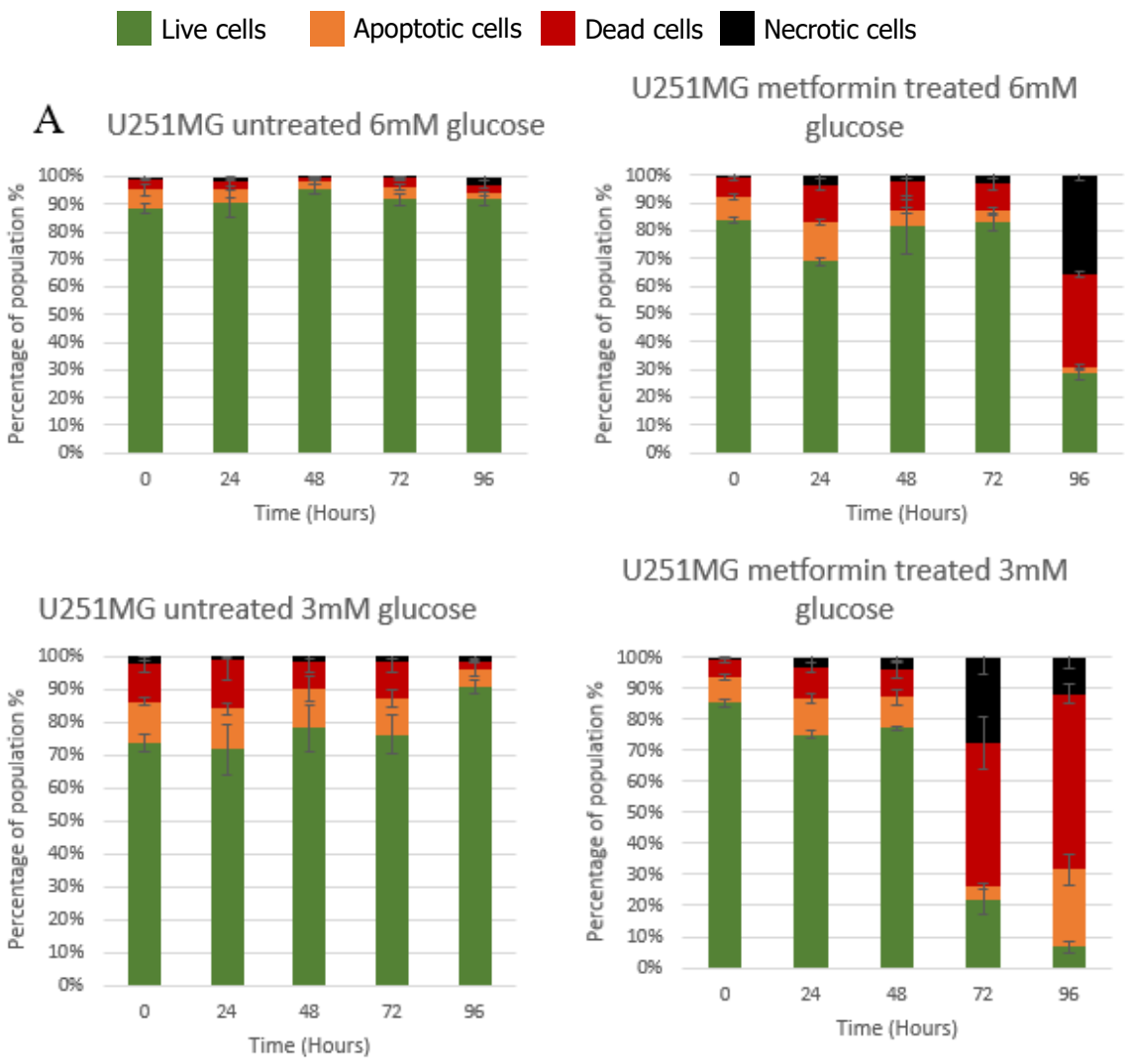

B

U251MG p-values 6mM glucose Untreated - Treated					
	0	24	48	72	96
Live cells	0.0358*	0.0342*	0.2724	0.0213*	0.0015*
Apoptotic Cells	0.245	0.2649	0.2228	0.1979	0.184
Dead cells	0.0946	0.0368*	0.2704	0.579	0.0056*
Necrotic Cells	0.6128	0.1022	0.2395	0.0972	0.008**

U251MG p-values 3mM glucose Untreated - Treated					
	0	24	48	72	96
Live cells	0.0161*	0.6466	0.8988	0.039*	0.0017*
Apoptotic Cells	0.0287*	0.7056	0.4414	0.1735	0.0634
Dead cells	0.0904	0.551	0.889	0.089	0.0041*
Necrotic Cells	0.466	0.2428	0.2809	0.0433*	0.0966

Figure 3.16a Apoptotic time courses for U251MG over 96 hours. A) Time course results. Coloured segments show % of cell population gated at each time point. Colours represent gating: Green – live cells, Orange – Apoptotic cells, Red – Dead cells, Black – Necrotic cells B) p-value results for statistical comparisons of each untreated and treated time point. Each level of statistical significance is denoted with a *.

U251MG										
6mM Glucose	Untreated					6mM Glucose	Treated			
%	0hr	24hr	48hr	72hr	96hr	%	0hr	24hr	48hr	72hr	96hr
Live cells	88.46	90.5	94.8	91.63	91.8	Live cells	83.73	68	81.36	82.8	28.76
Apoptotic cells	6.73	5	3.1	4.46	2	Apoptotic cells	8.73	14.5	5.1	4.1	2.13
Dead cells	3.96	2.5	1.16	3.266	3.43	Dead cells	6.56	13.2	10.7	9.7	33.7
Necrotic cells	0.83	1.8	0.4	0.6	2.8	Necrotic cells	1.2	3.4	2.16	3.33	36.06
3mM Glucose	Untreated					3mM Glucose	Treated			
%	0hr	24hr	48hr	72hr	96hr	%	0hr	24hr	48hr	72hr	96hr
Live cells	73.9	71.6	78.13	76.3	90.8	Live cells	85.43	75.16	77.16	22.13	6.6
Apoptotic cells	12.4	12.46	12.23	11.1	5.26	Apoptotic cells	8.4	11.63	10	4.167	25.03
Dead cells	11.5	14.96	8.167	10.87	2.6	Dead cells	5.4	9.86	9.1	46.1	56.6
Necrotic cells	2.16	0.9	1.433	1.767	1.33	Necrotic cells	0.8	3.3	3.73	27.6	11.8

Figure 3.16b Apoptotic time course figures for U251MG over 96 hours. Averaged numerical data for apoptotic time course. Cells grown in 3mM or 6mM glucose growth media were treated with or without metformin. Populations were measured every 24 hours by flow cytometry to assess levels of apoptosis. Values represent the percentage of the total population that fell within each gated quadrant. Colours represent gating: Green – live cells, Orange – Apoptotic cells, Red – Dead cells, White – Necrotic cells.

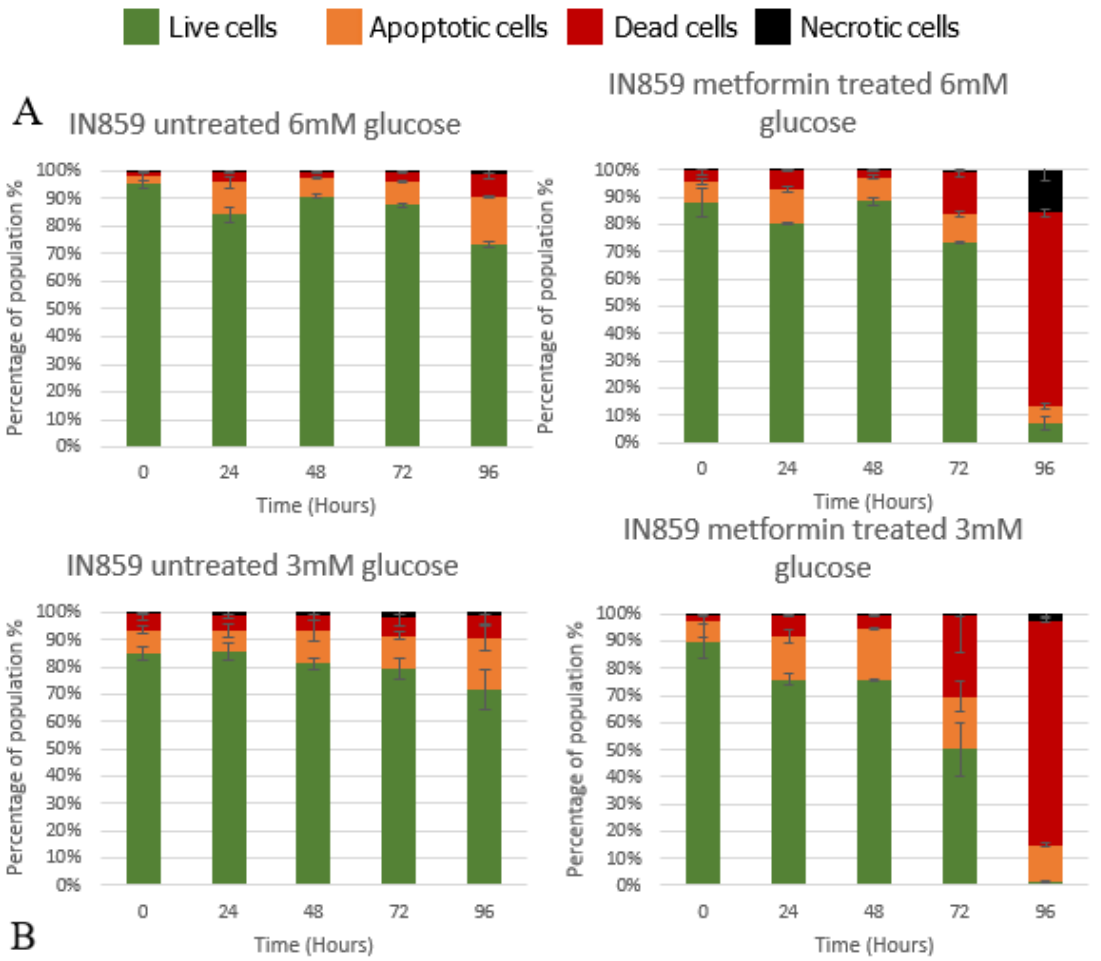

IN859 p-values 6mM glucose Untreated - Treated					
	0	24	48	72	96
Live cells	0.2057	0.3327	0.4226	0.0081**	0.0014**
Apoptotic Cells	0.1858	0.5118	0.4226	0.2733	0.2544
Dead cells	0.1798	0.0546	0.1296	0.0352*	0.0016**
Necrotic Cells	0.4226	1	0.667	0.4738	0.0537

IN859 p-values 3mM glucose Untreated - Treated					
	0	24	48	72	96
Live cells	0.5073	0.1327	0.1753	0.1617	0.0107*
Apoptotic Cells	0.7322	0.1647	0.2509	0.2463	0.4074
Dead cells	0.2902	0.329	0.7829	0.2916	0.0023**
Necrotic Cells	0.6697	0.4726	0.2932	0.0928	0.3075

Figure 3.17a Apoptotic time courses for IN859 over 96 hours. A) Time course results. Coloured segments show % of cell population gated at each time point. Colours represent gating: Green – live cells, Orange – Apoptotic cells, Red – Dead cells, Black – Necrotic cells B) p-value results for statistical comparisons of each untreated and treated time point. Each level of statistical significance is denoted with a *.

IN859										
6mM Glucose	Untreated					6mM Glucose	Treated			
%	0hr	24hr	48hr	72hr	96hr	%	0hr	24hr	48hr	72hr	96hr
Live cells	95.2	84.2	90.7	87.6	73.5	Live cells	86.4	80.5	88.6	73.2	7.2
Apoptotic cells	3	11.6	7	8.4	17.1	Apoptotic cells	7.4	12.5	8.7	10.7	6.4
Dead cells	1.4	3.8	1.8	3.6	8.3	Dead cells	4.2	6.5	2.3	15.4	70.6
Necrotic cells	0.4	0.4	0.5	0.4	1.1	Necrotic cells	0.4	0.4	0.3	0.6	15.7
3mM Glucose	Untreated					3mM Glucose	Treated			
%	0hr	24hr	48hr	72hr	96hr	%	0hr	24hr	48hr	72hr	96hr
Live cells	85.3	85.4	81.1	79.2	71.7	Live cells	89.8	75.9	75.7	50.2	1.3
Apoptotic cells	8.9	7.6	12.1	12.3	19.1	Apoptotic cells	7.2	15.8	18.7	19.2	13.5
Dead cells	5.9	6.1	5.6	6.9	8	Dead cells	2.1	7.7	5.2	29.7	82.7
Necrotic cells	0.5	0.8	1	1.4	1.1	Necrotic cells	0.7	0.4	0.2	0.8	2.4

Figure 3.17b Apoptotic time course figures for IN859 over 96 hours. Averaged numerical data for apoptotic time course. Cells grown in 3mM or 6mM glucose growth media were treated with or without metformin. Populations were measured every 24 hours by flow cytometry to assess levels of apoptosis. Values represent the percentage of the total population that fell within each gated quadrant. Colours represent gating: Green – live cells, Orange – Apoptotic cells, Red – Dead cells, White – Necrotic cells.

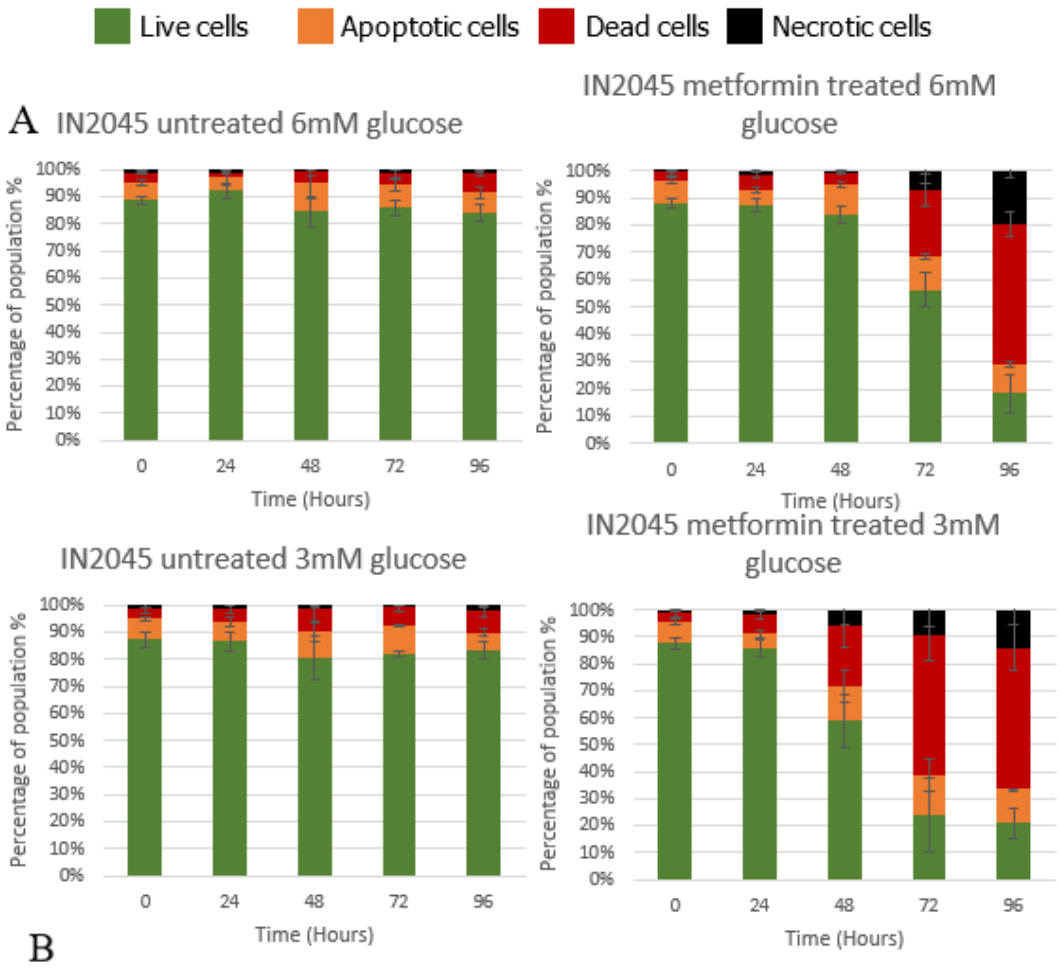

IN2045 p-values 6mM glucose Untreated - Treated					
	0	24	48	72	96
Live cells	0.1164	0.2372	0.7693	0.0785	0.0083**
Apoptotic Cells	0.6784	0.5207	0.8249	0.4037	0.8047
Dead cells	0.9483	0.0411*	0.9857	0.0739	0.0127*
Necrotic Cells	0.5225	0.5254	0.7757	0.3413	0.0114*

IN2045 p-values 3mM glucose Untreated - Treated					
	0	24	48	72	96
Live cells	0.7284	0.3676	0.2911	0.0586	0.0177*
Apoptotic Cells	0.2799	0.1736	0.2925	0.5209	0.0726
Dead cells	0.7418	0.0284*	0.37744	0.0583	0.0495*
Necrotic Cells	0.4522	0.3175	0.4229	0.2836	0.108

Figure 3.18a Apoptotic time courses for IN2045 over 96 hours. A) Time course results. Coloured segments show % of cell population gated at each time point. Colours represent gating: Green – live cells, Orange – Apoptotic cells, Red – Dead cells, Black – Necrotic cells B) p-value results for statistical comparisons of each untreated and treated time point. Each level of statistical significance is denoted with a *.

IN2045										
6mM Glucose	Untreated					6mM Glucose	Treated			
%	0hr	24hr	48hr	72hr	96hr	%	0hr	24hr	48hr	72hr	96hr
Live cells	88.7	92.2	84.7	86	84.1	Live cells	88	87.1	83.9	56.3	18.5
Apoptotic cells	6.8	4.8	10.4	8.2	7.4	Apoptotic cells	8.1	5.8	11.1	12.4	10.4
Dead cells	3.5	1.7	4.2	4.7	7.1	Dead cells	3.4	5.5	4.2	24.1	51.3
Necrotic cells	0.9	1.1	0.6	0.9	1.2	Necrotic cells	0.4	1.5	0.7	7.1	19.7
3mM Glucose	Untreated					3mM Glucose	Treated			
%	0hr	24hr	48hr	72hr	96hr	%	0hr	24hr	48hr	72hr	96hr
Live cells	87.3	86.7	80.9	82	83.3	Live cells	87.5	85.9	59	24.1	20.9
Apoptotic cells	7.6	7.1	9.4	10.4	6.7	Apoptotic cells	8.1	5.3	12.6	14.6	12.5
Dead cells	3.8	5	8.8	6.8	8	Dead cells	3.8	7.2	22.2	52.1	52.4
Necrotic cells	1.2	1.1	0.8	0.6	2	Necrotic cells	0.5	1.6	6	9	14.1

Figure 3.18b Apoptotic time course figures for IN2045 over 96 hours. Averaged numerical data for apoptotic time course. Cells grown in 3mM or 6mM glucose growth media were treated with or without metformin. Populations were measured every 24 hours by flow cytometry to assess levels of apoptosis. Values represent the percentage of the total population that fell within each gated quadrant. Colours represent gating: Green – live cells, Orange – Apoptotic cells, Red – Dead cells, White – Necrotic cells.

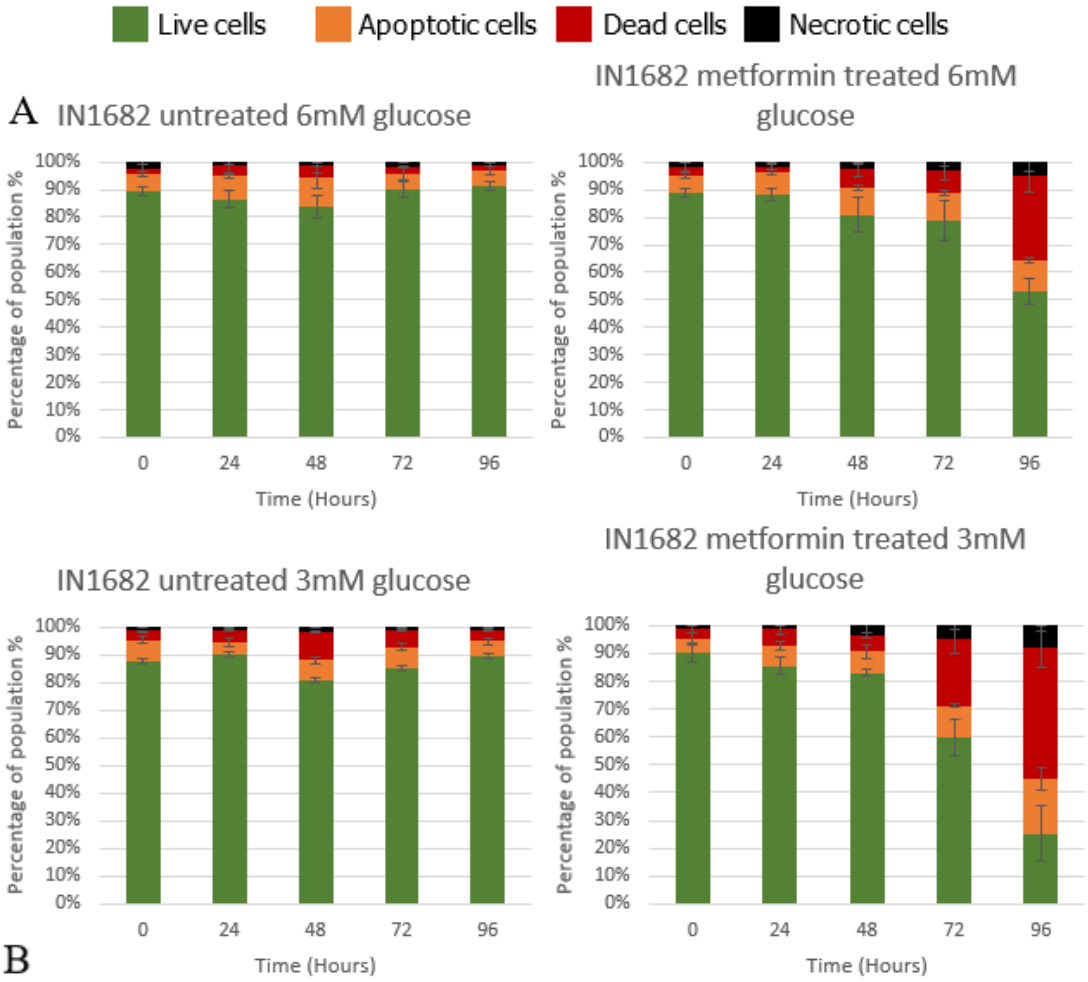

IN1682 p-values 6mM glucose Untreated - Treated					
	0	24	48	72	96
Live cells	0.8859	0.7258	0.4013	0.1698	0.0186*
Apoptotic Cells	0.4575	0.8327	0.4226	0.1836	0.2829
Dead cells	0.11	0.5075	0.3201	0.274	0.0479*
Necrotic Cells	0.4626	0.7324	0.2133	0.3047	0.393

IN1682 p-values 3mM glucose Untreated - Treated					
	0	24	48	72	96
Live cells	0.5877	0.1408	0.4433	0.0066**	0.0429*
Apoptotic Cells	0.4622	0.1939	0.9768	0.2172	0.1411
Dead cells	0.6027	0.0728	0.1774	0.0354*	0.038*
Necrotic Cells	0.5862	0.7295	0.5499	0.0572	0.0742

Figure 3.19a Apoptotic time courses for IN1682 over 96 hours. A) Time course results. Coloured segments show % of cell population gated at each time point. Colours represent gating: Green – live cells, Orange – Apoptotic cells, Red – Dead cells, Black – Necrotic cells B) p-value results for statistical comparisons of each untreated and treated time point. Each level of statistical significance is denoted with a *.

IN1682										
6mM Glucose	Untreated					6mM Glucose	Treated			
%	0hr	24hr	48hr	72hr	96hr	%	0hr	24hr	48hr	72hr	96hr
Live cells	89.2	86.5	83.7	90	91.5	Live cells	89	88.4	81	78.7	52.8
Apoptotic cells	6.4	8.3	10.8	5.6	5.4	Apoptotic cells	6	7.7	9.8	10.3	11.5
Dead cells	2.1	3.8	4.2	2.6	2	Dead cells	3.5	2.2	6.6	7.7	30.8
Necrotic cells	2.1	1.3	1.2	1.7	0.9	Necrotic cells	1.5	1.6	2.6	3.1	4.7
3mM Glucose	Untreated					3mM Glucose	Treated			
%	0hr	24hr	48hr	72hr	96hr	%	0hr	24hr	48hr	72hr	96hr
Live cells	87.5	90	80.5	85.2	89.2	Live cells	90.3	85.4	82.9	59.8	25.3
Apoptotic cells	7.6	4.1	7.5	7.4	5.6	Apoptotic cells	4.9	7.2	7.6	11.3	19.5
Dead cells	3.3	4.5	10.1	6.1	4.2	Dead cells	3.8	6.4	5.8	23.9	47.4
Necrotic cells	1.4	1	1.8	1.1	0.9	Necrotic cells	0.9	0.9	3.5	4.8	7.6

Figure 3.19b Apoptotic time course figures for IN1682 over 96 hours. Averaged numerical data for apoptotic time course. Cells grown in 3mM or 6mM glucose growth media were treated with or without metformin. Populations were measured every 24 hours by flow cytometry to assess levels of apoptosis. Values represent the percentage of the total population that fell within each gated quadrant. Colours represent gating: Green – live cells, Orange – Apoptotic cells, Red – Dead cells, White – Necrotic cells.

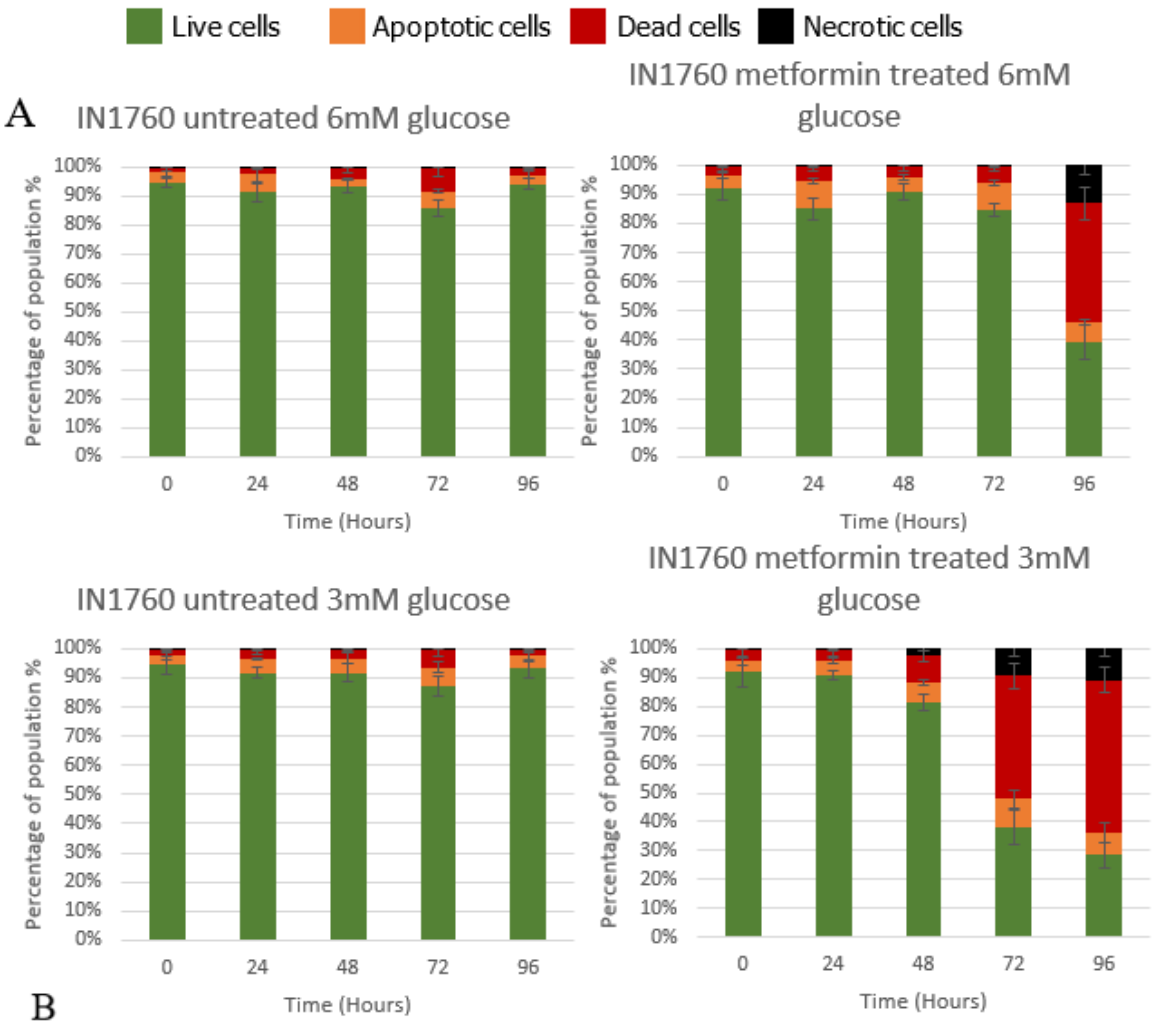

B

IN1760 p-values 6mM glucose Untreated - Treated					
	0	24	48	72	96
Live cells	0.3986	0.0114*	0.1045	0.663	0.0183*
Apoptotic Cells	0.1835	0.1856	0.2947	0.4226	0.2524
Dead cells	0.4036	0.1832	0.8539	0.3554	0.022*
Necrotic Cells	0.2893	0.4226	0.6254	0.6349	0.0573

IN1760 p-values 3mM glucose Untreated - Treated					
	0	24	48	72	96
Live cells	0.3873	0.272	0.0049*	0.0326*	0.0102*
Apoptotic Cells	0.7295	0.7515	0.1571	0.4687	0.492
Dead cells	0.4385	0.5665	0.0173*	0.0156*	0.0079*
Necrotic Cells	0.4226	0.4226	0.0419*	0.0626	0.0543

Figure 3.20a Apoptotic time courses for IN1760 over 96 hours. A) Time course results. Coloured segments show % of cell population gated at each time point. Colours represent gating: Green – live cells, Orange – Apoptotic cells, Red – Dead cells, Black – Necrotic cells B) p-value results for statistical comparisons of each untreated and treated time point. Each level of statistical significance is denoted with a *.

IN1760										
6mM Glucose	Untreated					6mM Glucose	Treated			
%	0hr	24hr	48hr	72hr	96hr	%	0hr	24hr	48hr	72hr	96hr
Live cells	94.3	91.1	93	85.6	93.8	Live cells	91.8	85	90.7	84.5	39.2
Apoptotic cells	3.7	6.6	2.8	5.8	3.3	Apoptotic cells	4.5	9.5	5.1	9.2	6.7
Dead cells	1.1	1.8	3.3	7.9	2.2	Dead cells	3.1	5	3.4	5.5	40.9
Necrotic cells	0.8	0.4	0.8	0.5	0.6	Necrotic cells	0.5	0.3	0.7	0.6	13.1
3mM Glucose	Untreated					3mM Glucose	Treated			
%	0hr	24hr	48hr	72hr	96hr	%	0hr	24hr	48hr	72hr	96hr
Live cells	94.2	91.8	91.7	87.3	93.3	Live cells	92	90.8	81.4	37.9	28.4
Apoptotic cells	3.6	4.7	4.8	6.2	4.1	Apoptotic cells	3.7	5.1	6.8	10	8
Dead cells	1.3	3	2.9	5.7	2	Dead cells	3.7	3.5	9.2	42.8	52.6
Necrotic cells	0.6	0.5	0.4	0.6	0.6	Necrotic cells	0.4	0.4	2.5	9.2	10.9

Figure 3.20b Apoptotic time course figures for IN1760 over 96 hours. Averaged numerical data for apoptotic time course. Cells grown in 3mM or 6mM glucose growth media were treated with or without metformin. Populations were measured every 24 hours by flow cytometry to assess levels of apoptosis. Values represent the percentage of the total population that fell within each gated quadrant. Colours represent gating: Green – live cells, Orange – Apoptotic cells, Red – Dead cells, White – Necrotic cells.

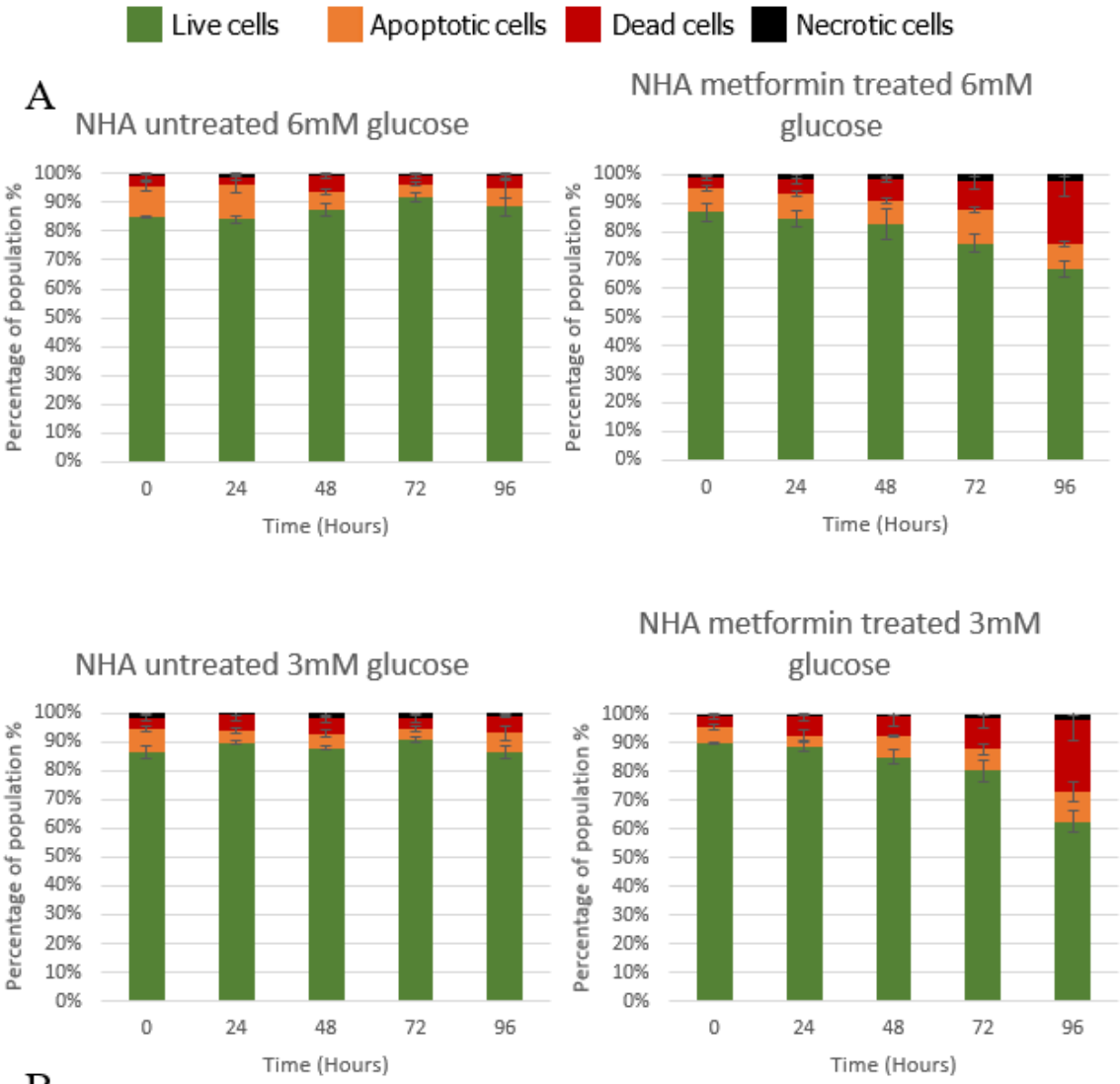

B

NHA p-values 6mM glucose Untreated - Treated					
	0	24	48	72	96
Live cells	0.5668	0.9604	0.361	0.0361*	0.0223*
Apoptotic Cells	0.1885	0.6869	0.4721	0.2047	0.2435
Dead cells	0.6525	0.0419*	0.3311	0.1803	0.0604
Necrotic Cells	0.6442	0.6983	0.3113	0.0482*	0.2096

NHA p-values 3mM glucose Untreated - Treated					
	0	24	48	72	96
Live cells	0.2379	0.4793	0.3952	0.1296	0.047*
Apoptotic Cells	0.2164	0.9883	0.192	0.3286	0.521
Dead cells	0.622	0.5685	0.7801	0.1478	0.1149
Necrotic Cells	0.292	0.5236	0.5417	0.6613	0.4341

Figure 3.21a Apoptotic time courses for NHA over 96 hours. A) Time course results. Coloured segments show % of cell population gated at each time point. Colours represent gating: Green – live cells, Orange – Apoptotic cells, Red – Dead cells, Black – Necrotic cells B) p-value results for statistical comparisons of each untreated and treated time point. Each level of statistical significance is denoted with a *.

NHA										
6mM Glucose	Untreated					6mM Glucose	Treated			
%	0hr	24hr	48hr	72hr	96hr	%	0hr	24hr	48hr	72hr	96hr
Live cells	84.9	84.1	87.1	90.6	88.3	Live cells	86.6	84.3	82.5	75.8	67.9
Apoptotic cells	10.4	11.8	6.6	4.4	6.4	Apoptotic cells	8.6	8.7	8.1	11.6	9.1
Dead cells	3.8	2.9	5.5	2.8	4.3	Dead cells	3.6	5	7.5	9.9	22
Necrotic cells	0.8	1.1	0.6	0.7	0.8	Necrotic cells	1	1.8	1.8	2.5	2.6
3mM Glucose	Untreated					3mM Glucose	Treated			
%	0hr	24hr	48hr	72hr	96hr	%	0hr	24hr	48hr	72hr	96hr
Live cells	86.1	89.7	87.8	90.9	86.2	Live cells	89.7	88.38	84.9	80.1	62.5
Apoptotic cells	8.4	3.9	4.9	3.9	6.6	Apoptotic cells	5.6	3.9	7.4	7.5	10.5
Dead cells	3.8	5.5	5.23	3.8	5.9	Dead cells	3.7	6.4	6.4	10.9	24.6
Necrotic cells	1.5	0.9	1.96	1.6	1.1	Necrotic cells	0.8	1.16	1.1	1.4	2.4

Figure 3.21b Apoptotic time course figures for NHA over 96 hours. Averaged numerical data for apoptotic time course. Cells grown in 3mM or 6mM glucose growth media were treated with or without metformin. Populations were measured every 24 hours by flow cytometry to assess levels of apoptosis. Values represent the percentage of the total population that fell within each gated quadrant. Colours represent gating: Green – live cells, Orange – Apoptotic cells, Red – Dead cells, White – Necrotic cells.

There were significant changes in the live population of metformin- treated U251MG cells at four-time points at 6 mM glucose (0, 24, 48 and 72 hours) and 3 points for 3mM glucose (0, 72 and 96 hours) (Figure 3.16). The changes at 72 hours and 96 hours are consistent with a decrease in live populations observed in other GBM cultures; however only, IN1760 also showed a similar change in live populations at 24 hours. the 24-hour time point, U251MG, IN2045 and NHA showed a significant increase in the dead cell population that did not persist to the next data point. Though all cultures showed significant decreases in live cells and increases in dead cell populations at the 96hour time point, IN859 showed this trend at 72 hours for 6 mM glucose and both IN1760 and IN2045 showed the same significant changes at 72 hours for 3mM glucose. Table 3.19 detailed the statistical average of each time course. Metformin treated NHA at 6mM glucose was the only time course that had a significant result (72h). All other time courses showed no significant changes in population level averaged across the time course.

Table 3.19 Results of paired t-test for cultures apoptotic time courses.

Time course p-values 6mM glucose Untreated - Treated						
	U251MG	IN859	IN2045	IN1682^{+}	IN1760^{+}	NHA^{+}
Live cells	0.1017	0.1879	0.1789	0.2433	0.2682	0.1535
Apoptotic Cells	0.29	0.9275	0.1594	0.3086	0.1989	0.5037
Dead cells	0.0684	0.2442	0.1879	0.2607	0.3377	0.1487
Necrotic Cells	0.2788	0.3703	0.2424	0.1627	0.3958	0.0193*

Time course p-values 3mM glucose Untreated - Treated						
	U251MG	IN859	IN2045	IN1682^{+}	IN1760^{+}	NHA^{+}
Live cells	0.2567	0.1733	0.1018	0.2328	0.1253	0.2145
Apoptotic Cells	0.9358	0.3467	0.1521	0.2682	0.062	0.3201
Dead cells	0.265	0.2659	0.102	0.245	0.1318	0.1891
Necrotic Cells	0.1794	0.8731	0.0993	0.1541	0.1368	0.9057

Results of paired t-test for cultures apoptotic time courses. Compares the statistical average of each treated time course against the untreated control. Results showing statistical significance denoted by *. Cultures marked with a $^{+}$ are *P53* wild type. Results identified only NHA having a statistically significant change in necrotic cells.

3.4.3 Comparison of glucose levels to apoptotic time course

Glucose concentration has been shown to impact the sensitivity of cancer cells to metformin (Zordoky *et al.*, 2014). Data from glucose levels from Figure 3.12 were aligned with the results of the apoptotic time course. Figures 3.22a and 3.22b display the overlay of the time course results of glucose concentration and metformin-induced cell death. Linear regression was used to assess the possible relationship between the amount of available media glucose and the percentage cell death.

Significant increases in the population of dead cells were seen in all the GBM cultures grown in media containing 3mM compared to 6mM glucose ($p<0.05$). Two of the short-term cultures with T*P53* aberrations, IN859 and IN2045, showed highly significant increases ($p<0.005$). However, significant increases in dead cells were not observed in any of the cultures grown in media containing at 6m, indicating that lower glucose levels significantly increase metformins toxicity. NHA showed no significant relationship between cell death and glucose concentrations, indicating that the increased sensitivity and cytotoxic effect identified in the 3mM time course is cancer-cell specific.

The results of this analysis show that the availability of glucose and the metabolism of cancer cells have a significant factor in the mechanism of metformin-induced cell death.

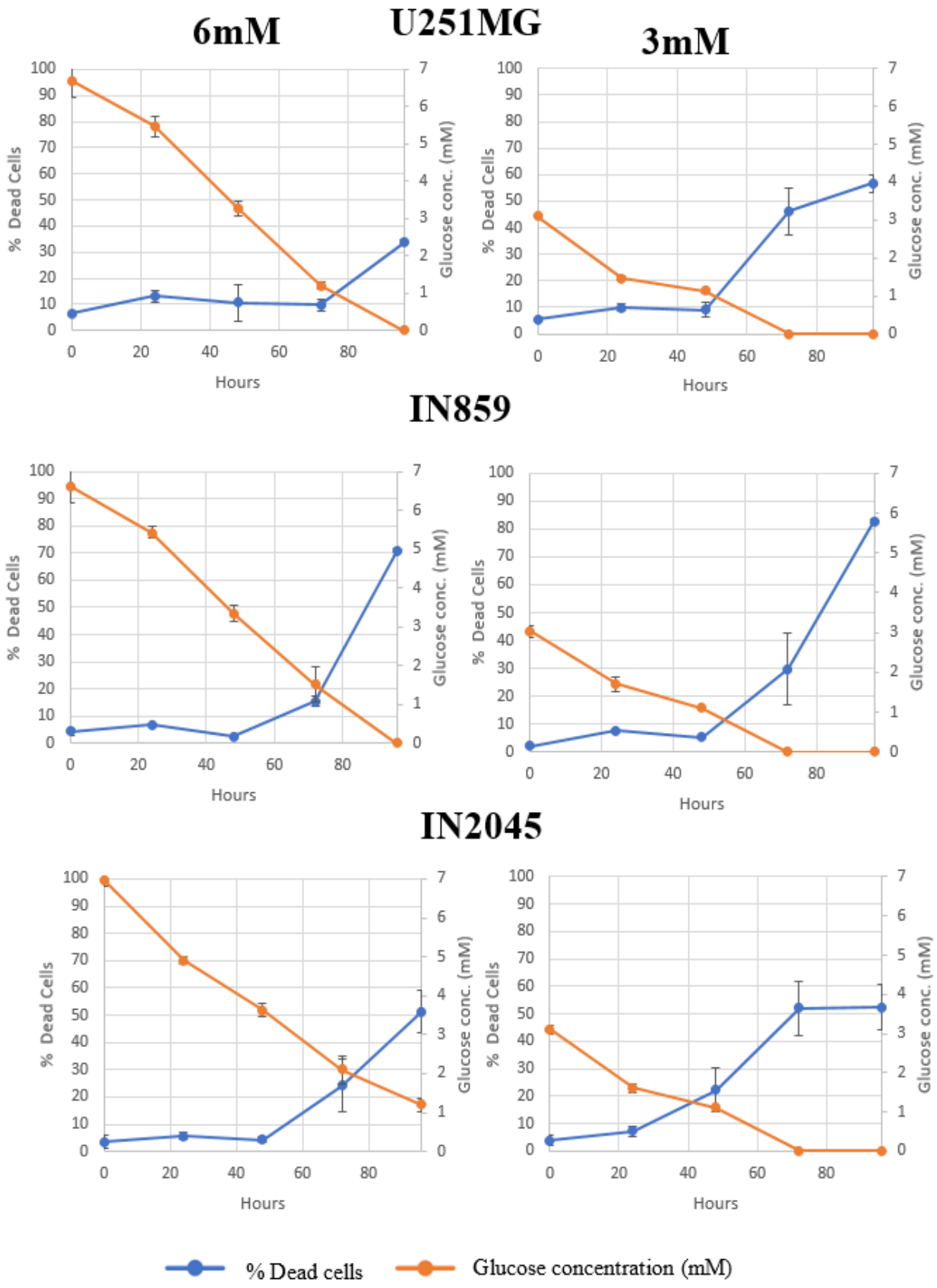

Figure 3.22a Results of glucose and cell death comparison *P53* aberrant cultures. Comparison analysis of glucose levels across time course compared with cell survival values taken from flow cytometry analysis for cultures U251MG, IN859 and IN1682. Flow cytometry values given as a percentage of population gated as dead cells. Glucose values measured in mM to two S.F.

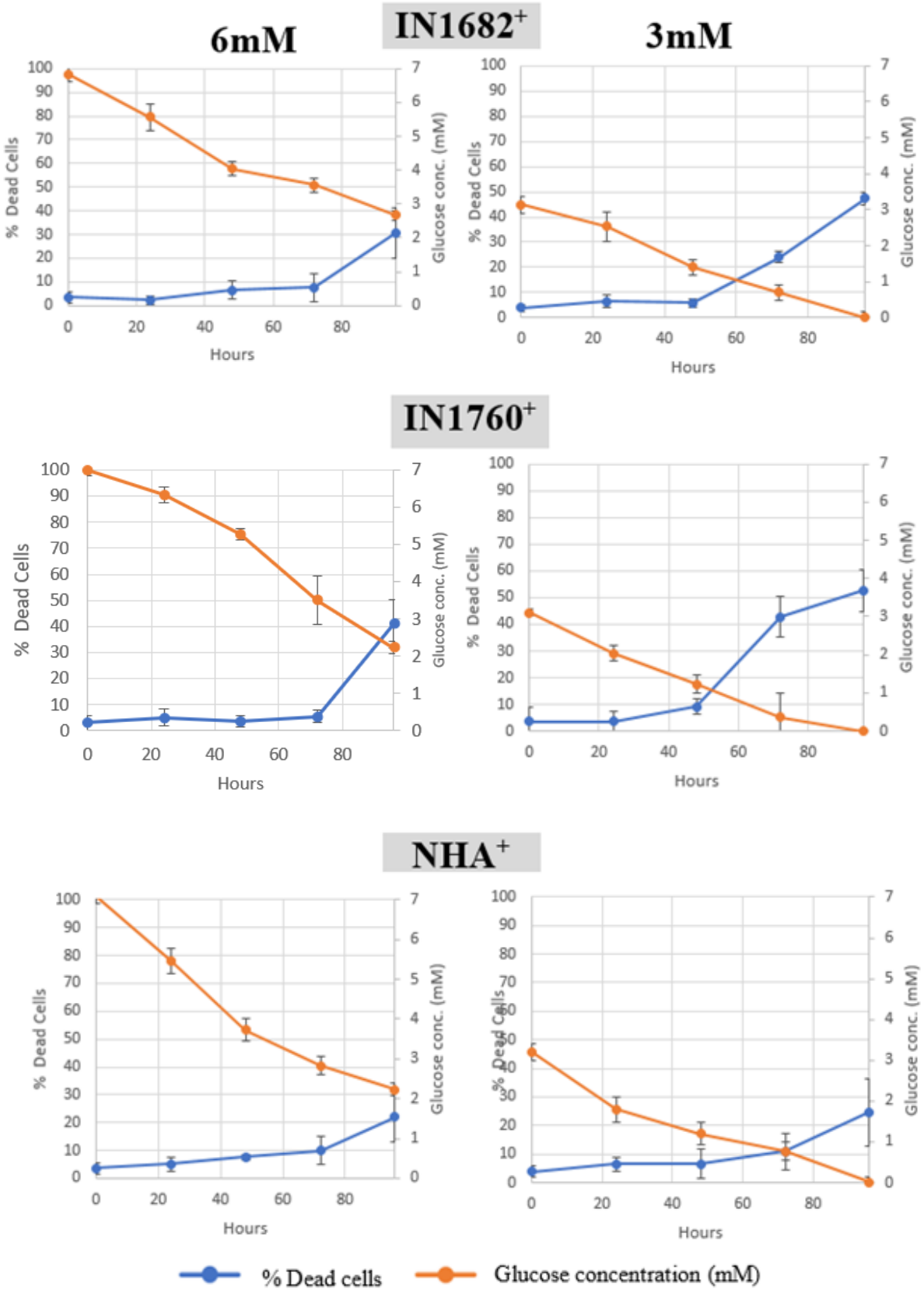

Figure 3.22a Results of glucose and cell death comparison *P53* wild type cultures. Comparison analysis of glucose levels across time course compared with cell survival values taken from flow cytometry analysis for cultures IN1760, IN2045 and NHA. Flow cytometry values given as a percentage of population gated as dead cells. Glucose values measured in mM to two S.F.

3.4.4 Mitochondria potential

Analysis of mitochondrial membranes was completed to determine whether the mitochondria play an important role in the mechanisms of metformin cytotoxicity (Choi and Lim, 2014; Wheaton *et al.*, 2014) Active measurement of mitochondrial membrane potential is affected by several factors and accurate assessment of the membrane can be completed with flow cytometry (Darzynkiewicz *et al.* 2001). JC-1 is a membrane-permeable lipophilic cationic fluorochrome able to penetrate cellular and mitochondria membranes (Cossarizza *et al.*, 1993). This feature allows its emission spectra to vary based on its relative concentration within cells and provide a reflection of ΔΨ. At low concentrations, JC-1 forms into monomers and at high concentrations it is able to aggregate into larger structures. This variation in behaviour enables the emission profile to be separated. When healthy cells are exposed to JC-1 it is taken up into the cell as monomers but is driven to accumulate with the mitochondria due to the polarized ΔΨ. Once enough JC-1 has penetrated the mitochondrial membrane, it begins to accumulate and form aggregates.

If the ΔΨ is depolarised JC-1 is unable to penetrate the mitochondria and remains as monomers in the cytoplasm of the cell. JC-1, in both forms, appears on the FL-1 (green) channel; however, the formation of aggregates creates a shift in the red emission which can be measured on FL-2 (red). By gating the cells using the parameters, it is possible to separate the monomer and aggregate populations and measure any changes in ΔΨ as shown in Figure 3.23a.

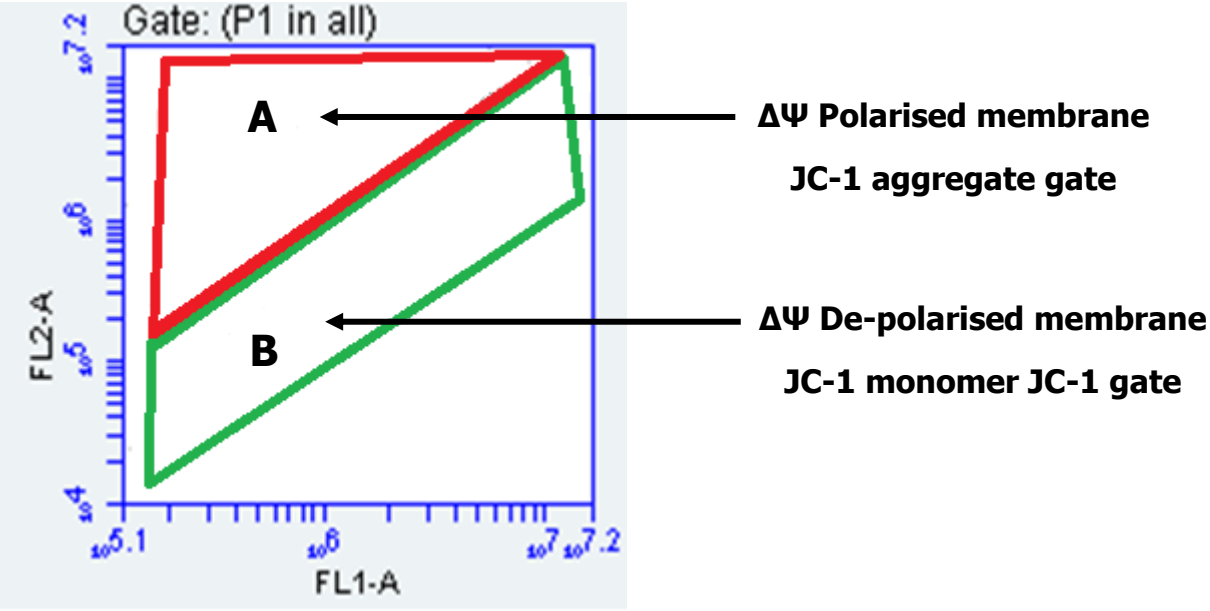

Figure 3.23a Flow cytometry gating for the separation of JC-1. Flow cytometry gating to separate monomer and aggregate populations of JC-1 in GBM cells. The red gate (A) selects for aggregate JC-1 populations that occur within the mitochondrial matrix. Populations in this gate have a polarised mitochondrial membrane that allows the JC-1 monomers to pass into the mitochondria, increase in concentration and form aggregates. The green gate (B) selects for monomer JC-1 populations that occur in the cytoplasm of cells. Populations in this gate have a de-polarised mitochondrial membrane that blocks JC-1 monomers entering the mitochondria. Monomers remain in the cytoplasm of the cells and do not form aggregates.

Five GBM cultures and NHA were assessed by flow cytometry for depolarisation of the mitochondrial membrane potential. Cells were treated with metformin for 96 hours with the ID_{50} concentrations in media containing 6mM glucose. Cells were analysed at 72-hour time point before the full completion of the cytotoxic time course.

Examples of mitochondrial depolarisation after 72 hours of 100μM camptothecin treatment are given in Figure 3.23b. Post-camptothecin treatment, the population of cells shifts to a higher reading on the FL1 channel. Positive depolarisation was defined by shifts from red P4 gate to green P5 gate.

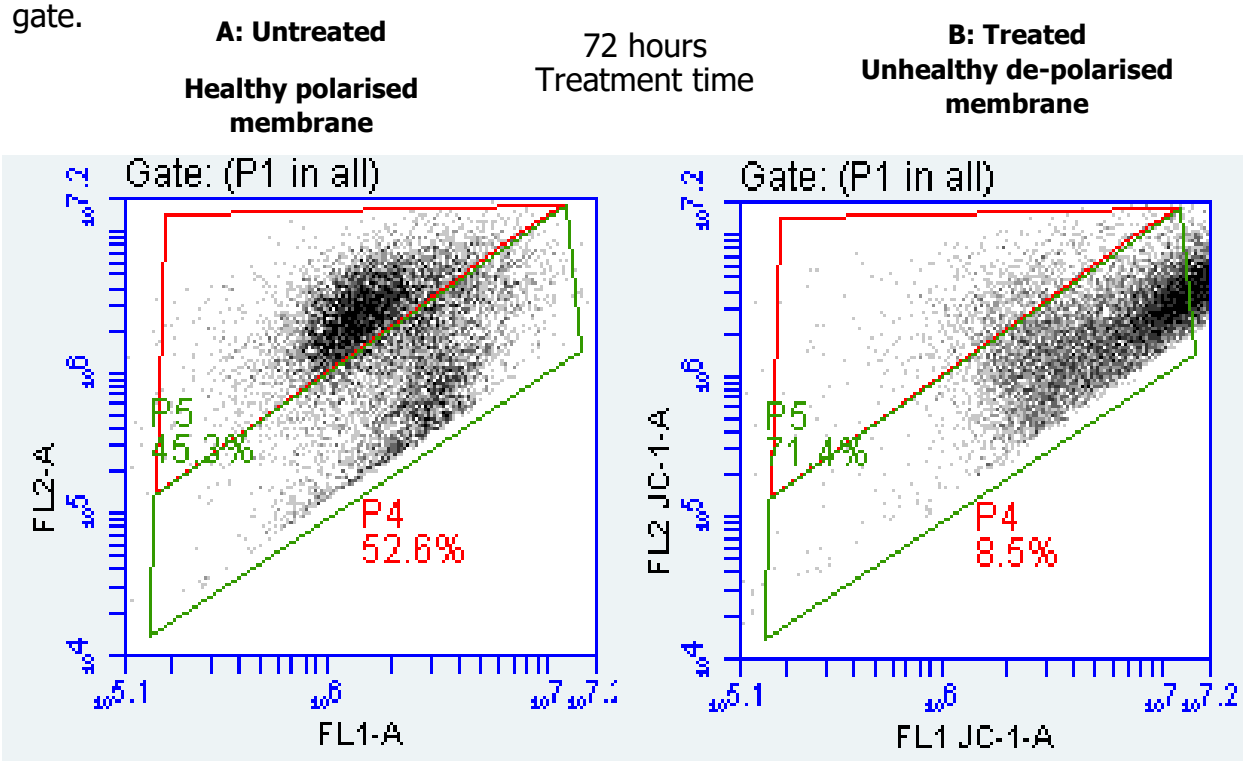

Figure 3.23b Depolarisation of the mitochondrial membrane by camptothecin. U251 MG cells were treated with 100μM camptothecin for 72 hours. Readings assessed based on FL1-A vs FL2-A readings. Apoptosis results in depolarisation of ΔΨ, shift in the FL1-A and reduction in FL2. Flow cytometry gating for depolarisation based on BD Biosciences template and adapted to GBM cultures based on repeat camptothecin treatments. Lower green gating (P5) shows JC-1 monomers unable to enter mitochondrial membrane, upper red gating (P4) shows the red shifted aggregated JC1 accumulating inside the mitochondria.

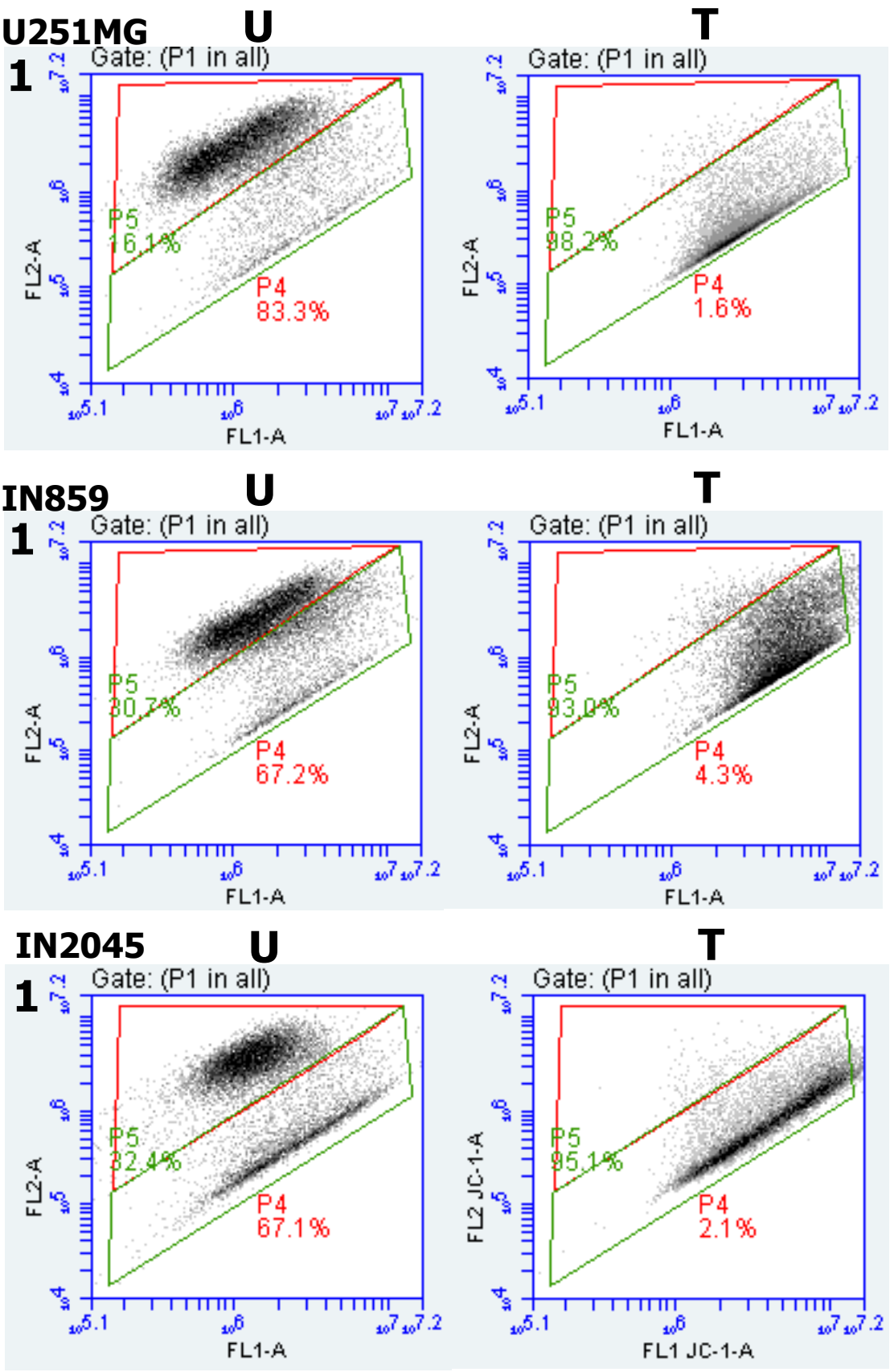

Figure 3.24a. Measurement of mitochondrial membrane potential in *P53* aberrant cultures. Red U-Untreated cultures, T-Cultures treated with metformin at 96 ID50 value. Lower green gating (P5) shows JC-1 monomers unable to enter mitochondrial membrane, upper red gating (P4) shows the red shifted aggregated JC1 accumulating inside the mitochondria.

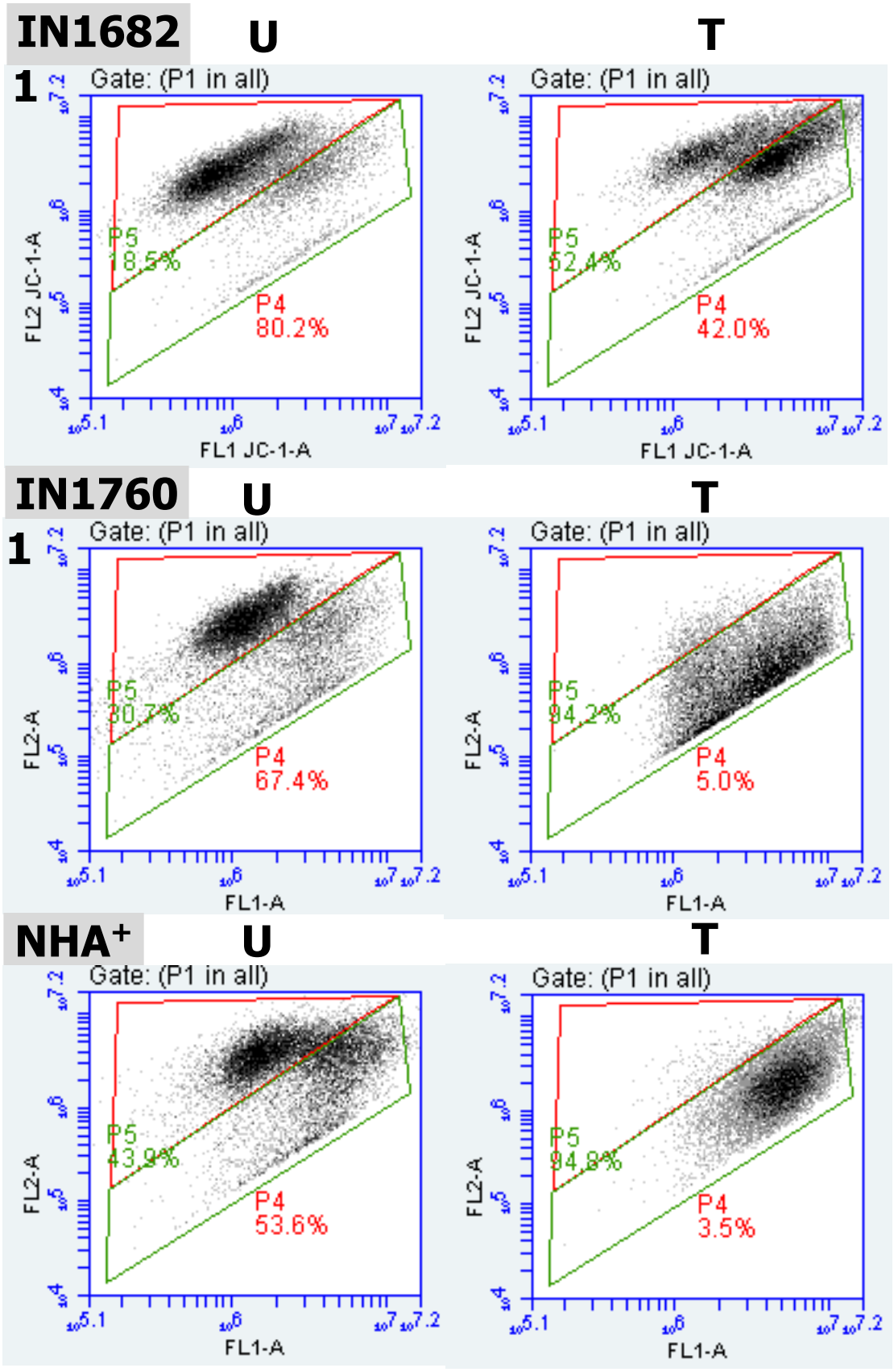

Figure 3.24b. Measurement of mitochondrial membrane potential in *P53* wild type cultures. Red U-Untreated cultures, T-Cultures treated with metformin at 96 ID50 value. Lower green gating (P5) shows JC-1 monomers unable to enter mitochondrial membrane, upper red gating (P4) shows the red shifted aggregated JC1 accumulating inside the mitochondria. Cultures marked with a $^{+}$ are *P53* wild type.

Results for all cultures are given in table 3.21. There were significant reductions in all JC-1 aggregate populations and significant increases in monomer population for all cultures. This shows that metformin had a significant effect on depolarising the mitochondrial membrane. There was no statistical difference between cultures based on *P53* status. Levels of monomers in untreated samples varied between cell cultures. The lowest monomer levels were seen in U251 17.50% (±1.51) and the highest values were seen in NHA 44.03% (±0.42). The lowest response was seen in IN1682 for which post treatment monomer values averaged to 55%. Examples of results for each culture are given in Figure 3.24a and Figure 3.24b. The experiments were not repeated under 3mM glucose conditions due to the strong positive response detected in mitochondrial membrane depolarisation for cells grown in media containing 6mM glucose. Results indicate significant depolarisation of the mitochondrial membrane occurs after 72 hours of metformin treatment at ID_{50} values at 96 hours. The cytotoxic effect of metformin can have an impact on the membrane and functions of mitochondria regardless of *P53* status.

Table 3.20 Mitochondrial membrane potential depolarisation assessments

	U		T	
	Aggregate[1]	Monomer[2]	Aggregate[1]	Monomer[2]
U251MG***	81.83 (±1.56)	17.5 (±1.51)	1.4 (±0.2)	98.36 (±0.15)
IN859***	69.43 (±2.11)	28.5 (±2.15)	4.2 (±0.56)	93.03 (±0.55)
IN2045**	60.06 (±6.11)	36.06 (±3.18)	1.1 (±0.89)	97.13 (±1.96)
IN1682+***	78.86 (±2.31)	19.9 (±2.34)	37.93 (±5.33)	55.6 (±4.87)
IN1760+***	65.66 (±1.5)	32.5 (±1.56)	4.133 (±0.78)	95.16 (±0.85)
NHA+***	53.56 (±0.45)	44.03 (±0.42)	3.1 (±0.4)	94.93 (±0.42)

Results of assessments of mitochondrial membrane across all cultures. Each level of statistical significance denoted by *. Cultures marked with a + are *P53* wild type. [1]Aggregate result represents JC-1 crossing the mitochondrial membrane and accumulating within. [2]Monomer results represent JC-1 accumulating in the cytoplasm of cells and remaining in a monomer form.

3.4.5 Cell cycle

Cell cycle analysis was carried out in five GBM cultures and NHA at 96 hours treatment with ID_{50} concentrations of metformin. Positive controls for apoptosis were created using 100μM camptothecin at 96 hours treatment which successfully generated sub-G1 populations and examples of induction of apoptosis and DNA fragmentation are given in Figure 3.25.

Cell cycle analysis is shown in Figures 3.26a and 3.26b and Tables 3.22 and 3.23. Five out of the six GBM cultures showed significant increases in G2/M population (Table 3.23). The *P53* aberrant cultures all showed increases above 12% and the *P53* wild-type IN1760 has a 7.7% (±3.8) increase in G2/M. IN1682 showed a non-significant increase of 4.2% (±8.3). All cultures demonstrated a reduction in G0/G1 populations, U251MG and IN1760 showed significant reductions in this population. The only culture to show a significant change in S-phase was U251MG with an increase of 6.5% (±0.3). All other cultures showed an increasing trend in S phase population; however, it was a non-significant result. IN2045 was the only culture to show a significant change in sub-G0/G1. The culture showed a significant decrease in the apoptotic population; however, this result was an average reduction of 0.7% (±0.2). U251MG proved most sensitive to cell cycle changes as it was the only culture to show a significant change in all its cell cycle stages. The experiments were not repeated under 3mM glucose conditions due to the positive cell cycle arrest observed in G2/M phase of cell cycle for cells grown in media containing 6mM glucose.

The results demonstrate that metformin treatment influences cell cycle progression through arrest at the G2/M step. The status of *P53* was not a factor in observed cell cycle response, IN1682 had a weak response and limited G2/M arrest. There was no significant increase in apoptotic population in any culture tested. This would indicate no fragmentation of DNA has occurred in the cultures. G0/G1 populations were not significantly affected in most populations and only a small non-significant increase was seen in S-phase in all short-term cultures, suggesting that the impact on cell cycle does not affect the checkpoints for either of the stages.

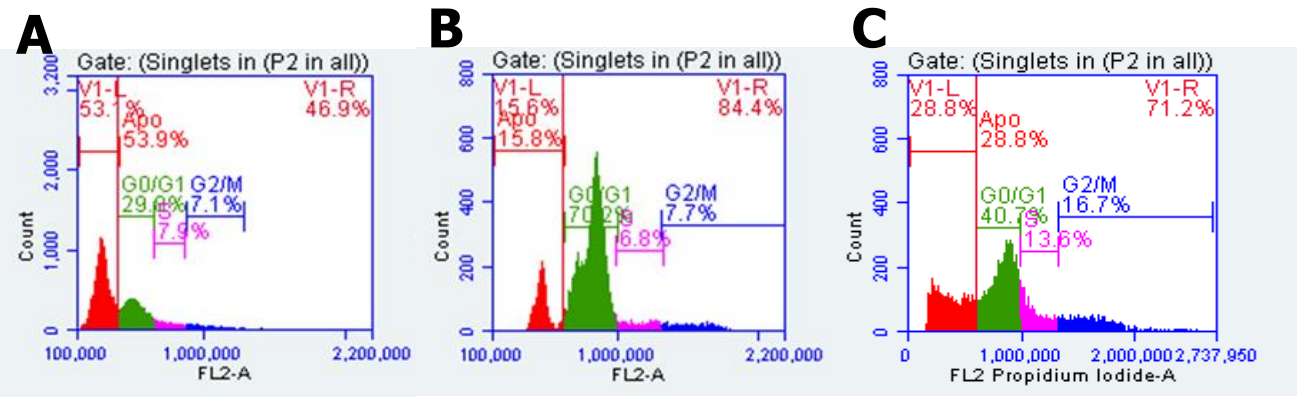

Figure 3.25 Camptothecin induced apoptotic positive cell cycle analysis. Cultures treated with 100µM camptothecin for 96 hours. Cultures measured after remove doublet cells. Apoptosis results in degradation of DNA producing stained fragments with low FL2 values. Apoptotic region labelled V1-L, normal cell cycle region labelled V1-R. Variation was observed between cells populations apoptotic presentation: A) U251MG – Wide peak that connects to G0/G1 population. B) IN1760 – Distinct sub population in sub-G0/G1 region separate from G0/G. C) IN859 – Wide population with no distinct peak. Populations coloured based on cell cycle stage: Red – Sub-G0/G1, Green – G0/G1, Pink – S-phase, Blue – G2/M.

Table 3.21 Cell cycle assessments

	G0/G1		S		G2/M		Apoptosis[1]	
	U	T	U	T	U	T	U	T
U251MG	73.7 (±6)	55.1 (±2)	2.3 (±0.2)	8.9 (±0.2)	23.3 (±5.7)	35.7 (±2.2)	0.7 (±0.3)	0.4 (±0.1)
IN859	66.2 (±6.1)	52.2 (±7.8)	7.1 (±1.1)	8.6 (±1.1)	25.5 (±6.5)	38.0 (±5.9)	1.2 (±0.5)	1.2 (±1.0)
IN2045	70.8 (±3.9)	53.3 (±4.4)	6.2 (±2.4)	12.2 (±2.4)	21.8 (±5.3)	34.0 (±5.1)	1.2 (±0.1)	0.5 (±0.2)
IN1682^{+}	66.4 (±2.8)	58.7 (±3.9)	10.6 (±2.1)	14.1 (±2.1)	20.3 (±5.2)	24.4 (±3.1)	2.8 (±0.9)	2.7 (±1.3)
IN1760^{+}	83.6 (±1.1)	73.3 (±4.7)	3.2 (±0.4)	4.8 (±0.4)	8.1 (±1.1)	15.8 (±0.9)	5.1 (±0.4)	6.1 (±0.2)
NHA^{+}	63.3 (±1.1)	58.1 (±8)	9.6 (±1.5)	12.2 (±2.1)	25.0 (±0.6)	25.1 (±4.2)	2.1 (±1.0)	4.5 (±1.7)

Results of cell cycle analysis of cultures after metformin. [1]Apoptosis value represent sub-G0/G1 populations. U- Untreated, T- Treated with metformin 96-hour ID50 value for 96 hours.

Table 3.22 Change in cell cycle populations

	G0/G1	S	G2/M	Apoptosis[1]
U251MG	-18.6% (±4.9) *	+6.5% (±0.3) **	+12.4% (±4.4) *	-0.4% (±0.3)
IN859	-14% (±7.5)	+1.5% (±4.6)	+12.5% (±3.3) *	0% (±0.9)
IN2045	-17.6% (±7.1)	+6.0% (±2.5)	+12.2% (±4.8) *	-0.7% (±0.2) *
IN1682^{+}	-7.6% (±6.4)	+3.5% (±5.2)	+4.2% (±8.3)	-0.1% (±2.3)
IN1760^{+}	-10.3% (±3.9) *	+1.7% (±3.8)	+7.7 (±0.3) *	+1.0% (±0.5)
NHA^{+}	-5.2% (±7.1)	+2.7% (±6.9)	+0.1% (±4.7)	+2.4% (±2.5)

Percentage changes in each cell population after 96-hours at ID50 metformin treatment. [1]Apoptosis value represent sub-G0/G1 populations. Each level of statistical significance denoted by *. Cultures marked with a $^{+}$ are *P53* wild type.

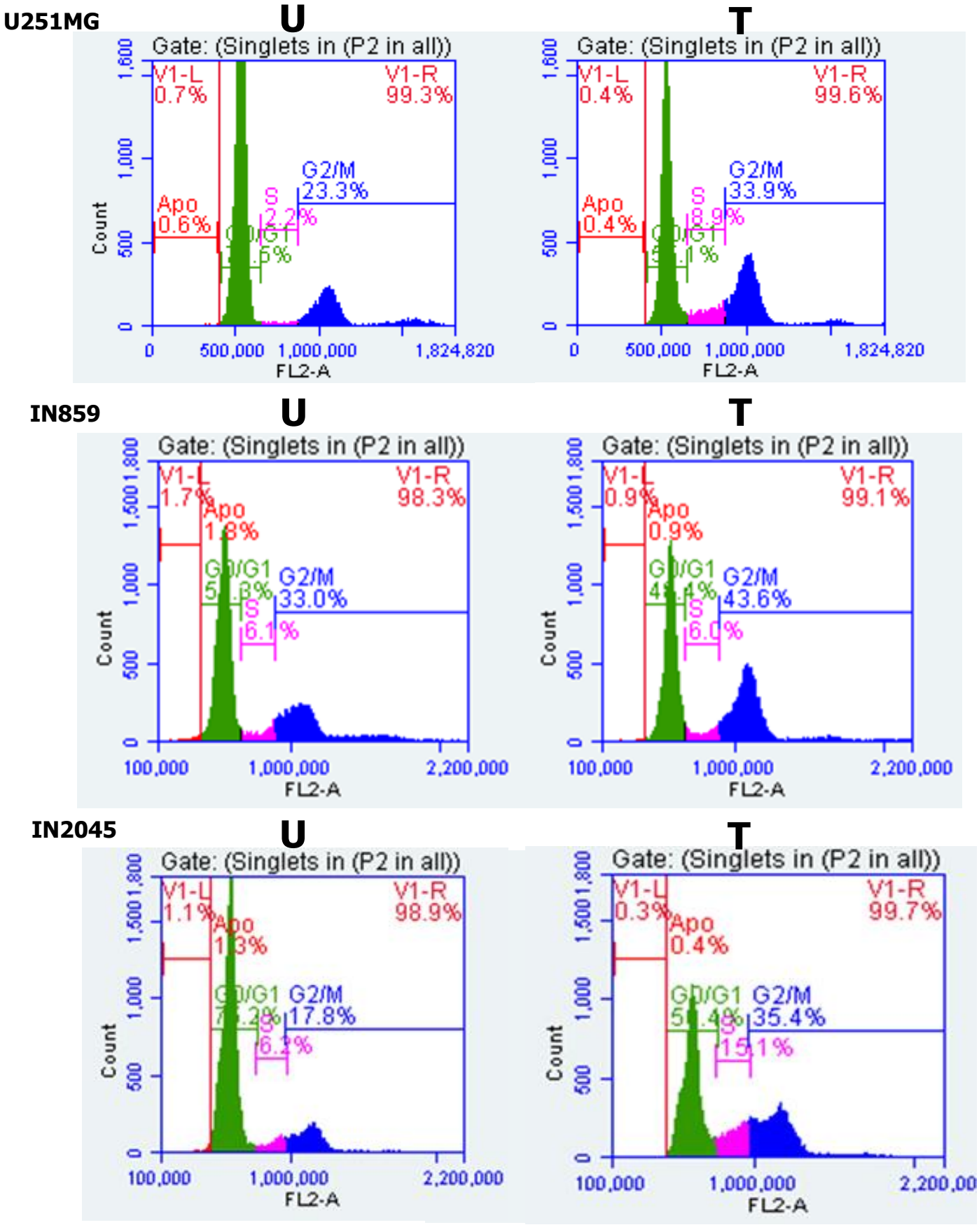

Figure 3.26a Cell cycle analysis in *P53* aberrant cultures. Cell cycle flow cytometry results of GBM cells, untreated (U) or treated (T) with ID_{50} metformin. DNA of cells stained with propidium iodide and measured on FL2-A. Gating of cell cycle stages based off untreated GBM sample. Populations coloured based on cell cycle stage: Red – Sub-G0/G1, Green – G0/G1, Pink – S-phase, Blue – G2/M. Increase in G2/M values of all GBM cultures indicative of G2/M cell cycle arrest.

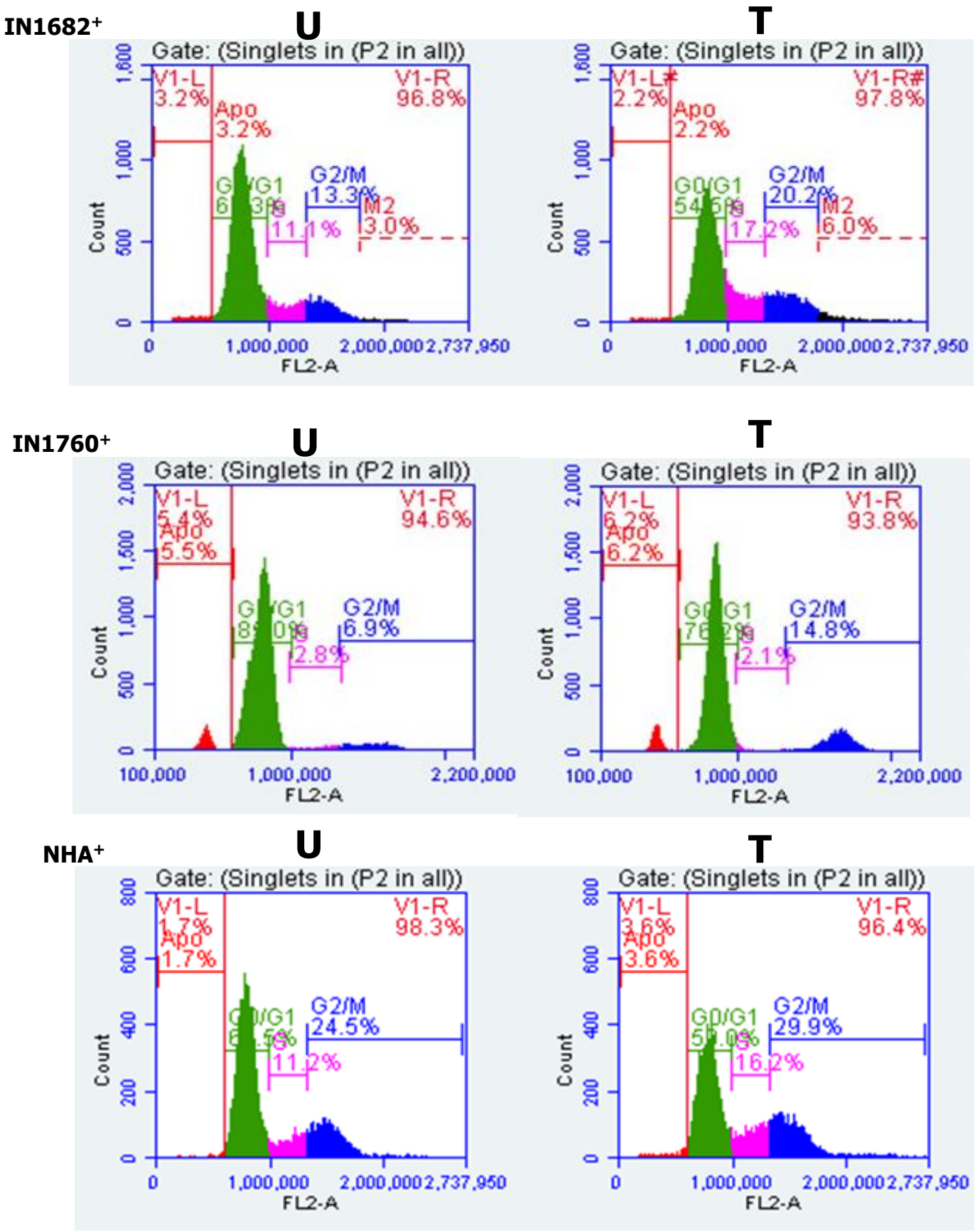

Figure 3.26b Cell cycle analysis in *P53* wild types cultures. Cell cycle flow cytometry results of GBM cells, untreated (U) or treated (T) with ID50 metformin. DNA of cells stained with propidium iodide and measured on FL2-A. Gating of cell cycle stages based off untreated GBM sample. Populations coloured based on cell cycle stage: Red – Sub-G0/G1, Green – G0/G1, Pink – S-phase, Blue – G2/M. Increase in G2/M values of all GBM cultures indicative of G2/M cell cycle arrest.

3.4.6 Caspase

Caspase 3/7 analysis was carried out on six cultures treated with 96-hour ID_{50} concentrations of metformin. Levels of caspase activity and SRB uptake were measured at 72 and 96 hours of drug treatment and normalised. A positive control for apoptosis was generated using 100μM camptothecin.

The normalised results show no significant change in caspase 3/7 readings in GBM cultures at all time points and glucose measurements. NHA showed a significant decrease in caspase activity at 96-hour time points in both glucose concentrations. There was no trend in the changes of caspase activity after metformin treatment at any time point in GBM culture. *P53* status of culture showed no difference in the observed response. Changes in relative light units (RLU) can be attributed to normal variation in generation of results. No metformin treated culture generated a RLU of above $5x10^5$ under any treatment conditions. Camptothecin (100μM) proved a strong positive control at inducing caspase activity in all cultures tested. The caspase activity detected for the camptothecin control exceeded an order of magnitude in all samples producing RLU values from $2x10^6$ up to $3.7x10^6$.

Results indicate that metformin does not affect caspase 3/7 activity at 72 or 96 hours of treatment in any GBM cultures. The RLU levels displayed by camptothecin show a strong increase in caspase apoptotic activity. This shows that the mechanism of cell death, following metformin treatment, in GBM appears to be independent of an increase of caspase 3/7 activity and this is not dependent on the *P53* status of the cell.

Table 3.23 Significance values for caspase 3/7 assay

P- Values for metformin treat cells in caspase 3/7 assay				
	3mM Glucose 72 hours	3mM Glucose 96 hours	6mM glucose 72 hours	6mM Glucose 96 Hours
U251MG	0.0592	0.0631	0.0721	0.0821
IN859	0.3817	0.2314	0.0811	0.624
IN12045	0.0871	0.0645	0.7456	0.5741
IN1682^{+}	0.7521	0.3645	0.4572	0.6521
IN1760^{+}	0.4761	0.9821	0.3451	0.9451
NHA^{+}	0.141	0.0495*	0.0789	0.0412*

Comparative p-value results for all changes in RLU from caspase 3/7 assay treated with ID50 metformin. Increasing levels of significance are marked with *. Cultures marked with a $^{+}$ are *P53* wild type.

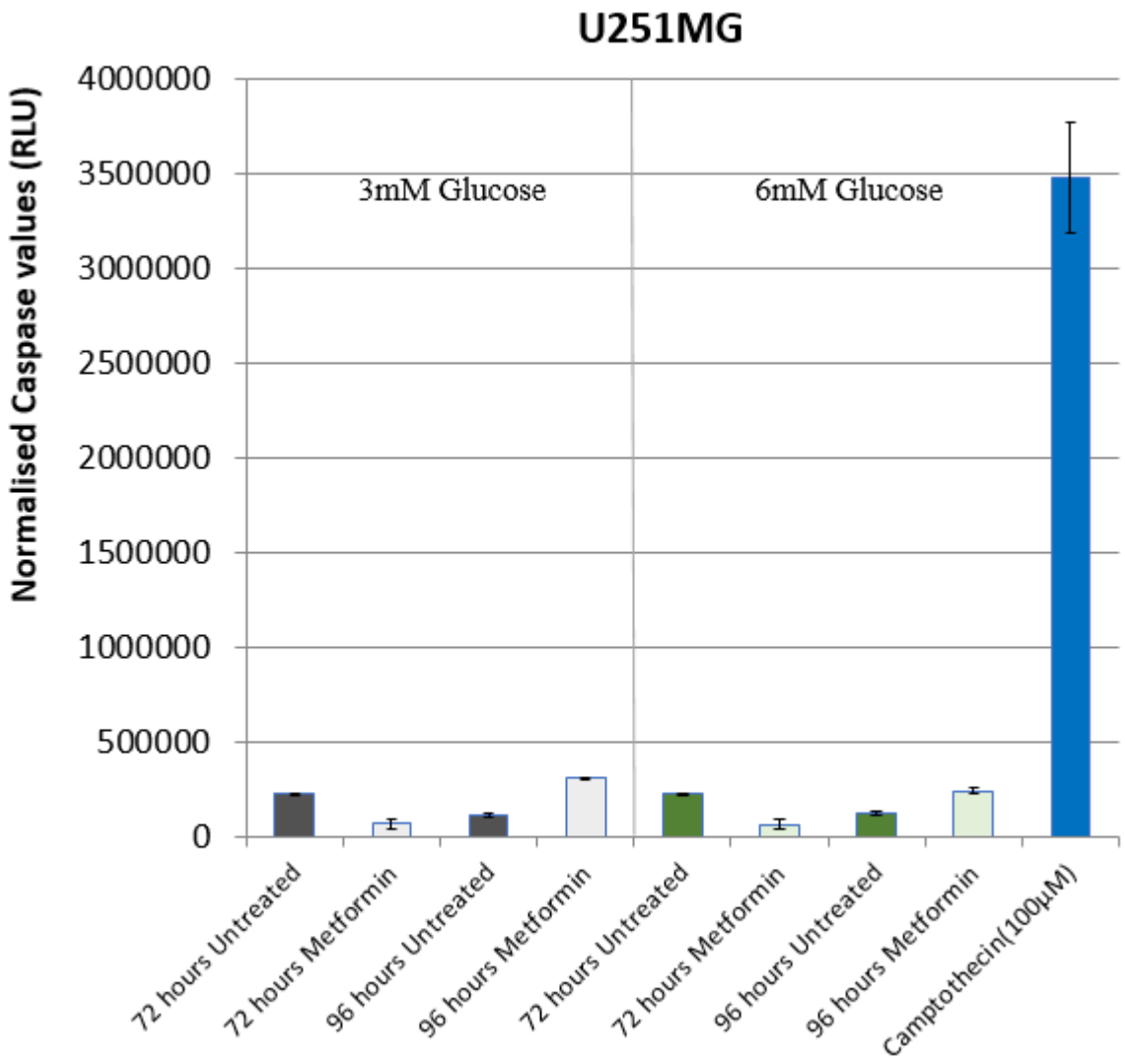

Figure 3.27a Caspase 3/7 assay results for U251MG. Results of measuring activity levels of caspase 3/7 in U251MG treated with 96-hour ID50 metformin with respect to glucose concentration. Readings taken at 72 and 96 hours. Normalised caspase value measured in relative light units normalised by an SRB control. 100μM camptothecin used to induce positive apoptosis. Value of camptothecin displayed are from 96-hour time point. Significant results marked with a * for each level of significance.

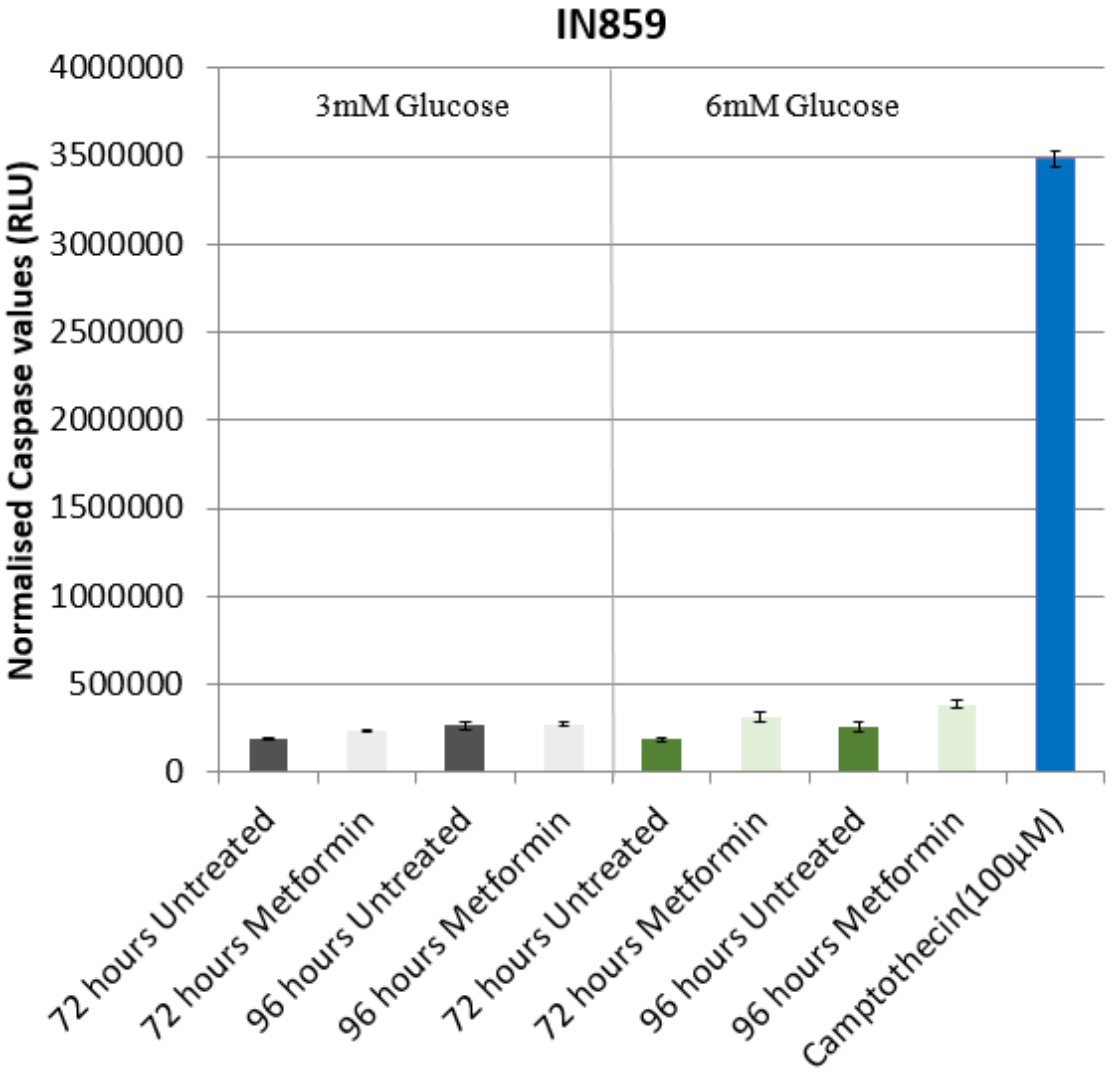

Figure 3.27b Caspase 3/7 assay results for IN859. Results of measuring activity levels of caspase 3/7 in IN859 treated with 96-hour ID50 metformin with respect to glucose concentration. Readings taken at 72 and 96 hours. Normalised caspase value measured in relative light units normalised by an SRB control. 100µM camptothecin used to induce positive apoptosis. Value of camptothecin displayed are from 96-hour time point. Significant results marked with a * for each level of significance.

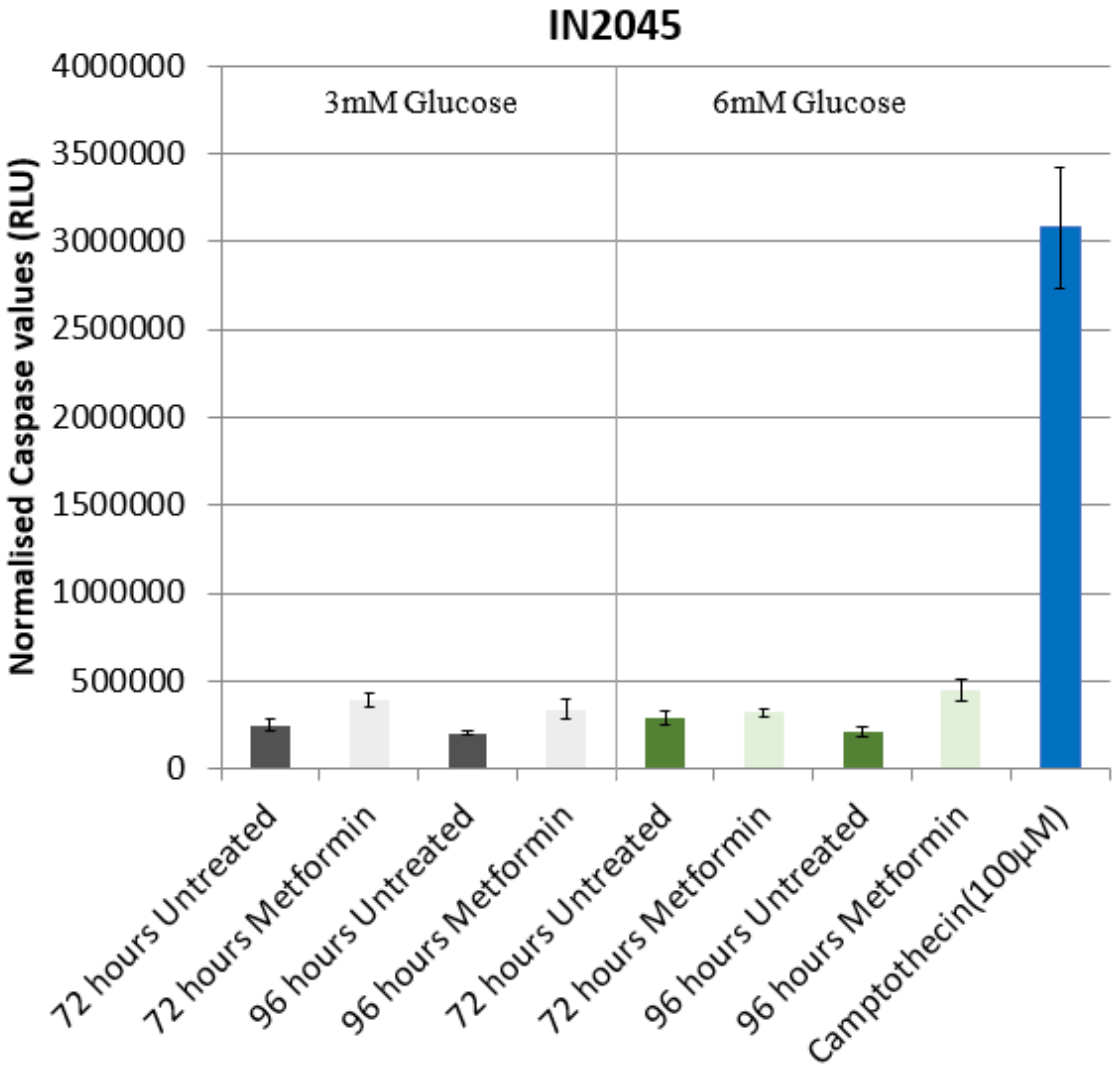

Figure 3.27c Caspase 3/7 assay results for IN2045. Results of measuring activity levels of caspase 3/7 in IN2045 treated with 96-hour ID50 metformin with respect to glucose concentration. Readings taken at 72 and 96 hours. Normalised caspase value measured in relative light units normalised by an SRB control. 100μM camptothecin used to induce positive apoptosis. Value of camptothecin displayed are from 96-hour time point. Significant results marked with a * for each level of significance.

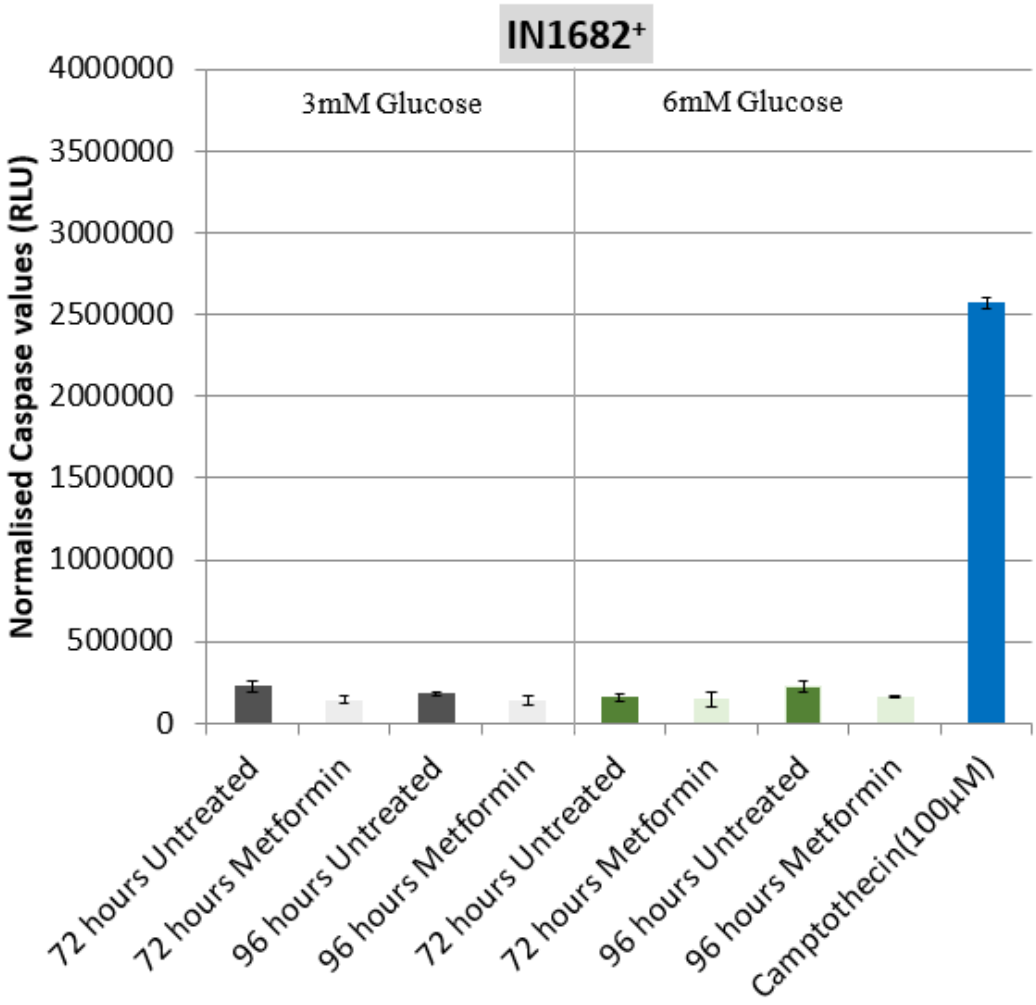

Figure 3.27d Caspase 3/7 assay results for IN1682. Results of measuring activity levels of caspase 3/7 in IN1682 treated with 96-hour ID50 metformin with respect to glucose concentration. Readings taken at 72 and 96 hours. Normalised caspase value measured in relative light units normalised by an SRB control. 100μM camptothecin used to induce positive apoptosis. Value of camptothecin displayed are from 96-hour time point. Cultures marked with a $^{+}$ are *P53* wild type. Significant results marked with a * for each level of significance.

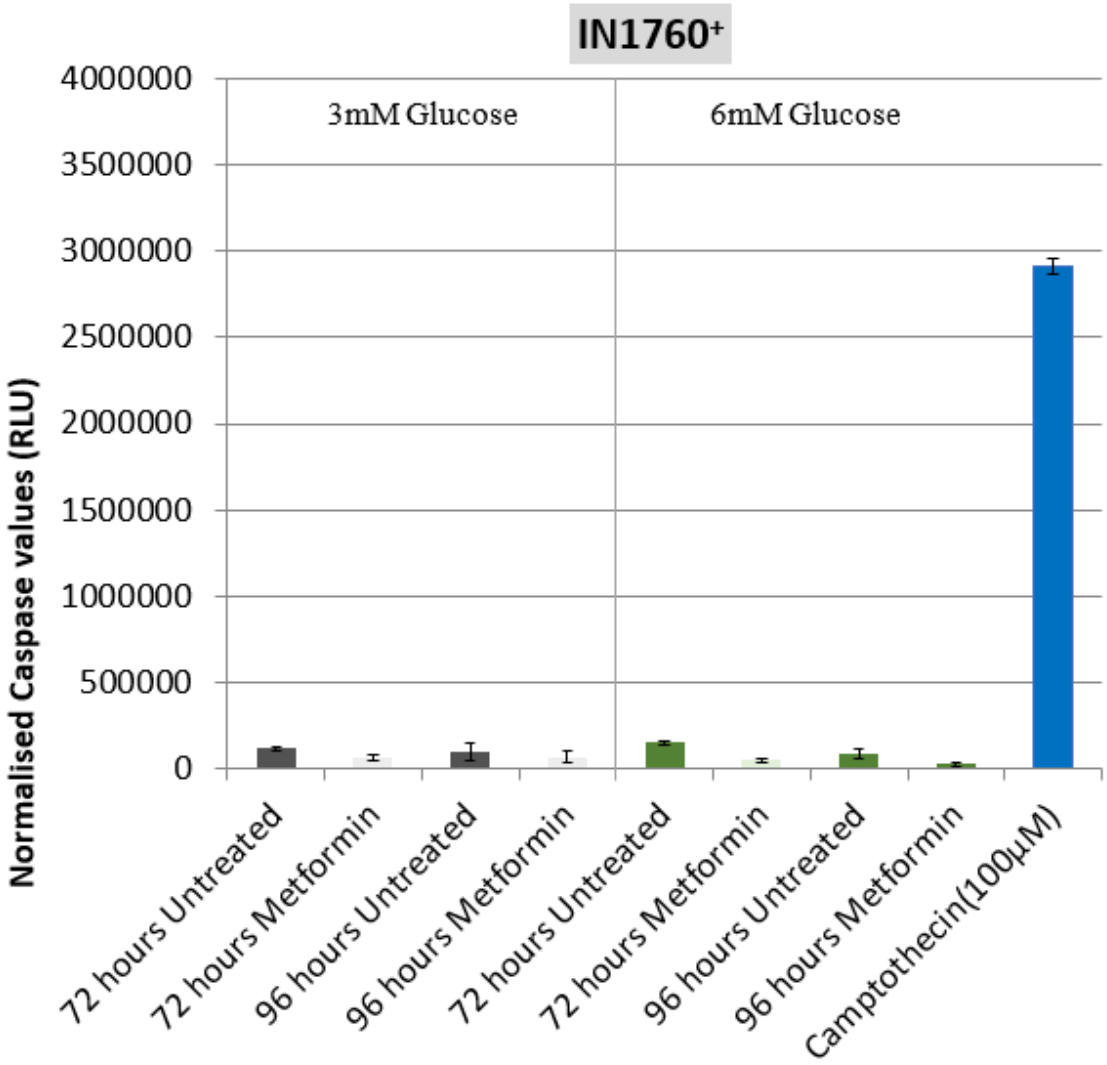

Figure 3.27e Caspase 3/7 assay results for IN1760. Results of measuring activity levels of caspase 3/7 in IN1760 treated with 96-hour ID50 metformin with respect to glucose concentration. Readings taken at 72 and 96 hours. Normalised caspase value measured in relative light units normalised by an SRB control. 100µM camptothecin used to induce positive apoptosis. Value of camptothecin displayed are from 96-hour time point. Cultures marked with a $^{+}$ are *P53* wild type. Significant results marked with a * for each level of significance.

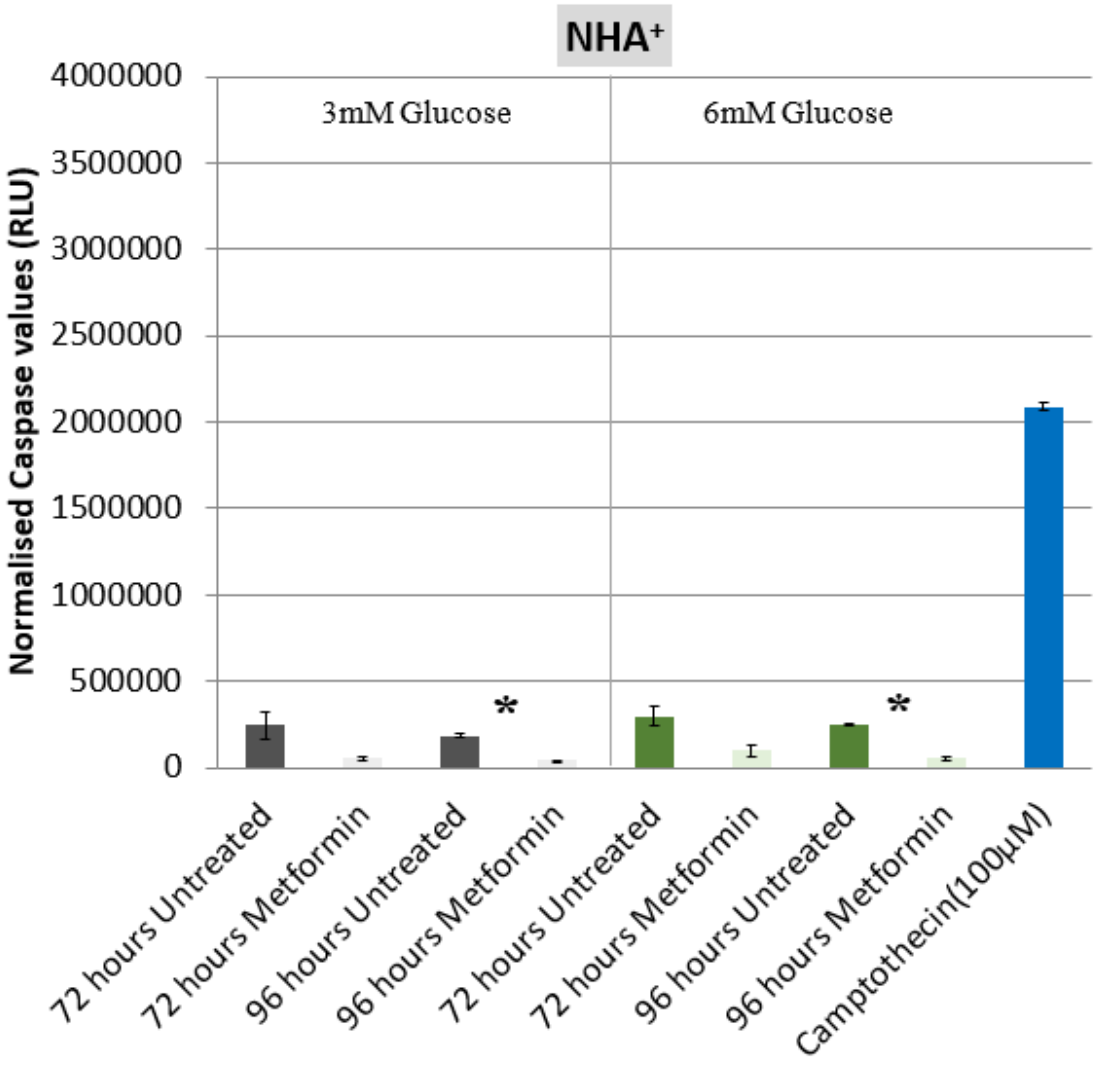

Figure 3.27f Caspase 3/7 assay results for NHA. Results of measuring activity levels of caspase 3/7 in NHA treated with 96-hour ID50 metformin with respect to glucose concentration. Readings taken at 72 and 96 hours. Normalised caspase value measured in relative light units normalised by an SRB control. 100μM camptothecin used to induce positive apoptosis. Value of camptothecin displayed are from 96-hour time point. Cultures marked with a $^{+}$ are *P53* wild type. Significant results marked with a * for each level of significance.

3.4.7 Summary

3.4.7.1 Apoptosis

Overall, the combined experiments show very little evidence in favour of a caspase dependent apoptotic pathway as the main mechanism of cell death in GBM from metformin treatment.

Results from the apoptotic time course showed that most of the cell death occurred at the 72 and 96-hour time points. This means that during the first 48 hours of exposure, metformin exerted little effect on the cells. Metformin is not metabolised within the human body, it is excreted in the same format it enters cells (Bailey, 2017; Hassan and Carlton, 2018). Metformin has been shown to be stable at physiological pH (Markowicz-Piasecka *et al.*, 2018) so over this period is unlikely to be broken down and concentrations should be maintained. Therefore, the lack of effect on the cells indicates that another mechanism may be mediating the cellular response to metformin. Levels of cell death in NHA were lower than the 50% that an ID_{50} dose should have generated. This discrepancy could be due to experimental differences with the SRB assay. The SRB assay is a measure of uptake of SRB into fixed cellular membranes (Skehan *et al.*, 1990). The ID_{50} values generated include reductions in proliferation in addition to measurement of cytotoxic effects, whereas the apoptotic flow cytometry assessment measure cell death only (Telford *et al.*, 1992). This may imply that metformin is mainly impacting NHA through reductions in proliferation. Cell cycle experiments demonstrated no Sub-G0 stained DNA, indicative of apoptotic cells (Pierre *et al.*, 2014) (Chen *et al.*, 2009). Instead a significant increase in G2/M region of all cultures indicates G2/M cell cycle arrest.

Induction of caspase was not observed in any culture. Caspase 3/7 are primary effectors at the end of the apoptotic caspase pathway, and hence the lack of a strong signal in any of the test cultures indicates that the metformin mediated response is independent of the caspase pathway. Though not common, caspase-independent pathways for cell death do occur in glioma (Du, *et al.* 2016). Cell death can also occur independently of caspase through necrosis or autophagy (Kitanaka and Kuchino, 1999; Kroemer and Martin, 2005). Metformin has been associated with induction of autophagy (Tomic *et al.*, 2011; Jivan *et al.*, 2017). The results given here indicate that mechanism of action for metformin in GBM is unlikely to function through caspase-mediated apoptosis.

3.4.7.2 Response to Metformin vs Glucose uptake

The data from the apoptotic time course shows that the majority of cell death occurred after 72 hours of exposure to metformin. The results of the regression analysis showed a significant relationship between glucose concentration and cell death was present in all the GBM culture time course experiments when cells were grown in media containing 3mM glucose. However, this relationship was not shown to be significant when cells were grown in media containing 6mM glucose. This shows that the metformin-mediated cell death is mediated by low/zero glucose conditions. For all cultures, the initial 3mM concentration of glucose in growth media was reduced to 1mM glucose by 72 hours. The cultures showed the highest values for cell death over the time course. The NHA culture was the only cell culture not to show a significant relationship between the change in glucose

concentration and cell death. Cell death was still detected, and glucose levels were also declining in the NHA cultures, so the lack of significance indicates that this is a cancer-specific relationship.

It has been previously shown by Zhuang *et al.* (2014) that sensitivity of cancer cells to metformin was modulated by the amount of glucose present within the growth media as higher glucose concentrations reduced the efficacy of metformin and had a protective effect on the cells. Once glucose levels were lowered, metformin-induced cell death increased due to a reduction in metformin-stimulated glycolysis. The comparison of the apoptotic time course data against the glucose values from section 3.4.3 has shown a similar response with the majority of cell death appearing once the glucose level drops to below 1.1mM. Reducing the starting glucose also showed a significant relationship in all GBM cultures.

Due to metformin observed effect of reducing blood glucose levels, it original name was glucophage, "the eater of glucose" (Fujioka *et al.*, 2005). This has since been corroborated with the effect of metformin treatment inducing cellular uptake of surrounding glucose (Koffert *et al.*, 2017).

3.4.7.3 Mitochondrial membrane

Depolarisation of the mitochondrial membrane was induced by metformin treatment. Metformin has been shown to impact mitochondria through inhibition of complex 1 of the mitochondria l respiratory chain (Owen *et al.*, 2000). In all GBM cultures, high levels of depolarisation were demonstrated, and this will impact metabolism within the cell and may lead to cell senescence (Ziegler *et al.*, 2015). Mitochondrial membrane depolarisation sometimes is a sign of apoptosis (Gyulkhandanyan *et al.*, 2015). This can lead to release of cytochrome C and activation of caspase apoptosis (Chen *et al.*, 2015). However, the caspase 3/7 assay showed no increase in activity, limiting the potential of this pathway being mediated by metformin. An alternative mechanism of action was proposed by Wheaton (2014). In a study using 293FT embryonal kidney cells, metformin impacted cell tumorigenesis through inhibition of mitochondrial complex I, causing a reduction in mitochondrial activity and cellular respiration. The depolarisation of the mitochondrial membrane demonstrated here could indicate that the mechanism of action of metformin within the cell is targeting the mitochondria and downstream effectors.

3.4.7.4 G2/M Cell cycle arrest

Cell cycle analysis showed a significant increase in G2/M phase post metformin treatment in four out of the five GBM cultures. The only one that did not demonstrate a significant increase was IN1682. This increase indicates that cells are arrested at this division check-point. This form of cell cycle arrest maybe indicative of DNA damage (Cho *et al.*, 2013) and damage to mitotic

spindle prevent progression the spindle assembly checkpoint (Fendzhi *et al.*,1998; Maria *et al.*, 2004).

Arrest at this checkpoint has been identified by Adeburg *et al.* (2017) who demonstrated in two GBM cell lines (Ln18, t*P53* mutant and LN229, t*P53* mutant) that mM doses of metformin could induce G2/M arrest after 72 hours treatment. Cell cycle arrest at this pre-mitosis checkpoint from metformin treatment has also been observed in several other tumour types. In a colorectal cancer cell line (HCT116) metformin was shown to cause an accumulation of tumour cells in the G2/M phase and delayed DNA repair cause by ionizing radiation exposure (Jeong *et al.*, 2015). This cell cycle arrest was seen in both cultures but more significantly in HCT116 *P53*-/- samples. G2/M has also been detected in drug-resistant leukaemia cells (Rodríguez-Lirio *et al.*, 2015). In epithelial ovarian cancer, two cell lines (OVCAR-3, OVCAR-4) showed cell cycle arrest in the S and G2/M phases after 72 hours of metformin treatment.

In contrast, metformin has also been seen to halt cells at the G0/G1 checkpoint. In oesophageal squamous cell carcinoma, metformin caused G0/G1 arrest in a *P53* dependent manner (Cai *et al.*, 2015). In glioma studies, metformin was shown to induce cell cycle arrest in G0/G1 phase, however this was only seen in the C6 rat glioma cell line (Isakovic *et al.*, 2007). This is the opposite of the results from this study. However, they also reported that significant levels of cell death were not induced by metformin treatment possibly due to the lower dosage of metformin used (5mM) and the differences between short term cultures and the C6 glioma cell line.

U251MG showed a significant increase in its S phase cell population post-metformin treatment, the only culture in which such a response was observed. Cell cycle arrest in S phase would be advantageous in drug treatment due to sensitising the cells to chemotherapy and radiotherapy DNA damage (Wang *et al.*, 2008). However, only U251MG showed a significant change, indicating this to be a feature gained by the cell line during long-term *in vitro* culture.

Though primarily a response to DNA damage, the G2/M check point is affected by other factors including mitochondria. Due to the high energy demand, the G2/M cell cycle check point is partly coordinated by mitochondria metabolism (Wang *et al.*, 2014). The mitochondria can also cause G2/M arrest through inhibition of the mitochondrial fission protein DRP1 (Qian *et al.*, 2012). This protein has been shown to be reduced and inhibited in metformin-treated endothelial cells leading to reduced mitochondrial fission in an AMPK dependent manner (Wang *et al.*, 2017). This work demonstrated that metformin does impact mitochondria in GBM with depolarisation of the mitochondrial membrane. Measurement of DRP1 in GBM cultures might indicate metformin is impacting G2/M arrest through this mechanism.

3.5 Metformins impact on miRNA expression

Pulito *et al.* (2014) examined the role of metformin in reprogramming the metabolism of cancer cells, potentially, through an interplay with miRNA expression. A literature review highlighted nine miRNAs (miR-26a, miR-33a, miR-140, miR-142, miR-192, miR-200, miR-205 miR-222 and let-7c) that were modulated by metformin treatment and had relevant known targets in cancer These miRNAs are summarised in Table 3.25. The metformin miRNA cancer targets have been identified from studies of several cancers including breast, lung and pancreatic but also included the effect of metformin on circulating miRNAs in diabetic patients.

3.5.1 TCGA miRNA GBM expression

To assess the relevance of the metformin miRNA targets in GBM, data on miRNA expression was taken from the TCGA database and analysed for normalised expression. The TCGA contained five sets of miRNA microarray expression data for GBMs. The full array output files were restricted but miRNA count data was obtained. This data contained information on the reads of each miRNA and, was normalised by reads per million miRNAs mapped. To account for variation between the arrays, the output value for each miRNA was normalised against the value of miR-16; a commonly used miRNA reference control (Davoren *et al.*, 2008). The relative expression of each miRNA, per million RNA was then mapped and is given in Figure 3.28.

Table 3.24 miRNA targets of metformin

miRNA	Change in expression	Target	Known target in cancer[1]	Reference
miR-140-5p	Down regulated	Circulating miRNA in diabetic patients	ADAM10	Kai Y *et al.*, 2014
			TGFBR1; FGF9	Yang H *et al.*, 2013
			DNMT1	Takata A *et al.*, 2013
			HDAC4	Song B *et al.*, 2009
miR-222	Down regulated	Lung cancer, Circulating miRNA in diabetic patients	*MGMT*	Quintavalle C *et al.*, 2013
			p27	le Sage C *et al.*, 2007
			ADIPOR1	Hwang MS *et al.*, 2013
			DKK2	Li Q *et al.*, 2013
			ADAM17	Xu K *et al.*, 2012
			PTPu	Quintavalle C *et al.*, 2012
			PTEN, p57	Garofalo M *et al.*, 2009; Wang Y *et al.*, 2013
miR-142-3p	Up regulation	Circulating miRNA in diabetic patients	ADCY9	Huang B *et al.*, 2009
miR-192	Up regulation	Pancreatic cancer	ZEB2	Wang B *et al.*, 2010
			Bcl2 VEGFA	Geng L *et al.*, 2013
let-7c	Up regulation	Pancreatic cancer	RAS	Johnson SM *et al.*, 2005
			TRIB2	Wang PY *et al.*, 2013
			Bcl-xL	Cui SY *et al.*, 2013
			ITGB3 MAP4K3	Zhao B *et al.*, 2014
			MYC	Nadiminty N *et al.*, 2012
			MMP11 PBX3	Han HB *et al.*, 2012
miR-26a	Up regulation	Breast cancer, Pancreatic cancer	EZH2	Lu J *et al.*, 2011
			HMGA2	Palmieri D *et al.*, 2012
miR-200 family	Up regulation	Murine embryonic fibroblasts	ZEB1	Park SM *et al.*, 2008
			ZEB2	Gregory PA *et al.*, 2008
			SLUG	Liu YN *et al.*, 2013
			E2F3	Feng B *et al.*, 2012
			SIRT1	Eades G *et al.*, 2011
miR-205	Up regulation	Lung cancer, Murine embryonic fibroblasts	LRP1	Song H, Bu G, 2009
			ZEB1 ZEB2	Gregory PA *et al.*, 2008
			PTEN	Greene SB *et al.*, 2010
			ERBB3	Wu H *et al.*, 2009
miR-33a	Up regulation	Breast Cancer	MYC	Blandino *et al.*, 2012
			TWIST	Zhou Y *et al.*, 2014
			PIM-1	Thomas M *et al.*, 2012

Data on identified miRNA targets of metformin treatment. [1]Known target gene of miRNA in cancer. Adapted from Pulito *et al.* (2014).

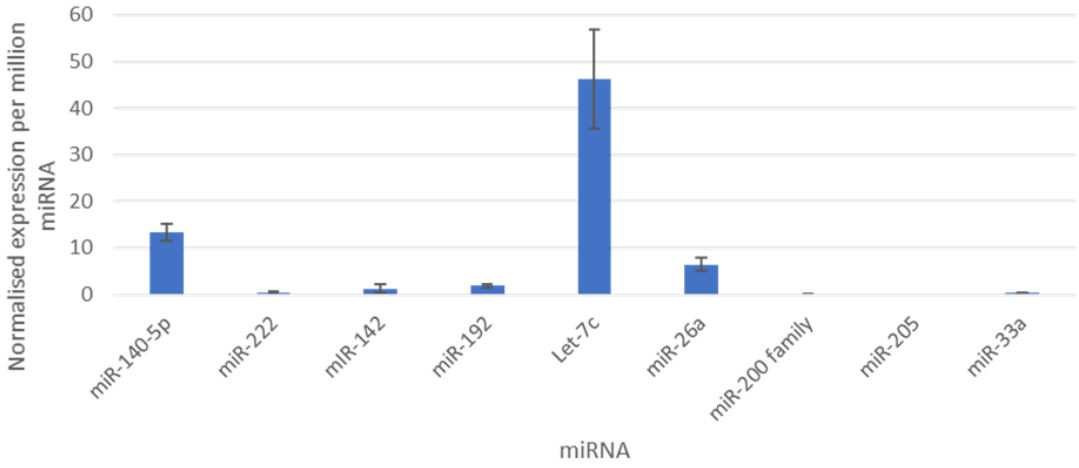

Figure 3.28 GBM normalised expression levels of miRNA targeted by metformin. GBM miRNA array expression data from five data files stored on the TCGA. Number of miRNA reads was mapped per million miRNAs read and then normalised against miR-16. miRNA samples with more than one version had all version averaged before normalisation.

Out of the nine miRNAs assessed, let-7c and miR-140 showed 10 times the expression levels of miR-16. Three miRNAs (miR-142, miR-192 and miR-26) showed similar or slightly raised expression values and four miRNA showed lower levels of expression.

3.5.2 Qualitative assessment of miRNA expression

Five short-term GBM cultures and the established GBM cell line U251MG were used to analyse the impact of metformin on miRNA expression. NHA was included as a control to assess relative expression of each miRNA in GBM cultures. This smaller cohort was representative of the larger culture panel, containing two *P53* wild type GBM cultures and three *P53* mutant cultures. All cultures were treated with ID_{50} values of metformin for 96 hours as given in table 3.2. After extraction and quantification, stem loop miRNA PCR was conducted on 100ng of total RNA. Amplification was successful for 4 of the miRNAs analysed as shown in Figure 3.29. All other cultures showed no band

for expression in either untreated or treated well for all repeats tested. It is unclear if this was from lack of expression in miRNA or an unsuccessful primer design. Two miRNA showed upregulation in metformin treated samples; miR-222 showed upregulation in five cultures (IN859, IN1979, IN1682, IN1760 and NHA) and miR-192 showed upregulation in four cultures (U251MG, IN1979, IN2045 and NHA). miR-140 showed upregulation in metformin treated sample of two cultures (IN1760 and NHA). Let-7c showed down regulation in the metformin treated samples of two cultures (IN2045 and NHA) and upregulation in two cultures (U251MG and IN1760). However qualitative results lacked an endogenous housekeeping control, due to lack of successful miR-16 PCR result and so results need to be quantitively analysed to assess absolute changes in expression.

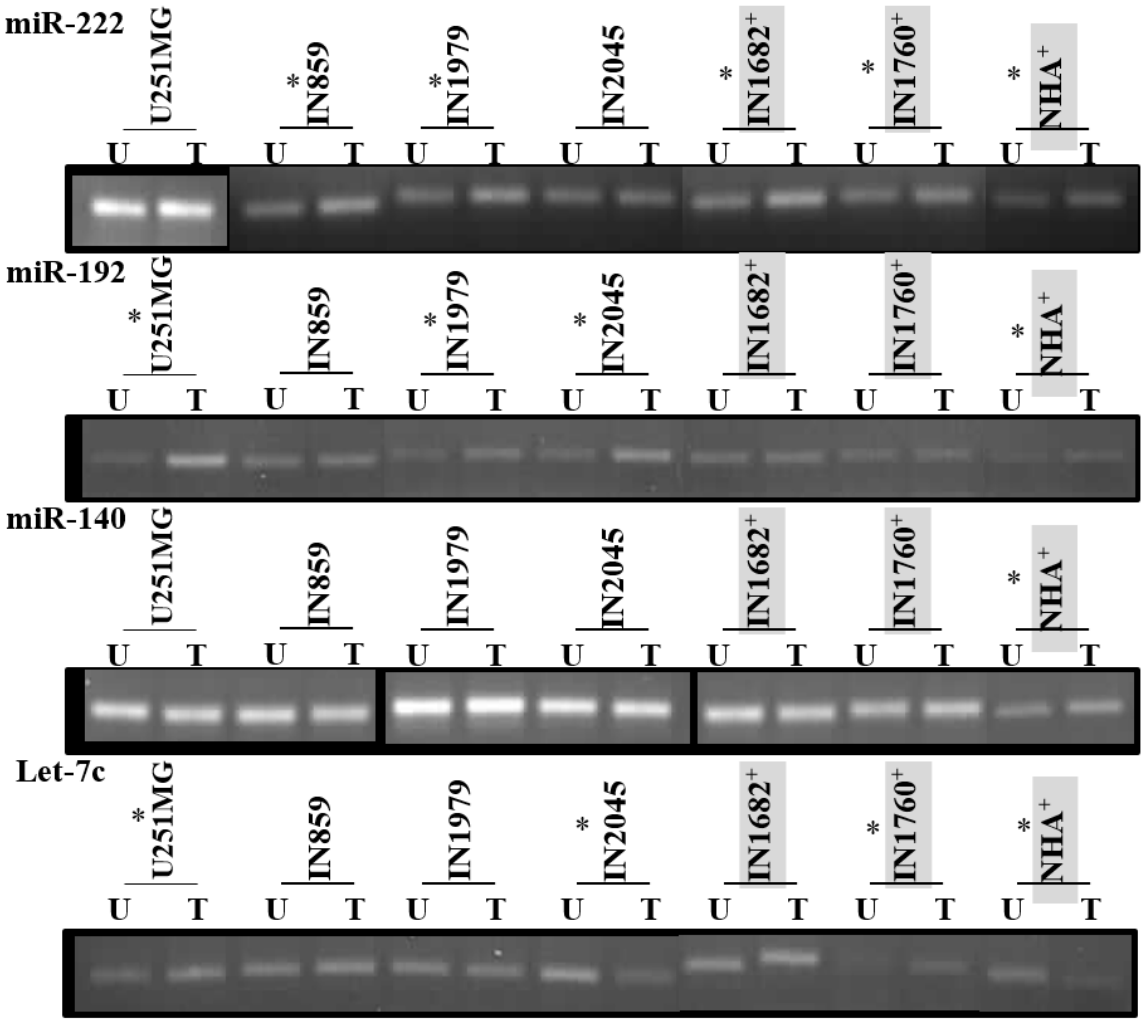

Figure 3.29 miRNA stem loop PCR results. GBM cultures and NHA results of stem loop PCR. Images shown are of samples showing positive band in either well. Results are paired by treatment type. U – Untreated control, T- Treated with metformin at 96-hour ID50. Cultures marked with a $^{+}$ and coloured grey are *P53* wild type samples. Paired samples with a * indicate samples with visible change in intensity of band after metformin treatment.

3.5.3 Quantitative assessment of miRNA expression

The seven cell cultures (U251MG, IN859, IN1979, IN2045, IN1682, IN1760 and NHA) used in Section 3.5.1 were analysed by real time quantitative PCR. From the total RNA samples extracted in 3.5.1, 100ng per sample was used for Q-PCR. As an endogenous control, the non-coding small nuclear RNA U6 was used (Lange *et al.*, 2017). Each culture was analysed twice. Initially, the fold-change in miRNA expression between untreated GBM and untreated NHA results was determined. The fold-change in expression following treatment with ID_{50} concentrations of metformin for 96 hours treatment was also assessed. Values for fold change were measured by 2^-ΔΔCt.

3.5.3.1 miR-222

All GBM cultures showed lower expression of miR-222 compared to NHA as shown in Figure 3.30. U251MG and IN2045 showed the highest expression levels at approximately a 0.4-fold change of NHA expression and expression was lowest in IN859 (0.02 fold). This low level of expression for miR-222 is consistent with the analysis of TCGA data described in Section 3.5.1 implies that miR-222 has expression levels in GBM lower than seen in normal tissue.

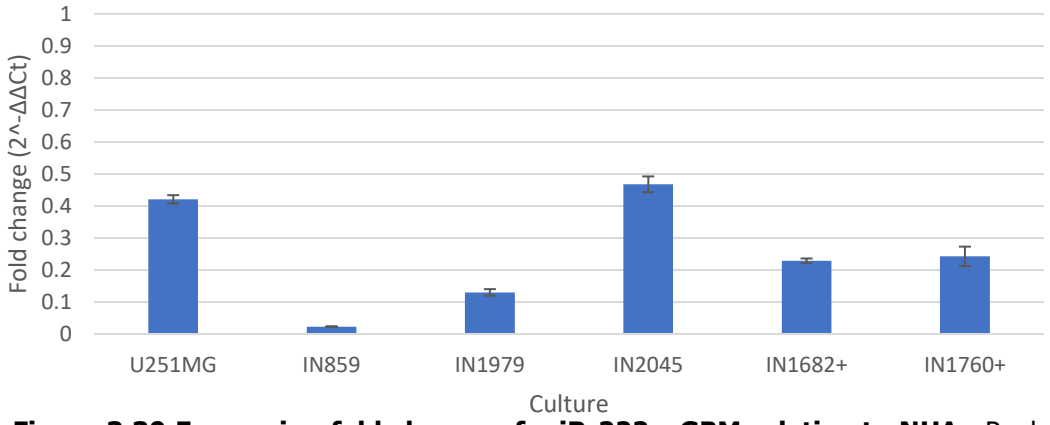

Figure 3.30 Expression fold change of miR-222 - GBM relative to NHA. Real time PCR analysis of miR-222 in GBM cultures. Fold change has been normalised against average expression level of miR-222 in NHA. Cultures marked with a + are *P53* wild type. All GBM cultures showed fold change values less than one, indicating a reduction in miR-222 expression in the GBM samples compared to NHA.

Metformin treatment had a varied effect on the culture panel as shown in Figure 3.31. Five cultures showed a reduction in fold change after metformin treatment. Two *P53* aberrant short-term cultures, IN859 and IN1979, showed increase in fold change greater than 1.5. The two cultures had the lowest expression relative to NHA. Even with this change in expression both cultures will still be lower than NHA. NHA also showed a reduction in miR-222

expression with metformin treatment. The results indicate that metformin has a culture specific impact on miRNA-222 and its expression.

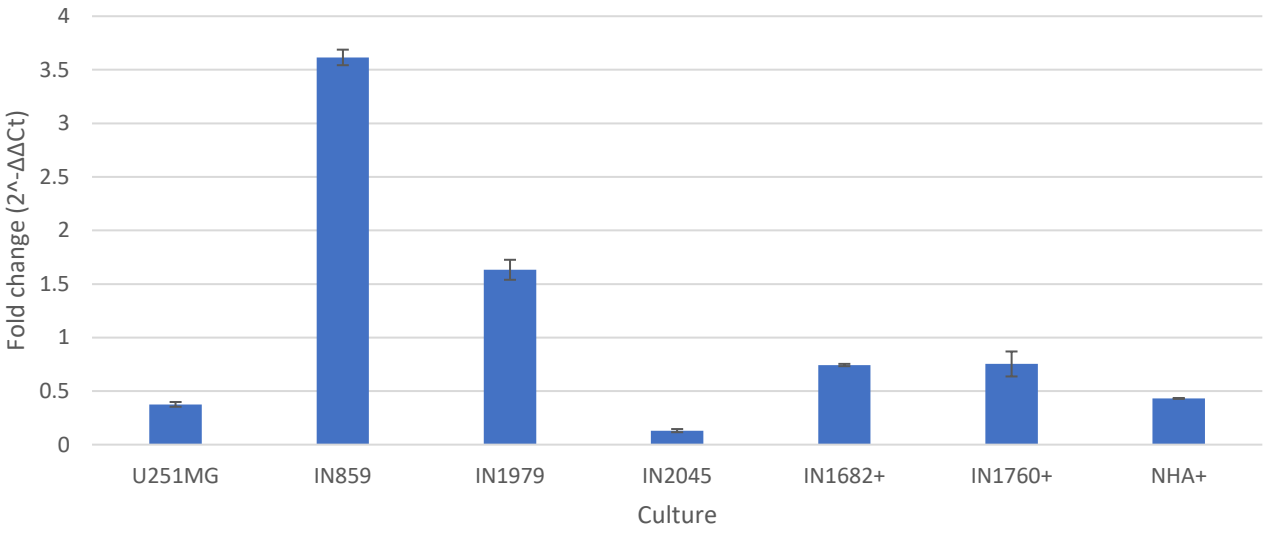

Figure 3.31 Expression fold change miR-222 post ID_{50} metformin treatment. Real time PCR analysis of miR-222 in GBM cultures and NHA treated with 96-hour ID_{50} metformin concentration. Fold change has been normalised against average expression level of miR-222 in an untreated cell culture. Cultures marked with a + are *P53* wild type. Two GBM cultures (IN859 and IN1979) showed fold change values greater than one, indicating an increase in miR-222 expression in the GBM samples after metformin treatment. Four GBM cultures (U251MG, IN2045, IN1682 and IN1760) and NHA showed fold change values less than one, indicating a decrease in miR-222 expression in the culture samples after metformin treatment.

3.5.3.2 miR-192

Only two GBM cultures showed higher expression of miR-192 than NHA, the *P53* mutant cultures IN1979 and IN2045. All other cultures expressed lower levels of miR-192 as shown in Figure 3.32. The low relative levels of miR-192 expression are in line with the analysis of TCGA data. In IN1979, expression, was x4.8 higher than NHA although this result did show the highest standard deviation of all the cultures. This result indicates that miR-192 has lower levels of expression in most GBM cultures when compared to normal tissue.

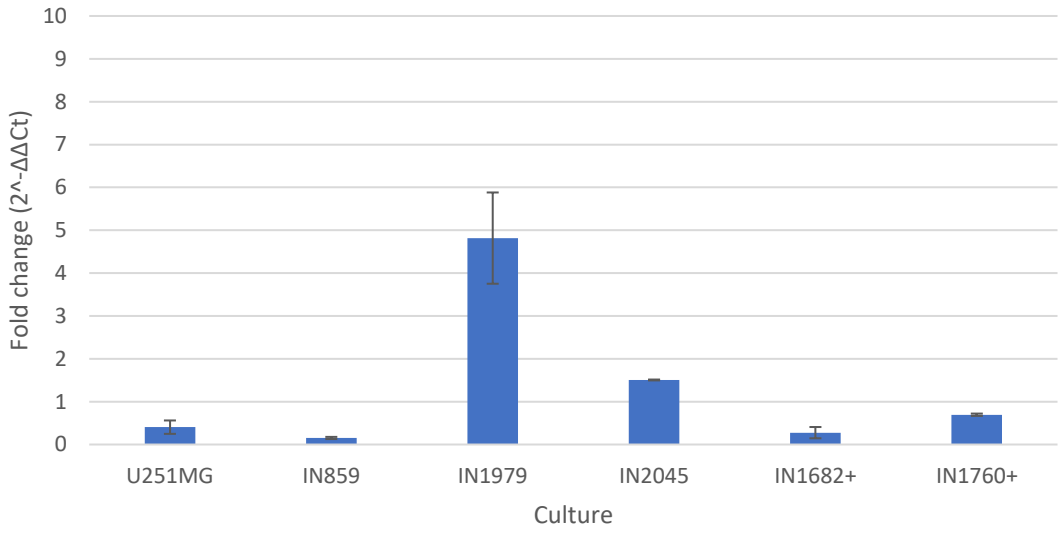

Figure 3.32 Expression fold change of miR-192 - GBM relative to NHA. Real time PCR analysis of miR-192 in GBM cultures. Fold change has been normalised against average expression level of miR-192 in NHA. Cultures marked with a + are *P53* wild type. Two GBM cultures (IN1979 and IN2045) showed fold change values greater than one, indicating an increase in miR-192 expression in the GBM samples compared to NHA. Four GBM cultures (U251MG, IN859, IN1682 and IN1760) showed fold change values less than one, indicating a reduction in miR-192 expression in the GBM samples compared to NHA.

All cultures tested showed an increase in expression of mir-192 after metformin treatment as shown in Figure 3.33. Three cultures showed a fold

change greater than 10, IN1760, IN1682 and IN859. IN1682 possessed the greatest increase with a fold change of 39. Both IN1682 and IN859 were among the smallest expression relative to NHA. The larger fold change exhibited by the samples may be explained by the initial low expression of miR-192 relative to NHA. The remaining cultures showed small increases with IN2045 only having a fold change of 3.3. NHA showed a fold change of 4.4 in line with the rest of the panel.

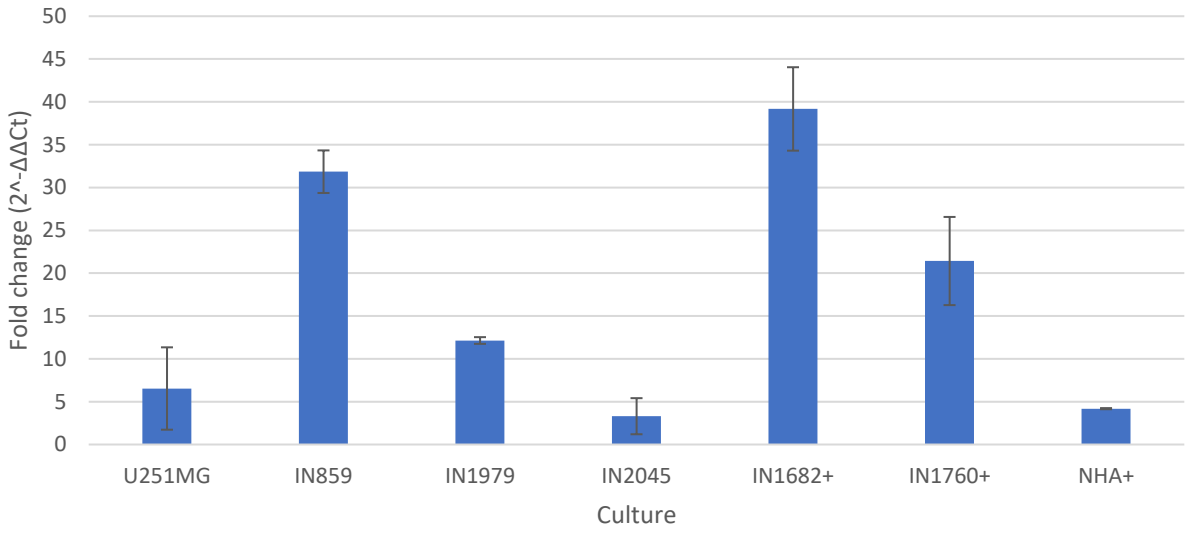

Figure 3.33 Expression fold change miR-192 post ID_{50} metformin treatment. Real time PCR analysis of miR-192 in GBM cultures and NHA treated with 96-hour ID_{50} metformin concentration. Fold change has been normalised against average expression level of miR-192 in an untreated cell culture. Cultures marked with a + are *P53* wild type. All GBM cultures and NHA showed fold change values greater than one, indicating an increase in miR-192 expression in the culture samples after metformin treatment.

3.5.3.3 miR-140

All but one culture showed lower expression of miR-140 when compared with NHA as shown in Figure 3.34. In the remaining culture, IN1682, expression was 5.3-fold higher than in NHA. In contrast, the TCGA data analysis showed that miR-140 is expressed in GBM samples.

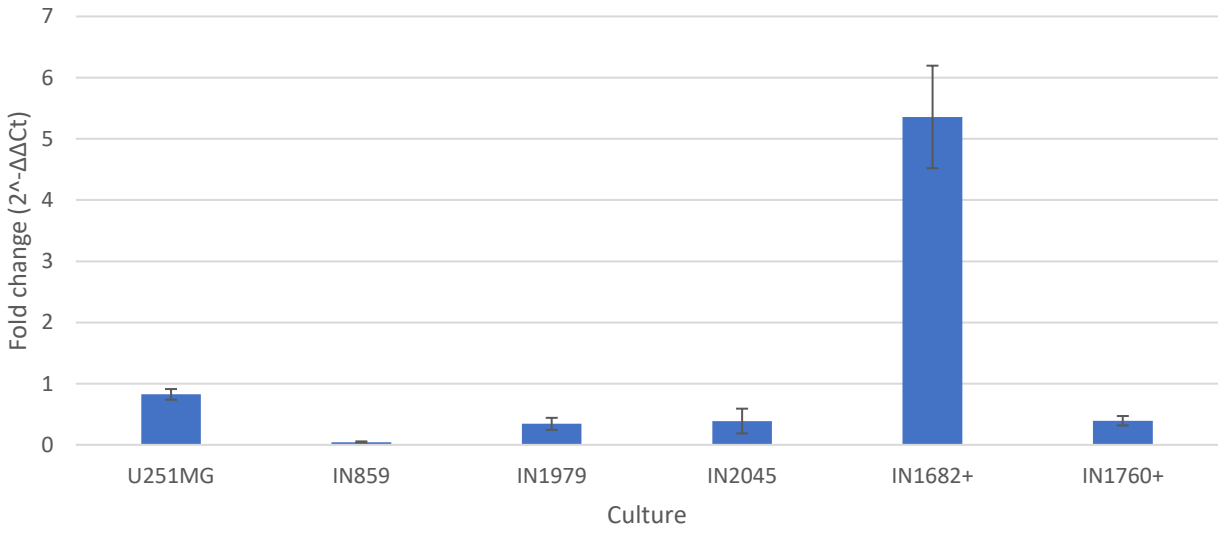

Figure 3.34 Expression fold change of miR-140 - GBM relative to NHA. Real time PCR analysis of miR-140 in GBM cultures. Fold change has been normalised against average expression level of miR-140 in NHA. Cultures marked with a + are *P53* wild type. One GBM culture (IN1682) showed fold change values greater than one, indicating an increase in miR-140 expression in the GBM sample compared to NHA. Five GBM cultures (U251MG, IN859, IN1979, IN2045, and IN1760) showed fold change values less than one, indicating a reduction in miR-140 expression in the GBM samples compared to NHA.

Metformin treatment increased the expression level of miR-140 in all cultures as shown in Figure 3.35 The greatest increase of >20 fold was observed in IN859. This culture possessed a negligible level of expression when compared with untreated NHA and hence, its larger fold change increase may be due to its low initial starting value. NHA did show a fold change of 1.4, this is nearly identical to the result for IN2045.

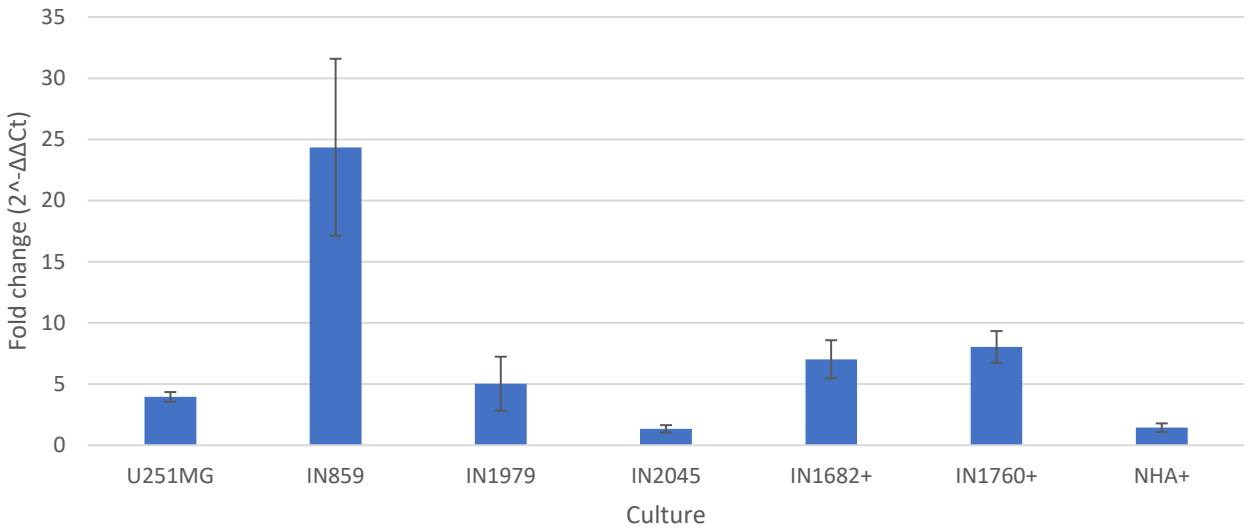

Figure 3.35 Expression fold change miR-140 post ID_{50} metformin treatment. Real time PCR analysis of miR-140 in GBM cultures and NHA treated with 96-hour ID_{50} metformin concentration. Fold change has been normalised against average expression level of miR-140 in an untreated cell culture. Cultures marked with a + are *P53* wild type. All GBM cultures and NHA showed fold change values greater than one, indicating an increase in miR-140 expression in the culture samples after metformin treatment.

3.5.3.4 Let-7c

Expression of Let-7c in GBM cultures were varied, as shown in Figure 3.36. Four cultures showed lower expression than NHA with fold change values less than 1 and two cultures, IN859 and IN2045, had fold change values below 0.15. Two cultures showed higher expression of Let-7c than NHA with, U251MG and IN1760 having fold change values of 1.24 and 1.8, respectively. The TCGA data analysis in Figure 3.28 showed, that relative to the other assed miRNA, let-7c had a higher expression level than average. The results when measured against NHA would imply most GBMs have lower levels of expression than normal cells. All three of the *P53* mutant cultures had a fold change less than 1, including two cultures with very low expression.

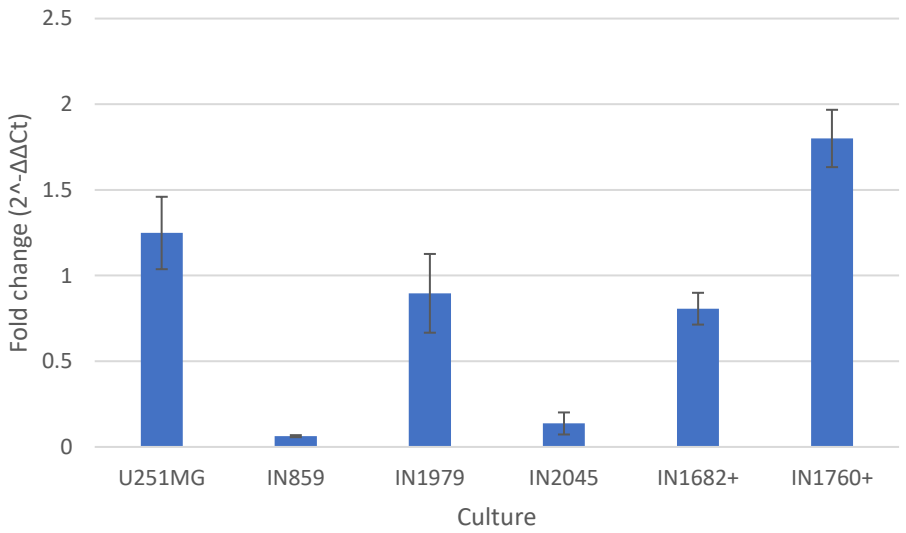

Figure 3.36 Expression fold change of Let-7c - GBM relative to NHA. Real time PCR analysis of let-7c in GBM cultures. Fold change has been normalised against average expression level of let-7c in NHA. Cultures marked with a + are *P53* wild type. Two GBM cultures (U251MG and IN1760) showed fold change values greater than one, indicating an increase in let-7c expression in the GBM sampled compared to NHA. Four GBM cultures showed fold change values less than one (IN859, IN1979, IN2045, and IN1682), indicating a reduction in let-7c expression in the GBM samples compared to NHA.

Expression of let-7c increased after metformin treatment in all GBM cultures as shown in Figure 3.37. Four of the cultures had fold changes > 2. U251MG has a fold change of 1.1 which was the lowest of all the GBM cultures. NHA showed a reduction in let-7c expression level after metformin treatment.

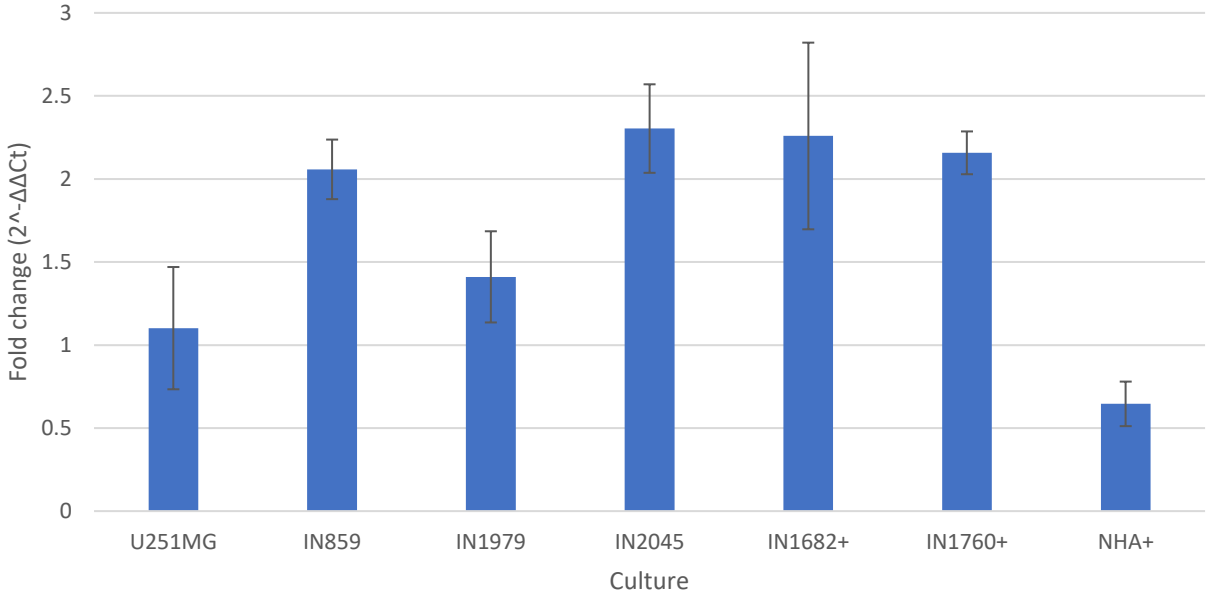

Figure 3.37 Expression fold change let-7c post ID_{50} metformin treatment. Real time PCR analysis of let-7c in GBM cultures and NHA treated with 96-hour ID_{50} metformin concentration. Fold change has been normalised against average expression level of let-7c in an untreated cell culture. Cultures marked with a + are *P53* wild type. All GBM cultures showed fold change values greater than one, indicating an increase in let-7c expression in the GBM samples after metformin treatment. NHA showed a fold change value less than one, indicating a decrease in let-7c expression in NHA after metformin treatment.

3.5.4 *P53* status and miRNA

Analysis of *P53* status with regard to miRNA expression is shown in Table 3.26. This analysis separates the six GBM cultures based on *P53* status and assesses if there is a significant difference in expression based on the cultures *P53* status. In all of the miRNA analysis conducted none showed any significant difference when analysed in relation to *P53* status. An overview of the results and this analysis shows the *P53* is not a defining factor for determining miRNA expression with regard to normal tissue. It is also not a determinant for differential expression of the miRNAs investigated after metformin treatment.

Table 3.25 Analysis of *P53* status with regard to miRNA expression

	p-Value	
	miRNA expression compared with NHA	miRNA expression after metformin treatment
miR-222	0.8869	0.5944
miR-192	0.4872	0.2015
miR-140	0.1829	0.8927
Let-7c	0.2482	0.3077

Results of un paired t-test to compare the difference in means of *P53* sub groups.

3.5.4 Summary

The TCGA data showed that most of the known metformin miRNA targets have low relative expression levels in GBM. Only miR-140 and let-7c showed large increase in quantity of miRNA compared with miR-16. Stem loop PCR was able to detect several expressed miRNAs in GBM samples and detect changes in expression. However, the lack of an endogenous control to compare the result against reduces the usefulness of the technique. Q-PCR combined with U6 as an endogenous control produced reliable data for all miRNA tested, all of which showed a change in expression after metformin treatment.

Although the initial levels of expression were low, metformin reduced miR-222 expression levels in 5 of the cultures. The remaining two had low levels of expression, below 0.2 with respect to NHA so with the resultant increase the cultures will still have minimal amounts of miR222. Although miR-222 is an important miRNA for growth and cardiac repair (Liu *et al.*, 2015), it has been reported to have implications in a range of cancers. A function of miR-222 is as a regulator of p27kip1, the cell cycle regulator and tumour suppressor. It has been reported that in glioma, high expression of miR-222 is linked with suppression of p27kip1 (le sage *et al.*, 2007) In lung cancer, metformin has been shown to reduce proliferation through inhibiting miR-222 and thus preventing it from inducing cell growth and cell cycle progression (Wang *et al.*, 2013). In breast cancer, the miR-222 promotes tumour aggressiveness and metastasis (Shah and Calin, 2011). It functions as key factor in melanoma development and dissemination while being propagated through exosomes (Felicetti *et al.*, 2016). However, the role is cancer specific, as miR-222 has been identified as a tumour suppressor in prostate cancer (Fuse *et al.*, 2012). In diabetic patients, miR222 can act to accelerate cell proliferation and has found to be upregulated. The factors are alleviated in type 2 diabetics through metformin treatment (Coleman *et al.*, 2013). Although low levels of miR-222 were present in all cultures tested, it has strong tumour promoting properties and metformin may have part of its anti-tumour action through suppression of this miRNA.

miR-192 expression levels in both the TCGA data analysis and GBM cultures was relatively low, although expression was elevated in one samples, IN1979.

The role of miR-192 has been identified as a tumour suppressor in a range of cancers. For renal cell carcinoma, miR-192 has been identified as functioning as part of a microRNA network, working alongside miR-193 and miR-215 to supress cell migration and invasion (Khella *et al.*, 2013). This is similar to other studies linking miR-192 and miR-215 to a *P53*-dependent up-regulation induced by genotoxic stress (Georges *et al.*, 2008). However, in the current study, there was no significant association between expression and *P53* status. It has been reported that miR-192 is a key regulator of transcription factors EGR1 and HOXB9 which control tumour angiogenesis (Kondetimmanahalli *et al.*, 2018). In colon cancer, overexpression of miR-192 inhibits metastatic colonization and sensitisizes cells to stress induced apoptosis (Geng *et al.*, 2014). However, miR-192 has conversely been negatively linked to cancer as well. In renal and ovarian cancers, low expression of miR-192 has been linked to poor clinical outcome (Kondetimmanahalli *et al.*, 2018). All cultures showed some upregulation of miR-192 with some showing large increases in expression after metformin treatment. The upregulation of miR-192 could be aiding metformins anti-tumour potential.

miR-140 showed very low levels of expression in all cultures except IN1682 that showed a 5-fold increase over NHA cells. This high-level expression is not significantly linked to *P53* status as IN1760 had a fold change of 0.39. This low level of expression in cultures and cell lines relatively to normal controls has also been reported in ovarian cancer (Lan *et al.*, 2015). This work also reported the role of miR-140 as a tumour suppressor. Overexpression in hepatocellular carcinoma inhibited proliferation and induced apoptosis. miR-

140 has also been linked with regulation of the Wnt signalling pathway (Barter *et al.*, 2015). In gliomas, miR-140-5p targets HOXA11-AS at 3'-UTR. HOXA11-AS has been linked with poor patient prognosis and shorter survival (Yan *et al.*, 2017). In colorectal cancer, it has been shown to be strongly associated with better survival through targeting of smad2 metastatic phenotype promotor (Zhai *et al.*, 2015).

Let-7c expression varied between GBM cultures. However, all the tumour cultures responded to metformin treatment with increased expression of Let-7c. Let-7c was also the only miRNA tested that showed a reduction in NHA, an inverse of the response seen in all of the GBM samples.

In cholangiocarcinoma, let-7c has been identified as a tumour suppressor reducing mamo sphere generation (Lin *et al.*, 2015). Let-7c also plays a role in chemo-resistance in bladder cancer, with decreased let-7c expression leading to reduced patient response (Vinal *et al.*, 2016). In glioma, let-7c has been linked to enforcing progression differentiation within the cell, reducing stem-like qualities (Degrauwe *et al.*, 2016). The mRNA binding factor IMP2 binds to miRNA recognition elements and prevents let-7c silencing. This would be consistent with the low to similar expression when compared with NHA. The upregulation from metformin treatment may lead to silencing of let-7c target genes. Phenformin has also been shown to increase let-7c expression in GBM cultures (Jiang *et al.*, 2015). Let-7c appears to have a tumour suppressor role in several cancers. Metformin may cause part of its cytotoxic and tumour supressing effects through this increase in miRNA expression.

The results here show that metformin has an impact on similar miRNAs to other cancer types as outlined by Pulito *et al.* (2014). GBM cultures did show a varied expression of miRNAs between cultures that was not linked to *P53* status. Metformin may exert some of its cytotoxic effect in GBM cultures through regulation of miRNA with tumour populations.

CHAPTER 4

Final discussion and conclusions

Chapter 4 - Final discussion and conclusions

4.1 Discussion

4.1.1 Metformin and *P53*

Sensitivity to metformin was shown to be significantly linked to *P53* aberrations. Cultures possessing *P53* mutations and deletions had significantly lower ID_{50} values than *P53* wild type cultures. The relationship between *P53* and metformin has been demonstrated in a range of cancers. However, the inverse of this relationship, requiring the activation of *P53* for sensitivity to metformin treatment has been observed in breast, hepatocellular, Hodgkin lymphoma, prostate, melanoma, and lung cancer (Ben Sahra *et al.*, 2010; Cerezo *et al.*, 2013; Do *et al.*, 2014; Gu *et al.*, 2015; Li *et al.*, 2015; Sun *et al.*, 2016; Shimazu *et al.*, 2017). In colorectal and uterine serous carcinoma, the effects of metformin were demonstrated to be *P53* independent (Sarfstein *et al.*, 2013; Abu el Maaty *et al.*, 2017). Buzzai *et al.*, (2007) demonstrated that *P53* aberrant colon cancer cell lines had increased sensitivity to metformin over *P53* wild type cell lines. They reported that under metformin induced cellular stress; wild type cells, but not aberrant cells, had an enhanced rate of glycolysis and reduced proliferation to increase cell survival. This was backed up by a study showing *P53* wild type had a role in protecting metabolically impaired cells under the effects of glucose and nutrient limitation (Jones *et al.*, 2005). The importance of nutrient deprivation was shown with the significant relationship of glucose concentration to cell death, as given in 3.4.3 and demonstrated in cancer and breast cell lines (Menendez *et al.*, 2012; Birsoy *et al.*, 2014). This implies that GBM with a *P53* mutation has potentially

higher sensitivity to metformin due to lack of metabolic control during glucose depravation.

4.1.2 Synergistic response of Temozolomide and Sorafenib

4.1.2.1 TMZ

A synergy between metformin and TMZ in GBM has been demonstrated before. Yu *et al.* (2015) reported that treating the U251MG and U87MG cell lines with metformin and TMZ has a significant effect on inhibiting proliferation, inducing apoptosis and reduced gliosphere formation. This work demonstrated the same synergistic response in U251MG. However, variation was present within the short term GBM cultures. Only two of the seven cultures showed a synergistic response. The response was not linked to *P53* status or *MGMT* methylation. Further characterisation of the cultures is needed before a relationship can be identified to explain the synergy results observed. TMZ has been shown to induce apoptosis in GBM through activation of AMPK upregulating and activating *P53* (Zhang *et al.* 2010). AMPK is a metabolic kinase, important in regulation of metabolism and proliferation of cells (Mihaylova and Shaw, 2011). The effects of AMPK activation have been shown to be augmented by, AMPK independent, AMPK agonists such as metformin (Liu *et al.*, 2014). The AMPK agonists act indirectly through metabolic stress to cause further physiological AMPK activation. This net increase of AMPK further sensitises cells to TMZ (Yu *et al.*, 2015).

In addition to this, metformin also impacts AKT as part of the mTOR pathway (Mahvash *et al.*, 2010). AKT activation and upregulation of the mTOR pathway is a common alteration in tumours and leads to increased cell proliferation and

survival (Alfonso *et al.*, 2005; Sharma *et al.*, 2015). Inhibition of AKT has been demonstrated to enhance the cytotoxicity of TMZ (Chen *et al.*, 2012). TMZ upregulates AKT however this is counteracted through metformin induced inhibition of AKT and the mTOR pathway (Yu *et al.*, 2015). This synergism of the two drugs leads to increased TMZ sensitivity in GBM cultures.

Lee *et al.* (2018) demonstrated using the cell lines U87MG, U251MG and A172 that in addition to the effects on AMPK and AKT, a metformin TMZ combination decreases expression of fatty acid synthase (FASN). Cancers with high FASN activity have increased proliferation (Swinnen *et al.*, 2002). In gliomas increased FASN activity has been correlated with WHO tumour grade (Grube *et al.*, 2014). The use of FASN inhibitors was linked to reduction in cell viability and survival (Yasumoto *et al.*, 2016).

4.1.2.2 Sorafenib

Sorafenib was shown to have a strong synergistic relation to metformin. All cultures showed an overall synergistic response to combination with only one culture (IN2045) showing some variation in its replicate results. As discussed in 3.2.4.1 the mechanism of synergy possibly stems from the dual pathway inhibition of the drug combination. Metformin impacting the cells through AMPK/AKT/mTOR and sorafenib impacting through RAF/MAPK (Aldea *et al.*, 2014). This joint effect of the pathways has been considered as an important therapeutic target for cancer cells (Chappell *et al.*, 2011; Asati *et al.*, 2016). The dual action of this drug has been hypothesised in hepatocellular carcinoma and is given in figure 4.1.

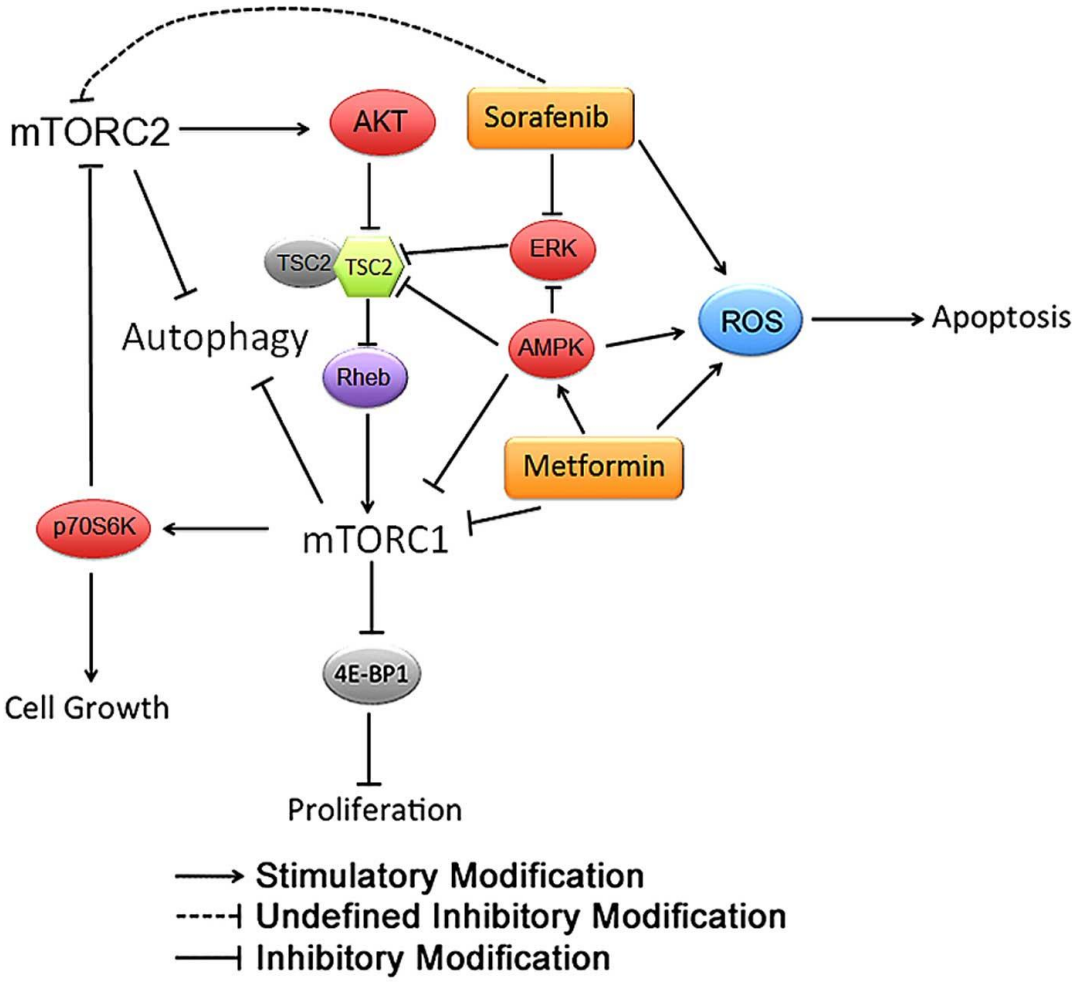

Figure 4.1 Proposed mechanism of metformin and sorafenib combination in hepatocellular carcinoma. When used in combination on hepatocellular carcinoma, metformin promotes activation of reactive oxygen species and upregulated AMPK causing mTORC1 inhibition. This is supported by sorafenib inhibiting mTORC2 by an unknown inhibitory mechanism. The co-operation of these two drugs regulation on both mTOR complexes may promote autophagy. (Ling *et al.*, 2016)

The pathways are commonly dysregulated in cancer and the effects of the inhibition have been observed in other cancers (Steelman et al, 2011). Molhoek *et al.* (2005) demonstrated a similar synergistic inhibition of the two pathways in human melanoma with B-Raf inhibitor and mTOR inhibitor rapamycin. Wang *et al.* (2008) demonstrated sorafenib combined with rapamycin had a synergistic response at inhibiting hepatocellular carcinoma in murine models. The simultaneous inhibition of these pathways impacts several downstream factors including apoptotic, proliferative and differentiation pathways (Vivek *et al.*, 2016). The results also demonstrate the importance of combination therapies and the use in the treatment of cancers. Several clinical trials have assessed sorafenib for use on GBM and showed moderate to no effect on progression free survival (Hainsworth *et al.*, 2010; Hegi *et al.*, 2011; Peereboom *et al.*, 2013). The addition of metformin creating a dual pathway synergistic combination treatment may prove more effective.

4.1.3 Metformin mechanism of cell death

The summary of the results of section 3.4 indicate no sign of induced apoptosis from metformin treatment. Apoptotic time course analysis showed no significant changes in phospholipid membrane prior to cell death. Caspase 3/7 levels showed no significant changes in activity post metformin treatment and assessed sub-G0/G1 populations showed no increase in cell cycle analysis. Mitochondrial membrane was depolarised in all cultures; however, this process can be independent of apoptosis and independent of caspase activation (Dussmann *et al.*, 2003; Ly *et al.*, 2003). *P53* did not have a significant impact on any apoptosis related cell death analysis.

Metformin may act through another mechanism of cell death, both autophagy and necrosis have been linked to metformin. One study linked metformin and simvastatin treatment to receptor-interacting protein kinases (Ripk) dependent necrosis (Babcook *et al.*, 2014). However, only U251MG, IN2045 and NHA showed significant changes in necrotic cell populations and was not consistent across the time course. All other cultures showed no significant change in necrotic cells, instead showing significant dead cells. Autophagy is another mechanism linked to metformin treatment. Autophagy can become triggered in response to cellular stress and increases in cellular metabolic demands (Zhineng *et al.*, 2011). Metformin can induce autophagy flux through regulation of AMPK (Zhang *et al.*, 2017). Sesen *et al.* (2015) demonstrated in GBM cell lines (U87MG and U251MG) metformin induced autophagy. Therefore, autophagy is a possible candidate alternative mechanism through which metformin induces cell death in GBM short term cultures.

A significant relationship between media glucose concentration and cell death over time was demonstrated in 3.4.3. Glucose deprivation has been highlighted as an important factor in metformins cancer cell lethality (Birsoy *et al.*, 2014). Menendez *et al.* (2012) demonstrated that glucose concentration has a protecting effect on metformin induced cell death in breast cancer cells. Dosages of glucose of 10Mmo/L resulted in low levels of cell death and cell cycle arrest in G0/G1 phase, glucose depletion lead to increases in cell death. After 96-hours of metformin treatment, GBM cells under glucose starvation showed G2/M arrest and high levels of cell death.

4.1.4 Metformin G2/M cell cycle arrest

Metformin induced G2/M cell cycle arrest in four of the five GBM cultures tested. IN1682 showed a non-significant increase in G2/M phase. Metformin has been shown to impact cells through G2/M arrest in GBM cell lines and other cancer types (Jeong *et al.*, 2015; Rodríguez-Lirio *et al.*, 2015; Adeburg *et al.*, 2017). Progression of the cell through cell cycle is managed by regulatory proteins called cyclin dependent kinases (CDK) that interact with cyclin proteins (Hydbring *et al.*, 2016). The G2/M phase transition is managed by CDK1 with cyclin A and progression through mitosis is managed by CDK1 with cyclin B (Vermeulen *et al.*, 2003). Lee *et al.* (2016) demonstrated that treatment with metformin in lung cancer cell lines correlated with downregulation of CDK1/cyclin B leading to cell cycle arrest. In human salivary adenocarcinoma cell lines, showed G2 cell cycle arrest due to decreased expression in CDK1 after 48 hours of 4mM metformin treatment (Guo *et al.*, 2015). The activation of CDK1/cyclin B complex is required in the progression of cell cycle from G2 to the mitotic M phase (Choi *et al.*, 2011). Measurement of CDK1/cyclin B and cyclin A may indicate if metformin utilises this mechanism to induce G2/M cell cycle arrest in GBM.

4.1.5 Metformin impact on miRNA expression

Metformin was shown to have an impact on the expression of four miRNA (miR-140, miR-192, miR-222 and let-7c). The miRNAs were outlined as known metformin cancer targets in Pulito *et al.* (2014). Five of the nine known metformin influenced miRNAs were not able to be detected in GBM cultures (miR-26a, miR-33a, miR-142, miR-200 and miR-205). Due to miRNAs abilities on post transcriptional regulation of mRNA, the dysregulation of pathways can

have a strong contribution to the tumour development, progression and therapeutic response (Iorio and Croce, 2012). MiRNA also have beneficial roles as diagnostic and prognostic biomarkers of cancer (Brown *et al.*, 2017). Metformins impact on reducing miR-222 expression could counteract proliferation and invasion (le sage *et al.*, 2007, Wang *et al.*, 2013). miR-192 has been outlined as a tumour suppressor and metformin was demonstrated to cause upregulation (Khella *et al.*, 2013). miR-140 has been identified as a tumour suppressor and metformin treatment showed upregulation (Yan *et al.*, 2017). Metformins impact on miR-192 and miR-140 could counteract tumour growth. Let-7c is a tumour suppressor that enforces cell progression and differentiation regulation, the miRNA showed upregulation from metformin treatment (Degrauwe *et al.*, 2016). The results may indicate that metformins mechanism of action within, the inhibition of GBM cultures, is through modulation of miRNA expression.

The differential expression of miRNA is being used to identify molecular subtypes within GBMS (Verzola *et al.*, 2018). This would enable improved molecular diagnosis and the generation of targeted therapeutics. In two of the miRNA analysed (miR-192 and miR-140) there was an outlier with differential expression to the rest of the GBM cultures. In miR-192, IN1979 showed increased expression and in miR-140, IN1682 showed an increased expression profile. The observed difference is not explained through *P53* status of the culture and may indicate molecular subtypes (Godlewski *et al.*, 2017).

4.2 Conclusion

This study showed the effect of metformin on a panel of short term GBM cell cultures. This unique group of cultures showed large variety in the response to metformin. The importance of this highlights the current over reliance in using immortal GBM cell lines and implies the possibility of generating results not representative of real GBM tumours.

Metformin cytotoxically kills GBM cells but sensitivity varies and is significantly modulated by *P53* status and the availability of glucose in the media. Phenformin also showed a significant link between *P53* and metformin sensitivity but at a magnitude lower in dosage. This highlights the possibility of other analogues or formulations of metformin having an even greater response. Phenformin is a discontinued drug, however the strong response shown here does suggest that other biguanides may possess strong anti-tumour properties. An obstacle in the application of other stronger biguanides will be overcoming the inherit negative side effects of biguanide drug use, that may need to be designed out to improve efficacy.

Glucose mediated metformin sensitivity was seen in all GBM cultures tested. The availability of glucose is an important factor when assessing the potential of metformin *in vivo*. Understanding the role of glucose, other metabolites and micro environment on GBM sensitivity to metformin will help understand and utilize biguanides as a treatment.

Metformin showed good synergy with sorafenib, this pairing should be further tested to see if it can be carried forward to clinical trials. Metformin also showed some synergy with TMZ. Further characterisation will allow for the

possible identification of this metformin induced TMZ sensitive molecular sub group. Increasing GBM sensitivity to TMZ may be beneficial for some patients when used as part of combined therapy.

We are progressing towards a new medical paradigm with personalised medical care, where treatment will be planned based on tumour molecular abnormality profile rather than tissue type or anatomical origin (Jackson *et al.*, 2015). The significant difference seen in *P53* aberrant cells clearly highlights that a sub-set of GBM tumours might be advisably treated with metformin.

The lack of detectable apoptotic cell death is also a novel result in GBM cell cultures. Reported cancer cells response to metformin varies between cancer type. This work identifies a non-caspase dependent, non-apoptotic cell death metformin response mediated by G2/M cell cycle arrest and mitochondria membrane depolarisation.

4.2.1 Limitations

There are several limitations inherent to this study and its techniques used.

The use of short term cultures was a strong feature of the study as it provided a more representative model of original GBM tumours. However, the panel of short term cultures needed to be further characterised, genetically and epigenetically, to make full use of the variety present within the panel. This would also enable a more complete understanding of the variation in cellular response and identify potential treatment sub-groups.

Short term cultures are more labour intensive compared to culturing immortal cells lines. This led to smaller groups of cultures being used for some

experiments. Due to the large variations in the culture doubling times it became a logistical problem to maintain many different short-term cultures, while also increasing the volume of each for experimental work. This issue could be alleviated by more efficient planning and work flow structuring. Completing all required experiments on smaller batches of similar cultures would unify experimental setups and treatment times.

Availability of biguanides for complete testing of metformin analogues was another limitation. The inability to source the drugs hindered expanding the scope of the work to the entire biguanide drug class.

Measurements of glucose levels within the culture media is an area of study not commonly assessed but the results demonstrated here are limited by the equipment used. The repurposed diabetic meter was shown to yield results similar to the glucose standards tested, however it did not have the ability to measure glucose levels below 1mM. The acquisition of a custom designed measurement tool would enable a greater level of reliability and accuracy in glucose measurement.

Analysis of cell death pathways was limited in the amount of techniques and avenues assessed. The analysis of apoptotic and cell cycle pathways needs examination at multiple points to definitively realise the complete mechanism of action utilised. In addition, the study did not assess necrosis or autophagy as possible mechanisms of metformin-based cell death. Analysis into these areas of work was outlined to be completed using western blotting and flow

cytometry. Problems arouse in the calibration of these techniques and no results were able to be reliably generated within the time frame of the work.

The results of miRNA expression analysis did identify changes attributed to metformin treatment, however due to the nature of the technique only a small number of miRNA were assessed. Realtime PCR gives accurate expression level analysis, but it is a time and resource intensive technique with a low volume of throughput. The inclusion of miRNA micro-arrays would further the scope of analysis beyond individual miRNA samples to all expression changes for each GBM culture.

4.3 Further study

This study has identified metformin has potential use as a GBM treatment and worth further investigation. There are several directions this research could take.

Metformin has a strong cytotoxic and metabolic effect on the cells, identifying the underlying mechanism of action utilized by metformin in GBM will help to identify potential partners and analogues. Western blotting and further flow cytometry would allow for this functional pathway analysis and should be the main start point of future research.

Targets and areas of interaction of metformin within the cell are not well understood. Due to metformins lack of breakdown within normal tissue, it should be possible to utilize low dosage fluorescently labelled metformin to assess where metformin accumulates with GBM cells (Ferrera *et al.*, 2012).

Follow up analysis using confocal microscopy could then generate 3D models to better visualise the results.

Due to its already existing use, metformin could easily be repurposed and approved for other treatments if shown to be effaceable. However new derivates of metformin may prove to have superior anti-cancer attributes and open new avenues for drug development (Lam *et al.*, 2018). Collaborating with other institutes to produce and test new chemicals would be a possible avenue of investigation but may be difficult to set up.

Glucose starvation conditions showed to be a significant factor in GBM sensitivity. Further analysis into availability of glucose and other metabolites could aid in improving GBM drug sensitivity. This may indicate that the use of calorie restrictive diets, for example ketogenic diets, will benefit patients and aid in improving outcomes. The fate of glucose in metformin treated cells will also aid in understanding the mechanisms that are utilised. Pathway analysis through use of ^{13}C-glucose labelling would allow for measurement of any kerb cycle and metabolic abnormalities (D'Alessandro *et al.*, 2015).

The improvement of cell culture modelling could be expanded on, primarily experimenting with different media types and different environmental conditions. The use of 3-D modelling and neuro spheres are the next step to closing the gap between scientific model and authentic growth conditions (Kaluzova *et al.*, 2015).

Hypoxia is a major factor that is not accommodated in the majority of cell culture work. The immense pressure and hyper-competitive densely packed

conditions present within a tumour are not represented by standard growth flasks and have effects on tumour proliferation (Mahase *et al.*, 2017). Growing all cultures within hypoxic incubators, and examined only in hypoxic work stations, would allow for experiments to be conducted under hypoxic conditions.

Metformin was demonstrated to affect the miRNA expression in GBM. Full analysis of all genomic miRNA through micro-arrays would generate a complete picture of metformins total effect on the miRNA expression profile for GBM.

The results of this work have shown that metformins mechanism of cell death within GBM appears to be non-caspase non-apoptotic and utilises other factors including availability of glucose and miRNAs. This shows that the scope of metformins action has a wide affect over the GBM metabolism and has potential inter-play between several factors.

The development of novel and repurposed treatments for GBM is a long and arduous process that has no guarantees of future success. The importance of this field of research will also likely grow over a time. If metformin, a derivate of metformin or another biguanide can prove to increase our understanding of GBM and cancer metabolism then its potential should not be overlooked.

Appendix

Appendix A -Metformin treatment 72 Hour Individual graphs

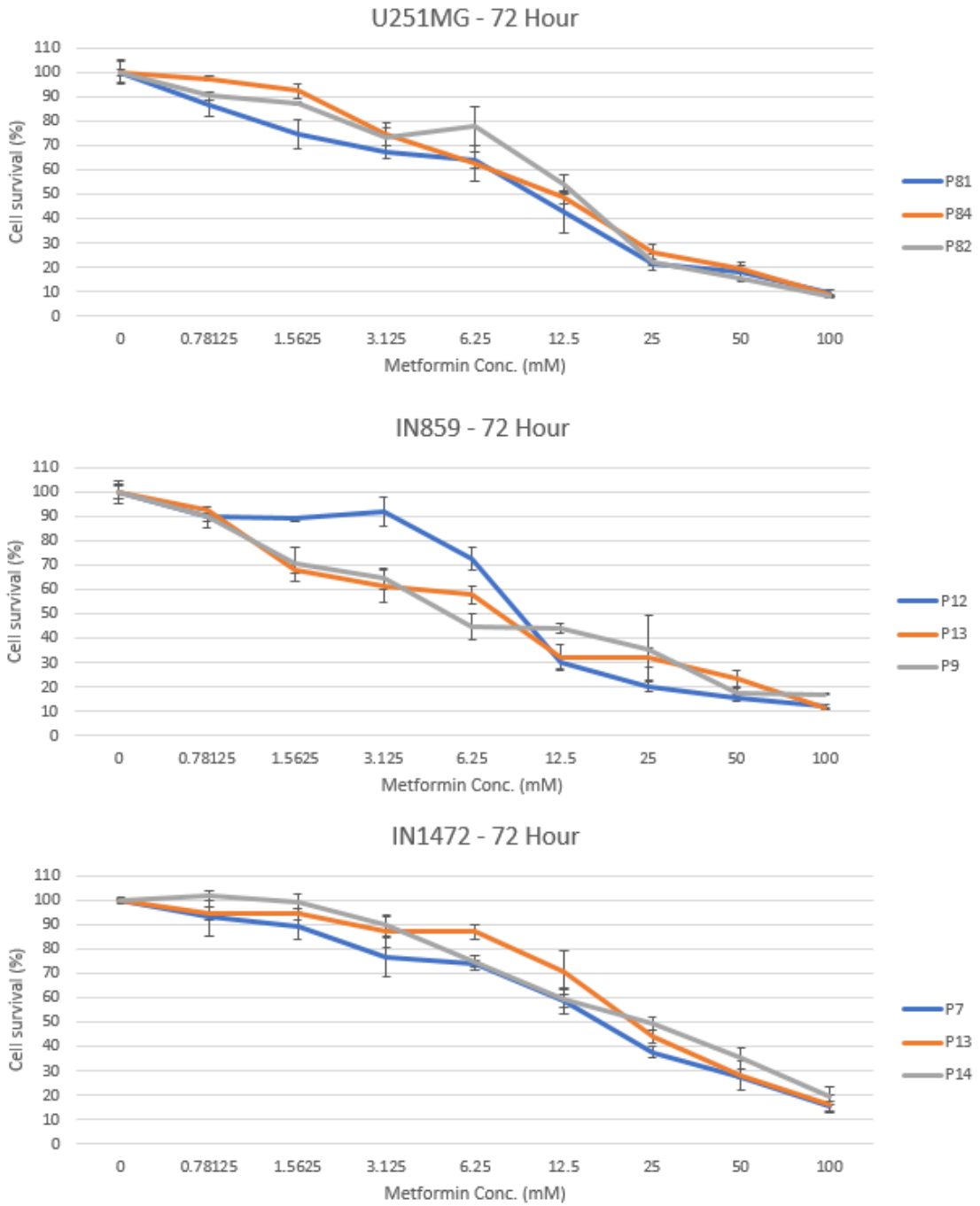

Appendix A1 72 Hour SRB cytotoxicity assays for metformin. Result of SRB assay used to determine ID50 of metformin at 72 hours. P – Passage of the culture.

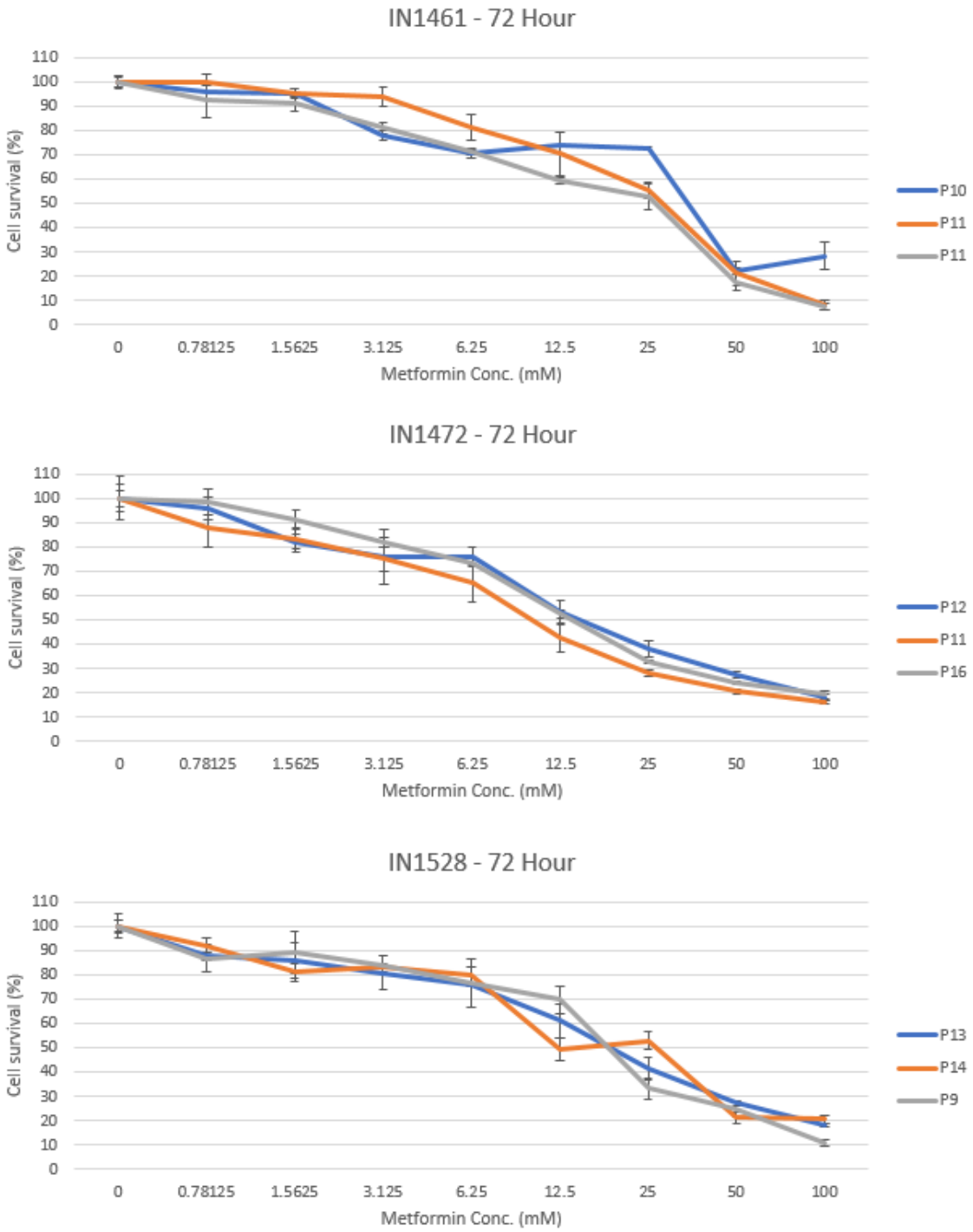

Appendix A2 72 Hour SRB cytotoxicity assays for metformin. Result of SRB assay used to determine ID50 of metformin at 72 hours. P – Passage of the culture.

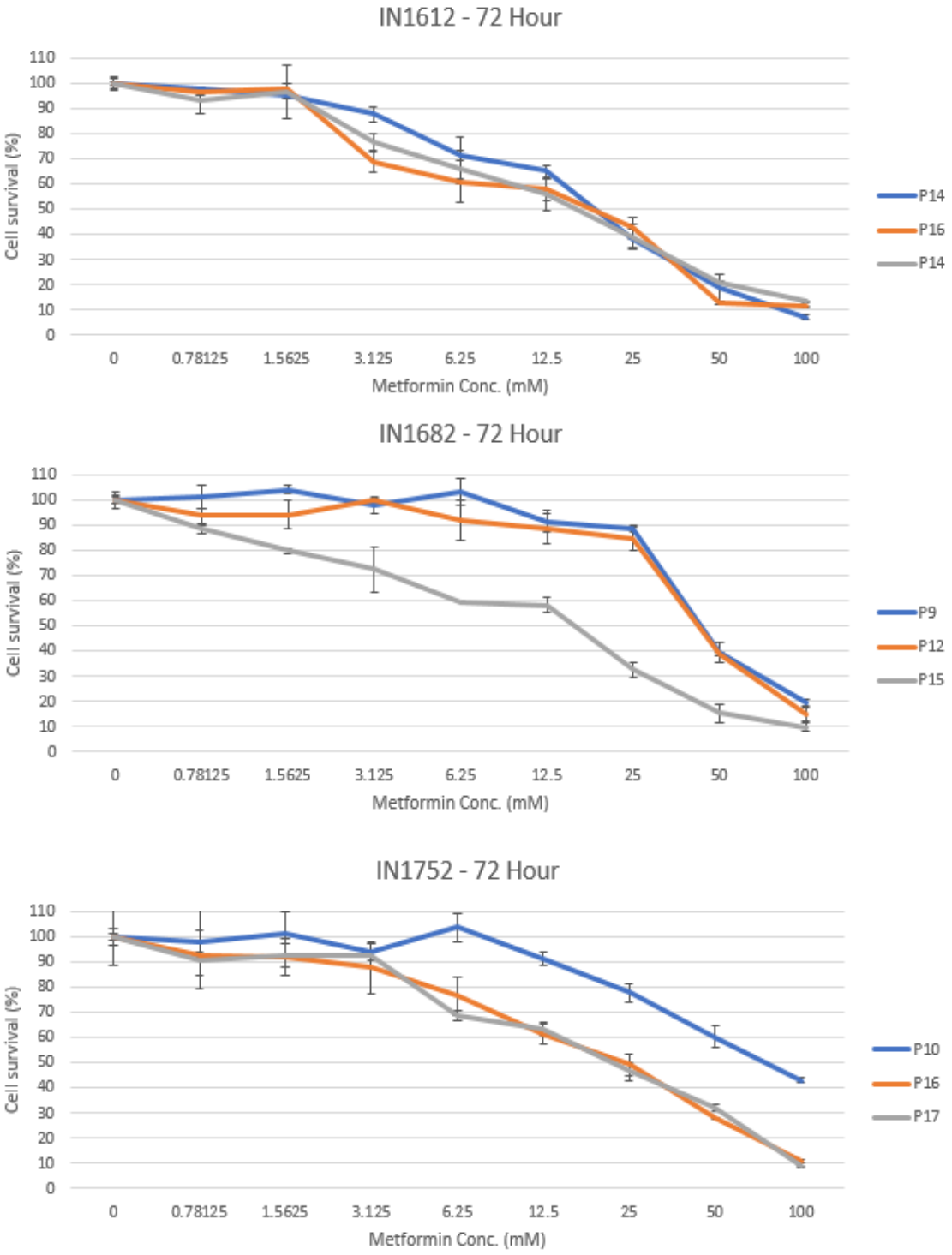

Appendix A3 72 Hour SRB cytotoxicity assays for metformin. Result of SRB assay used to determine ID50 of metformin at 72 hours. P – Passage of the culture.

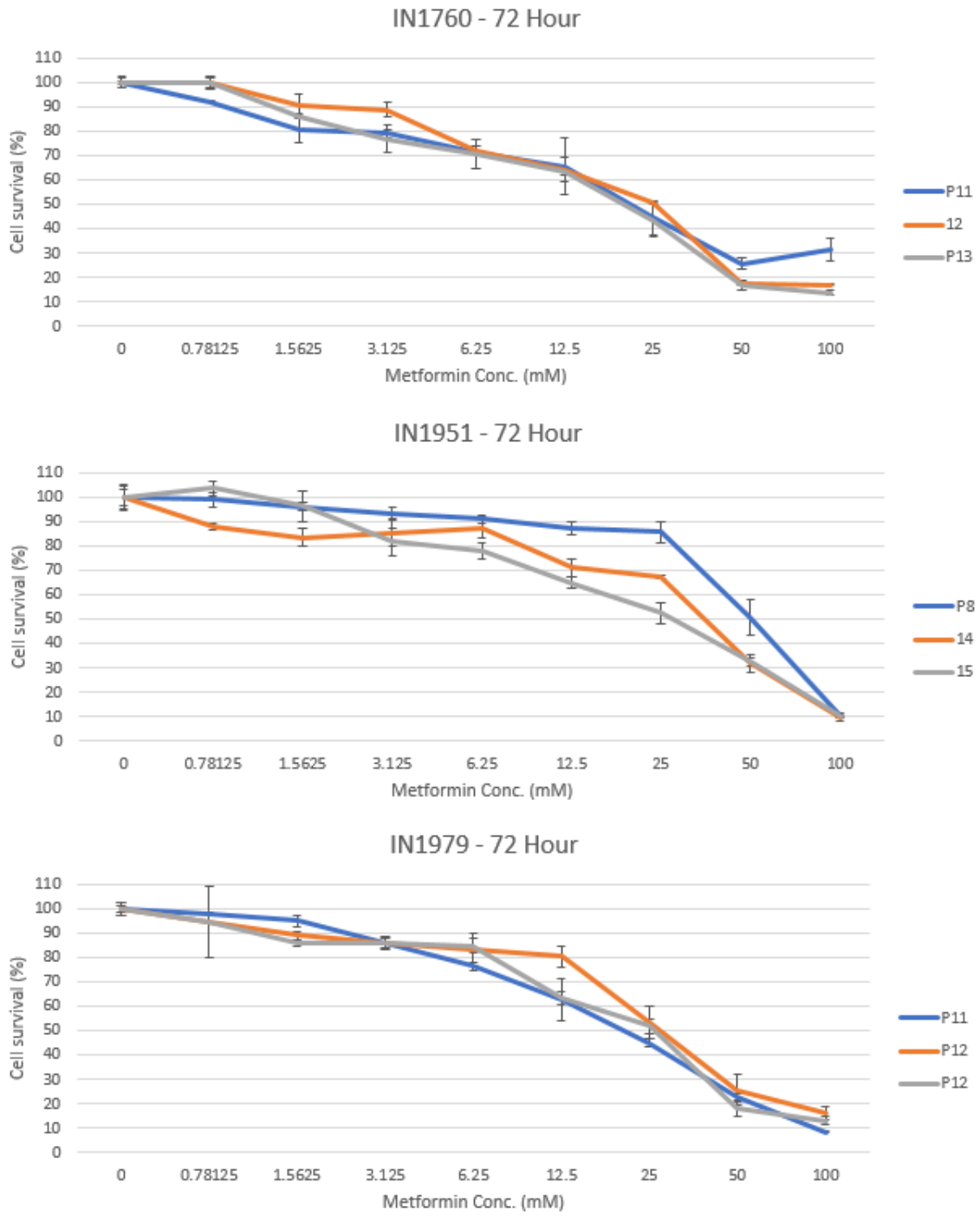

Appendix A4 72 Hour SRB cytotoxicity assays for metformin. Result of SRB assay used to determine ID50 of metformin at 72 hours. P – Passage of the culture.

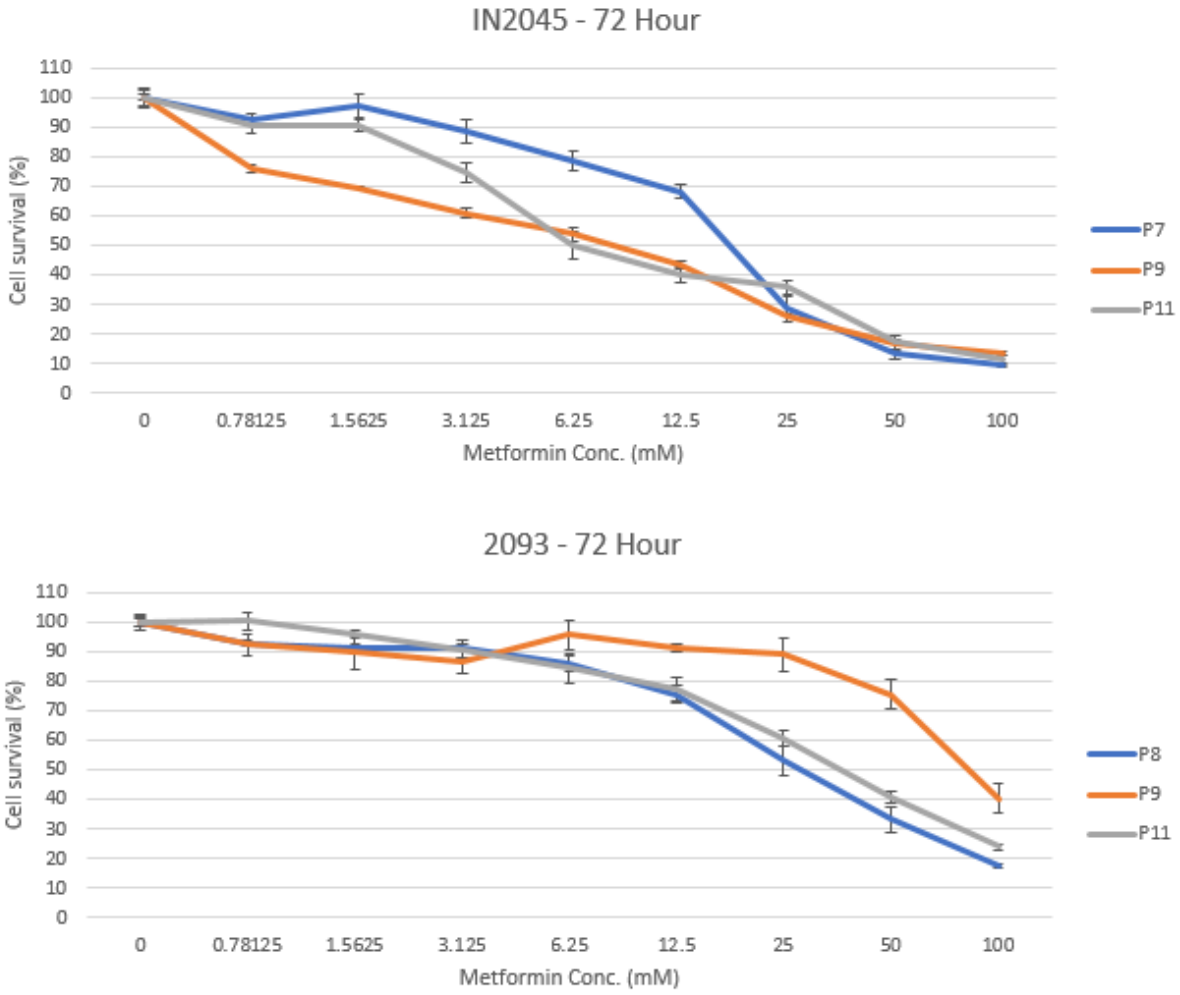

Appendix A5 72 Hour SRB cytotoxicity assays for metformin. Result of SRB assay used to determine ID50 of metformin at 72 hours. P – Passage of the culture.

Appendix B -Metformin treatment 96 Hour Individual graphs

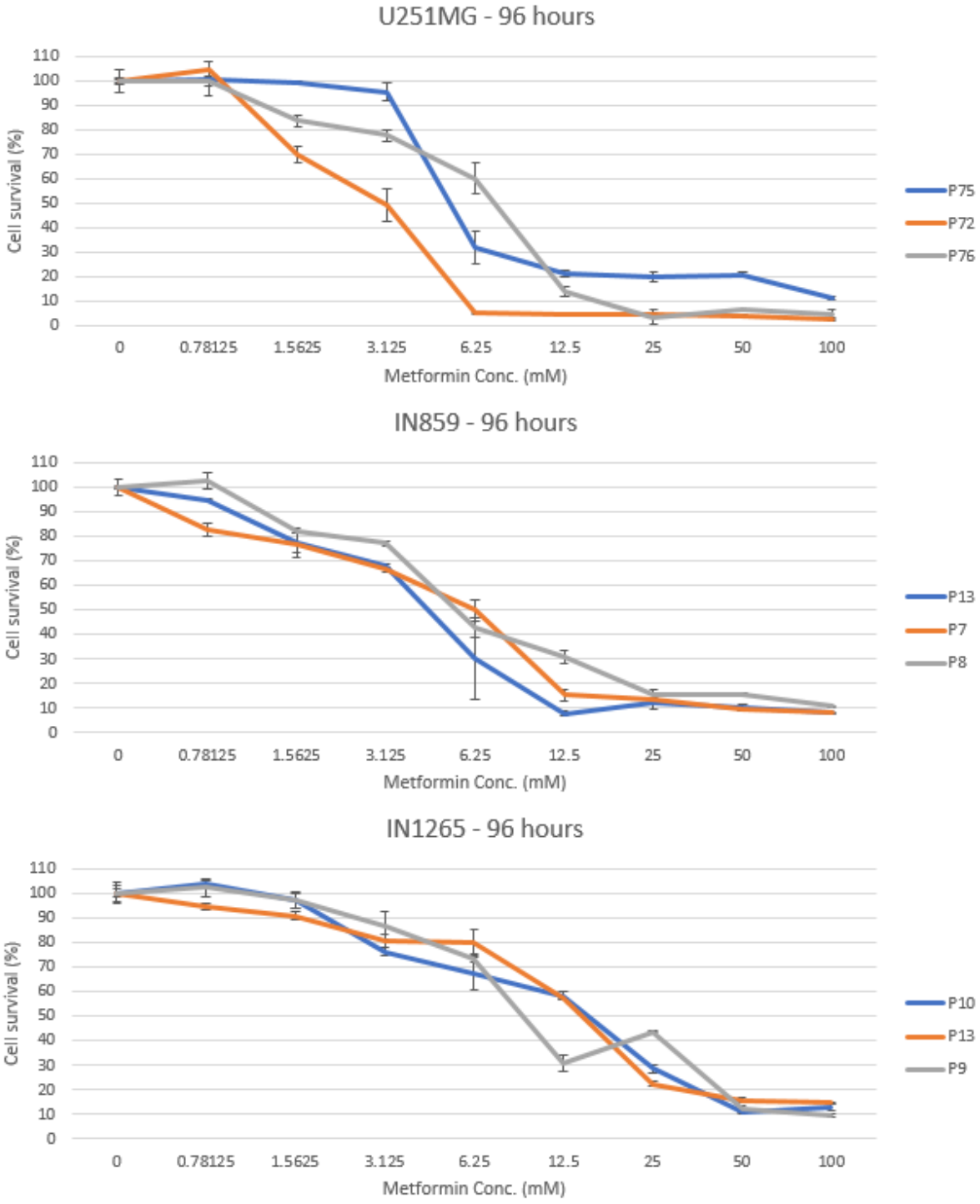

Appendix B1 96 Hour SRB cytotoxicity assays for metformin. Result of SRB assay used to determine ID50 of metformin at 96 hours. P – Passage of the culture.

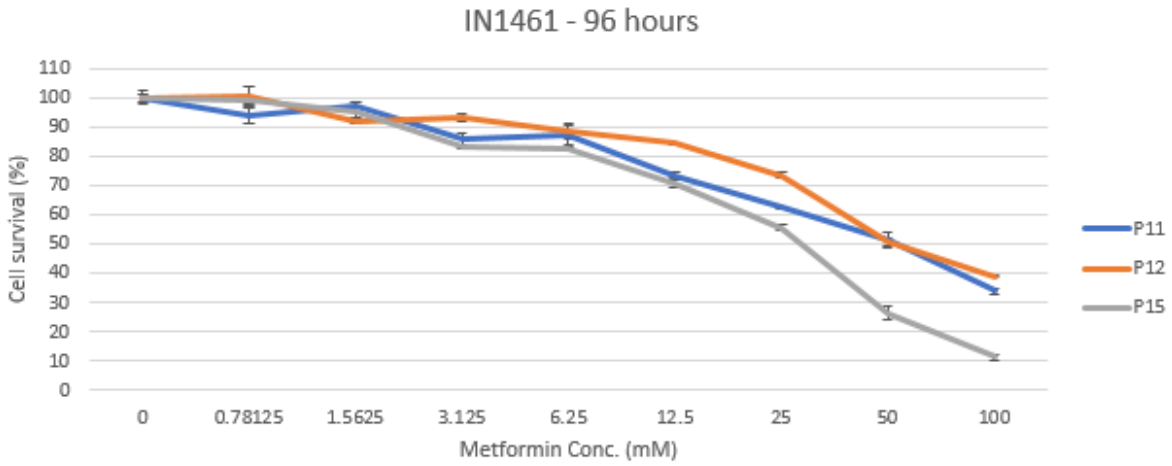

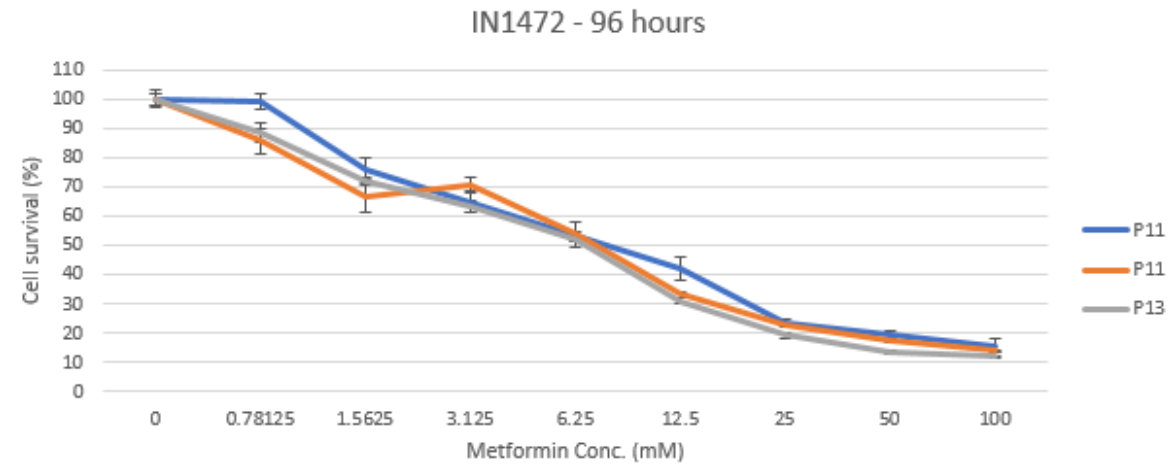

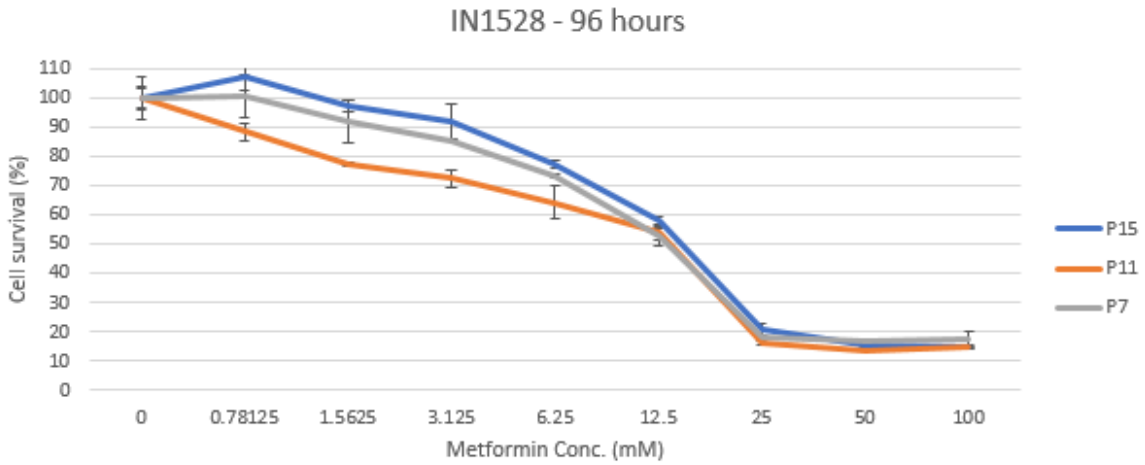

Appendix B2 96 Hour SRB cytotoxicity assays for metformin. Result of SRB assay used to determine ID50 of metformin at 96 hours. P – Passage of the culture.

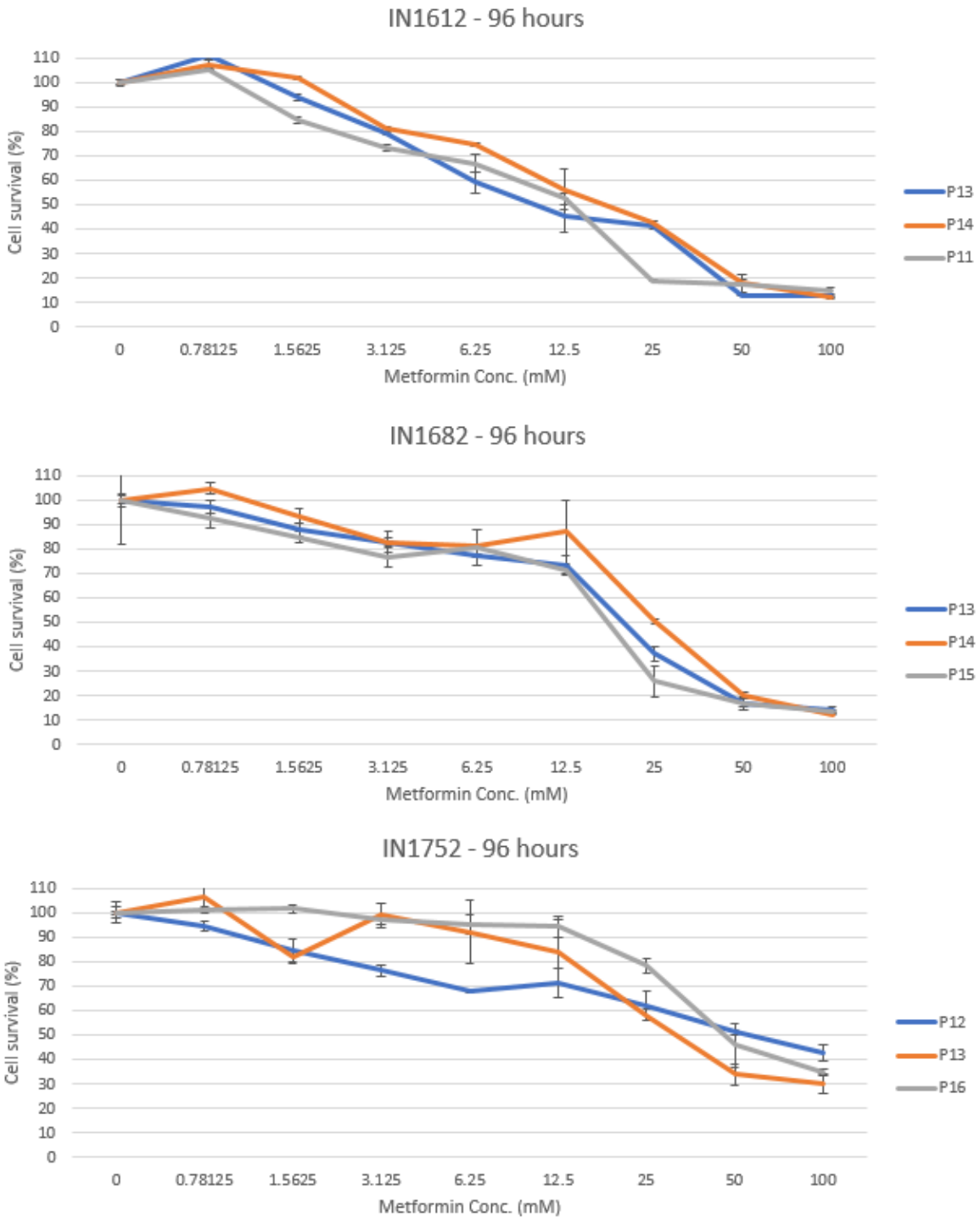

Appendix B3 96 Hour SRB cytotoxicity assays for metformin. Result of SRB assay used to determine ID50 of metformin at 96 hours. P – Passage of the culture.

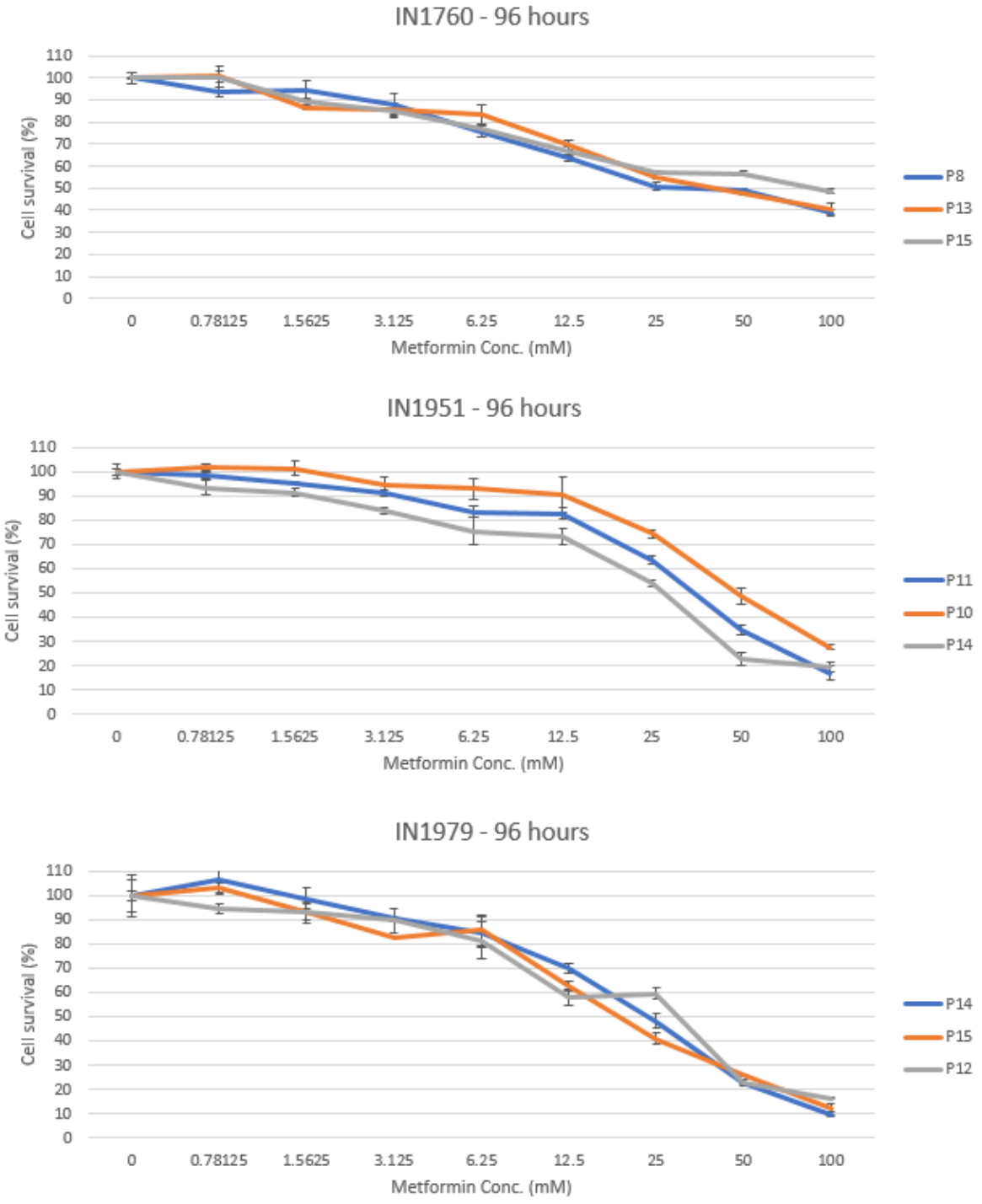

Appendix B4 96 Hour SRB cytotoxicity assays for metformin. Result of SRB assay used to determine ID50 of metformin at 96 hours. P – Passage of the culture.

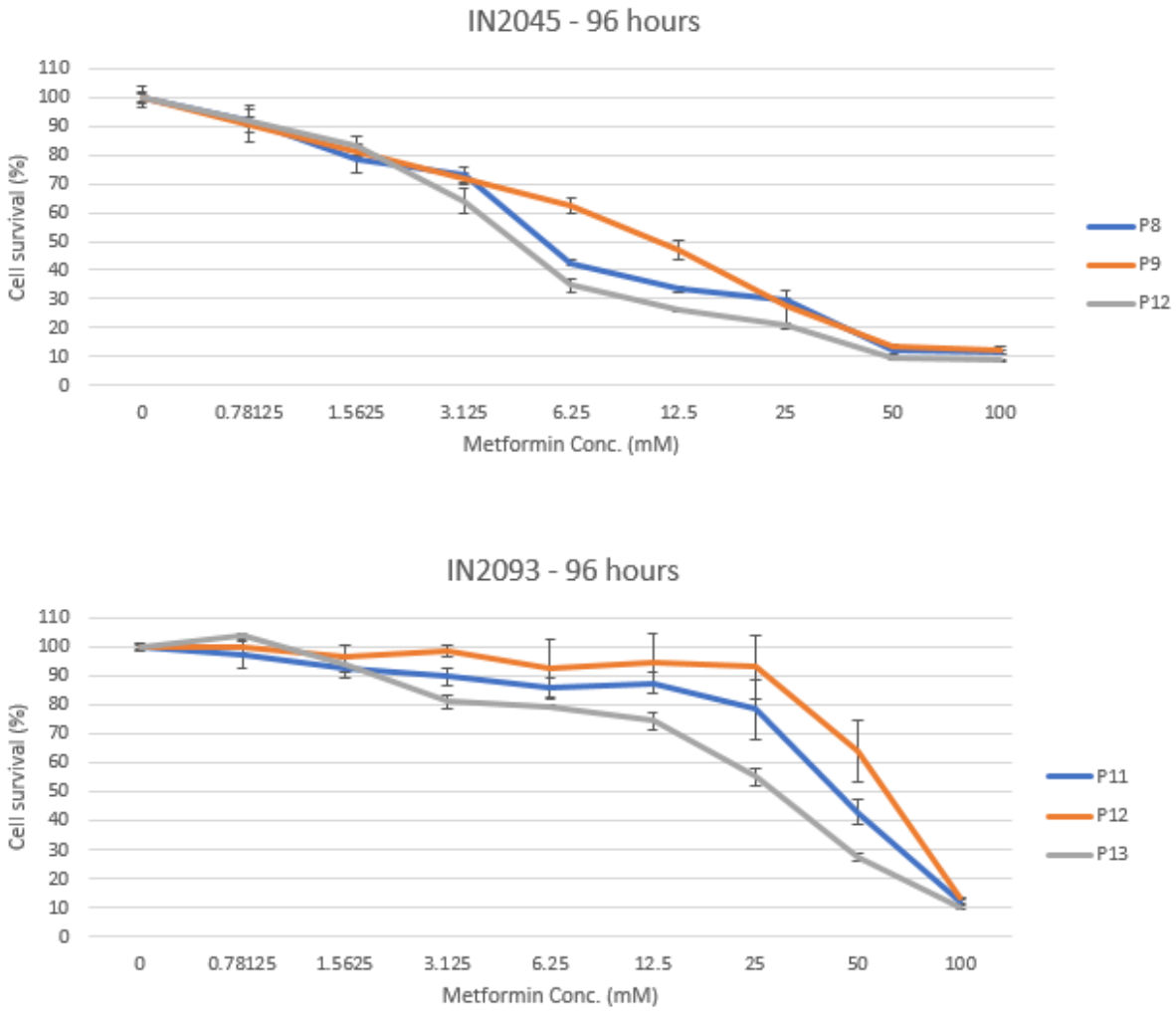

Appendix B5 96 Hour SRB cytotoxicity assays for metformin. Result of SRB assay used to determine ID50 of metformin at 96 hours. P – Passage of the culture.

Appendix C -Phenformin treatment 72 Hour Individual graphs

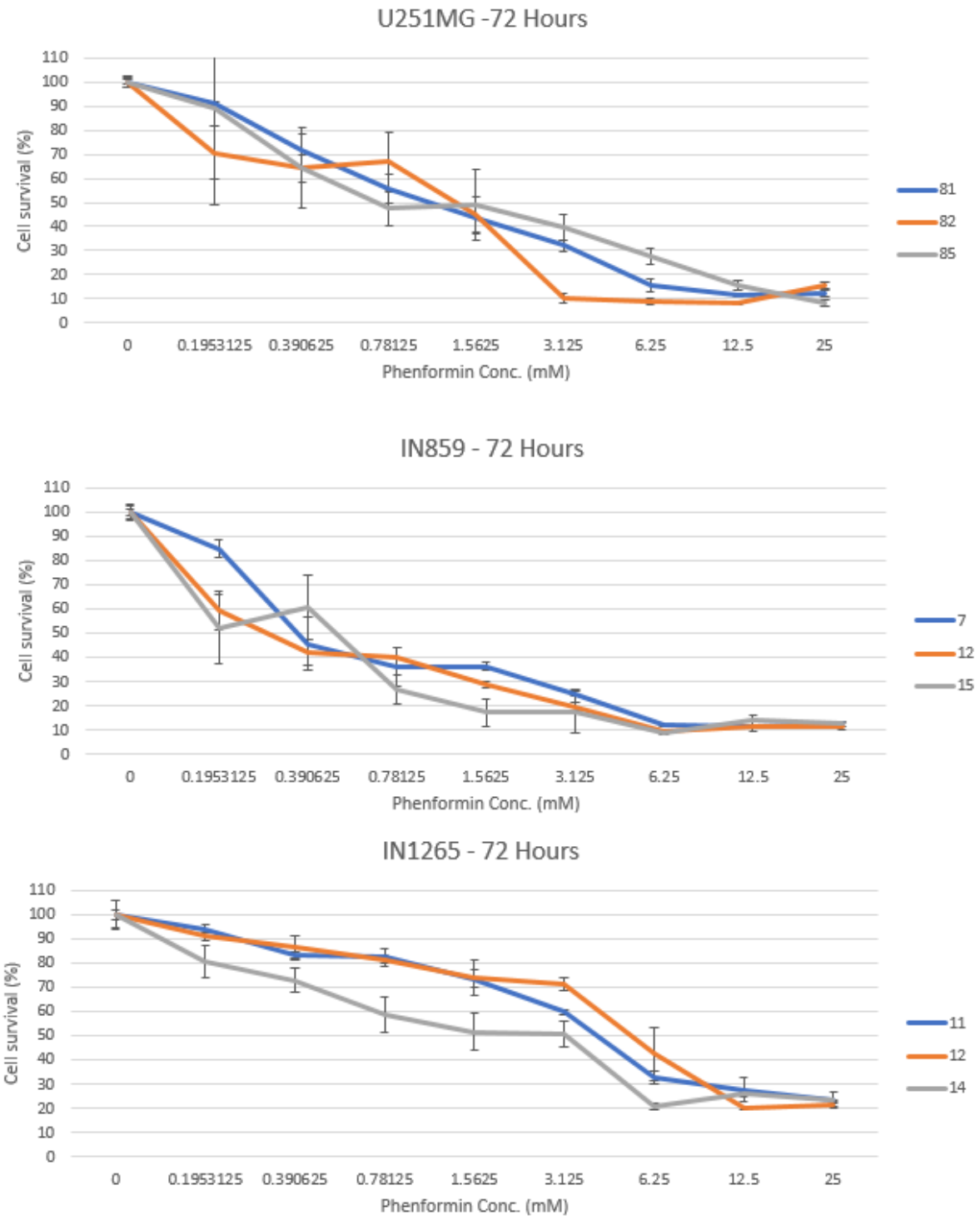

Appendix C1 72 Hour SRB cytotoxicity assays for phenformin. Result of SRB assay used to determine ID50 of phenformin at 72 hours. P – Passage of the culture.

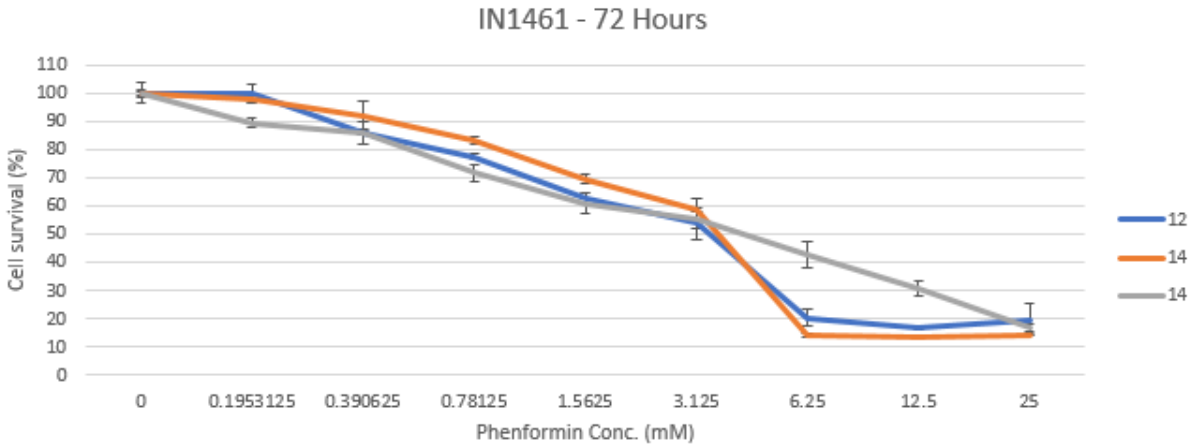

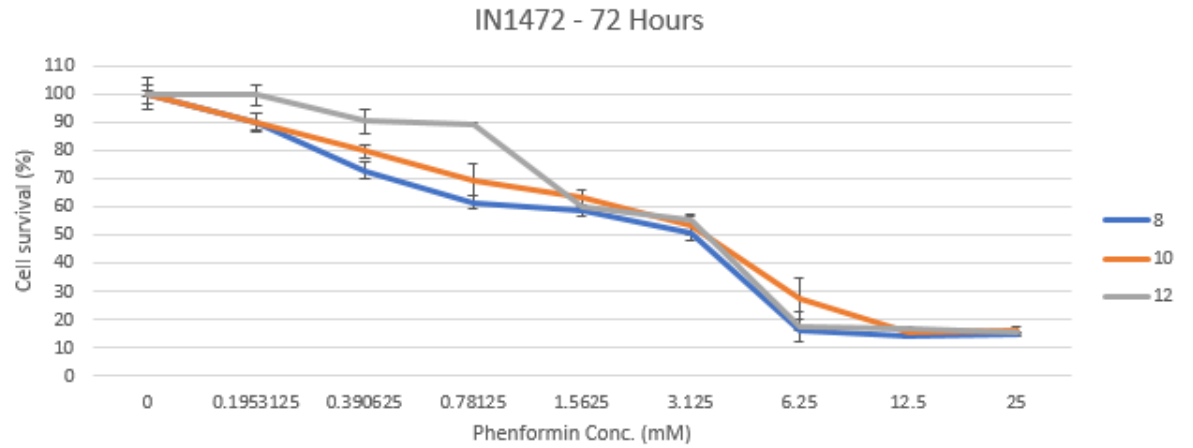

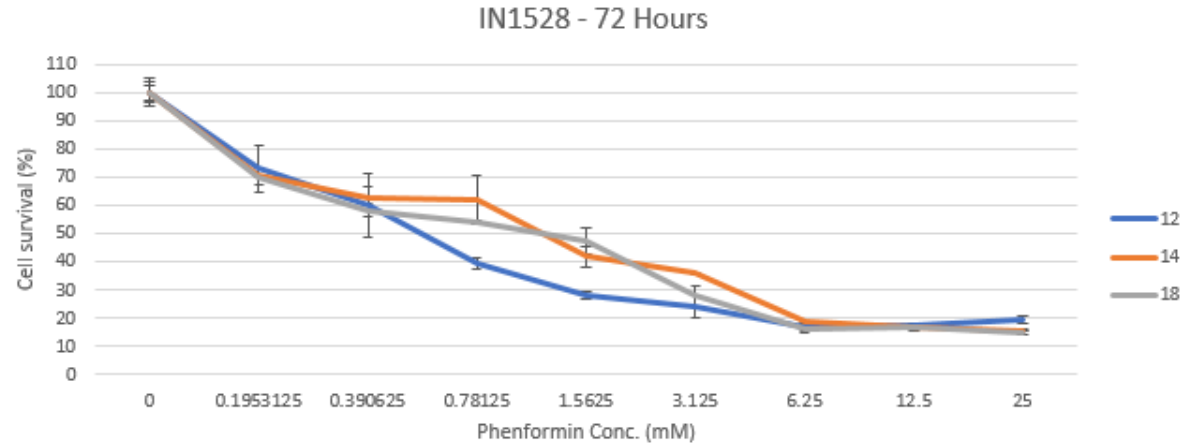

Appendix C2 72 Hour SRB cytotoxicity assays for phenformin. Result of SRB assay used to determine ID50 of phenformin at 72 hours. P – Passage of the culture.

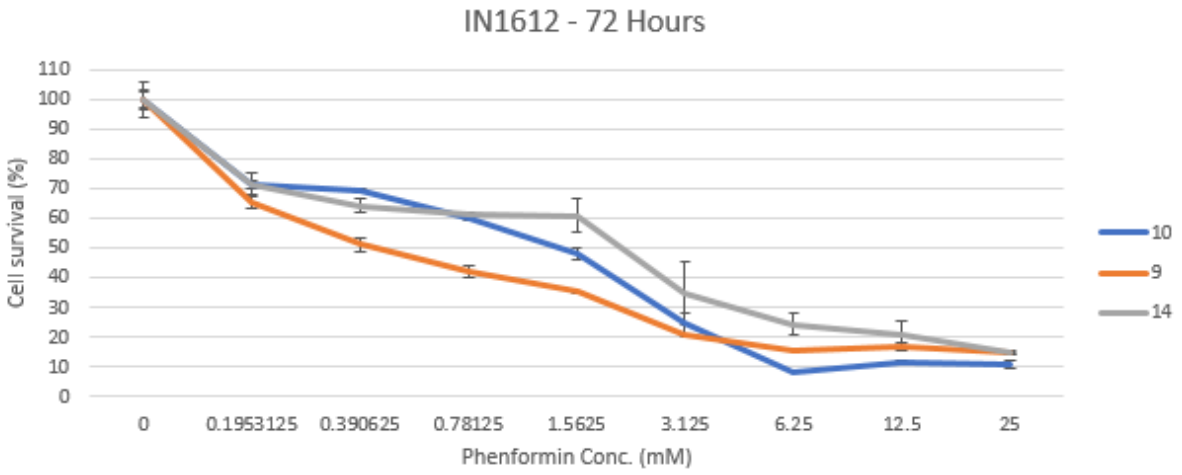

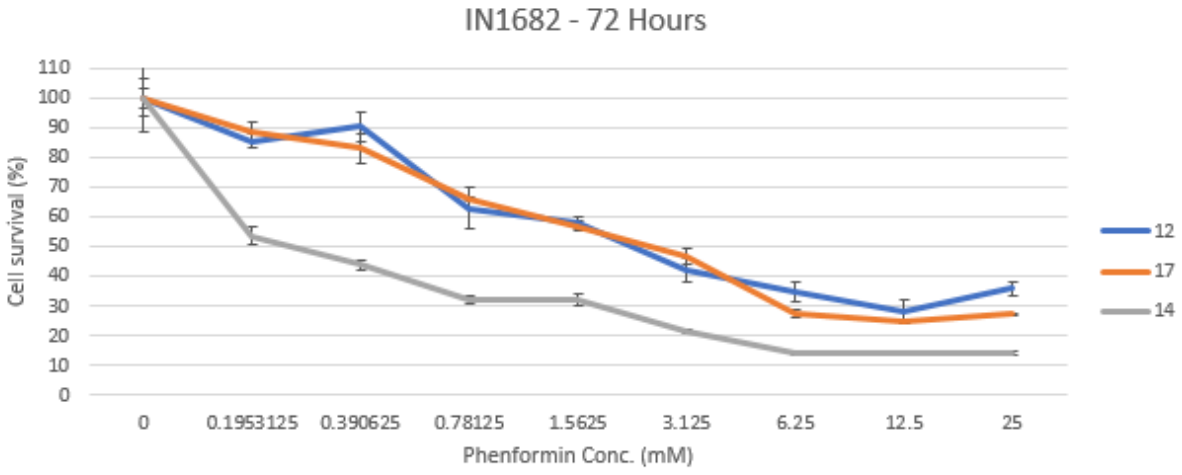

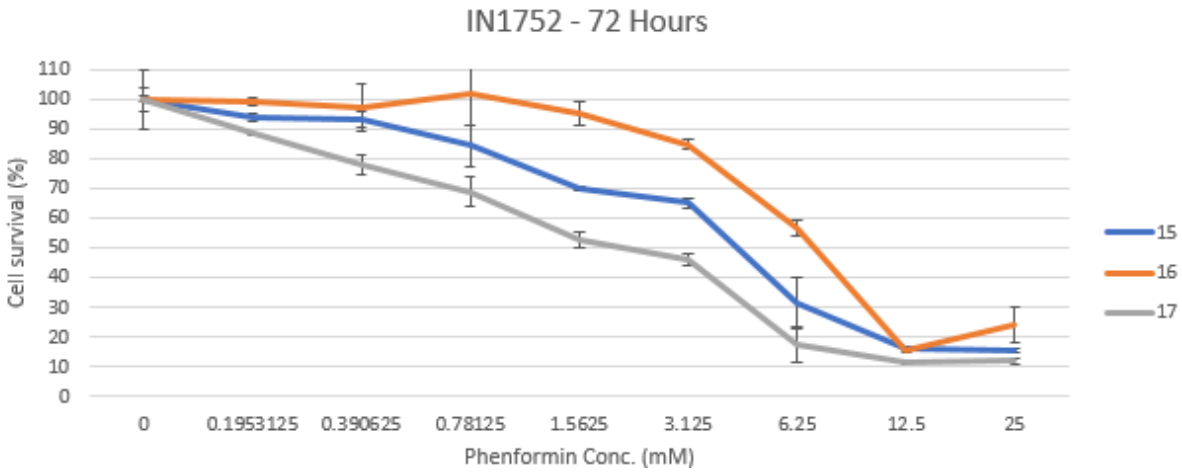

Appendix C3 72 Hour SRB cytotoxicity assays for phenformin. Result of SRB assay used to determine ID50 of phenformin at 72 hours. P – Passage of the culture.

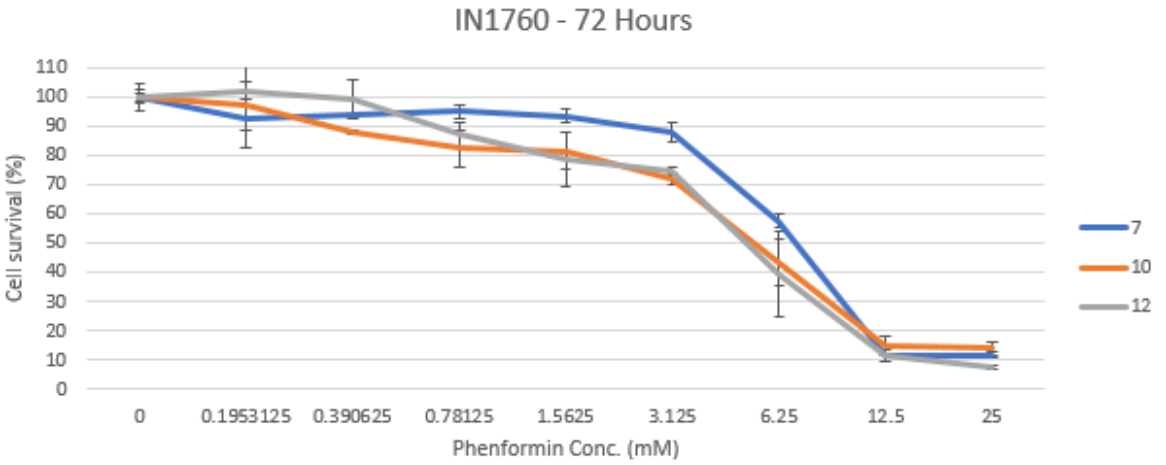

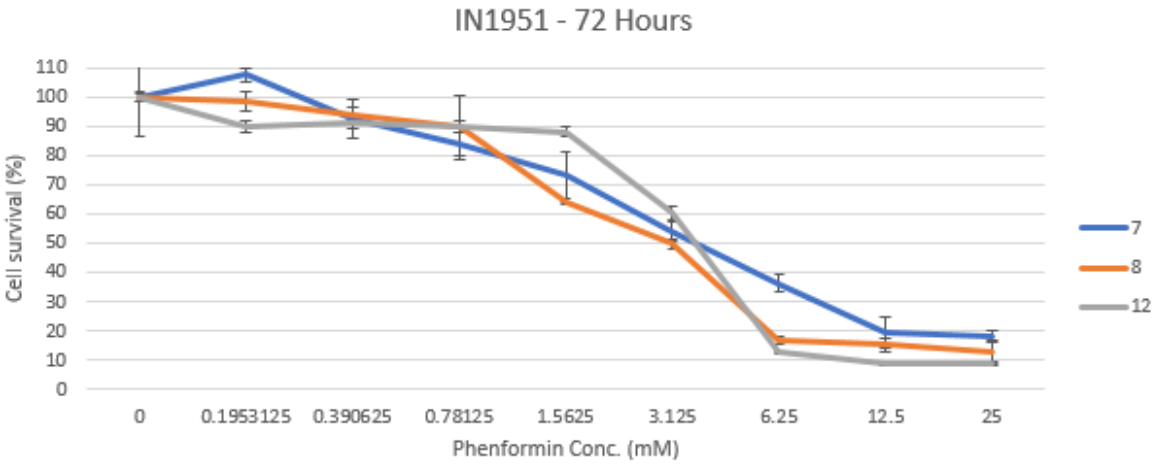

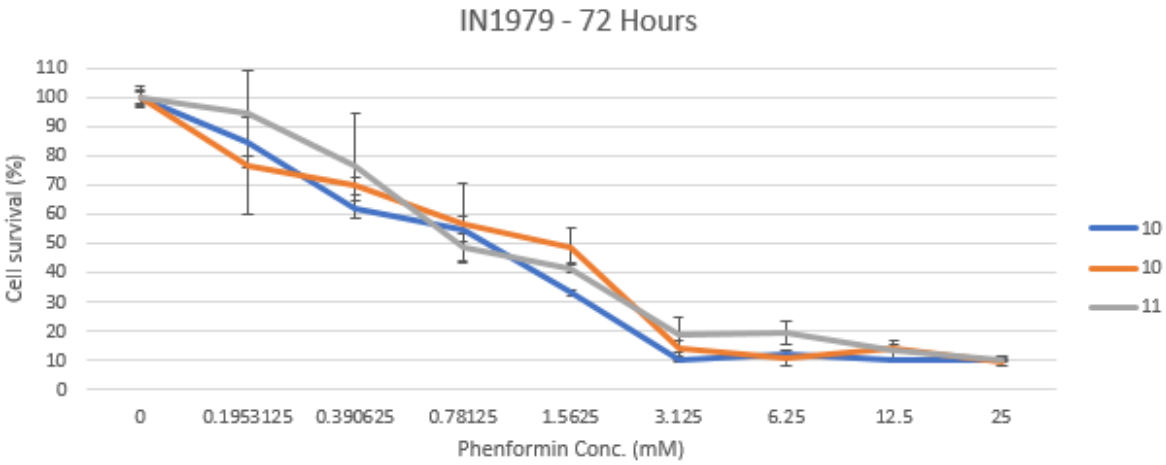

Appendix C4 72 Hour SRB cytotoxicity assays for phenformin. Result of SRB assay used to determine ID50 of phenformin at 72 hours. P – Passage of the culture.

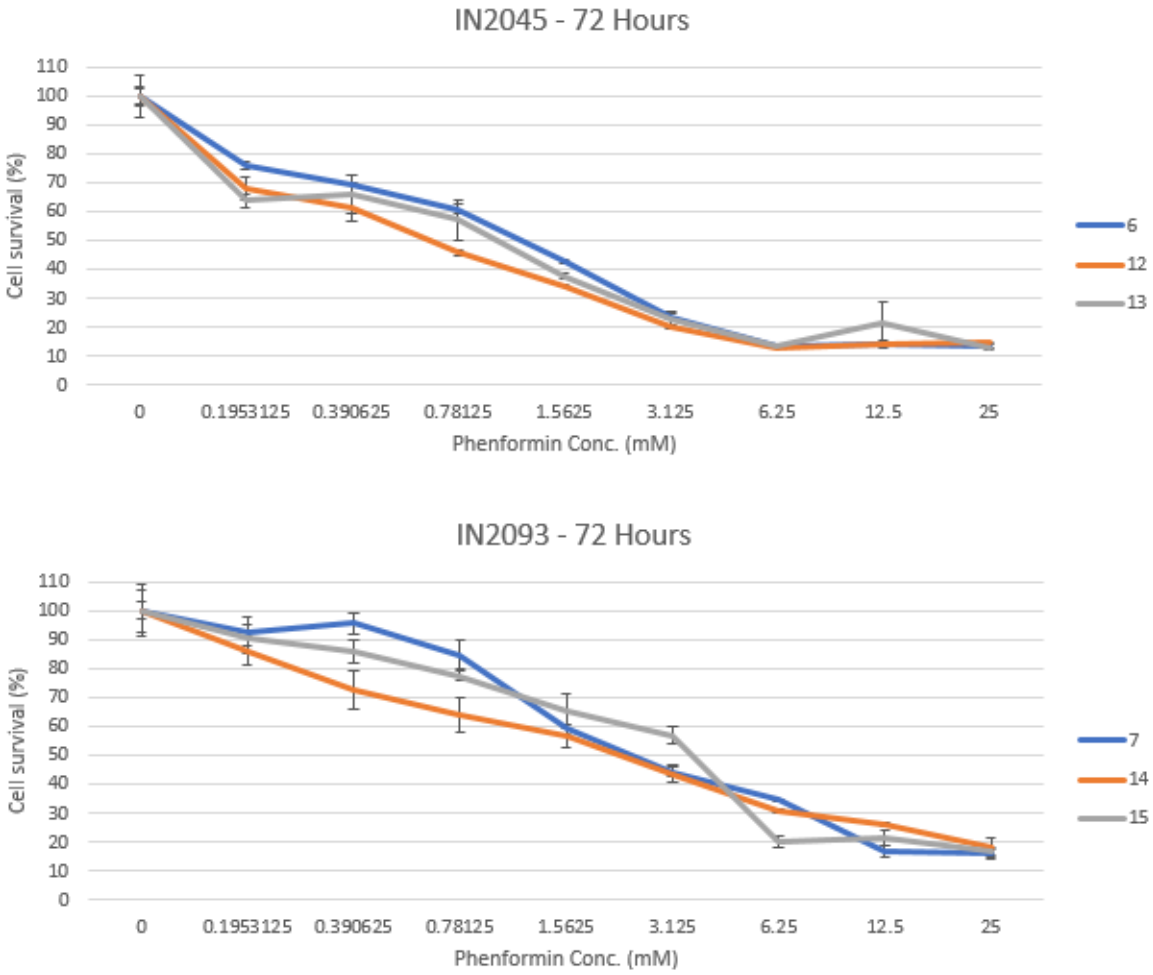

Appendix C5 72 Hour SRB cytotoxicity assays for phenformin. Result of SRB assay used to determine ID50 of phenformin at 72 hours. P – Passage of the culture.

Appendix 4 - Disulfiram drug combination graphs

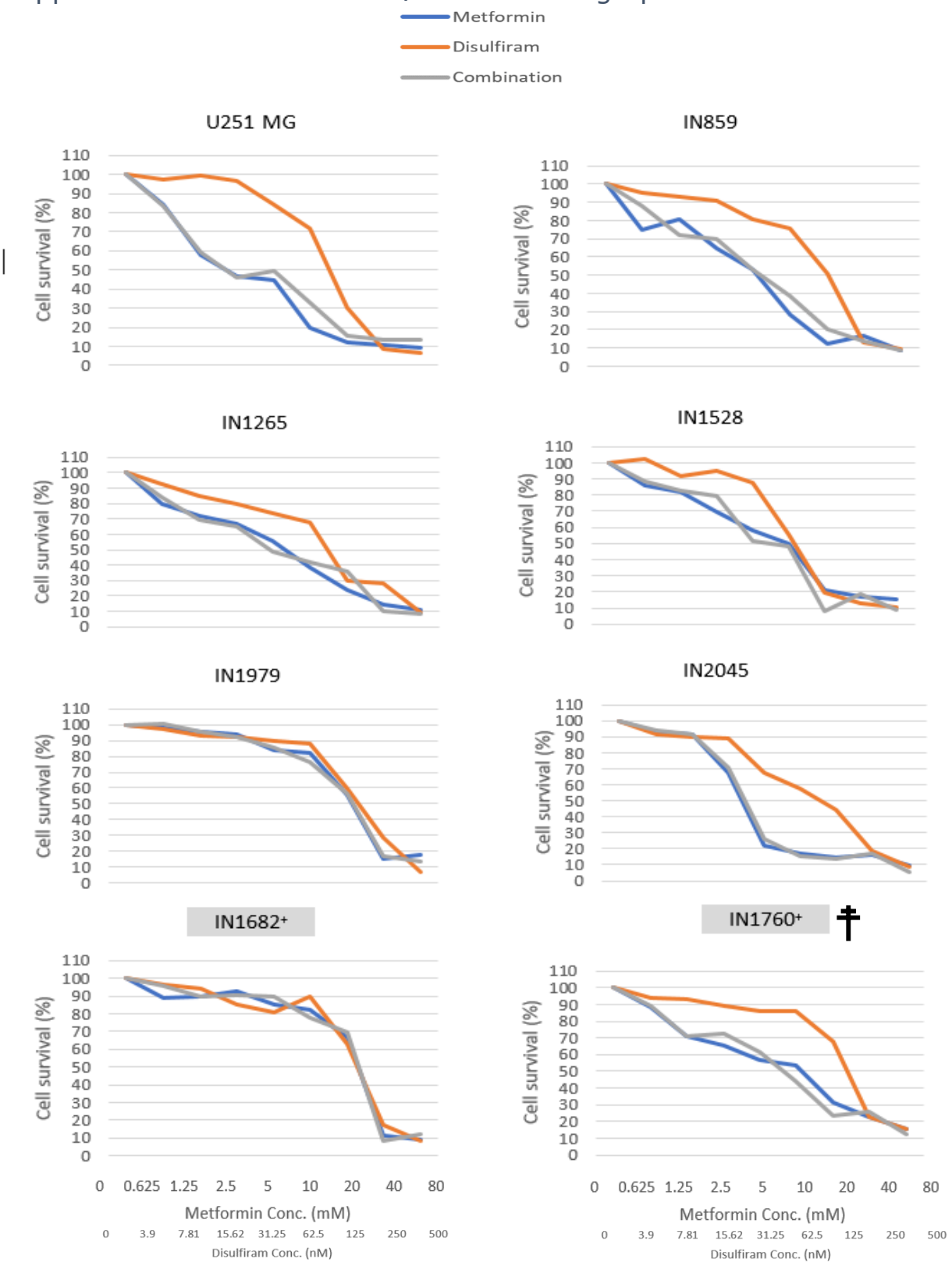

Appendix D1 – Graphs representing the combination synergy experiments of metformin alongside disulfiram. All culture tested in solo and combination treatment in equimolar dosages in a 96-hour period. Cultures that showed synergy marked with a †. Disulfiram results show higher ID50 curves than metformin. Combination curves of most graphs are similar to metformin treatment leading to antagonist results. All cultures marked with a + and shaded grey indicate *P53* wild type.

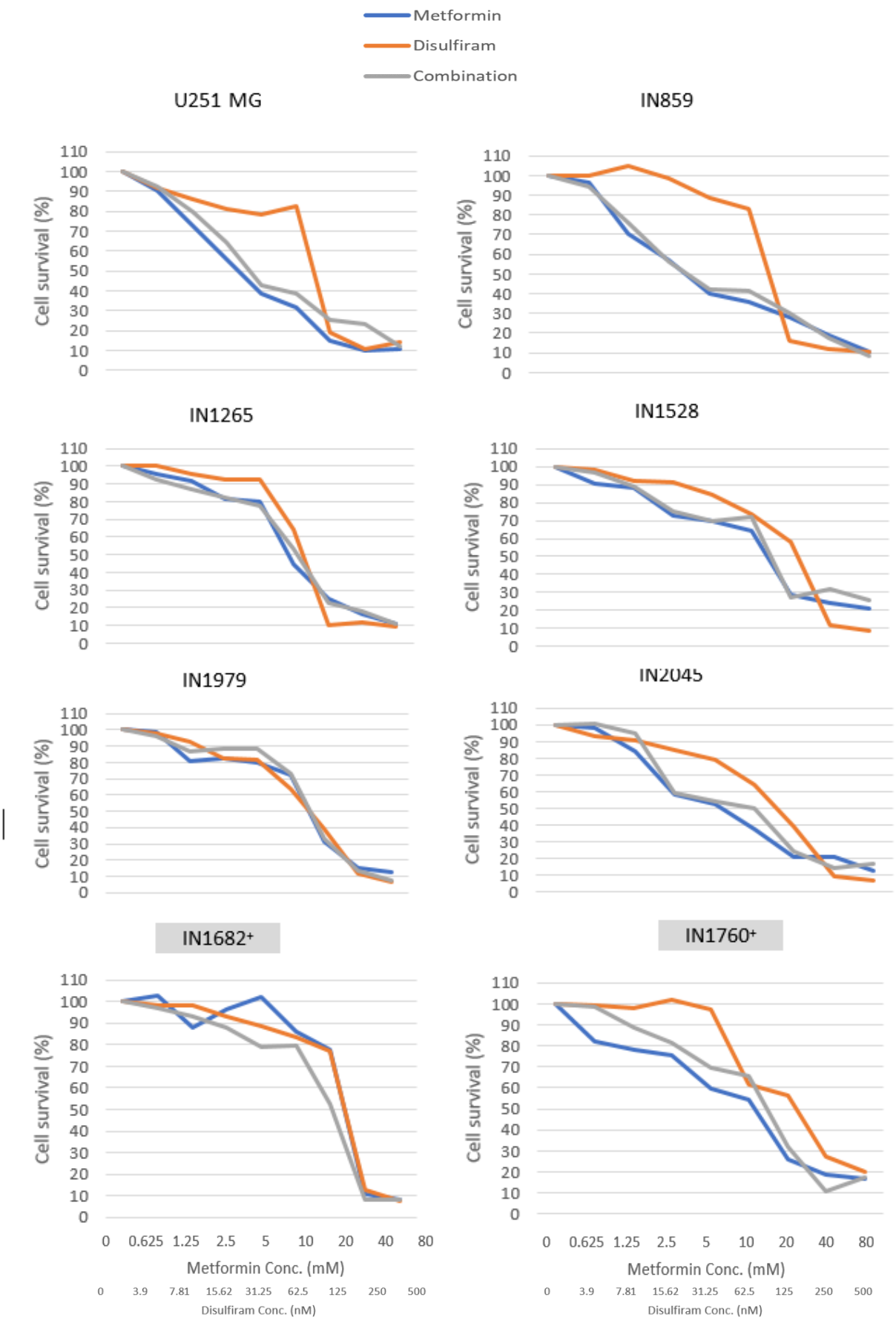

Appendix D2 – Graphs representing the combination synergy experiments of metformin alongside disulfiram. All culture tested in solo and combination treatment in equimolar dosages in a 96-hour period. Cultures that showed synergy marked with a †. Disulfiram results show higher ID50 curves than metformin. Combination curves of most graphs are similar to metformin treatment leading to antagonist results. All cultures marked with a + and shaded grey indicate *P53* wild type.

Appendix E - Temozolomide drug combination graphs

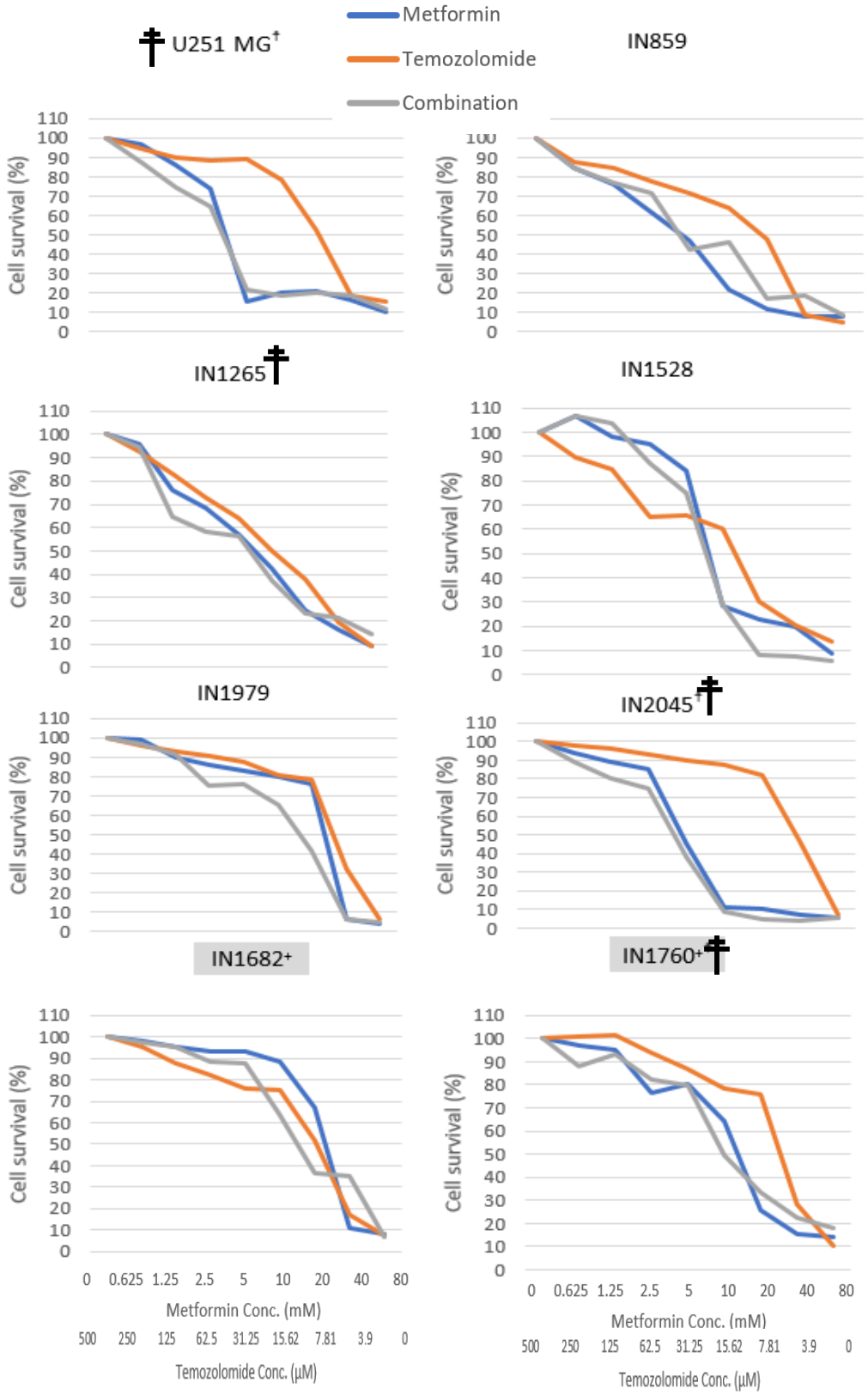

Appendix E1 – Graphs representing the combination synergy experiments of metformin alongside temozolomide supplemented with copper chloride. All culture tested in solo and combination treatment in equimolar dosages in a 96-hour period. Cultures that showed synergy marked with a †. Temozolomide results show lower ID50 curves than metformin. Combination curves of most graphs are similar to metformin treatment. All cultures marked with a + and shaded grey indicate *P53* wild type.

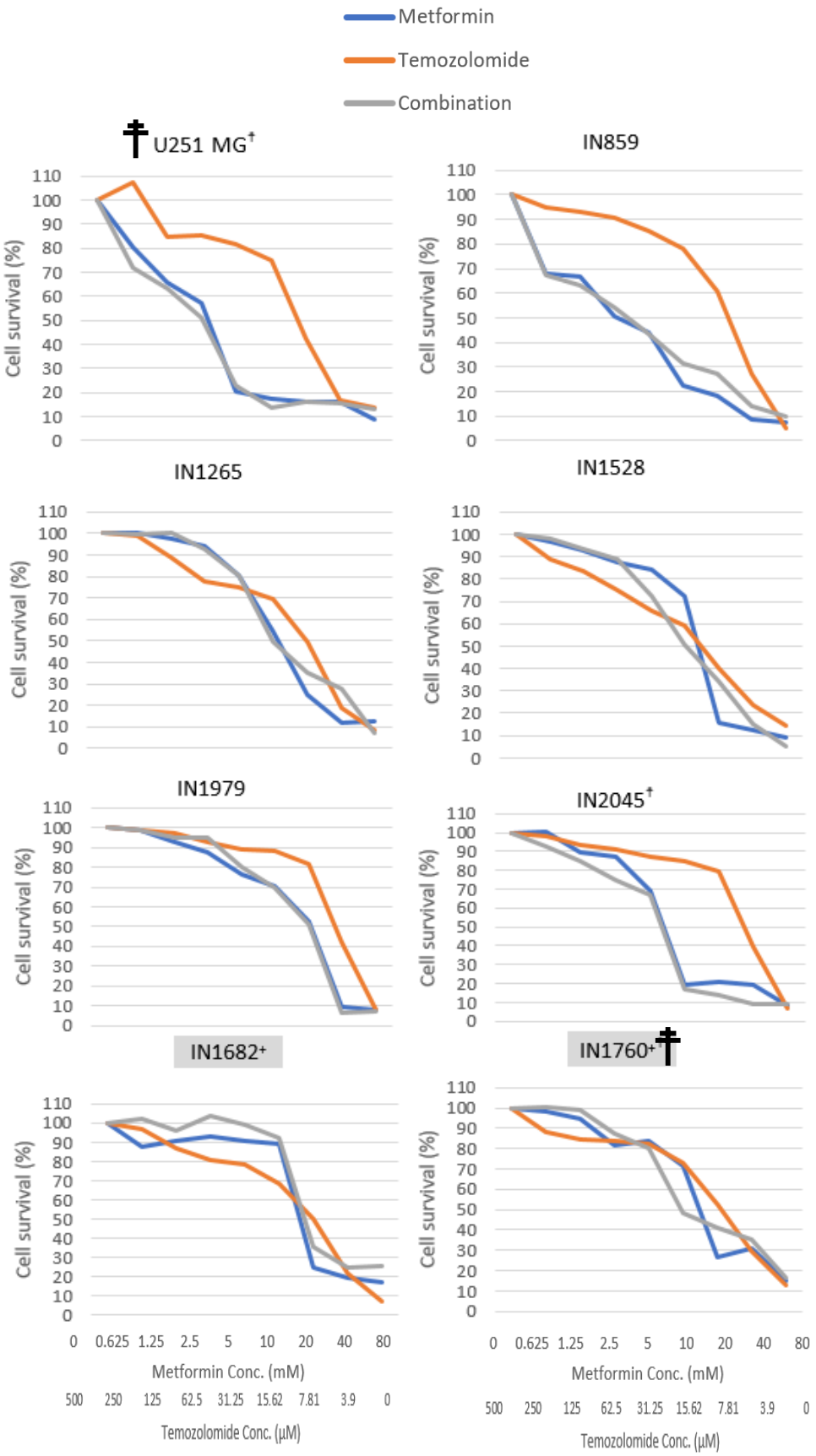

Appendix E2 – Graphs representing the combination synergy experiments of metformin alongside temozolomide supplemented with copper chloride. All culture tested in solo and combination treatment in equimolar dosages in a 96-hour period. Cultures that showed synergy marked with a †. Temozolomide results show lower ID50 curves than metformin. Combination curves of most graphs are similar to metformin treatment. All cultures marked with a + and shaded grey indicate *P53* wild type.

Appendix F - Sodium Oxamate drug combination graphs

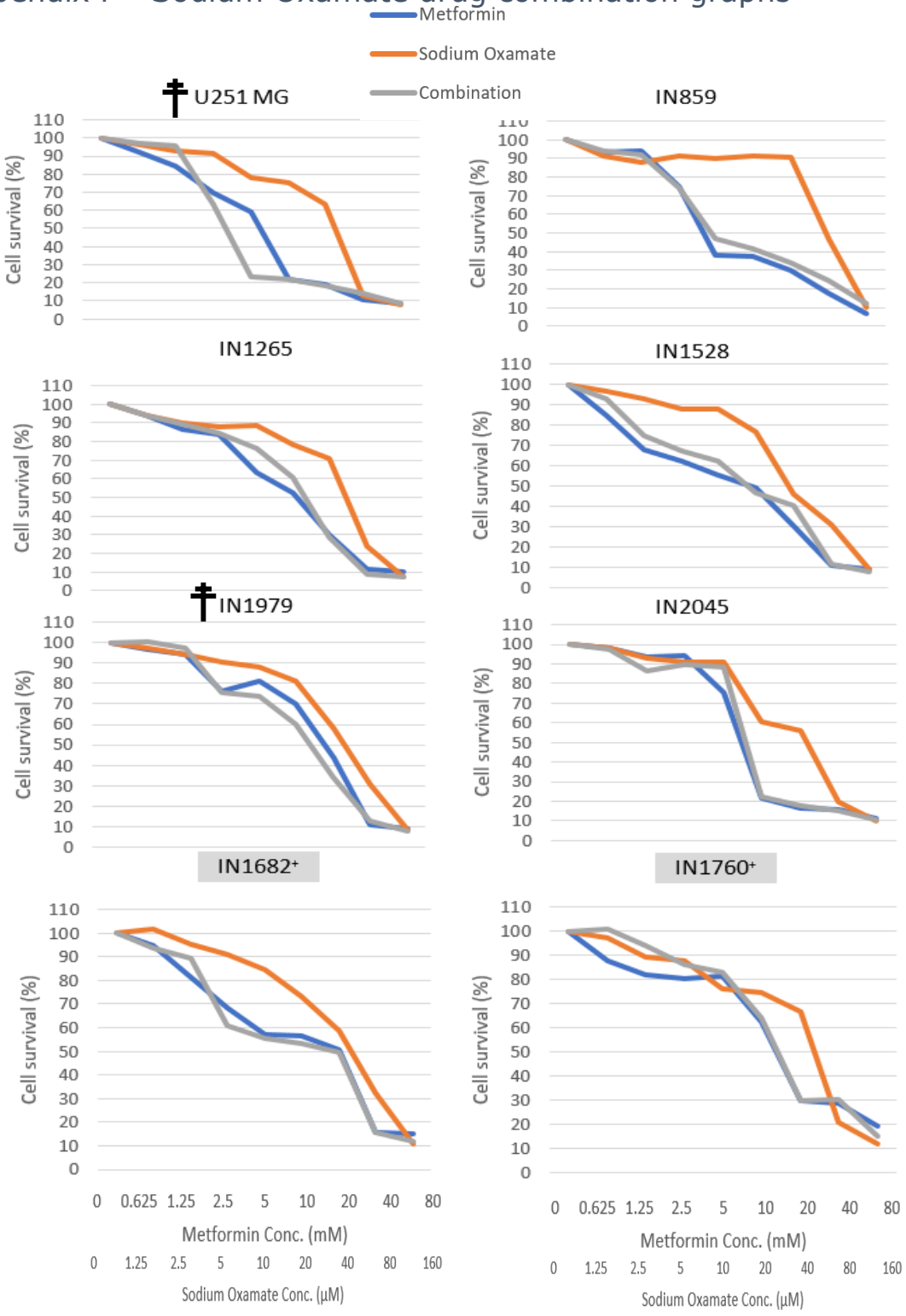

Appendix F1 – Graphs representing the combination synergy experiments of metformin alongside sodium oxamate. All culture tested in solo and combination treatment in equimolar dosages in a 96-hour period. Cultures that showed synergy marked with a †. Sodium oxamate showed synergy in U251MG but no other cultures tested. In all other cultures metformin mono treatment had the lowest ID50 values. All cultures marked with a + and shaded grey indicate *P53* wild type.

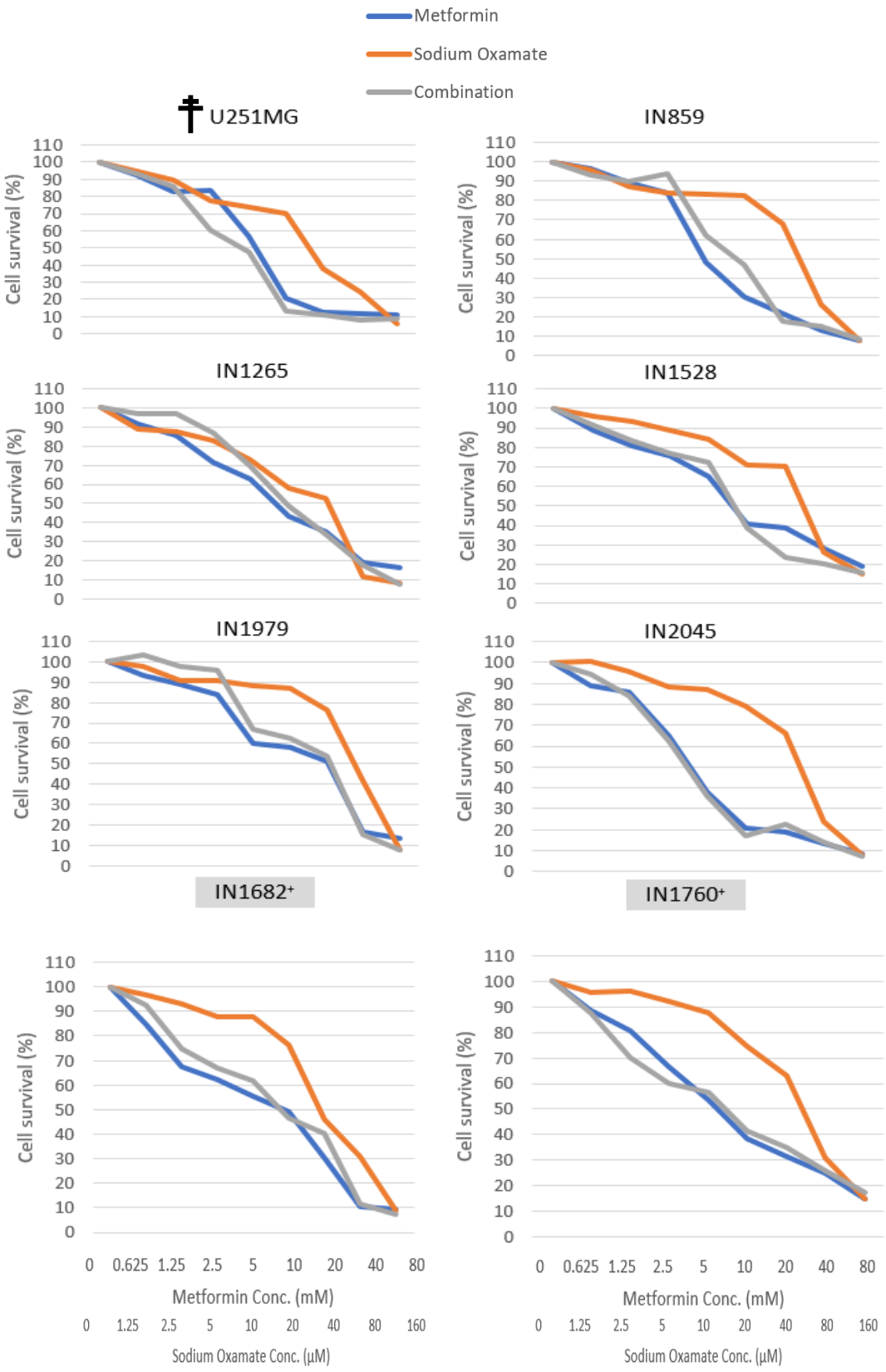

Appendix F2 – Graphs representing the combination synergy experiments of metformin alongside sodium oxamate. All culture tested in solo and combination treatment in equimolar dosages in a 96-hour period. Cultures that showed synergy marked with a †. Sodium oxamate showed synergy in U251MG but no other cultures tested. In all other cultures metformin mono treatment had the lowest ID50 values. All cultures marked with a + and shaded grey indicate *P53* wild type.

Appendix G - Sorafenib drug combination graphs

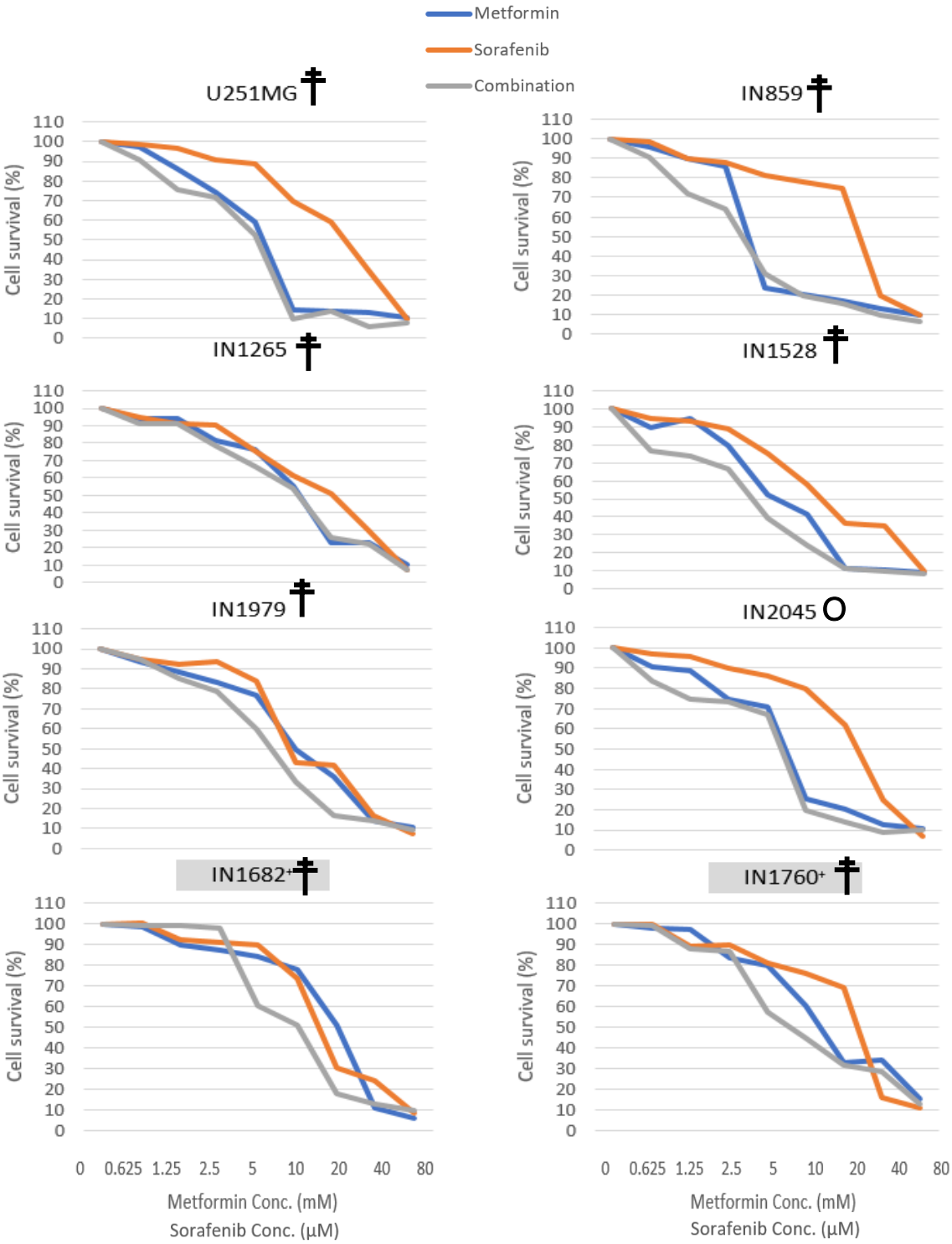

Appendix G1 – Graphs representing the combination synergy experiments of metformin alongside sorafenib. All culture tested in solo and combination treatment in equimolar dosages in a 96-hour period. Cultures that showed synergy marked with a †. All cultures showed strong synergy this is identifiable by the separation of the combination dosage response from the mono treatment results. [1]All cultures marked with a + and shaded grey indicate *P53* wild type. O marks a culture with an additive effect.

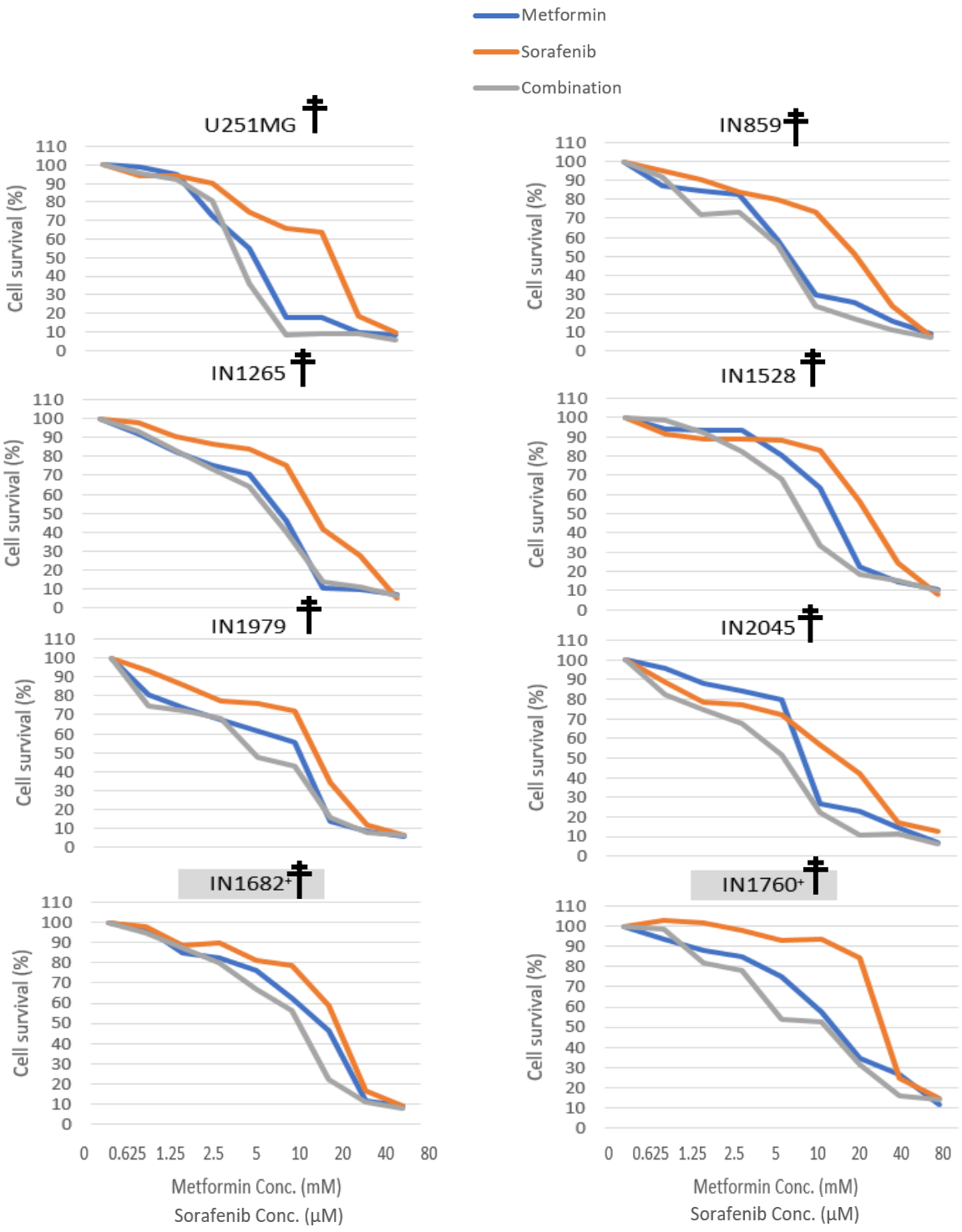

Appendix G2 – Graphs representing the combination synergy experiments of metformin alongside sorafenib. All culture tested in solo and combination treatment in equimolar dosages in a 96-hour period. Cultures that showed synergy marked with a †. All cultures showed strong synergy this is identifiable by the separation of the combination dosage response from the mono treatment results. [1]All cultures marked with a + and shaded grey indicate *P53* wild type. [O] marks a culture with an additive effect.

Appendix H - Apoptotic time course results

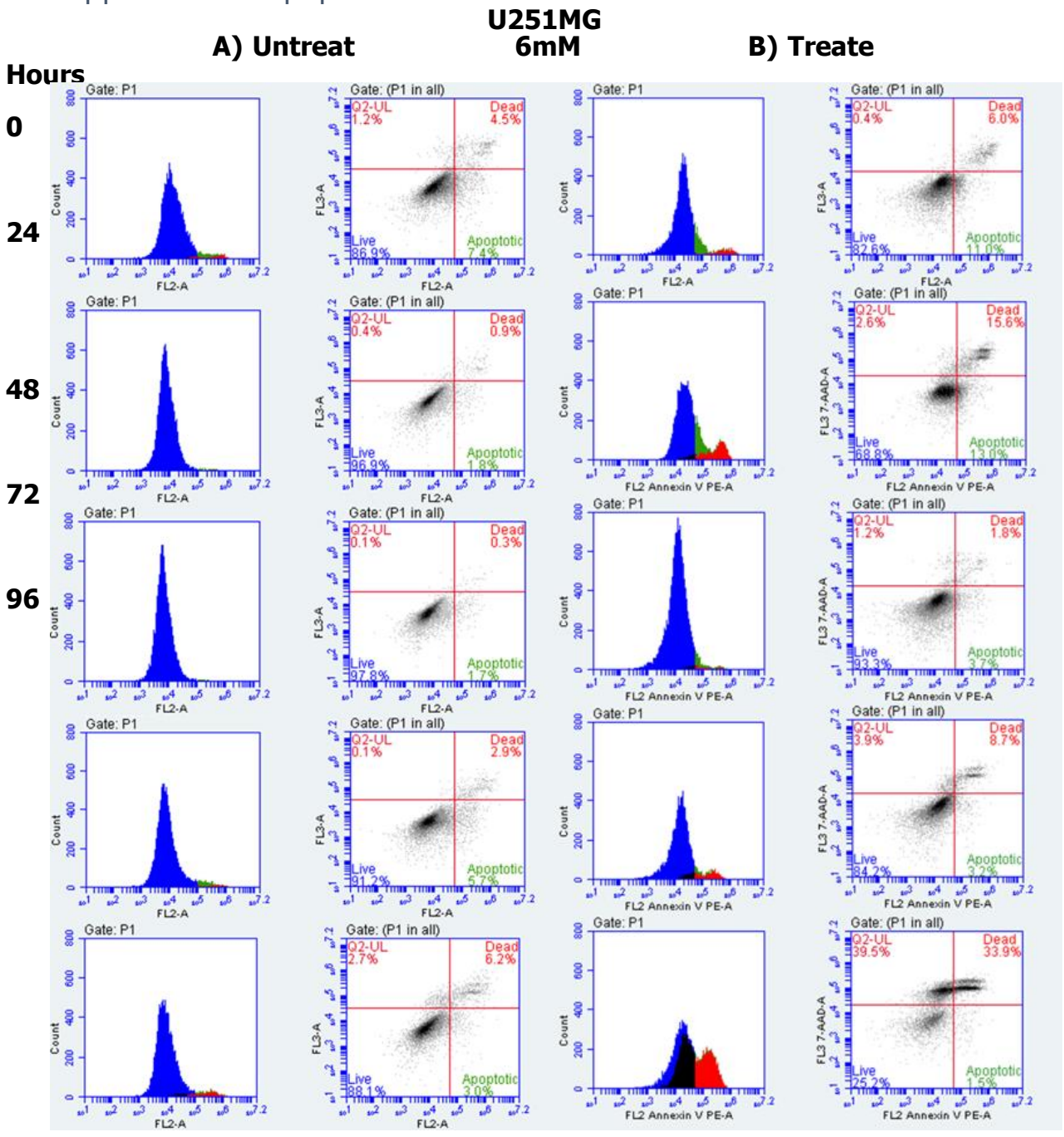

Appendix H1 i 96-hour apoptotic time course of U251MG treated with metformin in 6mM culture media. A) Untreated samples. Minimal variation in the live cell population over the time course. No increase in apoptosis. B) ID50 metformin treated samples. Blue – Live cells, Green – apoptotic cells, Red – Dead cells.

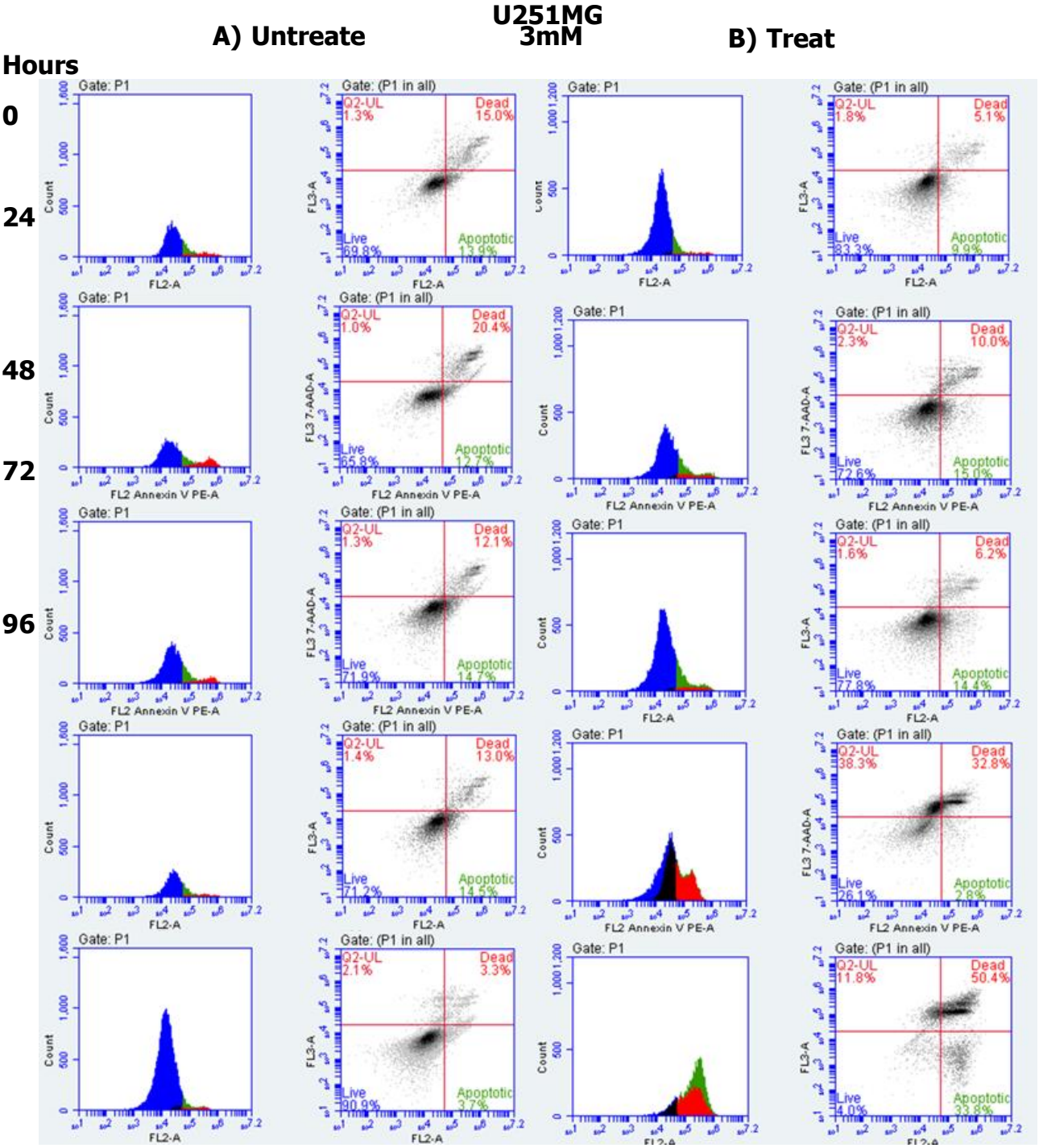

Appendix H1 ii 96-hour apoptotic time course of U251MG treated with metformin in 3mM culture media. A) Untreated samples. Minimal variation in the live cell population over the time course. No increase in apoptosis. B) ID50 metformin treated samples. Blue – Live cells, Green – apoptotic cells, Red – Dead cells.

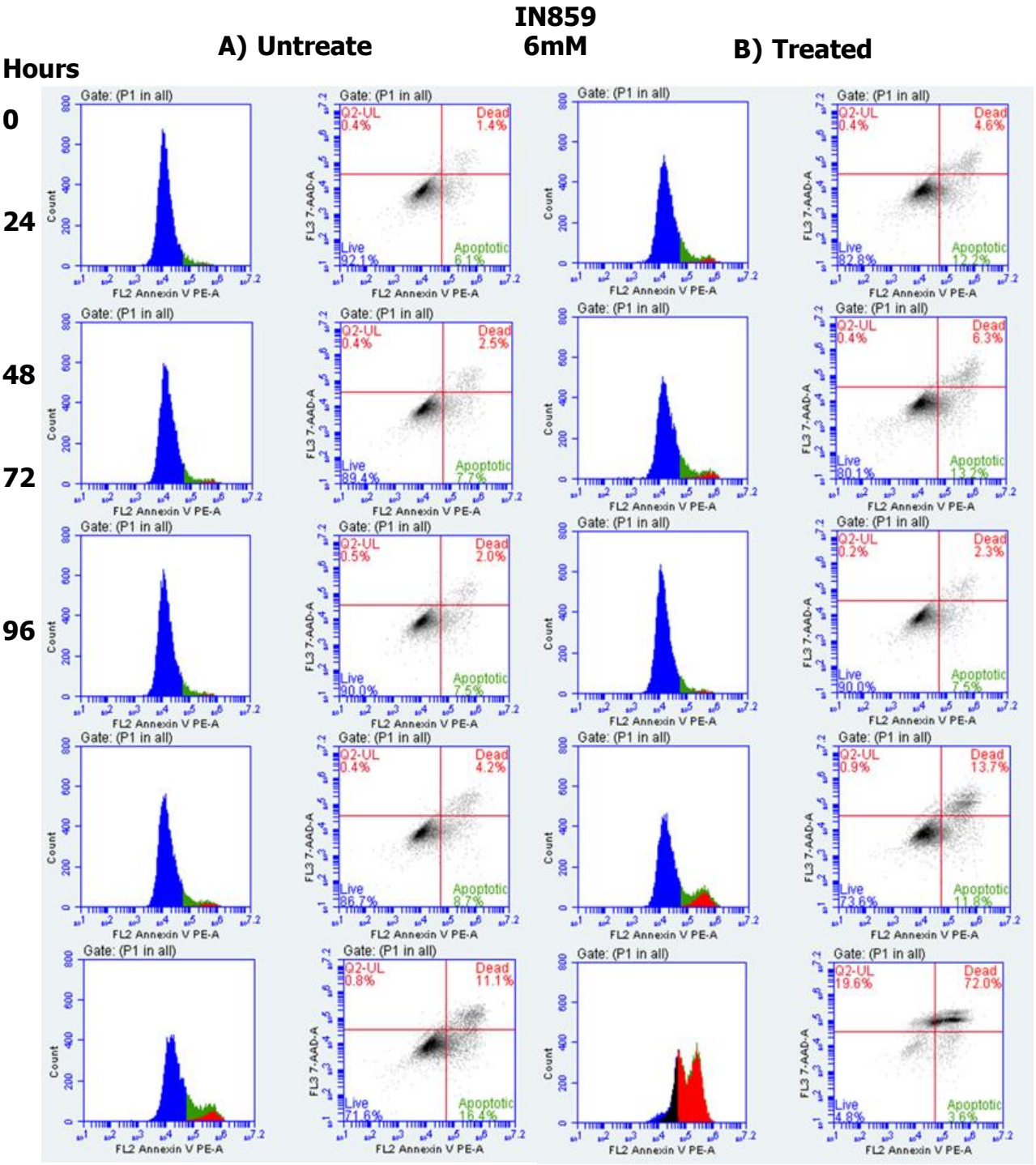

Appendix H2 i 96-hour apoptotic time course of IN859 treated with metformin in 6mM culture media. A) Untreated samples. Minimal variation in the live cell population over the time course. No increase in apoptosis. B) ID50 metformin treated samples. Blue – Live cells, Green – apoptotic cells, Red – Dead cells.

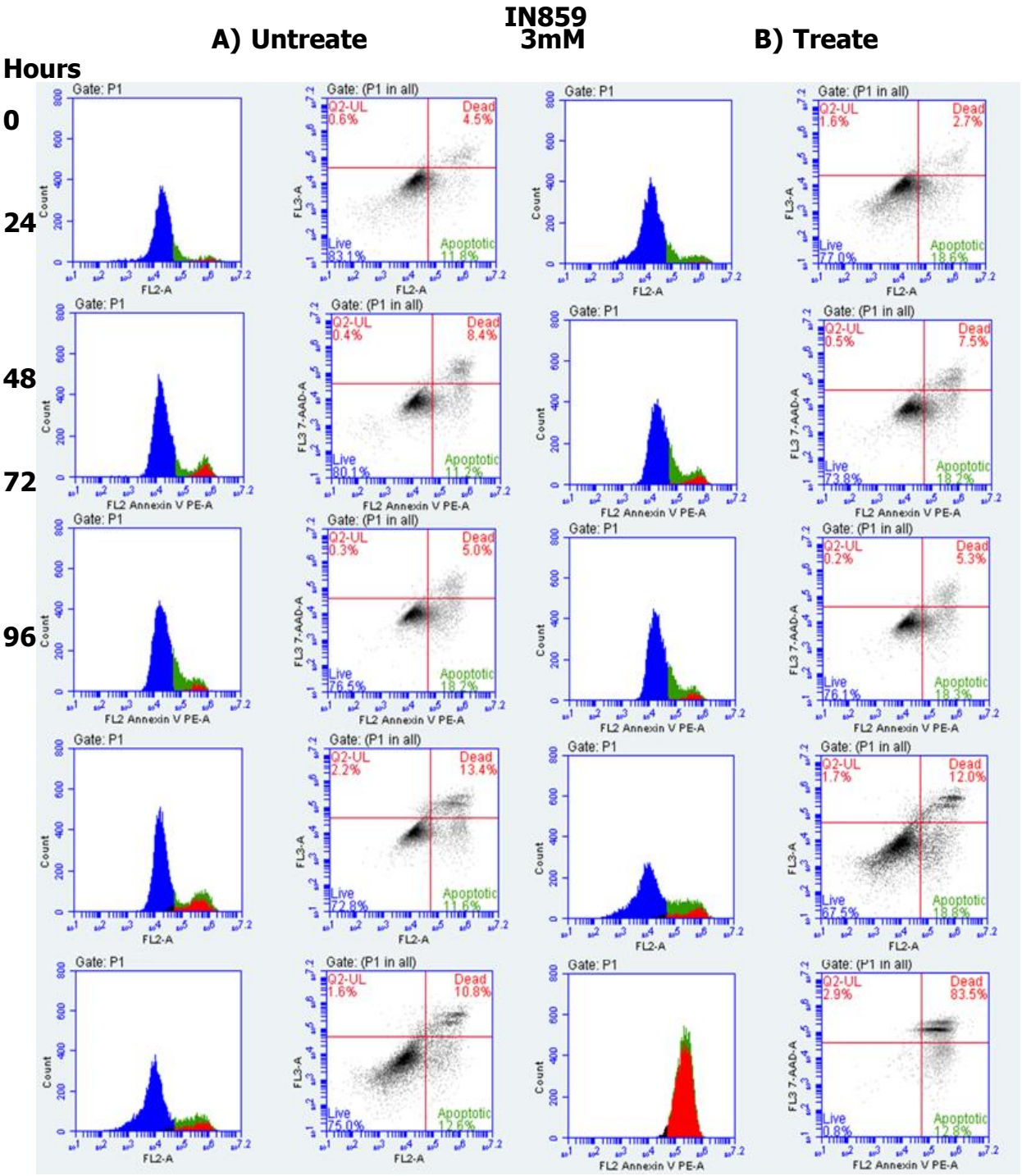

Appendix H2 ii 96-hour apoptotic time course of IN859 treated with metformin in 3mM culture media. A) Untreated samples. Minimal variation in the live cell population over the time course. No increase in apoptosis. B) ID50 metformin treated samples. Blue – Live cells, Green – apoptotic cells, Red – Dead cells.

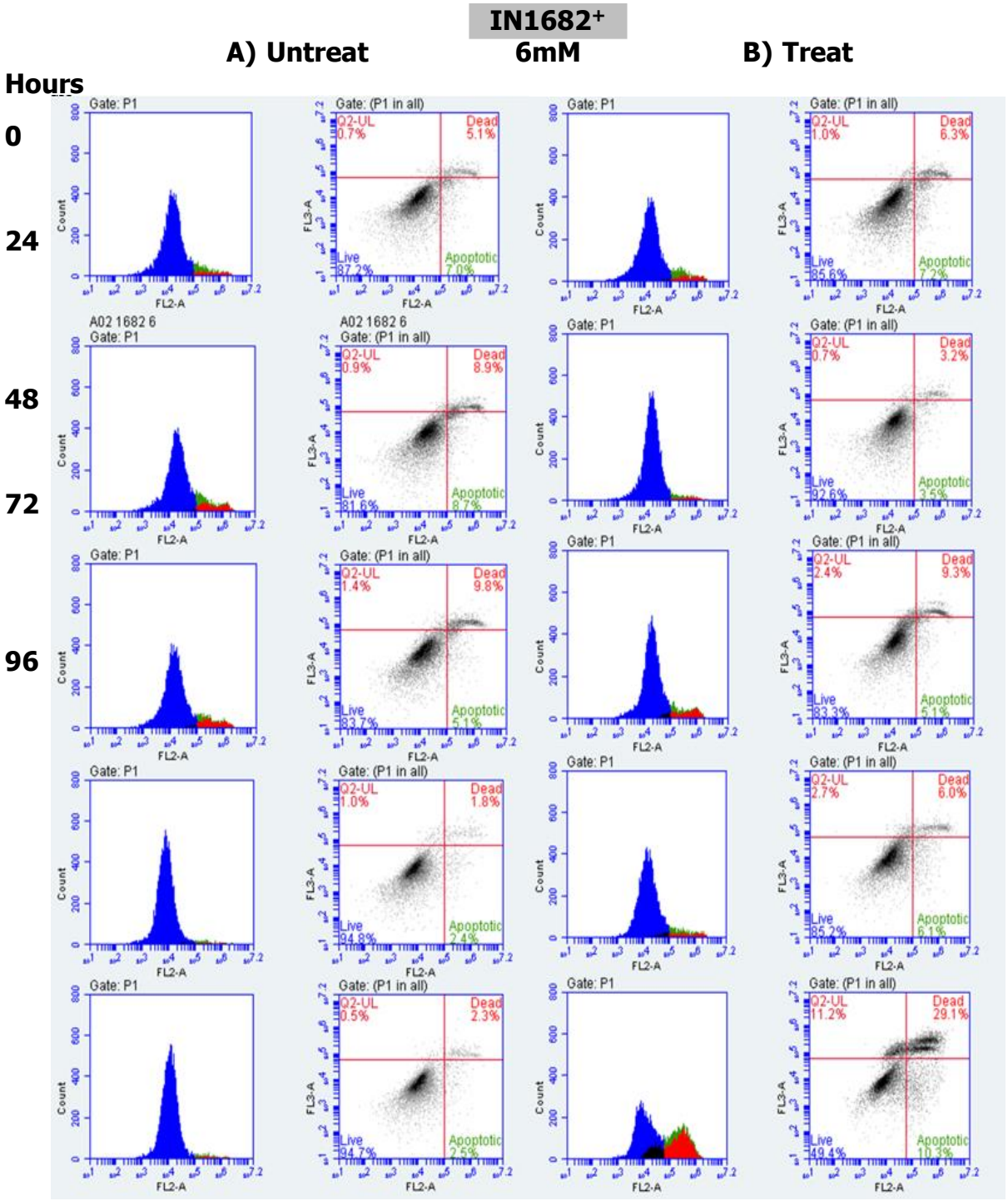

Appendix H3 i 96-hour apoptotic time course of IN1682 treated with metformin in 6mM culture media. A) Untreated samples. Minimal variation in the live cell population over the time course. No increase in apoptosis. B) ID50 metformin treated samples. Blue – Live cells, Green – apoptotic cells, Red – Dead cells.

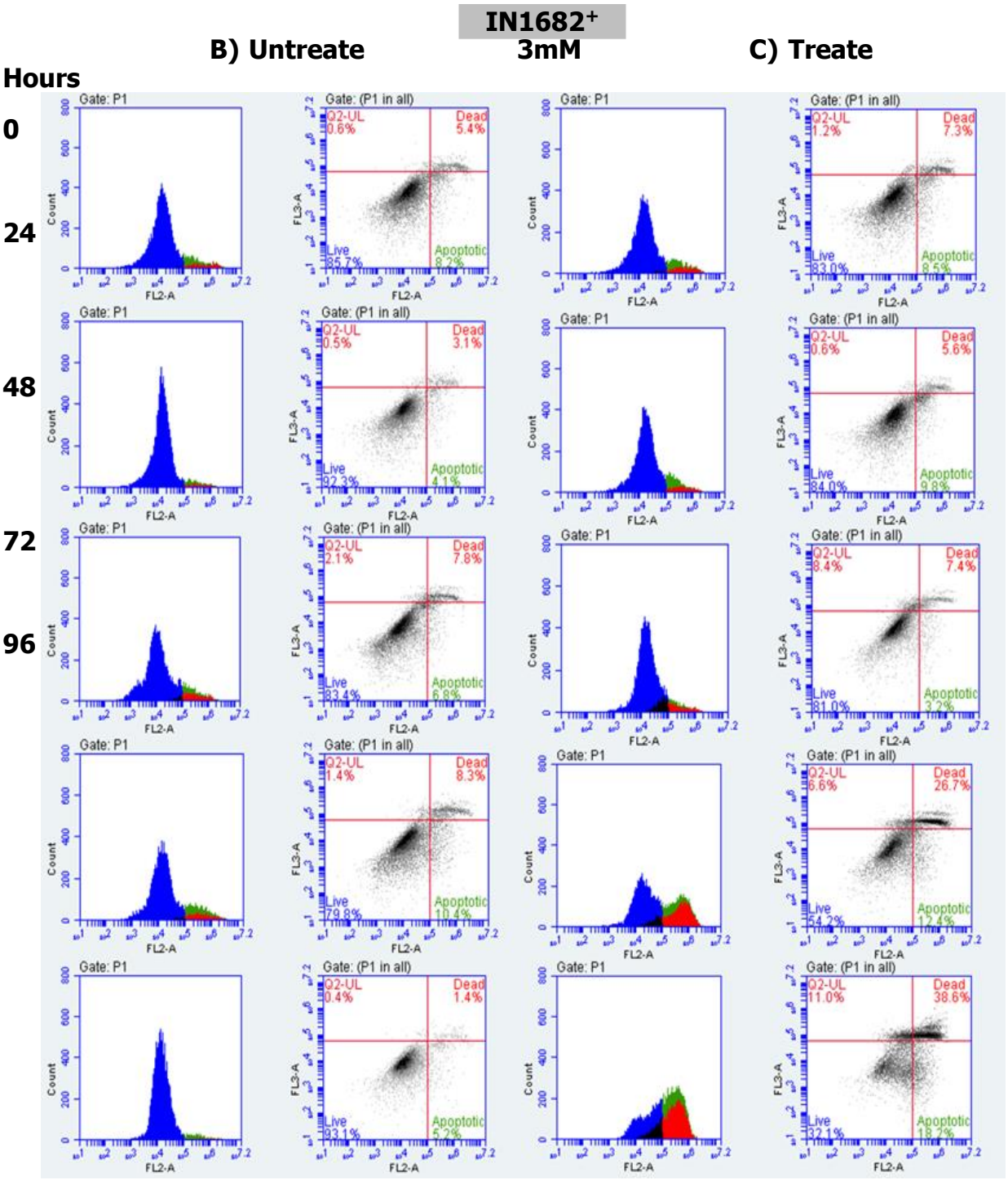

Appendix H3 ii 96-hour apoptotic time course of IN1682 treated with metformin in 3mM culture media. A) Untreated samples. Minimal variation in the live cell population over the time course. No increase in apoptosis. B) ID50 metformin treated samples. Blue – Live cells, Green – apoptotic cells, Red – Dead cells.

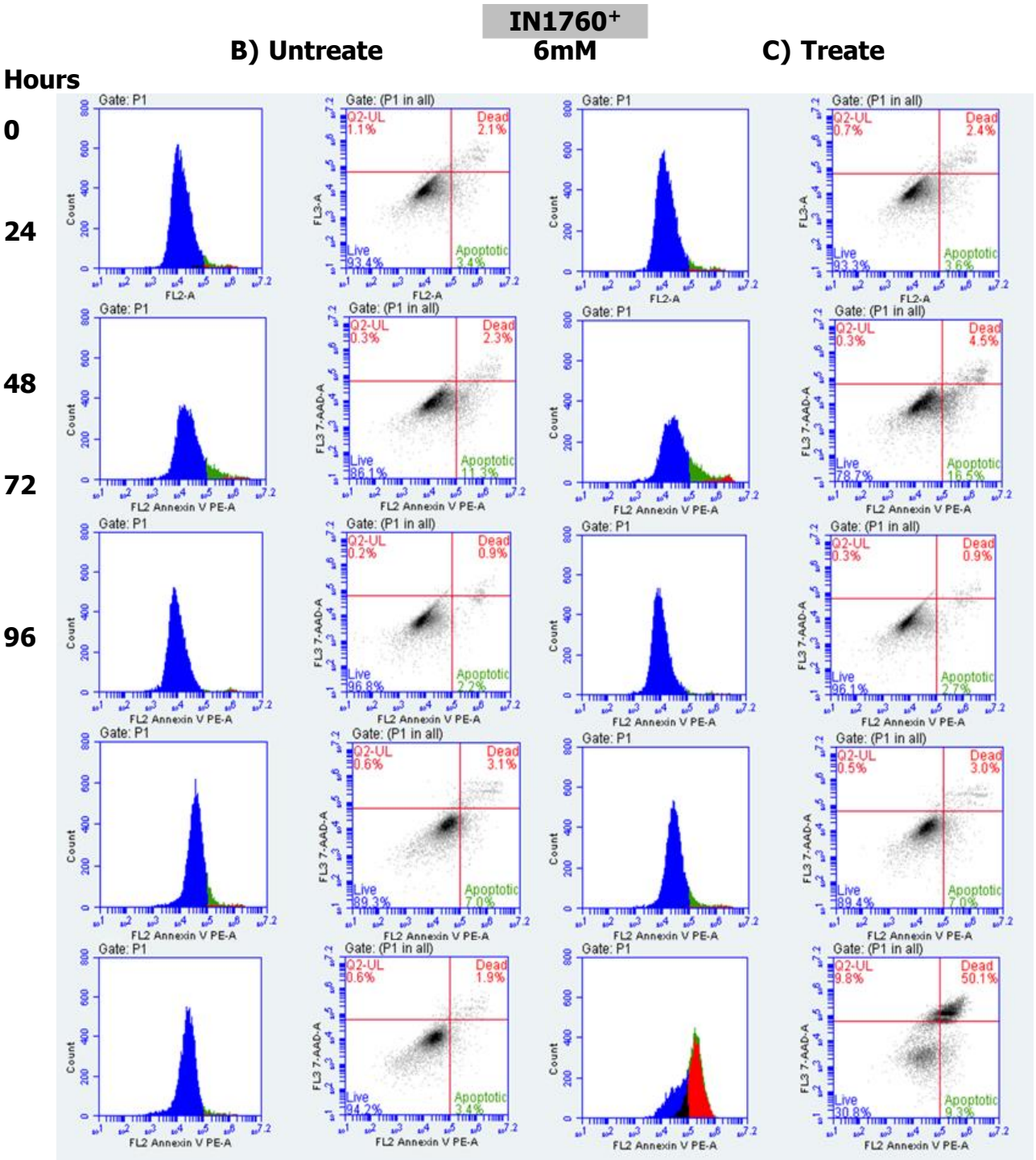

Appendix H4 i 96-hour apoptotic time course of IN1760 treated with metformin in 6mM culture media. A) Untreated samples. Minimal variation in the live cell population over the time course. No increase in apoptosis. B) ID50 metformin treated samples. Blue – Live cells, Green – apoptotic cells, Red – Dead cells.

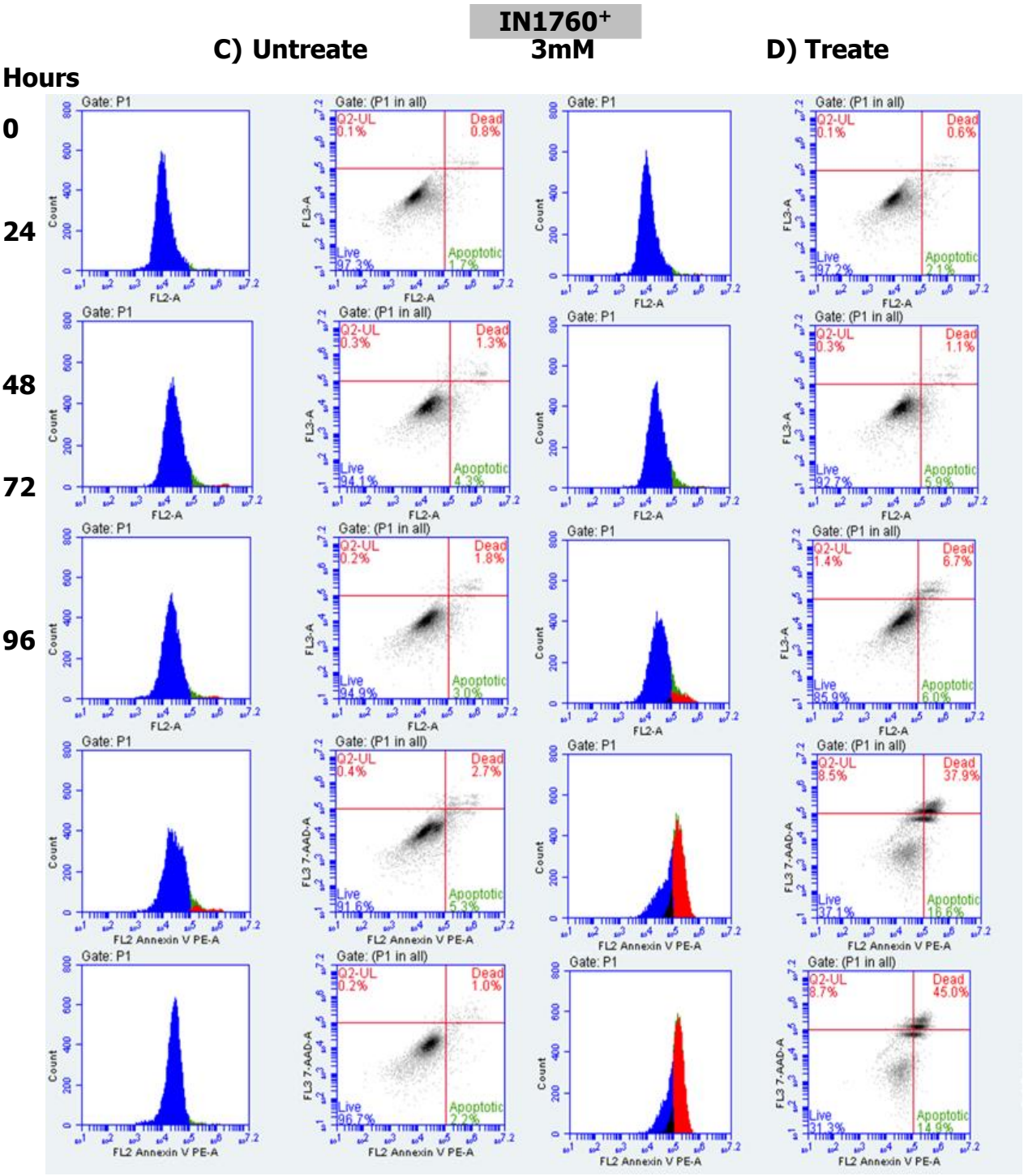

Appendix H4 ii 96-hour apoptotic time course of IN1760 treated with metformin in 3mM culture media. A) Untreated samples. Minimal variation in the live cell population over the time course. No increase in apoptosis. B) ID50 metformin treated samples. Blue – Live cells, Green – apoptotic cells, Red – Dead cells.

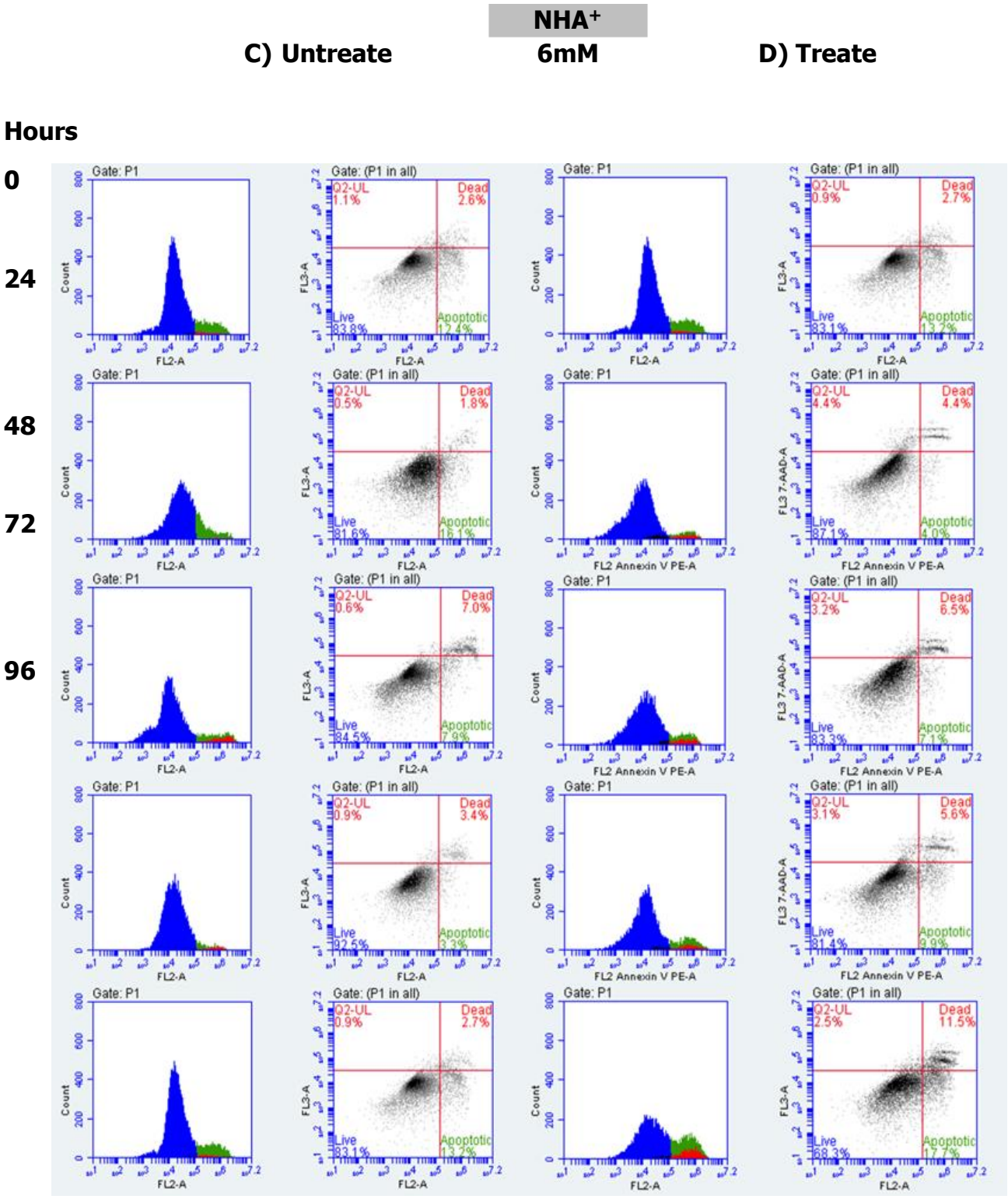

Appendix H5 i 96-hour apoptotic time course of NHA treated with metformin in 6mM culture media. A) Untreated samples. Minimal variation in the live cell population over the time course. No increase in apoptosis. B) ID50 metformin treated samples. Blue – Live cells, Green – apoptotic cells, Red – Dead cells.

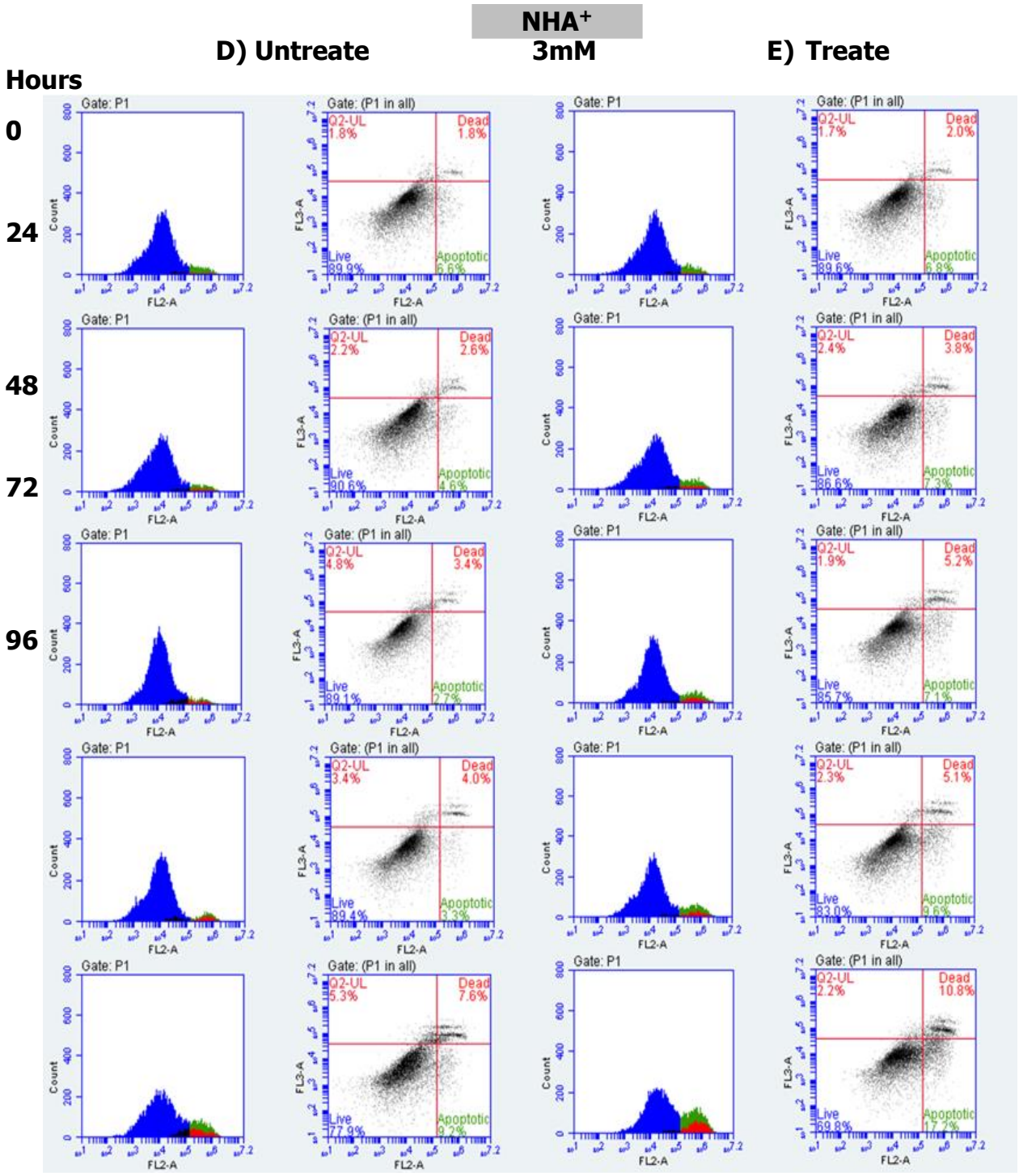

Appendix H5 ii 96-hour apoptotic time course of NHA treated with metformin in 3mM culture media. A) Untreated samples. Minimal variation in the live cell population over the time course. No increase in apoptosis. B) ID50 metformin treated samples. Blue – Live cells, Green – apoptotic cells, Red – Dead cells.

Appendix I - F-10 Growth media formulations used

11550 - Ham's F-10 Nutrient Mix

Catalog Number(s)

11550043

Components	Molecular Weight	Concentration (mg/L)	mM
Amino Acids			
Glycine	75.0	7.5	0.1
L-Alanine	89.0	9.0	0.101123594
L-Arginine hydrochloride	211.0	211.0	1.0
L-Asparagine-H2O	150.0	15.0	0.1
L-Aspartic acid	133.0	13.0	0.09774436
L-Cysteine	121.0	25.0	0.20661157
L-Glutamic Acid	147.0	14.7	0.1
L-Glutamine	146.0	146.0	1.0
L-Histidine hydrochloride-H2O	210.0	23.0	0.10952381
L-Isoleucine	131.0	2.6	0.019847328
L-Leucine	131.0	13.0	0.099236645
L-Lysine hydrochloride	183.0	29.0	0.15846995
L-Methionine	149.0	4.5	0.030201342
L-Phenylalanine	165.0	5.0	0.030303031
L-Proline	115.0	11.5	0.1
L-Serine	105.0	10.5	0.1
L-Threonine	119.0	3.6	0.0302521
L-Tryptophan	204.0	0.6	0.002941176
L-Tyrosine disodium salt dihydrate	261.0	2.62	0.010038313
L-Valine	117.0	3.5	0.02991453
Vitamins			
Biotin	244.0	0.024	9.836066E-5
Choline chloride	140.0	0.7	0.005
D-Calcium pantothenate	477.0	0.7	0.001467505
Folic Acid	441.0	1.3	0.002947846
Niacinamide	122.0	0.6	0.004918033
Pyridoxine hydrochloride	206.0	0.2	9.708738E-4
Riboflavin	376.0	0.4	0.001063829
Thiamine hydrochloride	337.0	1.0	0.002967359
Vitamin B12	1355.0	1.4	0.001033210
i-Inositol	180.0	0.5	0.002777778
Inorganic Salts			
Calcium Chloride (CaCl2) (anhyd.)	111.0	33.3	0.29999998
Cupric sulfate (CuSO4-5H2O)	250.0	0.0025	1.0E-5
Ferric sulfate (FeSO4-7H2O)	278.0	0.834	0.003
Magnesium Sulfate (MgSO4) (anhyd.)	120.0	74.62	0.6218334
Potassium Chloride (KCl)	75.0	285.0	3.8
Potassium Phosphate monobasic (KH2PO4)	136.0	83.0	0.6102941
Sodium Bicarbonate (NaHCO3)	84.0	1200.0	14.285714
Sodium Chloride (NaCl)	58.0	7400.0	127.586205
Sodium Phosphate dibasic (Na2HPO4) anhydrous	142.0	153.7	1.0823944
Zinc sulfate (ZnSO4-7H2O)	288.0	0.03	1.0416666E-4
Other Components			
D-Glucose (Dextrose)	180.0	1100.0	6.111111
Hypoxanthine Na	159.0	4.7	0.029559746
Lipoic Acid	206.0	0.2	9.708738E-4
Phenol Red	376.4	1.2	0.003188097
Sodium Pyruvate	110.0	110.0	1.0
Thymidine	242.0	0.7	0.002892562

Appendix I1 Formulation of F-10 from Gibco Life Technologies. Standard formulation of F-10 used for culturing of all cultures.

Ham´s F-10 Medium		P04-13501
	Components	mg/L
Inorganic Salts	Calcium chloride x 2H2O	34,091
	Copper(II) sulfate x $5H_2O$	0,0025
	Iron(II) sulfate x $7H_2O$	0,834
	Magnesium sulfate dried	110,01
	Potassium dihydrogen phosphate	83,00
	Potassium chloride	285,00
	Sodium chloride	6900,00
	di-Sodium hydrogen phosphate	153,70
	Zinc sulfate x $7H_2O$	0,029
Other Components	D(+)-Glucose anhydrous	0,00
	HEPES	0,00
	Hypoxanthine	4,08
	DL-α-Lipoic acid	0,21
	Phenol red	1,20
	Sodium pyruvate	110,00
	Deoxythymidine	0,73
Aminoacids	L-Alanine	8,91
	L-Arginine x HCl	211,00
	L-Asparagine x H_2O	15,00
	L-Aspartic acid	13,30
	L-Cysteine x HCl x H_2O	25,12
	stable Glutamine	150,00
	L-Glutamic acid	14,70
	Glycine	7,51
	L-Histidine x HCl x H_2O	21,00
	L-Isoleucine	2,60
	L-Leucine	13,10
	L-Lysine x HCl	29,30
	L-Methionine	4,48
	L-Phenylalanine	4,96
	L-Proline	11,50
	L-Serine	10,50
	L-Threonine	3,57
	L-Tryptophane	0,60
	L-Tyrosine	2,81
	L-Valine	3,50
Vitamins	D(+)-Biotin	0,024
	D-Calcium pantothenate	0,715
	Choline chloride	0,698
	Folic acid	1,320
	myo-Inositol	0,541
	Nicotinamide	0,615
	Pyridoxine x HCl	0,210
	Riboflavine	0,376
	Thiamine x HCl	1,010
	Vitamin B_{12}	1,360
	Natriumhydrogencarbonat	1,2 g/l

Appendix I2 Formulation of F-10 from PAN Biotech. Formulation of F-10 used for all glucose experiments. PAN F-10 was supplemented with Glucose from Sigma UK.

References

Aapro, M.S. and Alberts, D.S. (1981) High-dose dexamethasone for prevention of cis-platin-induced vomiting. Cancer chemotherapy and pharmacology , 7(1), pp. 11-14 .

Abbruzzese, C., Matteoni, S., Signore, M., Cardone, L., Nath, K., Glickson, J.D. and Paggi, M.G. (2017) Drug repurposing for the treatment of glioblastoma multiforme. Journal of Experimental & Clinical Cancer Research , 36(1), pp. 169 .

Abdul-Ghani, M. and DeFronzo, R.A. (2017) Is It Time to Change the Type 2 Diabetes Treatment Paradigm? Yes! GLP-1 RAs Should Replace Metformin in the Type 2 Diabetes Algorithm. Diabetes care , 40(8), pp. 1121-1127 .

Adeberg, S., Bernhardt, D., Harrabi, S.B., Nicolay, N., Rieber, J., Koenig, L., Repka, M., Mohr, A., Abdollahi, A. and Weber, K. (2017) Metformin Enhanced *in vitro* Radiosensitivity Associates with G2/M Cell Cycle Arrest and Elevated pAMPK Levels in Glioblastoma. Radiology and Oncology , 51(4), .

Aldea, M.D., Petrushev, B., Soritau, O., Tomuleasa, C.I., Berindan-Neagoe, I., Filip, A.G., Chereches, G., Cenariu, M., Craciun, L. and Tatomir, C. (2014) Metformin plus sorafenib highly impacts temozolomide-resistant glioblastoma stem-like cells.

Alifieris, C. and Trafalis, D.T. (2015) Glioblastoma multiforme: Pathogenesis and treatment. Pharmacology & therapeutics , 152pp. 63-82 .

Applied Biosystems (2011) Endogenous Controls for Real-Time Quantitation of miRNA Using TaqMan ® MicroRNA Assays.Available at:

<http://www3.appliedbiosystems.com/cms/groups/mcb_marketing/documents/generaldocuments/cms_044972.pdf>.

Arevalo, O., Valenzuela, R., Esquenazi, Y., Rao, M., Tran, B., Zhu, J., Bhattacharjee, M., Doyle, N. and Riascos, R. (2017) The 2016 World Health Organization Classification of Tumors of the Central Nervous System: A Practical Approach for Gliomas, Part 2. Isocitrate Dehydrogenase Status—Imaging Correlation. Neurographics , 7(5), pp. 344-349 .

Arkin, M.R., Tang, Y. and Wells, J.A. (2014) Small-molecule inhibitors of protein-protein interactions: progressing toward the reality. Chemistry & biology , 21(9), pp. 1102-1114 .

Armulik, A., Genové, G., Mäe, M., Nisancioglu, M.H., Wallgard, E., Niaudet, C., He, L., Norlin, J., Lindblom, P. and Strittmatter, K. (2010) Pericytes regulate the blood–brain barrier. Nature , 468(7323), pp. 557 .

Asati, V., Mahapatra, D.K. and Bharti, S.K. (2016) PI3K/Akt/mTOR and Ras/Raf/MEK/ERK signaling pathways inhibitors as anticancer agents: structural and pharmacological perspectives. European journal of medicinal chemistry , 109pp. 314-341 .

Ashkenazi, A. (2015) Targeting the extrinsic apoptotic pathway in cancer: lessons learned and future directions. The Journal of clinical investigation , 125(2), pp. 487-489 .

Babcook, M., Sramkoski, R., Fujioka, H., Daneshgari, F., Almasan, A., Shukla, S., Nanavaty, R. and Gupta, S. (2014) Combination simvastatin and metformin

induces G1-phase cell cycle arrest and Ripk1-and Ripk3-dependent necrosis in C4-2B osseous metastatic castration-resistant prostate cancer cells. Cell death & disease , 5(11), pp. e1536 .

Badie, B., Schartner, J., Prabakaran, S., Paul, J. and Vorpahl, J. (2001) Expression of Fas ligand by microglia: possible role in glioma immune evasion. Journal of neuroimmunology , 120(1-2), pp. 19-24 .

Bailey, C., Wilcock, C. and Scarpello, J. (2008) Metformin and the intestine. Diabetologia , 51(8), pp. 1552 .

Bailey, C.J. (2017) Metformin: historical overview. Diabetologia , 60(9), pp. 1566-1576 .

Bailey, C.J. and Day, C. (2004) Metformin: its botanical background. Practical diabetes , 21(3), pp. 115-117 .

Bailey, C.J. and Turner, R.C. (1996) Metformin. New England Journal of Medicine , 334(9), pp. 574-579 .

Bailey, P. and Cushing, H. (1925) Microchemical Color Reactions as an Aid to the Identification and Classification of Brain Tumors. Proceedings of the National Academy of Sciences of the United States of America , 11(1), pp. 82-84 .

Balding, E., Ververis, K. and Karagiannis, T.C. (2014) Molecular Aspects of the Warburg Effect. in Molecular mechanisms and physiology of disease. Springer, pp.371-382.

Ballabh, P., Braun, A. and Nedergaard, M. (2004) The blood–brain barrier: an overview: structure, regulation, and clinical implications. Neurobiology of disease , 16(1), pp. 1-13 .

Banko, M.R., Allen, J.J., Schaffer, B.E., Wilker, E.W., Tsou, P., White, J.L., Villén, J., Wang, B., Kim, S.R. and Sakamoto, K. (2011) Chemical genetic screen for AMPKα2 substrates uncovers a network of proteins involved in mitosis. Molecular cell , 44(6), pp. 878-892 .

Bara, J.J., Richards, R.G., Alini, M. and Stoddart, M.J. (2014) Concise review: Bone marrow-derived mesenchymal stem cells change phenotype following *in vitro* culture: implications for basic research and the clinic. Stem cells , 32(7), pp. 1713-1723 .

Barker, F.G.,2nd, Simmons, M.L., Chang, S.M., Prados, M.D., Larson, D.A., Sneed, P.K., Wara, W.M., Berger, M.S., Chen, P., Israel, M.A. and Aldape, K.D. (2001) EGFR overexpression and radiation response in glioblastoma multiforme. International journal of radiation oncology, biology, physics , 51(2), pp. 410-418 .

Barter, M.J., Tselepi, M., Gómez, R., Woods, S., Hui, W., Smith, G.R., Shanley, D.P., Clark, I.M. and Young, D.A. (2015) Genome-Wide MicroRNA and Gene Analysis of Mesenchymal Stem Cell Chondrogenesis Identifies an Essential Role and Multiple Targets for miR-140-5p. Stem Cells , 33(11), pp. 3266-3280 .

Basu, S. and Murphy, M.E. (2016) Genetic Modifiers of the p53 Pathway. Cold Spring Harbor perspectives in medicine , 6(4), pp. a026302 .

Bell, E.H., Zhang, P., Fisher, B.J., Macdonald, D.R., McElroy, J.P., Lesser, G.J., Fleming, J., Chakraborty, A.R., Liu, Z. and Becker, A.P. (2018) Association of MGMT Promoter Methylation Status With Survival Outcomes in Patients With High-Risk Glioma Treated With Radiotherapy and Temozolomide: An Analysis From the NRG Oncology/RTOG 0424 Trial. JAMA oncology .

Bellacosa, A., Kumar, C.C., Di Cristofano, A. and Testa, J.R. (2005) Activation of AKT kinases in cancer: implications for therapeutic targeting. Advances in Cancer Research , 94pp. 29-86 .

Ben Sahra, I., Laurent, K., Giuliano, S., Larbret, F., Ponzio, G., Gounon, P., Le Marchand-Brustel, Y., Giorgetti-Peraldi, S., Cormont, M., Bertolotto, C., Deckert, M., Auberger, P., Tanti, J.F. and Bost, F. (2010) Targeting cancer cell metabolism: the combination of metformin and 2-deoxyglucose induces p53-dependent apoptosis in prostate cancer cells. Cancer research , 70(6), pp. 2465-2475 .

Ben Sahra, I., Regazzetti, C., Robert, G., Laurent, K., Le Marchand-Brustel, Y., Auberger, P., Tanti, J.F., Giorgetti-Peraldi, S. and Bost, F. (2011) Metformin, independent of AMPK, induces mTOR inhibition and cell-cycle arrest through REDD1. Cancer research , 71(13), pp. 4366-4372 .

Benitez, J.A., Ma, J., D'Antonio, M., Boyer, A., Camargo, M.F., Zanca, C., Kelly, S., Khodadadi-Jamayran, A., Jameson, N.M. and Andersen, M. (2017) PTEN regulates glioblastoma oncogenesis through chromatin-associated complexes of DAXX and histone H3. 3. Nature communications , 8pp. 15223 .

Berezikov, E., Chung, W., Willis, J., Cuppen, E. and Lai, E.C. (2007) Mammalian mirtron genes. Molecular cell , 28(2), pp. 328-336 .

Berghoff, A.S., Kiesel, B., Widhalm, G., Rajky, O., Ricken, G., Wöhrer, A., Dieckmann, K., Filipits, M., Brandstetter, A. and Weller, M. (2014) Programmed death ligand 1 expression and tumor-infiltrating lymphocytes in glioblastoma. Neuro-oncology , 17(8), pp. 1064-1075 .

Bertoli, C. and de Bruin, Robertus Antonius Maria (2014) Cell Division: Turning cell cycle entry on its head. Elife , 3pp. e03475 .

Birsoy, K., Possemato, R., Lorbeer, F.K., Bayraktar, E.C., Thiru, P., Yucel, B., Wang, T., Chen, W.W., Clish, C.B. and Sabatini, D.M. (2014) Metabolic determinants of cancer cell sensitivity to glucose limitation and biguanides. Nature , 508(7494), pp. 108 .

Blandino, G., Valerio, M., Cioce, M., Mori, F., Casadei, L., Pulito, C., Sacconi, A., Biagioni, F., Cortese, G. and Galanti, S. (2012) Metformin elicits anticancer effects through the sequential modulation of DICER and c-MYC. Nature communications , 3pp. 865 .

Bleeker, F.E., Molenaar, R.J. and Leenstra, S. (2012) Recent advances in the molecular understanding of glioblastoma. Journal of neuro-oncology , 108(1), pp. 11-27 .

Block, L., Schemling, L., Couto, A., Mourão, S. and Bresolin, T. (2009) Pharmaceutical equivalence of metformin tablets with various binders. Revista de Ciências Farmacêuticas Básica e Aplicada , 29(1), pp. 29-35 .

Blume-Peytavi, U., Shapiro, J., Messenger, A.G., Hordinsky, M.K., Zhang, P., Quiza, C., Doshi, U. and Olsen, E.A. (2016) Efficacy and Safety of Once-Daily Minoxidil Foam 5% Versus Twice-Daily Minoxidil Solution 2% in Female Pattern Hair Loss: A Phase III, Randomized, Investigator-Blinded Study. Journal of drugs in dermatology : JDD , 15(7), pp. 883-889 .

Bogdahn, U., Hau, P., Stockhammer, G., Venkataramana, N., Mahapatra, A., Suri, A.a., Balasubramaniam, A., Nair, S., Oliushine, V. and Parfenov, V. (2010) Targeted therapy for high-grade glioma with the TGF-β2 inhibitor trabedersen: results of a randomized and controlled phase IIb study. Neuro-oncology , 13(1), pp. 132-142 .

Brat, D.J. and Van Meir, E.G. (2004) Vaso-occlusive and prothrombotic mechanisms associated with tumor hypoxia, necrosis, and accelerated growth in glioblastoma. Laboratory investigation , 84(4), pp. 397-405

Brenneman, B.R., Floyd, D.H., Harris, T. and Purow, B. (2016) Assessing and augmenting the immune response to glioblastoma using repurposed pharmaceuticals .

Bridges, H.R., Jones, A.J., Pollak, M.N. and Hirst, J. (2014) Effects of metformin and other biguanides on oxidative phosphorylation in mitochondria. The Biochemical journal , 462(3), pp. 475-487 .

Bromage, D.I. and Yellon, D.M. (2015) The pleiotropic effects of metformin: time for prospective studies. Cardiovascular diabetology , 14(1), pp. 109 .

Brose, M.S., Nutting, C., Jarzab, B., Elisei, R., Siena, S., Bastholt, L., de la Fouchardiere, C., Pacini, F., Paschke, R. and Shong, Y.K. (2013) Sorafenib in locally advanced or metastatic patients with radioactive iodine-refractory differentiated thyroid cancer: The phase III DECISION trial. .

Brown, D., Croce, C. and Nana-Sinkam, S. (2017) Clinical and Therapeutic Applications of MicroRNA in Cancer. in Translating MicroRNAs to the Clinic. Elsevier, pp.17-37.

Buckanovich, R.J., Brown, J., Shank, J., Griffith, K.A., Reynolds, R.K., Johnston, C., McLean, K., Uppal, S., Liu, J.R. and Cabrera, L. (2017) A phase II clinical trial of metformin as a cancer stem cell targeting agent in stage IIc/III/IV ovarian, fallopian tube, and primary peritoneal cancer. .

Budihardjo, I., Oliver, H., Lutter, M., Luo, X. and Wang, X. (1999) Biochemical pathways of caspase activation during apoptosis. Annual Review of Cell and Developmental Biology , 15(1), pp. 269-290 .

Butkytė, S., Čiupas, L., Jakubauskienė, E., Vilys, L., Mocevicius, P., Kanopka, A. and Vilkaitis, G. (2016) Splicing-dependent expression of microRNAs of mirtron origin in human digestive and excretory system cancer cells. Clinical epigenetics , 8(1), pp. 33 .

Butte, M.J., Keir, M.E., Phamduy, T.B., Sharpe, A.H. and Freeman, G.J. (2007) Programmed death-1 ligand 1 interacts specifically with the B7-1 costimulatory molecule to inhibit T cell responses. Immunity , 27(1), pp. 111-122 .

Buzzai, M., Jones, R.G., Amaravadi, R.K., Lum, J.J., DeBerardinis, R.J., Zhao, F., Viollet, B. and Thompson, C.B. (2007) Systemic treatment with the antidiabetic drug metformin selectively impairs p53-deficient tumor cell growth. Cancer research , 67(14), pp. 6745-6752 .

Cancer Genome Atlas Research Network (2008) Comprehensive genomic characterization defines human glioblastoma genes and core pathways. Nature , 455(7216), pp. 1061 .

Carlsson, S.K., Brothers, S.P. and Wahlestedt, C. (2014) Emerging treatment strategies for glioblastoma multiforme. EMBO molecular medicine , 6(11), pp. 1359-1370 .

Castedo, M., Perfettini, J., Roumier, T., Andreau, K., Medema, R. and Kroemer, G. (2004) Cell death by mitotic catastrophe: a molecular definition. Oncogene , 23(16), pp. 2825-2837 .

Cerezo, M., Tichet, M., Abbe, P., Ohanna, M., Lehraiki, A., Rouaud, F., Allegra, M., Giacchero, D., Bahadoran, P., Bertolotto, C., Tartare-Deckert, S., Ballotti, R. and Rocchi, S. (2013) Metformin blocks melanoma invasion and metastasis development in AMPK/p53-dependent manner. Molecular cancer therapeutics , 12(8), pp. 1605-1615 .

Chae, Y.K., Arya, A., Malecek, M.K., Shin, D.S., Carneiro, B., Chandra, S., Kaplan, J., Kalyan, A., Altman, J.K., Platanias, L. and Giles, F. (2016) Repurposing metformin for cancer treatment: current clinical studies. Oncotarget , 7(26), pp. 40767-40780 .

Chahlavi, A., Rayman, P., Richmond, A.L., Biswas, K., Zhang, R., Vogelbaum, M., Tannenbaum, C., Barnett, G. and Finke, J.H. (2005) Glioblastomas induce T-lymphocyte death by two distinct pathways involving gangliosides and CD70. Cancer research , 65(12), pp. 5428-5438 .

Chan, J.A., Krichevsky, A.M. and Kosik, K.S. (2005) MicroRNA-21 is an antiapoptotic factor in human glioblastoma cells. Cancer research , 65(14), pp. 6029-6033 .

Chang, Z., Meng, F., Zhang, Z., Mao, G., Huang, Z., Liao, W. and He, A. (2018) MicroRNA-193b-3p Regulates Matrix Metalloproteinase 19 Expression in Interleukin-1β-Induced Human Chondrocytes. Journal of cellular biochemistry .

Chappell, W.H., Steelman, L.S., Long, J.M., Kempf, R.C., Abrams, S.L., Franklin, R.A., Basecke, J., Stivala, F., Donia, M., Fagone, P., Malaponte, G., Mazzarino, M.C., Nicoletti, F., Libra, M., Maksimovic-Ivanic, D., Mijatovic, S., Montalto, G., Cervello, M., Laidler, P., Milella, M., Tafuri, A., Bonati, A., Evangelisti, C., Cocco, L., Martelli, A.M. and McCubrey, J.A. (2011) Ras/Raf/MEK/ERK and PI3K/PTEN/Akt/mTOR inhibitors: rationale and importance to inhibiting these pathways in human health. Oncotarget , 2(3), pp. 135-164 .

Chaudhry, A., Benson, L., Varshaver, M., Farber, O., Weinberg, U., Kirson, E. and Palti, Y. (2015) NovoTTF™-100A System (Tumor Treating Fields) transducer array layout planning for glioblastoma: a NovoTAL™ system user study. World journal of surgical oncology , 13(1), pp. 316 .

Chen, C., Ridzon, D.A., Broomer, A.J., Zhou, Z., Lee, D.H., Nguyen, J.T., Barbisin, M., Xu, N.L., Mahuvakar, V.R., Andersen, M.R., Lao, K.Q., Livak, K.J. and Guegler, K.J. (2005) Real-time quantification of microRNAs by stem-loop RT-PCR. Nucleic acids research , 33(20), pp. e179 .

Chen, L., Han, L., Shi, Z., Zhang, K., Liu, Y., Zheng, Y., Jiang, T., Pu, P., Jiang, C. and Kang, C. (2012) LY294002 enhances cytotoxicity of temozolomide in glioma by down-regulation of the PI3K/Akt pathway. Molecular medicine reports , 5(2), pp. 575-579 .

Chen, P., Wang, A.Y. and DePinho, R.A. (2018) Lysyl oxidase secreted by PTEN-deficient glioblastoma cells recruits macrophages and promotes malignant growth .

Chen, T., Tian, X., Liu, C., Ge, J., Chu, X. and Li, Y. (2015) Fluorescence activation imaging of cytochrome c released from mitochondria using aptameric nanosensor. Journal of the American Chemical Society , 137(2), pp. 982-989 .

Cheng, C.K., Fan, Q. and Weiss, W.A. (2009) PI3K signaling in glioma—animal models and therapeutic challenges. Brain pathology , 19(1), pp. 112-120 .

Choi, H.J., Fukui, M. and Zhu, B.T. (2011) Role of cyclin B1/Cdc2 up-regulation in the development of mitotic prometaphase arrest in human breast cancer cells treated with nocodazole. PloS one , 6(8), pp. e24312 .

Choi, Y.W. and Lim, I.K. (2014) Sensitization of metformin-cytotoxicity by dichloroacetate via reprogramming glucose metabolism in cancer cells. Cancer letters , 346(2), pp. 300-308 .

Chou, T.C. (2010) Drug combination studies and their synergy quantification using the Chou-Talalay method. Cancer research , 70(2), pp. 440-446 .

Christofk, H.R., Vander Heiden, M.G., Harris, M.H., Ramanathan, A., Gerszten, R.E., Wei, R., Fleming, M.D., Schreiber, S.L. and Cantley, L.C. (2008) The M2 splice isoform of pyruvate kinase is important for cancer metabolism and tumour growth. Nature , 452(7184), pp. 230 .

Christopher, A.F., Kaur, R.P., Kaur, G., Kaur, A., Gupta, V. and Bansal, P. (2016) MicroRNA therapeutics: Discovering novel targets and developing specific therapy. Perspectives in clinical research , 7(2), pp. 68-74 .

Coleman, C.B., Lightell Jr, D.J., Moss, S.C., Bates, M., Eugene Parrino, P. and Cooper Woods, T. (2013) Elevation of miR-221 and-222 in the Internal Mammary Arteries of Diabetic Subjects and Normalization with Metformin. Molecular and cellular endocrinology .

Cossarizza, A., Baccaranicontri, M., Kalashnikova, G. and Franceschi, C. (1993) A new method for the cytofluorometric analysis of mitochondrial membrane potential using the J-aggregate forming lipophilic cation 5, 5′, 6, 6′-tetrachloro-1, 1′, 3, 3′-tetraethylbenzimidazolcarbocyanine iodide (JC-1). Biochemical and biophysical research communications , 197(1), pp. 40-45 .

Cui, Y., Yi, L., Zhao, J. and Jiang, Y. (2017) Long noncoding RNA HOXA11-AS functions as miRNA sponge to promote the glioma tumorigenesis through targeting miR-140-5p. DNA and cell biology , 36(10), pp. 822-828 .

Cui, S.Y., Huang, J.Y., Chen, Y.T., Song, H.Z., Feng, B., Huang, G.C., Wang, R., Chen, L.B. and De, W. (2013) Let-7c governs the acquisition of chemo- or radioresistance and epithelial-to-mesenchymal transition phenotypes in docetaxel-resistant lung adenocarcinoma. Molecular cancer research : MCR , 11(7), pp. 699-713 .

D'Alessandro, A., Slaughter, A.L., Peltz, E.D., Moore, E.E., Silliman, C.C., Wither, M., Nemkov, T., Bacon, A.W., Fragoso, M. and Banerjee, A. (2015) Trauma/hemorrhagic shock instigates aberrant metabolic flux through glycolytic pathways, as revealed by preliminary 13 C-glucose labeling metabolomics. Journal of translational medicine , 13(1), pp. 253 .

Darzynkiewicz,Z., Bedner,E. and Smolewski,P. (2001) Flow cytometry in analysis of cell cycle and apoptosis Seminars in hematology. Elsevier, pp.179-193.

Darzynkiewicz, Z. and Zhao, H. Cell cycle analysis by flow cytometry. Els .

Davoren, P.A., McNeill, R.E., Lowery, A.J., Kerin, M.J. and Miller, N. (2008) Identification of suitable endogenous control genes for microRNA gene expression analysis in human breast cancer. BMC molecular biology , 9(1), pp. 76 .

de Groot, J.F., Fuller, G., Kumar, A.J., Piao, Y., Eterovic, K., Ji, Y. and Conrad, C.A. (2010) Tumor invasion after treatment of glioblastoma with bevacizumab: radiographic and pathologic correlation in humans and mice. Neuro-oncology , 12(3), pp. 233-242 .

De Robertis, A., Valensin, S., Rossi, M., Tunici, P., Verani, M., De Rosa, A., Giordano, C., Varrone, M., Nencini, A., Pratelli, C., Benicchi, T., Bakker, A., Hill, J., Sangthongpitag, K., Pendharkar, V., Liu, B., Ng, F.M., Then, S.W., Jing Tai, S., Cheong, S.M., He, X., Caricasole, A. and Salerno, M. (2013) Identification and characterization of a small-molecule inhibitor of Wnt signaling in glioblastoma cells. Molecular cancer therapeutics , 12(7), pp. 1180-1189 .

DeFronzo, R.A., Goodman, A.M. and Multicenter Metformin Study Group (1995) Efficacy of metformin in patients with non-insulin-dependent diabetes mellitus. New England Journal of Medicine , 333(9), pp. 541-549 .

DeFronzo, R., Fleming, G.A., Chen, K. and Bicsak, T.A. (2016) Metformin-associated lactic acidosis: current perspectives on causes and risk. Metabolism-Clinical and Experimental , 65(2), pp. 20-29 .

Degrauwe, N., Schlumpf, T.B., Janiszewska, M., Martin, P., Cauderay, A., Provero, P., Riggi, N., Suvà, M., Paro, R. and Stamenkovic, I. (2016) The RNA binding protein IMP2 preserves glioblastoma stem cells by preventing let-7 target gene silencing. Cell reports , 15(8), pp. 1634-1647 .

Delgado-Lopez, P. and Corrales-Garcia, E. (2016) Survival in glioblastoma: a review on the impact of treatment modalities. Clinical and Translational Oncology , 18(11), pp. 1062-1071 .

Denli, A.M., Tops, B.B., Plasterk, R.H., Ketting, R.F. and Hannon, G.J. (2004) Processing of primary microRNAs by the Microprocessor complex. Nature , 432(7014), pp. 231 .

Denny, B.J., Wheelhouse, R.T., Stevens, M.F., Tsang, L.L. and Slack, J.A. (1994) NMR and molecular modeling investigation of the mechanism of activation of the antitumor drug temozolomide and its interaction with DNA. Biochemistry , 33(31), pp. 9045-9051 .

Do, M.T., Kim, H.G., Choi, J.H. and Jeong, H.G. (2014) Metformin induces microRNA-34a to downregulate the Sirt1/Pgc-1α/Nrf2 pathway, leading to increased susceptibility of wild-type p53 cancer cells to oxidative stress and therapeutic agents. Free Radical Biology and Medicine , 74pp. 21-34 .

Dowling, R.J., Parulekar, W.R., Gelmon, K.A., Shepherd, L.E., Virk, S., Ennis, M., Mao, F., Ligibel, J.A., Hershman, D.L. and Rastogi, P. (2018) CA15-3/MUC1 in CCTG MA-32 (NCT01101438): A phase III RCT of the effect of metformin vs.placebo on invasive disease free and overall survival in early stage breast cancer (BC). .

Dowling, R.J., Zakikhani, M., Fantus, I.G., Pollak, M. and Sonenberg, N. (2007) Metformin inhibits mammalian target of rapamycin-dependent translation initiation in breast cancer cells. Cancer research , 67(22), pp. 10804-10812 .

Dussmann, H., Rehm, M., Kogel, D. and Prehn, J.H. (2003) Outer mitochondrial membrane permeabilization during apoptosis triggers caspase-independent mitochondrial and caspase-dependent plasma membrane potential depolarization: a single-cell analysis. Journal of cell science , 116(Pt 3), pp. 525-536 .

Eades, G., Yao, Y., Yang, M., Zhang, Y., Chumsri, S. and Zhou, Q. (2011) miR-200a regulates SIRT1 expression and epithelial to mesenchymal transition (EMT)-like transformation in mammary epithelial cells. The Journal of biological chemistry , 286(29), pp. 25992-26002 .

Eckel-Passow, J.E., Lachance, D.H., Molinaro, A.M., Walsh, K.M., Decker, P.A., Sicotte, H., Pekmezci, M., Rice, T., Kosel, M.L. and Smirnov, I.V. (2015) Glioma groups based on 1p/19q, IDH, and TERT promoter mutations in tumors. New England Journal of Medicine , 372(26), pp. 2499-2508 .

Eggen, T. and Lillo, C. (2012) Antidiabetic II drug metformin in plants: uptake and translocation to edible parts of cereals, oily seeds, beans, tomato, squash, carrots, and potatoes. Journal of Agricultural and Food Chemistry , 60(28), pp. 6929-6935 .

Elmore, S. (2007) Apoptosis: a review of programmed cell death. Toxicologic pathology , 35(4), pp. 495-516 .

England, B., Huang, T. and Karsy, M. (2013) Current understanding of the role and targeting of tumor suppressor p53 in glioblastoma multiforme. Tumor Biology , 34(4), pp. 2063-2074 .

Esteller, M., Garcia-Foncillas, J., Andion, E., Goodman, S.N., Hidalgo, O.F., Vanaclocha, V., Baylin, S.B. and Herman, J.G. (2000) Inactivation of the DNA-repair gene MGMT and the clinical response of gliomas to alkylating agents. N Engl j Med , 2000(343), pp. 1350-1354 .

Eulalio, A., Huntzinger, E. and Izaurralde, E. (2008) Getting to the root of miRNA-mediated gene silencing. Cell , 132(1), pp. 9-14 .

Evan, G.I. and Vousden, K.H. (2001) Proliferation, cell cycle and apoptosis in cancer. Nature , 411(6835), pp. 342-348 .

Evans, J.M., Donnelly, L.A., Emslie-Smith, A.M., Alessi, D.R. and Morris, A.D. (2005) Metformin and reduced risk of cancer in diabetic patients. BMJ (Clinical research ed.) , 330(7503), pp. 1304-1305 .

Fabian, M.R. and Sonenberg, N. (2012) The mechanics of miRNA-mediated gene silencing: a look under the hood of miRISC. Nature Structural and Molecular Biology , 19(6), pp. 586 .

Fan, Q. and Weiss, W.A. (2011) Autophagy and Akt promote survival in glioma. Autophagy .

Felicetti, F., Feo, A., Coscia, C., Puglisi, R., Pedini, F., Pasquini, L., Bellenghi, M., Errico, M.C., Pagani, E. and Carè, A. (2016) Exosome-mediated transfer of miR-222 is sufficient to increase tumor malignancy in melanoma. Journal of translational medicine , 14(1), pp. 56 .

Feng, B., Wang, R., Song, H. and Chen, L. (2012) MicroRNA-200b reverses chemoresistance of docetaxel-resistant human lung adenocarcinoma cells by targeting E2F3. Cancer , 118(13), pp. 3365-3376 .

Ferrera, J.F. and Martinez, L.E. (2012) Synthesis of Fluorescent labeled Metformin. Rollins College Student-Faculty Collaborative Research Program, 2012 Annual Report pp. 41 .

Feustel, S.M., Meissner, M. and Liesenfeld, O. (2012) Toxoplasma gondii and the blood-brain barrier. Virulence , 3(2), pp. 182-192 .

Finlay, C.A., Hinds, P.W. and Levine, A.J. (1989) The p53 proto-oncogene can act as a suppressor of transformation. Cell , 57(7), pp. 1083-1093 .

Franceschi, E., Tosoni, A., Minichillo, S., Depenni, R., Paccapelo, A., Bartolini, S., Michiara, M., Pavesi, G., Urbini, B. and Crisi, G. (2018) The prognostic role of gender and MGMT methylation status in glioblastoma patients: the female power. World Neurosurgery .

Frezza, C., Zheng, L., Folger, O., Rajagopalan, K.N., MacKenzie, E.D., Jerby, L., Micaroni, M., Chaneton, B., Adam, J. and Hedley, A. (2011) Haem oxygenase is synthetically lethal with the tumour suppressor fumarate hydratase. Nature , 477(7363), pp. 225 .

Fujioka, K., Brazg, R., Raz, I., Bruce, S., Joyal, S., Swanink, R. and Pans, M. (2005) Efficacy, dose–response relationship and safety of once-daily extended-release metformin (Glucophage® XR) in type 2 diabetic patients with inadequate glycaemic control despite prior treatment with diet and

exercise: results from two double-blind, placebo-controlled studies. Diabetes, Obesity and Metabolism , 7(1), pp. 28-39 .

Fulda, S. and Debatin, K. (2006) Extrinsic versus intrinsic apoptosis pathways in anticancer chemotherapy. Oncogene , 25(34), pp. 4798-4811 .

Fulda, S. and Kögel, D. (2015) Cell death by autophagy: emerging molecular mechanisms and implications for cancer therapy. Oncogene , 34(40), pp. 5105 .

Fuse, M., Kojima, S., Enokida, H., Chiyomaru, T., Yoshino, H., Nohata, N., Kinoshita, T., Sakamoto, S., Naya, Y. and Nakagawa, M. (2012) Tumor suppressive microRNAs (miR-222 and miR-31) regulate molecular pathways based on microRNA expression signature in prostate cancer. Journal of human genetics , 57(11), pp. 691-699 .

Gao, Q., Lei, T. and Ye, F. (2013) Therapeutic targeting of EGFR-activated metabolic pathways in glioblastoma. Expert opinion on investigational drugs , 22(8), pp. 1023-1040 .

Garofalo, M., Di Leva, G., Romano, G., Nuovo, G., Suh, S., Ngankeu, A., Taccioli, C., Pichiorri, F., Alder, H. and Secchiero, P. (2009) miR-221&222 regulate TRAIL resistance and enhance tumorigenicity through PTEN and TIMP3 downregulation. Cancer cell , 16(6), pp. 498-509 .

Gatenby, R.A. and Gillies, R.J. (2004) Why do cancers have high aerobic glycolysis? Nature Reviews Cancer , 4(11), pp. 891 .

Gee, H., Buffa, F., Camps, C., Ramachandran, A., Leek, R., Taylor, M., Patil, M., Sheldon, H., Betts, G. and Homer, J. (2011) The small-nucleolar RNAs commonly used for microRNA normalisation correlate with tumour pathology and prognosis. British journal of cancer , 104(7), pp. 1168-1177 .

Geng, B., Liang, M., Ye, X. and Zhao, W. (2015) Association of CA 15-3 and CEA with clinicopathological parameters in patients with metastatic breast cancer. Molecular and clinical oncology , 3(1), pp. 232-236 .

Geng, L., Chaudhuri, A., Talmon, G., Wisecarver, J.L., Are, C., Brattain, M. and Wang, J. (2014) MicroRNA-192 suppresses liver metastasis of colon cancer. Oncogene , 33(46), pp. 5332-5340

Georges, S.A., Biery, M.C., Kim, S.Y., Schelter, J.M., Guo, J., Chang, A.N., Jackson, A.L., Carleton, M.O., Linsley, P.S., Cleary, M.A. and Chau, B.N. (2008) Coordinated regulation of cell cycle transcripts by p53-Inducible microRNAs, miR-192 and miR-215. Cancer research , 68(24), pp. 10105-10112 .

Gilbert, M.R., Dignam, J.J., Armstrong, T.S., Wefel, J.S., Blumenthal, D.T., Vogelbaum, M.A., Colman, H., Chakravarti, A., Pugh, S. and Won, M. (2014) A randomized trial of bevacizumab for newly diagnosed glioblastoma. New England Journal of Medicine , 370(8), pp. 699-708 .

Godlewski,J., Rooj,A., Mineo,M., Chiocca,E. and Bronisz,A. (2017) THE ROLE OF NON-CODING RNAS IN GBM STEM-LIKE CELLS SUBTYPE IDENTITY MAINTENANCE AND TRANSITION NEURO-ONCOLOGY. OXFORD UNIV PRESS INC JOURNALS DEPT, 2001 EVANS RD, CARY, NC 27513 USA, pp.26-26.

Goldberg, R.M., Sargent, D.J., Morton, R.F., Fuchs, C.S., Ramanathan, R.K., Williamson, S.K., Findlay, B.P., Pitot, H.C. and Alberts, S.R. (2004) A randomized controlled trial of fluorouracil plus leucovorin, irinotecan, and oxaliplatin combinations in patients with previously untreated metastatic colorectal cancer. Journal of Clinical Oncology , 22(1), pp. 23-30 .

Goldstein, I., Tseng, L., Creanga, D., Stecher, V. and Kaminetsky, J.C. (2016) Efficacy and safety of sildenafil by age in men with erectile dysfunction. The journal of sexual medicine , 13(5), pp. 852-859 .

Gonnissen, A., Isebaert, S., McKee, C.M., Muschel, R.J. and Haustermans, K. (2017) The Effect of Metformin and GANT61 Combinations on the Radiosensitivity of Prostate Cancer Cells. International journal of molecular sciences , 18(2), pp. 399 .

Goodwin, M.L., Gladden, L.B., Nijsten, M.W. and Jones, K.B. (2015) Lactate and cancer: revisiting the Warburg effect in an era of lactate shuttling. Frontiers in nutrition , 1pp. 27 .

Gozuacik, D. and Kimchi, A. (2004) Autophagy as a cell death and tumor suppressor mechanism. Oncogene , 23(16), pp. 2891 .

Greene, S.B., Herschkowitz, J.I. and Rosen, J.M. (2010) The ups and downs of miR-205: identifying the roles of miR-205 in mammary gland development and breast cancer. RNA biology , 7(3), pp. 300-304 .

Gregory, P.A., Bert, A.G., Paterson, E.L., Barry, S.C., Tsykin, A., Farshid, G., Vadas, M.A., Khew-Goodall, Y. and Goodall, G.J. (2008) The miR-200 family

and miR-205 regulate epithelial to mesenchymal transition by targeting ZEB1 and SIP1. Nature cell biology , 10(5), pp. 593-601 .

Gregory, R.I., Yan, K., Amuthan, G., Chendrimada, T., Doratotaj, B., Cooch, N. and Shiekhattar, R. (2004) The Microprocessor complex mediates the genesis of microRNAs. Nature , 432(7014), pp. 235 .

Grube, S., Dünisch, P., Freitag, D., Klausnitzer, M., Sakr, Y., Walter, J., Kalff, R. and Ewald, C. (2014) Overexpression of fatty acid synthase in human gliomas correlates with the WHO tumor grade and inhibition with Orlistat reduces cell viability and triggers apoptosis. Journal of neuro-oncology , 118(2), pp. 277-287 .

Gstraunthaler, G. (2003) Alternatives to the use of fetal bovine serum: serum-free cell culture. Altex , 20(4), pp. 275-281 .

Gu, C., Cheng, J., Zhang, B., Yang, S., Xie, F., Sun, J., Huang, L., Yu, J. and Li, M. (2017) Protopanaxadiol and metformin synergistically inhibit estrogen-mediated proliferation and anti-autophagy effects in endometrial cancer cells. American journal of translational research , 9(9), pp. 4071 .

Gu, J.J., Zhang, Q., Mavis, C., Czuczman, M.S. and Hernandez-Ilizaliturri, F.J. (2015) Metformin Induces p53-Dependent Mitochondrial Stress in Therapy-Sensitive and-Resistant Lymphoma Pre-Clinical Model and Primary Patients Sample with B-Cell Non-Hodgkin Lymphoma (NHL) .

Guo, Y., Yu, T., Yang, J., Zhang, T., Zhou, Y., He, F., Kurago, Z., Myssiorek, D., Wu, Y., Lee, P. and Li, X. (2015) Metformin inhibits salivary

adenocarcinoma growth through cell cycle arrest and apoptosis. American journal of cancer research , 5(12), pp. 3600-3611 .

Gyulkhandanyan, A.V., Mutlu, A., Freedman, J. and Leytin, V. (2015) Mitochondrial permeability transition pore (MPTP)-dependent and-independent pathways of mitochondrial membrane depolarization, cell shrinkage and microparticle formation during platelet apoptosis. British journal of haematology , 169(1), pp. 142-145 .

Hainsworth, J.D., Ervin, T., Friedman, E., Priego, V., Murphy, P.B., Clark, B.L. and Lamar, R.E. (2010) Concurrent radiotherapy and temozolomide followed by temozolomide and sorafenib in the first-line treatment of patients with glioblastoma multiforme. Cancer , 116(15), pp. 3663-3669 .

Ham, R. (1963) An improved nutrient solution for diploid Chinese hamster and human cell lines. Experimental cell research , 29(3), pp. 515-526

Han, G., Gong, H., Wang, Y., Guo, S. and Liu, K. (2015) AMPK/mTOR-mediated inhibition of survivin partly contributes to metformin-induced apoptosis in human gastric cancer cell. Cancer biology & therapy , 16(1), pp. 77-87 .

Han, H., Gu, J., Zuo, H., Chen, Z., Zhao, W., Li, M., Ji, D., Lu, Y. and Zhang, Z. (2012) Let-7c functions as a metastasis suppressor by targeting MMP11 and PBX3 in colorectal cancer. The Journal of pathology , 226(3), pp. 544-555 .

Hanisch, B., Abbas, B., Kratz, W. and Schueuermann, G. (2004) Human drugs in aquatic ecosystems: approach for the environmental risk assessment of

drug residues. Umweltwissenschaften und Schadstoff-Forschung , 16(4), pp. 223-238 .

Hata, A. and Lieberman, J. (2015) Dysregulation of microRNA biogenesis and gene silencing in cancer. Science signaling , 8(368), pp. re3 .

Hay, N. and Sonenberg, N. (2004) Upstream and downstream of mTOR. Genes & development , 18(16), pp. 1926-1945 .

Heckman-Stoddard, B.M., DeCensi, A., Sahasrabuddhe, V.V. and Ford, L.G. (2017) Repurposing metformin for the prevention of cancer and cancer recurrence. Diabetologia , 60(9), pp. 1639-1647 .

Hegi, M.E., Diserens, A., Gorlia, T., Hamou, M., de Tribolet, N., Weller, M., Kros, J.M., Hainfellner, J.A., Mason, W. and Mariani, L. (2005) MGMT gene silencing and benefit from temozolomide in glioblastoma. New England Journal of Medicine , 352(10), pp. 997-1003 .

Hegi, M.E., Diserens, A.C., Bady, P., Kamoshima, Y., Kouwenhoven, M.C., Delorenzi, M., Lambiv, W.L., Hamou, M.F., Matter, M.S., Koch, A., Heppner, F.L., Yonekawa, Y., Merlo, A., Frei, K., Mariani, L. and Hofer, S. (2011) Pathway analysis of glioblastoma tissue after preoperative treatment with the EGFR tyrosine kinase inhibitor gefitinib--a phase II trial. Molecular cancer therapeutics , 10(6), pp. 1102-1112 .

Heras-Sandoval, D., Pérez-Rojas, J.M., Hernández-Damián, J. and Pedraza-Chaverri, J. (2014) The role of PI3K/AKT/mTOR pathway in the modulation of

autophagy and the clearance of protein aggregates in neurodegeneration. Cellular signalling , 26(12), pp. 2694-2701 .

Hesketh, P.J. (2008) Chemotherapy-induced nausea and vomiting. New England Journal of Medicine , 358(23), pp. 2482-2494 .

Hill, C., Hunter, S.B. and Brat, D.J. (2003) Genetic Markers in Glioblastoma: Prognostic Significance and Future Therapeutic Implications: On: Impact of Genotype Morphology on the Prognosis of Glioblastoma. Schmidt MC Antweiler S, Urban N, *et al.* J Neuropathol Ex Neurol 2002; 61: 321–328. Advances in Anatomic Pathology , 10(4), pp. 212-217 .

Hiller, K. and Metallo, C.M. (2013) Profiling metabolic networks to study cancer metabolism. Current opinion in biotechnology , 24(1), pp. 60-68 .

Hong, C., Piazza, M., Ho, W. and Zhuang, Z. (2015) Bi-02disruption Of Perivascular Astrocytic Foot Processes Characterizes Mri Enhancement In Pediatric Brain Tumors. Neuro-oncology , 17(Suppl 3), pp. iii2 .

Hong, I.S., Ipema, H.J., Gabay, M.P. and Lodolce, A.E. (2011) Medication Repurposing: New Uses for Old Drugs. Journal of Pharmacy Technology , 27(3), pp. 132-140 .

Honn, K.V., Singley, J.A. and Chavin, W. (1975) Fetal bovine serum: a multivariate standard. Proceedings of the Society for Experimental Biology and Medicine , 149(2), pp. 344-347 .

Howlader, N., Noone, A., Krapcho, M., Garshell, J., Neyman, N., Altekruse, S., Kosary, C., Yu, M., Ruhl, J. and Tatalovich, Z. (2016) SEER Cancer Statistics Review, 1975–2012, National Cancer Institute; 2015 .

Huang, B., Zhao, J., Lei, Z., Shen, S., Li, D., Shen, G.X., Zhang, G.M. and Feng, Z.H. (2009) miR-142-3p restricts cAMP production in CD4+CD25- T cells and CD4+CD25+ TREG cells by targeting AC9 mRNA. EMBO reports , 10(2), pp. 180-185 .

Hunt, T. (2002) Molecular biology of the cell: A problems approach. Garland Science.

Hwang, M.S., Yu, N., Stinson, S.Y., Yue, P., Newman, R.J., Allan, B.B. and Dornan, D. (2013) miR-221/222 targets adiponectin receptor 1 to promote the epithelial-to-mesenchymal transition in breast cancer. PloS one , 8(6), pp. e66502 .

Hydbring, P., Malumbres, M. and Sicinski, P. (2016) Non-canonical functions of cell cycle cyclins and cyclin-dependent kinases. Nature reviews Molecular cell biology , 17(5), pp. 280 .

Inoki, K., Zhu, T. and Guan, K. (2003) TSC2 mediates cellular energy response to control cell growth and survival. Cell , 115(5), pp. 577-590 .

Iorio, M.V. and Croce, C.M. (2012) MicroRNA dysregulation in cancer: diagnostics, monitoring and therapeutics. A comprehensive review. EMBO molecular medicine , 4(3), pp. 143-159 .

Islam, M.N., Masud, M.K., Haque, M.H., Hossain, M.S.A., Yamauchi, Y., Nguyen, N. and Shiddiky, M.J. (2017) RNA biomarkers: diagnostic and prognostic potentials and recent developments of electrochemical biosensors. Small Methods , 1(7), pp. 1700131 .

Jeon, S., Chandel, N.S. and Hay, N. (2012) AMPK regulates NADPH homeostasis to promote tumour cell survival during energy stress. Nature , 485(7400), pp. 661 .

Jiang, W., Cazacu, S., Xiang, C., Brodie, Z., Shackelford, D. and Brodie, C. (2015) ATPS-04REPURPOSING PHENFORMIN FOR THE TREATMENT OF GLIOBLASTOMA: ROLE OF THE H19/LET-7/STAT3 AXIS. Neuro-oncology , 17(Suppl 5), pp. v18 .

Jiang, W., Finniss, S., Cazacu, S., Xiang, C., Brodie, Z., Mikkelsen, T., Poisson, L., Shackelford, D.B. and Brodie, C. (2016) Repurposing phenformin for the targeting of glioma stem cells and the treatment of glioblastoma. Oncotarget , 7(35), pp. 56456-56470 .

Jivan, R., Peres, J., Damelin, L.H., Wadee, R., Veale, R.B., Prince, S. and Mavri-Damelin, D. (2017) Disulfiram with or without metformin inhibits oesophageal squamous cell carcinoma *in vivo*. Cancer letters , 417pp. 1-10 .

Johnson, S.M., Grosshans, H., Shingara, J., Byrom, M., Jarvis, R., Cheng, A., Labourier, E., Reinert, K.L., Brown, D. and Slack, F.J. (2005) RAS is regulated by the let-7 microRNA family. Cell , 120(5), pp. 635-647 .

Jordan, K., Kasper, C. and Schmoll, H. (2005) Chemotherapy-induced nausea and vomiting: current and new standards in the antiemetic prophylaxis and treatment. European journal of cancer , 41(2), pp. 199-205 .

Kai, Y., Peng, W., Ling, W., Jiebing, H. and Zhuan, B. (2014) Reciprocal effects between microRNA-140-5p and ADAM10 suppress migration and invasion of human tongue cancer cells. Biochemical and biophysical research communications , 448(3), pp. 308-314 .

Kaiser, A.M. and Attardi, L.D. (2018) Deconstructing networks of p53-mediated tumor suppression *in vivo*. Cell death and differentiation , 25(1), pp. 93 .

Kaluzova, M., Bouras, A., Machaidze, R. and Hadjipanayis, C.G. (2015) Targeted therapy of glioblastoma stem-like cells and tumor non-stem cells using cetuximab-conjugated iron-oxide nanoparticles. Oncotarget , 6(11), pp. 8788-8806 .

Kandoth, C., McLellan, M.D., Vandin, F., Ye, K., Niu, B., Lu, C., Xie, M., Zhang, Q., McMichael, J.F. and Wyczalkowski, M.A. (2013) Mutational landscape and significance across 12 major cancer types. Nature , 502(7471), pp. 333 .

Kasznicki, J., Sliwinska, A. and Drzewoski, J. (2014) Metformin in cancer prevention and therapy. Annals of translational medicine , 2(6), pp. 57-5839.2014.06.01 .

Kawamata, T., Yoda, M. and Tomari, Y. (2011) Multilayer checkpoints for microRNA authenticity during RISC assembly. EMBO reports , 12(9), pp. 944-949 .

Khella, H.W., Bakhet, M., Allo, G., Jewett, M.A., Girgis, A.H., Latif, A., Girgis, H., Von Both, I., Bjarnason, G.A. and Yousef, G.M. (2013) miR-192, miR-194 and miR-215: a convergent microRNA network suppressing tumor progression in renal cell carcinoma. Carcinogenesis , 34(10), pp. 2231-2239 .

Kim, J., Robertson, G., Akbani, R., Lerner, S.P., Weinstein, J.N., Getz, G. and Kwiatkowski, D.J. (2018) Genomic Assessment of Muscle-Invasive Bladder Cancer: Insights from the Cancer Genome Atlas (TCGA) Project. in Precision Molecular Pathology of Bladder Cancer. Springer, pp.43-64.

Kim, Y.C. and Guan, K. (2015) mTOR: a pharmacologic target for autophagy regulation. The Journal of clinical investigation , 125(1), pp. 25-32 .

Kitambi, S.S., Toledo, E.M., Usoskin, D., Wee, S., Harisankar, A., Svensson, R., Sigmundsson, K., Kalderen, C., Niklasson, M., Kundu, S., Aranda, S., Westermark, B., Uhrbom, L., Andang, M., Damberg, P., Nelander, S., Arenas, E., Artursson, P., Walfridsson, J., Forsberg Nilsson, K., Hammarstrom, L.G.J. and Ernfors, P. (2014) RETRACTED: Vulnerability of glioblastoma cells to catastrophic vacuolization and death induced by a small molecule. Cell , 157(2), pp. 313-328 .

Kleihues, P. and Sobin, L.H. (2000) World Health Organization classification of tumors. Cancer , 88(12), pp. 2887-2887 .

Kobayashi, S. (2015) Choose delicately and reuse adequately: the newly revealed process of autophagy. Biological and Pharmaceutical Bulletin , 38(8), pp. 1098-1103 .

Koffert, J.P., Mikkola, K., Virtanen, K.A., Andersson, A.D., Faxius, L., Hallsten, K., Heglind, M., Guiducci, L., Pham, T., Silvola, J.M.U., Virta, J., Eriksson, O., Kauhanen, S.P., Saraste, A., Enerback, S., Iozzo, P., Parkkola, R., Gomez, M.F. and Nuutila, P. (2017) Metformin treatment significantly enhances intestinal glucose uptake in patients with type 2 diabetes: Results from a randomized clinical trial. Diabetes research and clinical practice , 131pp. 208-216 .

Kondetimmanahalli, R., Gharpure, K.M., Wu, S.Y., Lopez-Berestein, G. and Sood, A.K. (2018) Noncoding RNAs: Novel Targets in Anticancer Drug Development. in Cancer and Noncoding RNAs. Elsevier, pp.447-459.

Koopman, G., Reutelingsperger, C.P., Kuijten, G.A., Keehnen, R.M., Pals, S.T. and van Oers, M.H. (1994) Annexin V for flow cytometric detection of phosphatidylserine expression on B cells undergoing apoptosis. Blood , 84(5), pp. 1415-1420 .

Kordes, S., Pollak, M.N., Zwinderman, A.H., Mathôt, R.A., Weterman, M.J., Beeker, A., Punt, C.J., Richel, D.J. and Wilmink, J.W. (2015) Metformin in patients with advanced pancreatic cancer: a double-blind, randomised, placebo-controlled phase 2 trial. The Lancet Oncology , 16(7), pp. 839-847 .

Korshunov, A., Schrimpf, D., Ryzhova, M., Sturm, D., Chavez, L., Hovestadt, V., Sharma, T., Habel, A., Burford, A. and Jones, C. (2017) H3-/IDH-wild type pediatric glioblastoma is comprised of molecularly and prognostically distinct

subtypes with associated oncogenic drivers. Acta Neuropathologica , 134(3), pp. 507-516 .

Kosma, C.I., Lambropoulou, D.A. and Albanis, T.A. (2015) Comprehensive study of the antidiabetic drug metformin and its transformation product guanylurea in Greek wastewaters. Water research , 70pp. 436-448 .

Kroemer, G. and Martin, S.J. (2005) Caspase-independent cell death. Nature medicine , 11(7), pp. 725-730 .

Laezza, C., D'Alessandro, A., Di Croce, L., Picardi, P., Ciaglia, E., Pisanti, S., Malfitano, A.M., Comegna, M., Faraonio, R. and Gazzerro, P. (2015) p53 regulates the mevalonate pathway in human glioblastoma multiforme. Cell death & disease , 6(10), pp. e1909 .

Lai, C. and Kuo, K. (2005) The critical component to establish *in vitro* BBB model: Pericyte. Brain Research Reviews , 50(2), pp. 258-265 .

Lalau, J. and Kajbaf, F. (2014) Interpreting the consequences of metformin accumulation in an emergency context: impact of the time frame on the blood metformin levels. International journal of endocrinology , 2014.

Lam, T.G., Jeong, Y.S., Kim, S. and Ahn, S. (2018) New metformin derivative HL 156A prevents oral cancer progression by inhibiting the insulin-like growth factor/AKT/mammalian target of rapamycin pathways. Cancer science , 109(3), pp. 699-709 .

Lan, H., Chen, W., He, G. and Yang, S. (2015) miR-140-5p inhibits ovarian cancer growth partially by repression of PDGFRA. Biomedicine & Pharmacotherapy , 75pp. 117-122 .

Lawrence, M.S., Stojanov, P., Mermel, C.H., Robinson, J.T., Garraway, L.A., Golub, T.R., Meyerson, M., Gabriel, S.B., Lander, E.S. and Getz, G. (2014) Discovery and saturation analysis of cancer genes across 21 tumour types. Nature , 505(7484), pp. 495 .

le Sage, C., Nagel, R., Egan, D.A., Schrier, M., Mesman, E., Mangiola, A., Anile, C., Maira, G., Mercatelli, N. and Ciafrè, S.A. (2007) Regulation of the p27Kip1 tumor suppressor by miR-221 and miR-222 promotes cancer cell proliferation. The EMBO journal , 26(15), pp. 3699-3708 .

Lee, S.B., Frattini, V., Bansal, M., Castano, A.M., Sherman, D., Hutchinson, K., Bruce, J.N., Califano, A., Liu, G. and Cardozo, T. (2016) An ID2-dependent mechanism for VHL inactivation in cancer. Nature , 529(7585), pp. 172 .

Lee, J.E., Lim, J.H., Hong, Y.K. and Yang, S.H. (2018) High-Dose Metformin Plus Temozolomide Shows Increased Anti-tumor Effects in Glioblastoma *In vitro* and *In vivo* Compared with Monotherapy. Cancer research and treatment : official journal of Korean Cancer Association .

Lee, K.M., Lee, M., Lee, J., Kim, S.W., Moon, H.G., Noh, D.Y. and Han, W. (2016) Enhanced anti-tumor activity and cytotoxic effect on cancer stem cell population of metformin-butyrate compared with metformin HCl in breast cancer. Oncotarget , 7(25), pp. 38500-38512 .

Lewandowicz, G., Harding, B., Harkness, W., Hayward, R., Thomas, D. and Darling, J. (2000) Chemosensitivity in childhood brain tumours *in vitro*: evidence of differential sensitivity to lomustine (CCNU) and vincristine. European journal of cancer , 36(15), pp. 1955-1964 .

Li, F., Ambrosini, G., Chu, E.Y., Plescia, J., Tognin, S., Marchisio, P.C. and Altieri, D.C. (1998) Control of apoptosis and mitotic spindle checkpoint by survivin. Nature , 396(6711), pp. 580 .

Li, P., Zhao, M., Parris, A.B., Feng, X. and Yang, X. (2015) p53 is required for metformin-induced growth inhibition, senescence and apoptosis in breast cancer cells. Biochemical and biophysical research communications , 464(4), pp. 1267-1274 .

Li, Q., Shen, K., Zhao, Y., He, X., Ma, C., Wang, L., Wang, B., Liu, J. and Ma, J. (2013) MicroRNA-222 promotes tumorigenesis via targeting DKK2 and activating the Wnt/β-catenin signaling pathway. FEBS letters , 587(12), pp. 1742-1748 .

Liberti, M.V. and Locasale, J.W. (2016) The Warburg effect: how does it benefit cancer cells? Trends in biochemical sciences , 41(3), pp. 211-218 .

Licchesi, J.D. and Herman, J.G. (2009) Methylation-specific PCR. DNA Methylation: Methods and Protocols pp. 305-323 .

Lin, K., Ye, H., Han, B., Wang, W., Wei, P., He, B., Li, X. and Chen, Y. (2016) Genome-wide screen identified let-7c/miR-99a/miR-125b regulating tumor

progression and stem-like properties in cholangiocarcinoma. Oncogene , 35(26), pp. 3376-3386 .

Lin, S. and Gregory, R.I. (2015) MicroRNA biogenesis pathways in cancer. Nature reviews cancer , 15(6), pp. 321-333 .

Lin, T., Ma, Q., Zhang, Y., Zhang, H., Yan, J. and Gao, C. (2018) MicroRNA-27a functions as an oncogene in human osteosarcoma by targeting CCNG1. Oncology Letters , 15(1), pp. 1067-1071 .

Lindqvist, L.M., Tandoc, K., Topisirovic, I. and Furic, L. (2018) Cross-talk between protein synthesis, energy metabolism and autophagy in cancer. Current opinion in genetics & development , 48pp. 104-111 .

Ling, S., Song, L., Fan, N., Feng, T., Liu, L., Yang, X., Wang, M., Li, Y., Tian, Y. and Zhao, F. (2017) Combination of metformin and sorafenib suppresses proliferation and induces autophagy of hepatocellular carcinoma via targeting the mTOR pathway. International journal of oncology , 50(1), pp. 297-309 .

Lipton, J.O. and Sahin, M. (2014) The neurology of mTOR. Neuron , 84(2), pp. 275-291 .

Liu, J., Guo, S., Li, Q., Yang, L., Xia, Z., Zhang, L., Huang, Z. and Zhang, N. (2013) Phosphoglycerate dehydrogenase induces glioma cells proliferation and invasion by stabilizing forkhead box M1. Journal of neuro-oncology , 111(3), pp. 245-255 .

Liu, P., Brown, S., Goktug, T., Channathodiyil, P., Kannappan, V., Hugnot, J., Guichet, P., Bian, X., Armesilla, A. and Darling, J. (2012) Cytotoxic effect of

disulfiram/copper on human glioblastoma cell lines and ALDH-positive cancer-stem-like cells. British journal of cancer , 107(9), pp. 1488 .

Liu, X., Xiao, J., Zhu, H., Wei, X., Platt, C., Damilano, F., Xiao, C., Bezzerides, V., Boström, P. and Che, L. (2015) miR-222 is necessary for exercise-induced cardiac growth and protects against pathological cardiac remodeling. Cell metabolism , 21(4), pp. 584-595 .

Liu, Y., Yin, J., Abou-Kheir, W., Hynes, P., Casey, O., Fang, L., Yi, M., Stephens, R., Seng, V. and Sheppard-Tillman, H. (2013) MiR-1 and miR-200 inhibit EMT via Slug-dependent and tumorigenesis via Slug-independent mechanisms. Oncogene , 32(3), pp. 296-306 .

Liu, P., Wang, Z., Brown, S., Kannappan, V., Tawari, P.E., Jiang, W., Irache, J.M., Tang, J.Z., Armesilla, A.L., Darling, J.L., Tang, X. and Wang, W. (2014) Liposome encapsulated Disulfiram inhibits NFkappaB pathway and targets breast cancer stem cells *in vitro* and *in vivo*. Oncotarget , 5(17), pp. 7471-7485 .

Liu, X., Chhipa, R.R., Pooya, S., Wortman, M., Yachyshin, S., Chow, L.M., Kumar, A., Zhou, X., Sun, Y., Quinn, B., McPherson, C., Warnick, R.E., Kendler, A., Giri, S., Poels, J., Norga, K., Viollet, B., Grabowski, G.A. and Dasgupta, B. (2014) Discrete mechanisms of mTOR and cell cycle regulation by AMPK agonists independent of AMPK. Proceedings of the National Academy of Sciences of the United States of America , 111(4), pp. E435-44 .

Llovet, J.M., Ricci, S., Mazzaferro, V., Hilgard, P., Gane, E., Blanc, J., de Oliveira, A.C., Santoro, A., Raoul, J. and Forner, A. (2008) Sorafenib in

advanced hepatocellular carcinoma. New England journal of medicine , 359(4), pp. 378-390 .

Locasale, J.W., Grassian, A.R., Melman, T., Lyssiotis, C.A., Mattaini, K.R., Bass, A.J., Heffron, G., Metallo, C.M., Muranen, T. and Sharfi, H. (2011) Phosphoglycerate dehydrogenase diverts glycolytic flux and contributes to oncogenesis. Nature genetics , 43(9), pp. 869 .

Lord, S., Liu, D., Haider, S., Gaude, E., Teoh, E., Neel, P., Zhang, Q., Gleeson, F., Wakelam, M. and Frezza, C. (2016) Abstract LB-200: Integrating dynamic 18F-FDG PET-CT, tumor metabolomics and functional genomics to understand metformin's pharmacodynamic effects in breast cancer: results of a phase 0 clinical trial .

Lord, J.M., Flight, I.H. and Norman, R.J. (2003) Metformin in polycystic ovary syndrome: systematic review and meta-analysis. BMJ (Clinical research ed.) , 327(7421), pp. 951-953 .

Lou, G., Ma, N., Xu, Y., Jiang, L., Yang, J., Wang, C., Jiao, Y. and Gao, X. (2015) Differential distribution of U6 (RNU6-1) expression in human carcinoma tissues demonstrates the requirement for caution in the internal control gene selection for microRNA quantification. International journal of molecular medicine , 36(5), pp. 1400-1408 .

Loubiere, C., Clavel, S., Gilleron, J., Harisseh, R., Fauconnier, J., Ben-Sahra, I., Kaminski, L., Laurent, K., Herkenne, S. and Lacas-Gervais, S. (2017) The energy disruptor metformin targets mitochondrial integrity via modification of calcium flux in cancer cells. Scientific reports , 7(1), pp. 5040 .

Louis, D.N., Ohgaki, H., Wiestler, O.D., Cavenee, W.K., Burger, P.C., Jouvet, A., Scheithauer, B.W. and Kleihues, P. (2007) The 2007 WHO classification of tumours of the central nervous system. Acta Neuropathologica , 114(2), pp. 97-109 .

Lowe, S.W. and Lin, A.W. (2000) Apoptosis in cancer. Carcinogenesis , 21(3), pp. 485-495 .

Lu, J., He, M.L., Wang, L., Chen, Y., Liu, X., Dong, Q., Chen, Y.C., Peng, Y., Yao, K.T., Kung, H.F. and Li, X.P. (2011) MiR-26a inhibits cell growth and tumorigenesis of nasopharyngeal carcinoma through repression of EZH2. Cancer research , 71(1), pp. 225-233 .

Lucey, B.P., Nelson-Rees, W.A. and Hutchins, G.M. (2009) Henrietta Lacks, HeLa cells, and cell culture contamination. Archives of Pathology & Laboratory Medicine , 133(9), pp. 1463-1467 .

Luissint, A., Artus, C., Glacial, F., Ganeshamoorthy, K. and Couraud, P. (2012) Tight junctions at the blood brain barrier: physiological architecture and disease-associated dysregulation. Fluids and Barriers of the CNS , 9(1), pp. 23 .

Ly, J.D., Grubb, D. and Lawen, A. (2003) The mitochondrial membrane potential (Δψm) in apoptosis; an update. Apoptosis , 8(2), pp. 115-128 .

Maachani, U.B., Tandle, A., Shankavaram, U., Kramp, T. and Camphausen, K. (2016) Modulation of miR-21 signaling by MPS1 in human glioblastoma. Oncotarget , 7(33), pp. 52912-52927 .

Madiraju, A.K., Erion, D.M., Rahimi, Y., Zhang, X., Braddock, D.T., Albright, R.A., Prigaro, B.J., Wood, J.L., Bhanot, S. and MacDonald, M.J. (2014) Metformin suppresses gluconeogenesis by inhibiting mitochondrial glycerophosphate dehydrogenase. Nature , 510(7506), pp. 542 .

Mahase, S., Rattenni, R.N., Wesseling, P., Leenders, W., Baldotto, C., Jain, R. and Zagzag, D. (2017) Hypoxia-mediated mechanisms associated with antiangiogenic treatment resistance in glioblastomas. The American journal of pathology , 187(5), pp. 940-953 .

Maier, H.J. and Britton, P. (2012) Involvement of autophagy in coronavirus replication. Viruses , 4(12), pp. 3440-3451 .

Manzine, P.R., Pelucchi, S., Horst, M.A., Vale, F.A., Pavarini, S.C., Audano, M., Mitro, N., Di Luca, M., Marcello, E. and Cominetti, M.R. (2018) microRNA 221 Targets ADAM10 mRNA and is Downregulated in Alzheimer's Disease. Journal of Alzheimer's Disease (Preprint), pp. 1-11 .

Markowicz-Piasecka, M., Huttunen, K.M., Mikiciuk-Olasik, E. and Sikora, J. (2018) Biocompatible sulfenamide and sulfonamide derivatives of metformin can exert beneficial effects on plasma haemostasis. Chemico-biological interactions , 280pp. 15-27 .

Martínez-Reyes, I., Diebold, L.P., Kong, H., Schieber, M., Huang, H., Hensley, C.T., Mehta, M.M., Wang, T., Santos, J.H. and Woychik, R. (2016) TCA cycle and mitochondrial membrane potential are necessary for diverse biological functions. Molecular cell , 61(2), pp. 199-209 .

Maruthur, N.M., Tseng, E., Hutfless, S., Wilson, L.M., Suarez-Cuervo, C., Berger, Z., Chu, Y., Iyoha, E., Segal, J.B. and Bolen, S. (2016) Diabetes Medications as Monotherapy or Metformin-Based Combination Therapy for Type 2 DiabetesA Systematic Review and Meta-analysisDiabetes Medications as Monotherapy or Metformin-Based Combination Therapy. Annals of Internal Medicine , 164(11), pp. 740-751 .

Massey, T. and Robertson, N. (2018) Repurposing drugs to treat neurological diseases. Journal of neurology pp. 1-3 .

McGuire, S. (2016) World Cancer Report 2014. Geneva, Switzerland: World Health Organization, International Agency for Research on Cancer, WHO Press, 2015. Advances in nutrition (Bethesda, Md.) , 7(2), pp. 418-419 .

McNeill, K.A. (2016) Epidemiology of brain tumors. Neurologic clinics , 34(4), pp. 981-998 .

Melstrom, K. and Sentovich, S.M. (2017) Colon and Rectal Surgical Emergencies. in Surgical Emergencies in the Cancer Patient. Springer, pp.177-187.

Menendez, J.A., Oliveras-Ferraros, C., Cufí, S., Corominas-Faja, B., Joven, J., Martin-Castillo, B. and Vazquez-Martin, A. (2012) Metformin is synthetically lethal with glucose withdrawal in cancer cells. Cell cycle , 11(15), pp. 2782-2792 .

Merchant, M.S., Geller, J.I., Baird, K., Chou, A.J., Galli, S., Charles, A., Amaoko, M., Rhee, E.H., Price, A., Wexler, L.H., Meyers, P.A., Widemann, B.C.,

Tsokos, M. and Mackall, C.L. (2012) Phase I trial and pharmacokinetic study of lexatumumab in pediatric patients with solid tumors. Journal of clinical oncology : official journal of the American Society of Clinical Oncology , 30(33), pp. 4141-4147 .

Messaoudi, K., Clavreul, A. and Lagarce, F. (2015) Toward an effective strategy in glioblastoma treatment. Part I: resistance mechanisms and strategies to overcome resistance of glioblastoma to temozolomide. Drug discovery today .

Meyer, M., Reimand, J., Lan, X., Head, R., Zhu, X., Kushida, M., Bayani, J., Pressey, J.C., Lionel, A.C., Clarke, I.D., Cusimano, M., Squire, J.A., Scherer, S.W., Bernstein, M., Woodin, M.A., Bader, G.D. and Dirks, P.B. (2015) Single cell-derived clonal analysis of human glioblastoma links functional and genomic heterogeneity. Proceedings of the National Academy of Sciences of the United States of America , 112(3), pp. 851-856 .

Mihaylova, M.M. and Shaw, R.J. (2011) The AMPK signalling pathway coordinates cell growth, autophagy and metabolism. Nature cell biology , 13(9), pp. 1016 .

Miroshnikova, Y.A., Mouw, J.K., Barnes, J.M., Pickup, M.W., Lakins, J.N., Kim, Y., Lobo, K., Persson, A.I., Reis, G.F. and McKnight, T.R. (2016) Tissue mechanics promote IDH1-dependent HIF1α–tenascin C feedback to regulate glioblastoma aggression. Nature cell biology , 18(12), pp. 1336 .

Miskimins, W.K., Ahn, H.J., Kim, J.Y., Ryu, S., Jung, Y. and Choi, J.Y. (2014) Synergistic anti-cancer effect of phenformin and oxamate. PloS one , 9(1), pp. e85576 .

Molenaar, R.J., Verbaan, D., Lamba, S., Zanon, C., Jeuken, J.W., Boots-Sprenger, S.H., Wesseling, P., Hulsebos, T.J., Troost, D. and Van Tilborg, A.A. (2014) The combination of IDH1 mutations and MGMT methylation status predicts survival in glioblastoma better than either IDH1 or MGMT alone. Neuro-oncology , 16(9), pp. 1263-1273 .

Molhoek, K.R., Brautigan, D.L. and Slingluff, C.L. (2005) Synergistic inhibition of human melanoma proliferation by combination treatment with B-Raf inhibitor BAY43-9006 and mTOR inhibitor Rapamycin. Journal of translational medicine , 3(1), pp. 39 .

Monga, V., Jones, K. and Chang, S. (2017) CLINICAL RELEVANCE OF MOLECULAR MARKERS IN GLIOMAS. Revista Médica Clínica Las Condes , 28(3), pp. 343-351 .

Muller, P.A. and Vousden, K.H. (2014) Mutant p53 in cancer: new functions and therapeutic opportunities. Cancer cell , 25(3), pp. 304-317 .

Muller, P.A. and Vousden, K.H. (2013) p53 mutations in cancer. Nature cell biology , 15(1), pp. 2

Munoz, J.L., Rodriguez-Cruz, V., Greco, S.J., Nagula, V., Scotto, K.W. and Rameshwar, P. (2014) Temozolomide induces the production of epidermal

growth factor to regulate MDR1 expression in glioblastoma cells. Molecular cancer therapeutics , 13(10), pp. 2399-2411 .

Nadiminty, N., Tummala, R., Lou, W., Zhu, Y., Zhang, J., Chen, X., eVere White, R.W., Kung, H.J., Evans, C.P. and Gao, A.C. (2012) MicroRNA let-7c suppresses androgen receptor expression and activity via regulation of Myc expression in prostate cancer cells. The Journal of biological chemistry , 287(2), pp. 1527-1537 .

Nair, V., Sreevalsan, S., Basha, R., Abdelrahim, M., Abudayyeh, A., Rodrigues Hoffman, A. and Safe, S. (2014) Mechanism of metformin-dependent inhibition of mammalian target of rapamycin (mTOR) and Ras activity in pancreatic cancer: role of specificity protein (Sp) transcription factors. The Journal of biological chemistry , 289(40), pp. 27692-27701 .

Nakamura, S. and Yoshimori, T. (2017) New insights into autophagosome-lysosome fusion. Journal of cell science , 130(7), pp. 1209-1216 .

Narita, Y. (2015) Bevacizumab for glioblastoma. Therapeutics and clinical risk management , 11pp. 1759-1765 .

Nattrass, M. and Alberti, K.G. (1978) Biguanides. Diabetologia , 14(2), pp. 71-74 .

Nduom, E.K., Weller, M. and Heimberger, A.B. (2015) Immunosuppressive mechanisms in glioblastoma. Neuro-oncology , 17(suppl_7), pp. vii9-vii14 .

Nestor, C.E., Ottaviano, R., Reinhardt, D., Cruickshanks, H.A., Mjoseng, H.K., McPherson, R.C., Lentini, A., Thomson, J.P., Dunican, D.S. and Pennings, S.

(2015) Rapid reprogramming of epigenetic and transcriptional profiles in mammalian culture systems. Genome biology , 16(1), pp. 11 .

Niccoli, T., Cabecinha, M., Tillmann, A., Kerr, F., Wong, C.T., Cardenes, D., Vincent, A.J., Bettedi, L., Li, L. and Grönke, S. (2016) Increased glucose transport into neurons rescues Aβ toxicity in Drosophila. Current Biology , 26(17), pp. 2291-2300 .

Niemuth, N.J. and Klaper, R.D. (2015) Emerging wastewater contaminant metformin causes intersex and reduced fecundity in fish. Chemosphere , 135pp. 38-45 .

Noushmehr, H., Weisenberger, D.J., Diefes, K., Phillips, H.S., Pujara, K., Berman, B.P., Pan, F., Pelloski, C.E., Sulman, E.P. and Bhat, K.P. (2010) Identification of a CpG island methylator phenotype that defines a distinct subgroup of glioma. Cancer cell , 17(5), pp. 510-522 .

Nunez, R. (2001) DNA measurement and cell cycle analysis by flow cytometry. Current Issues in Molecular Biology , 3pp. 67-70 .

Oberoi, R.K., Parrish, K.E., Sio, T.T., Mittapalli, R.K., Elmquist, W.F. and Sarkaria, J.N. (2015) Strategies to improve delivery of anticancer drugs across the blood–brain barrier to treat glioblastoma. Neuro-oncology , 18(1), pp. 27-36 .

Occhipinti, G., Giulietti, M., Principato, G. and Piva, F. (2016) The choice of endogenous controls in exosomal microRNA assessments from biofluids. Tumor Biology , 37(9), pp. 11657-11665 .

Ohgaki, H. and Kleihues, P. (2007) Genetic pathways to primary and secondary glioblastoma. The American journal of pathology , 170(5), pp. 1445-1453 .

Owen, M.R., Doran, E. and Halestrap, A.P. (2000) Evidence that metformin exerts its anti-diabetic effects through inhibition of complex 1 of the mitochondrial respiratory chain. The Biochemical journal , 348 Pt 3pp. 607-614 .

Pai, S.I., Wu, G.S., Ozoren, N., Wu, L., Jen, J., Sidransky, D. and El-Deiry, W.S. (1998) Rare loss-of-function mutation of a death receptor gene in head and neck cancer. Cancer research , 58(16), pp. 3513-3518 .

Palmieri, D., D'angelo, D., Valentino, T., De Martino, I., Ferraro, A., Wierinckx, A., Fedele, M., Trouillas, J. and Fusco, A. (2012) Downregulation of HMGA-targeting microRNAs has a critical role in human pituitary tumorigenesis. Oncogene , 31(34), pp. 3857-3865 .

Papagiannakopoulos, T., Shapiro, A. and Kosik, K.S. (2008) MicroRNA-21 targets a network of key tumor-suppressive pathways in glioblastoma cells. Cancer research , 68(19), pp. 8164-8172 .

Park, S.M., Gaur, A.B., Lengyel, E. and Peter, M.E. (2008) The miR-200 family determines the epithelial phenotype of cancer cells by targeting the E-cadherin repressors ZEB1 and ZEB2. Gees & development , 22(7), pp. 894-907 .

Parsa, A.T., Waldron, J.S., Panner, A., Crane, C.A., Parney, I.F., Barry, J.J., Cachola, K.E., Murray, J.C., Tihan, T. and Jensen, M.C. (2007) Loss of tumor

suppressor PTEN function increases B7-H1 expression and immunoresistance in glioma. Nature medicine , 13(1), pp. 84 .

Parzych, K.R. and Klionsky, D.J. (2014) An overview of autophagy: morphology, mechanism, and regulation. Antioxidants & redox signaling , 20(3), pp. 460-473 .

Patel, M., McCully, C., Godwin, K. and Balis, F.M. (2003) Plasma and cerebrospinal fluid pharmacokinetics of intravenous temozolomide in non-human primates. Journal of neuro-oncology , 61(3), pp. 203-207 .

Peereboom, D.M., Ahluwalia, M.S., Ye, X., Supko, J.G., Hilderbrand, S.L., Phuphanich, S., Nabors, L.B., Rosenfeld, M.R., Mikkelsen, T. and Grossman, S.A. (2013) NABTT 0502: a phase II and pharmacokinetic study of erlotinib and sorafenib for patients with progressive or recurrent glioblastoma multiforme. Neuro-oncology , 15(4), pp. 490-496 .

Philips, A., Henshaw, D.L., Lamburn, G. and O'Carroll, M.J. (2018) Brain tumours: rise in Glioblastoma Multiforme incidence in England 1995–2015 suggests an adverse environmental or lifestyle factor. Journal of environmental and public health , 2018.

Philpott, N.J., Turner, A.J., Scopes, J., Westby, M., Marsh, J.C., Gordon-Smith, E.C., Dalgleish, A.G. and Gibson, F.M. (1996) The use of 7-amino actinomycin D in identifying apoptosis: simplicity of use and broad spectrum of application compared with other techniques. Blood , 87(6), pp. 2244-2251 .

Piantadosi, S. (2017) Clinical trials: a methodologic perspective. John Wiley & Sons.

Pirola, C.J., Fernandez Gianotti, T., Castano, G.O., Mallardi, P., San Martino, J., Mora Gonzalez Lopez Ledesma, M., Flichman, D., Mirshahi, F., Sanyal, A.J. and Sookoian, S. (2015) Circulating microRNA signature in non-alcoholic fatty liver disease: from serum non-coding RNAs to liver histology and disease pathogenesis. Gut , 64(5), pp. 800-812 .

Pollak, M.N. (2012) Investigating metformin for cancer prevention and treatment: the end of the beginning. Cancer discovery , 2(9), pp. 778-790 .

Ponten, J. and MACINTYRE, E.H. (1968) Long term culture of normal and neoplastic human glia. Acta Pathologica Microbiologica Scandinavica , 74(4), pp. 465-486 .

Ponten, J. and Westermark, B. (1978) Properties of human malignant glioma cells *in vitro*. Medical biology , 56(4), pp. 184-193 .

Poteet, E., Choudhury, G.R., Winters, A., Li, W., Ryou, M.G., Liu, R., Tang, L., Ghorpade, A., Wen, Y., Yuan, F., Keir, S.T., Yan, H., Bigner, D.D., Simpkins, J.W. and Yang, S.H. (2013) Reversing the Warburg effect as a treatment for glioblastoma. The Journal of biological chemistry , 288(13), pp. 9153-9164 .

Prins, R.M., Soto, H., Konkankit, V., Odesa, S.K., Eskin, A., Yong, W.H., Nelson, S.F. and Liau, L.M. (2011) Gene expression profile correlates with T-cell infiltration and relative survival in glioblastoma patients vaccinated with

dendritic cell immunotherapy. Clinical cancer research : an official journal of the American Association for Cancer Research , 17(6), pp. 1603-1615 .

Pryor, R. and Cabreiro, F. (2015) Repurposing metformin: an old drug with new tricks in its binding pockets. The Biochemical journal , 471(3), pp. 307-322 .

Pulito, C., Donzelli, S., Muti, P., Puzzo, L., Strano, S. and Blandino, G. (2014) microRNAs and cancer metabolism reprogramming: the paradigm of metformin. Annals of translational medicine , 2(6), .

Pyonteck, S.M., Akkari, L., Schuhmacher, A.J., Bowman, R.L., Sevenich, L., Quail, D.F., Olson, O.C., Quick, M.L., Huse, J.T. and Teijeiro, V. (2013) CSF-1R inhibition alters macrophage polarization and blocks glioma progression. Nature medicine , 19(10), pp. 1264 .

Quintavalle, C., Garofalo, M., Zanca, C., Romano, G., Iaboni, M., De Caro, M del Basso, Martinez-Montero, J., Incoronato, M., Nuovo, G. and Croce, C. (2012) miR-221/222 overexpession in human glioblastoma increases invasiveness by targeting the protein phosphate PTPμ. Oncogene , 31(7), pp. 858-868 .

Quintavalle, C., Mangani, D., Roscigno, G., Romano, G., Diaz-Lagares, A., Iaboni, M., Donnarumma, E., Fiore, D., De Marinis, P. and Soini, Y. (2013) MiR-221/222 target the DNA methyltransferase MGMT in glioma cells. PloS one , 8(9), pp. e74466 .

Ramirez, Y.P., Weatherbee, J.L., Wheelhouse, R.T. and Ross, A.H. (2013) Glioblastoma multiforme therapy and mechanisms of resistance. Pharmaceuticals , 6(12), pp. 1475-1506 .

Rattan, R., Giri, S., Hartmann, L.C. and Shridhar, V. (2011) Metformin attenuates ovarian cancer cell growth in an AMP-kinase dispensable manner. Journal of Cellular and Molecular Medicine , 15(1), pp. 166-178 .

Rattan, R., Graham, R.P., Maguire, J.L., Giri, S. and Shridhar, V. (2011) Metformin suppresses ovarian cancer growth and metastasis with enhancement of cisplatin cytotoxicity *in vivo*. Neoplasia , 13(5), pp. 483-491 .

Reardon, D.A., Freeman, G., Wu, C., Chiocca, E.A., Wucherpfennig, K.W., Wen, P.Y., Fritsch, E.F., Curry, W.T., Sampson, J.H. and Dranoff, G. (2014) Immunotherapy advances for glioblastoma. Neuro-oncology , 16(11), pp. 1441-1458 .

Reya, T., Morrison, S.J., Clarke, M.F. and Weissman, I.L. (2001) Stem cells, cancer, and cancer stem cells. Nature , 414(6859), pp. 105 .

Roberts, S. and Speirs, V. (2017) Advances in the development of improved animal-free models for use in breast cancer biomedical research. Biophysical reviews , 9(4), pp. 321-327 .

Rodríguez-Lirio, A., Pérez-Yarza, G., Fernández-Suárez, M., Alonso-Tejerina, E., Boyano, M. and Asumendi, A. (2015) Metformin induces cell cycle arrest and apoptosis in drug-resistant leukemia cells. Leukemia research and treatment , 2015.

Saisho, Y. (2015) Metformin and inflammation: its potential beyond glucose-lowering effect. Endocrine, Metabolic & Immune Disorders-Drug Targets (Formerly Current Drug Targets-Immune, Endocrine & Metabolic Disorders) , 15(3), pp. 196-205 .

Salani, B., Del Rio, A., Marini, C., Sambuceti, G., Cordera, R. and Maggi, D. (2014) Metformin, cancer and glucose metabolism. Endocrine-related cancer , 21(6), pp. R461-71 .

Salpeter, S.R., Greyber, E., Pasternak, G.A. and Salpeter, E.E. (2010) Risk of fatal and nonfatal lactic acidosis with metformin use in type 2 diabetes mellitus. The Cochrane Library .

Sankar, A., Sythana, S., Jhansi, A., Shanmugasundharam, P. and Aumithra, M. (2013) Development and validation for simultaneous estimation of sitagliptin and metformin in pharmaceutical dosage form using RP-HPLC method. International Journal of Pharma Tech Research , 5(4), pp. 1736-1744 .

Sansom, C. (2009) Temozolomide--Birth of a blockbuster-The history of anti-cancer drug temozolomide can be traced back over 30 years--And it all started with some novel nitrogen chemistry. Chemistry World , 6(7), pp. 48 .

Santa-Maria, I., Alaniz, M.E., Renwick, N., Cela, C., Fulga, T.A., Van Vactor, D., Tuschl, T., Clark, L.N., Shelanski, M.L., McCabe, B.D. and Crary, J.F. (2015) Dysregulation of microRNA-219 promotes neurodegeneration through post-transcriptional regulation of tau. The Journal of clinical investigation , 125(2), pp. 681-686 .

Sarfstein, R., Friedman, Y., Attias-Geva, Z., Fishman, A., Bruchim, I. and Werner, H. (2013) Metformin downregulates the insulin/IGF-I signaling pathway and inhibits different uterine serous carcinoma (USC) cells proliferation and migration in p53-dependent or-independent manners. PloS one , 8(4), pp. e61537

Saxton, R.A. and Sabatini, D.M. (2017) mTOR signaling in growth, metabolism, and disease. Cell , 168(6), pp. 960-976 .

Scheurer, M., Michel, A., Brauch, H., Ruck, W. and Sacher, F. (2012) Occurrence and fate of the antidiabetic drug metformin and its metabolite guanylurea in the environment and during drinking water treatment. Water research , 46(15), pp. 4790-4802 .

Schiff, D., Jaeckle, K.A., Anderson, S.K., Galanis, E., Giannini, C., Buckner, J.C., Stella, P., Flynn, P.J., Erickson, B.J. and Schwerkoske, J.F. (2018) Phase 1/2 trial of temsirolimus and sorafenib in the treatment of patients with recurrent glioblastoma: North Central Cancer Treatment Group Study/Alliance N0572. Cancer .

Schnerch, D., Yalcintepe, J., Schmidts, A., Becker, H., Follo, M., Engelhardt, M. and Wasch, R. (2012) Cell cycle control in acute myeloid leukemia. American journal of cancer research , 2(5), pp. 508-528 .

Schultz, S., Pinsky, G.S., Wu, N.C., Chamberlain, M.C., Rodrigo, A.S. and Martin, S.E. (2005) Fine needle aspiration diagnosis of extracranial glioblastoma multiforme: Case report and review of the literature. CytoJournal , 2pp. 19-6413-2-19 .

Segawa, K. and Nagata, S. (2015) An apoptotic ‘eat me’signal: phosphatidylserine exposure. Trends in cell biology , 25(11), pp. 639-650 .

Sesen, J., Dahan, P., Scotland, S.J., Saland, E., Dang, V., Lemarié, A., Tyler, B.M., Brem, H., Toulas, C. and Moyal, E.C. (2015) Metformin inhibits growth of human glioblastoma cells and enhances therapeutic response. PloS one , 10(4), pp. e0123721 .

Shah, M.Y. and Calin, G.A. (2011) MicroRNAs miR-221 and miR-222: a new level of regulation in aggressive breast cancer. Genome Med , 3(8), pp. 56 .

Sharma, N., Nanta, R., Sharma, J., Gunewardena, S., Singh, K.P., Shankar, S. and Srivastava, R.K. (2015) PI3K/AKT/mTOR and sonic hedgehog pathways cooperate together to inhibit human pancreatic cancer stem cell characteristics and tumor growth. Oncotarget , 6(31), pp. 32039-32060 .

Sheu-Gruttadauria, J. and MacRae, I.J. (2018) Phase Transitions in the Assembly and Function of Human miRISC. Cell , 173(4), pp. 946-957. e16 .

Shimazu, K., Tada, Y., Morinaga, T., Shingyoji, M., Sekine, I., Shimada, H., Hiroshima, K., Namiki, T., Tatsumi, K. and Tagawa, M. (2017) Metformin produces growth inhibitory effects in combination with nutlin-3a on malignant mesothelioma through a cross-talk between mTOR and p53 pathways. BMC cancer , 17(1), pp. 309 .

Siegel, R.L., Miller, K.D. and Jemal, A. (2016) Cancer statistics, 2016. CA: a cancer journal for clinicians , 66(1), pp. 7-30 .

Singh, D., Chan, J.M., Zoppoli, P., Niola, F., Sullivan, R., Castano, A., Liu, E.M., Reichel, J., Porrati, P., Pellegatta, S., Qiu, K., Gao, Z., Ceccarelli, M., Riccardi, R., Brat, D.J., Guha, A., Aldape, K., Golfinos, J.G., Zagzag, D., Mikkelsen, T., Finocchiaro, G., Lasorella, A., Rabadan, R. and Iavarone, A. (2012) Transforming fusions of FGFR and TACC genes in human glioblastoma. Science (New York, N.Y.) , 337(6099), pp. 1231-1235 .

Sinnett-Smith, J., Kisfalvi, K., Kui, R. and Rozengurt, E. (2013) Metformin inhibition of mTORC1 activation, DNA synthesis and proliferation in pancreatic cancer cells: dependence on glucose concentration and role of AMPK. Biochemical and biophysical research communications , 430(1), pp. 352-357 .

Skehan, P., Storeng, R., Scudiero, D., Monks, A., McMahon, J., Vistica, D., Warren, J.T., Bokesch, H., Kenney, S. and Boyd, M.R. (1990) New colorimetric cytotoxicity assay for anticancer-drug screening. JNCI: Journal of the National Cancer Institute , 82(13), pp. 1107-1112 .

Soda, Y., Myskiw, C., Rommel, A. and Verma, I.M. (2013) Mechanisms of neovascularization and resistance to anti-angiogenic therapies in glioblastoma multiforme. Journal of molecular medicine , 91(4), pp. 439-448 .

Song, B., Wang, Y., Xi, Y., Kudo, K., Bruheim, S., Botchkina, G.I., Gavin, E., Wan, Y., Formentini, A. and Kornmann, M. (2009) Mechanism of chemoresistance mediated by miR-140 in human osteosarcoma and colon cancer cells. Oncogene , 28(46), pp. 4065-4074 .

Song, H. and Bu, G. (2009) MicroRNA-205 inhibits tumor cell migration through down-regulating the expression of the LDL receptor-related protein 1. Biochemical and biophysical research communications , 388(2), pp. 400-405 .

Speirs, V., Green, A., Walton, D., Kerin, M., Fox, J., Carleton, P., Desai, S. and Atkin, S. (1998) Short-term primary culture of epithelial cells derived from human breast tumours. British journal of cancer , 78(11), pp. 1421 .

Spoerri, L., Oo, Z.Y., Larsen, J.E., Haass, N.K., Gabrielli, B. and Pavey, S. (2015) Cell cycle checkpoint and dna damage response defects as anticancer targets: from molecular mechanisms to therapeutic opportunities. in Stress Response Pathways in Cancer. Springer, pp.29-49.

Steelman, L.S., Chappell, W.H., Abrams, S.L., Kempf, R.C., Long, J., Laidler, P., Mijatovic, S., Maksimovic-Ivanic, D., Stivala, F., Mazzarino, M.C., Donia, M., Fagone, P., Malaponte, G., Nicoletti, F., Libra, M., Milella, M., Tafuri, A., Bonati, A., Basecke, J., Cocco, L., Evangelisti, C., Martelli, A.M., Montalto, G., Cervello, M. and McCubrey, J.A. (2011) Roles of the Raf/MEK/ERK and PI3K/PTEN/Akt/mTOR pathways in controlling growth and sensitivity to therapy-implications for cancer and aging. Aging , 3(3), pp. 192-222 .

Stupp, R., Taillibert, S., Kanner, A.A., Kesari, S., Steinberg, D.M., Toms, S.A., Taylor, L.P., Lieberman, F., Silvani, A. and Fink, K.L. (2015) Maintenance therapy with tumor-treating fields plus temozolomide vs temozolomide alone for glioblastoma: a randomized clinical trial. Jama , 314(23), pp. 2535-2543 .

Sun, R.C. and Denko, N.C. (2014) Hypoxic regulation of glutamine metabolism through HIF1 and SIAH2 supports lipid synthesis that is necessary for tumor growth. Cell metabolism , 19(2), pp. 285-292 .

Sun, Y., Tao, C., Huang, X., He, H., Shi, H., Zhang, Q. and Wu, H. (2016) Metformin induces apoptosis of human hepatocellular carcinoma HepG2 cells by activating an AMPK/p53/miR-23a/FOXA1 pathway. OncoTargets and therapy , 9pp. 2845-2853 .

Swinnen, J.V., Roskams, T., Joniau, S., Van Poppel, H., Oyen, R., Baert, L., Heyns, W. and Verhoeven, G. (2002) Overexpression of fatty acid synthase is an early and common event in the development of prostate cancer. International journal of cancer , 98(1), pp. 19-22 .

Takata, A., Otsuka, M., Yoshikawa, T., Kishikawa, T., Hikiba, Y., Obi, S., Goto, T., Kang, Y.J., Maeda, S. and Yoshida, H. (2013) MicroRNA-140 acts as a liver tumor suppressor by controlling NF-κB activity by directly targeting DNA methyltransferase 1 (Dnmt1) expressio. Hepatology , 57(1), pp. 162-170 .

Takata, F., Dohgu, S., Matsumoto, J., Machida, T., Kaneshima, S., Matsuo, M., Sakaguchi, S., Takeshige, Y., Yamauchi, A. and Kataoka, Y. (2013) Metformin induces up-regulation of blood–brain barrier functions by activating AMP-activated protein kinase in rat brain microvascular endothelial cells. Biochemical and biophysical research communications , 433(4), pp. 586-590 .

Tanaka, R., Tomosugi, M., Horinaka, M., Sowa, Y. and Sakai, T. (2015) Metformin causes G1-phase arrest via down-regulation of MiR-221 and

enhances TRAIL sensitivity through DR5 up-regulation in pancreatic cancer cells. PLoS One , 10(5), pp. e0125779 .

Telford, W.G., King, L.E. and Fraker, P.J. (1992) Comparative evaluation of several DNA binding dyes in the detection of apoptosis-associated chromatin degradation by flow cytometry. Cytometry Part A , 13(2), pp. 137-143 .

Ter Laak, T. and Baken, K. (2014) The occurrence, fate and ecological and human health risks of metformin and guanylurea in the water cycle-A literature review. The Water Research Institute.KWR , 24.

Thomas, K., Reid, M. and Langford, K. (2010) Methodology for the analysis of selected pharmaceuticals and drugs of abuse in sediments and sludge. Norwegian Institute for Water Research (NIVA) .

Thomas, M., Lange-Grünweller, K., Weirauch, U., Gutsch, D., Aigner, A., Grünweller, A. and Hartmann, R. (2012) The proto-oncogene Pim-1 is a target of miR-33a. Oncogene , 31(7), pp. 918-928 .

Thorpe, T.A. (2007) History of plant tissue culture. Molecular biotechnology , 37(2), pp. 169-180 .

Tiwarekar, V., Wohlfahrt, J., Fehrholz, M., Scholz, C.J., Kneitz, S. and Schneider-Schaulies, J. (2018) APOBEC3G-regulated host factors interfere with measles virus replication: role of REDD1 and mTORC1 inhibition. Journal of virology .

Tomczak, K., Czerwinska, P. and Wiznerowicz, M. (2015) The Cancer Genome Atlas (TCGA): an immeasurable source of knowledge. Contemporary oncology (Poznan, Poland) , 19(1A), pp. A68-77 .

Tomic, T., Botton, T., Cerezo, M., Robert, G., Luciano, F., Puissant, A., Gounon, P., Allegra, M., Bertolotto, C. and Bereder, J. (2011) Metformin inhibits melanoma development through autophagy and apoptosis mechanisms. Cell death & disease , 2(9), pp. e199 .

Torre, L.A., Bray, F., Siegel, R.L., Ferlay, J., Lortet-Tieulent, J. and Jemal, A. (2015) Global cancer statistics, 2012. CA: a cancer journal for clinicians , 65(2), pp. 87-108 .

Torsvik, A., Stieber, D., Enger, P.Ø., Golebiewska, A., Molven, A., Svendsen, A., Westermark, B., Niclou, S.P., Olsen, T.K. and Chekenya Enger, M. (2014) U-251 revisited: genetic drift and phenotypic consequences of long-term cultures of glioblastoma cells. Cancer medicine , 3(4), pp. 812-824 .

Trautwein, C., Berset, J., Wolschke, H. and Kümmerer, K. (2014) Occurrence of the antidiabetic drug Metformin and its ultimate transformation product Guanylurea in several compartments of the aquatic cycle. Environment international , 70pp. 203-212 .

Trembath, D.G., Lal, A., Kroll, D.J., Oberlies, N.H. and Riggins, G.J. (2007) A novel small molecule that selectively inhibits glioblastoma cells expressing EGFRvIII. Molecular cancer , 6(1), pp. 30 .

Tsai, H.H., Lai, H.Y., Chen, Y.C., Li, C.F., Huang, H.S., Liu, H.S., Tsai, Y.S. and Wang, J.M. (2017) Metformin promotes apoptosis in hepatocellular carcinoma through the CEBPD-induced autophagy pathway. Oncotarget , 8(8), pp. 13832-13845 .

van den Bent, M.J., Dubbink, H.J., Marie, Y., Brandes, A.A., Taphoorn, M.J., Wesseling, P., Frenay, M., Tijssen, C.C., Lacombe, D., Idbaih, A., van Marion, R., Kros, J.M., Dinjens, W.N., Gorlia, T. and Sanson, M. (2010) IDH1 and IDH2 mutatons are prognostic but not predictive for outcome in anaplastic oligodendroglial tumors: a report of the European Organization for Research and Treatment of Cancer Brain Tumor Group. Clinical cancer research : an official journal of the American Association for Cancer Research , 16(5), pp. 1597-1604 .

Van Tellingen, O., Yetkin-Arik, B., De Gooijer, M., Wesseling, P., Wurdinger, T. and De Vries, H. (2015) Overcoming the blood–brain tumor barrier for effective glioblastoma treatment. Drug Resistance Updates , 19pp. 1-12

Vander Heiden, M.G., Cantley, L.C. and Thompson, C.B. (2009) Understanding the Warburg effect: the metabolic requirements of cell proliferation. Science (New York, N.Y.) , 324(5930), pp. 1029-1033 .

Verhaak, R.G., Hoadley, K.A., Purdom, E., Wang, V., Qi, Y., Wilkerson, M.D., Miller, C.R., Ding, L., Golub, T. and Mesirov, J.P. (2010) Integrated genomic analysis identifies clinically relevant subtypes of glioblastoma characterized by abnormalities in PDGFRA, IDH1, EGFR, and NF1. Cancer cell , 17(1), pp. 98-110 .

Vermeulen, K., Van Bockstaele, D.R. and Berneman, Z.N. (2003) The cell cycle: a review of regulation, deregulation and therapeutic targets in cancer. Cell proliferation , 36(3), pp. 131-149 .

Verzola, L.F.S., Vidotto, T. and Squire, J.A. (2018) Abstract B58: The effect of differential miRNA expression in glioblastoma multiforme molecular subtypes .

Vichai, V. and Kirtikara, K. (2006) Sulforhodamine B colorimetric assay for cytotoxicity screening. Nature protocols , 1(3), pp. 1112-1116 .

Vinall, R.L., Tepper, C.G., Ripoll, A.A., Gandour-Edwards, R.F., Durbin-Johnson, B.P., Yap, S.A., Ghosh, P.M. and deVere White, R.W. (2016) Decreased expression of let-7c is associated with non-response of muscle-invasive bladder cancer patients to neoadjuvant chemotherapy. Genes & cancer , 7(3-4), pp. 86 .

Viollet, B., Guigas, B., Sanz Garcia, N., Leclerc, J., Foretz, M. and Andreelli, F. (2012) Cellular and molecular mechanisms of metformin: an overview. Clinical science (London, England : 1979) , 122(6), pp. 253-270 .

von Karstedt, S., Montinaro, A. and Walczak, H. (2017) Exploring the TRAILs less travelled: TRAIL in cancer biology and therapy. Nature Reviews Cancer , 17(6), pp. 352-366 .

von Pawel, J., Harvey, J.H., Spigel, D.R., Dediu, M., Reck, M., Cebotaru, C.L., Humphreys, R.C., Gribbin, M.J., Fox, N.L. and Camidge, D.R. (2014) Phase II Trial of Mapatumumab, a Fully Human Agonist Monoclonal Antibody to Tumor

Necrosis Factor-Related Apoptosis-Inducing Ligand Receptor 1 (TRAIL-R1), in Combination With Paclitaxel and Carboplatin in Patients With Advanced Non–Small-Cell Lung Cancer. Clinical lung cancer , 15(3), pp. 188-196. e2 .

Wahl, D.R. and Venneti, S. (2018) Cancer Metabolism. in Imaging and Metabolism. Springer, pp.129-154.

Wang, F., Xu, J., Liu, H., Liu, Z. and Xia, F. (2016) Metformin induces apoptosis by microRNA-26a-mediated downregulation of myeloid cell leukaemia-1 in human oral cancer cells. Molecular medicine reports , 13(6), pp. 4671-4676 .

Wang, P., Sun, Y., Zhang, S., Pang, M., Zhang, H., Gao, S., Zhang, C., Lv, C. and Xie, S. (2013) Let-7c inhibits A549 cell proliferation through oncogenic TRIB2 related factors. FEBS letters , 587(16), pp. 2675-2681 .

Wang, Y., Dai, W., Chu, X., Yang, B., Zhao, M. and Sun, Y. (2013) Metformin inhibits lung cancer cells proliferation through repressing microRNA-222. Biotechnology Letters , 35(12), .

Wang, B., Herman-Edelstein, M., Koh, P., Burns, W., Jandeleit-Dahm, K., Watson, A., Saleem, M., Goodall, G.J., Twigg, S.M., Cooper, M.E. and Kantharidis, P. (2010) E-cadherin expression is regulated by miR-192/215 by a mechanism that is independent of the profibrotic effects of transforming growth factor-beta. Diabetes , 59(7), pp. 1794-1802 .

Wang, Q., Zhang, M., Torres, G., Wu, S., Ouyang, C., Xie, Z. and Zou, M.H. (2017) Metformin Suppresses Diabetes-Accelerated Atherosclerosis via the

Inhibition of Drp1-Mediated Mitochondrial Fission. Diabetes , 66(1), pp. 193-205 .

Wang, Z., Zhou, J., Fan, J., Qiu, S.J., Yu, Y., Huang, X.W. and Tang, Z.Y. (2008) Effect of rapamycin alone and in combination with sorafenib in an orthotopic model of human hepatocellular carcinoma. Clinical cancer research : an official journal of the American Association for Cancer Research , 14(16), pp. 5124-5130 .

Watanabe, C. (1918) Studies in the metabolic changes induced by administration of guanidine bases. J.biol.Chem. , 33pp. 253 .

Watkins, S., Robel, S., Kimbrough, I.F., Robert, S.M., Ellis-Davies, G. and Sontheimer, H. (2014) Disruption of astrocyte–vascular coupling and the blood–brain barrier by invading glioma cells. Nature communications , 5pp. 4196 .

Werner, E.A. and Bell, J. (1922) CCXIV.—The preparation of methylguanidine, and of ββ-dimethylguanidine by the interaction of dicyanodiamide, and methylammonium and dimethylammonium chlorides respectively. Journal of the Chemical Society, Transactions , 121pp. 1790-1794 .

Westermark, B., Ponten, J. and Hugosson, R. (1973) Determinants for the establishment of permanent tissue culture lines from human gliomas. Acta Pathologica Microbiologica Scandinavica Section a Pathology , 81(6), pp. 791-805 .

Wheaton, W.W., Weinberg, S.E., Hamanaka, R.B., Soberanes, S., Sullivan, L.B., Anso, E., Glasauer, A., Dufour, E., Mutlu, G.M. and Budigner, G.S. (2014) Metformin inhibits mitochondrial complex I of cancer cells to reduce tumorigenesis. Elife , 3pp. e02242 .

Wild, C.P. and Stewart, B.W. (2014) World Cancer Report 2014. World Health Organization.

Wilson, R.C. and Doudna, J.A. (2013) Molecular mechanisms of RNA interference. Annual review of biophysics , 42pp. 217-239 .

Wong, A., Ye, M., Levy, A., Rothstein, J., Bergles, D. and Searson, P.C. (2013) The blood-brain barrier: an engineering perspective. Frontiers in neuroengineering , 6pp. 7 .

Wong, H.A., El Fatimy, R., Onodera, C., Wei, Z., Yi, M., Mohan, A., Gowrisankaran, S., Karmali, P., Marcusson, E. and Wakimoto, H. (2015) The Cancer Genome Atlas analysis predicts microRNA for targeting cancer growth and vascularization in glioblastoma. Molecular Therapy , 23(7), pp. 1234-1247 .

World Health Organization (2017) WHO model list of essential medicines: 20th list, March 2017.

World Health Organization (2002) WHO Model List of Essential Medicines, 2002. Available from: left angle bracket http://www.who.int/medicines/publications/essentialmedicines/en/right angle bracket .

Wu, H., Zhu, S. and Mo, Y. (2009) Suppression of cell growth and invasion by miR-205 in breast cancer. Cell research , 19(4), pp. 439-448 .

Wu, K., He, J., Pu, W. and Peng, Y. (2018) The Role of Exportin-5 in MicroRNA Biogenesis and Cancer. Genomics, proteomics & bioinformatics .

Würth, R., Pattarozzi, A., Gatti, M., Bajetto, A., Corsaro, A., Parodi, A., Sirito, R., Massollo, M., Marini, C. and Zona, G. (2013) Metformin selectively affects human glioblastoma tumor-initiating cell viability: A role for metformin-induced inhibition of Akt. Cell Cycle , 12(1), pp. 145-156 .

Xiang, M., Zeng, Y., Yang, R., Xu, H., Chen, Z., Zhong, J., Xie, H., Xu, Y. and Zeng, X. (2014) U6 is not a suitable endogenous control for the quantification of circulating microRNAs. Biochemical and biophysical research communications , 454(1), pp. 210-214 .

Xie, F. (2015) miRNA primer designerAvailable at: <https://www.ecu.edu/>.

Xu, H., Zong, H., Ma, C., Ming, X., Shang, M., Li, K., He, X., Du, H. and Cao, L. (2017) Epidermal growth factor receptor in glioblastoma. Oncology letters , 14(1), pp. 512-516 .

Xu, K., Liang, X., Shen, K., Sun, L., Cui, D., Zhao, Y., Tian, J., Ni, L. and Liu, J. (2012) MiR-222 modulates multidrug resistance in human colorectal carcinoma by down-regulating ADAM-17. Experimental cell research , 318(17), pp. 2168-2177 .

Yamazaki, Y. and Kanekiyo, T. (2017) Blood-brain barrier dysfunction and the pathogenesis of Alzheimer's disease. International journal of molecular sciences , 18(9), pp. 1965 .

Yan, H., Parsons, D.W., Jin, G., McLendon, R., Rasheed, B.A., Yuan, W., Kos, I., Batinic-Haberle, I., Jones, S. and Riggins, G.J. (2009) IDH1 and IDH2 mutations in gliomas. New England Journal of Medicine , 360(8), pp. 765-773 .

Yan, J., Kong, L., Hu, J., Gabrusiewicz, K., Dibra, D., Xia, X., Heimberger, A.B. and Li, S. (2015) FGL2 as a multimodality regulator of tumor-mediated immune suppression and therapeutic target in gliomas. JNCI: Journal of the National Cancer Institute , 107(8), .

Yang, H., Fang, F., Chang, R. and Yang, L. (2013) MicroRNA-140-5p suppresses tumor growth and metastasis by targeting transforming growth factor β receptor 1 and fibroblast growth factor 9 in hepatocellular carcinoma. Hepatology , 58(1), pp. 205-217 .

Yang, J., Wei, J., Wu, Y., Wang, Z., Guo, Y., Lee, P. and Li, X. (2015) Metformin induces ER stress-dependent apoptosis through miR-708-5p/NNAT pathway in prostate cancer. Oncogenesis , 4(6), pp. e158 .

Yang, L., Lin, C., Wang, L., Guo, H. and Wang, X. (2012) Hypoxia and hypoxia-inducible factors in glioblastoma multiforme progression and therapeutic implications. Experimental cell research , 318(19), pp. 2417-2426 .

Yang, C.H., Pfeffer, S.R., Sims, M., Yue, J., Wang, Y., Linga, V.G., Paulus, E., Davidoff, A.M. and Pfeffer, L.M. (2015) The oncogenic microRNA-21 inhibits the tumor suppressive activity of FBXO11 to promote tumorigenesis. The Journal of biological chemistry , 290(10), pp. 6037-6046 .

Yasumoto, Y., Miyazaki, H., Vaidyan, L.K., Kagawa, Y., Ebrahimi, M., Yamamoto, Y., Ogata, M., Katsuyama, Y., Sadahiro, H. and Suzuki, M. (2016) Inhibition of fatty acid synthase decreases expression of stemness markers in glioma stem cells. PloS one , 11(1), pp. e0147717 .

Ye, J., Mancuso, A., Tong, X., Ward, P.S., Fan, J., Rabinowitz, J.D. and Thompson, C.B. (2012) Pyruvate kinase M2 promotes de novo serine synthesis to sustain mTORC1 activity and cell proliferation. Proceedings of the National Academy of Sciences of the United States of America , 109(18), pp. 6904-6909 .

Yee, D., Paoloni, M., van't Veer, L., Sanil, A., Yau, C., Forero, A., Chien, A., Wallace, A., Moulder, S. and Albain, K. (2017) Abstract P6-11-04: The evaluation of ganitumab/metformin plus standard neoadjuvant therapy in high-risk breast cancer: Results from the I-SPY 2 trial .

Yousaf, H. and Kemp, C. (2018) 1353: Metformin And Chronic Kidney Disease Type B Lactic Acidosis. Critical Care Medicine , 46(1), pp. 660 .

Yu, Z., Zhao, G., Xie, G., Zhao, L., Chen, Y., Yu, H., Zhang, Z., Li, C. and Li, Y. (2015) Metformin and temozolomide act synergistically to inhibit growth of glioma cells and glioma stem cells *in vitro* and *in vivo*. Oncotarget , 6(32), pp. 32930-32943 .

Zakikhani, M., Blouin, M., Piura, E. and Pollak, M.N. (2010) Metformin and rapamycin have distinct effects on the AKT pathway and proliferation in breast cancer cells. Breast cancer research and treatment , 123(1), pp. 271-279 .

Zhai, X., Yang, Y., Wan, J., Zhu, R. and Wu, Y. (2013) Inhibition of LDH-A by oxamate induces G2/M arrest, apoptosis and increases radiosensitivity in nasopharyngeal carcinoma cells. Oncology reports , 30(6), pp. 2983-2991 .

Zhai, H., Fesler, A., Ba, Y., Wu, S. and Ju, J. (2015) Inhibition of colorectal cancer stem cell survival and invasive potential by hsa-miR-140-5p mediated suppression of Smad2 and autophagy. Oncotarget , 6(23), pp. 19735-19746 .

Zhang, C., Zhang, J., Zhang, A., Shi, Z., Han, L., Jia, Z., Yang, W., Wang, G., Jiang, T. and You, Y. (2010) MiR-221 and miR-222 target PUMA to induce cell survival in glioblastoma. Molecular cancer , 9(1), pp. 229 .

Zhang, D., Xuan, J., Zheng, B., Zhou, Y., Lin, Y., Wu, Y., Zhou, Y., Huang, Y., Wang, Q. and Shen, L. (2017) Metformin improves functional recovery after spinal cord injury via autophagy flux stimulation. Molecular neurobiology , 54(5), pp. 3327-3341 .

Zhang, W.B., Wang, Z., Shu, F., Jin, Y.H., Liu, H.Y., Wang, Q.J. and Yang, Y. (2010) Activation of AMP-activated protein kinase by temozolomide contributes to apoptosis in glioblastoma cells via p53 activation and mTORC1 inhibition. The Journal of biological chemistry , 285(52), pp. 40461-40471 .

Zhao, B., Han, H., Chen, J., Zhang, Z., Li, S., Fang, F., Zheng, Q., Ma, Y., Zhang, J. and Wu, N. (2014) MicroRNA let-7c inhibits migration and invasion

of human non-small cell lung cancer by targeting ITGB3 and MAP4K3. Cancer letters , 342(1), pp. 43-51 .

Zhao, Y., Liu, H., Riker, A.I., Fodstad, O., Ledoux, S.P., Wilson, G.L. and Tan, M. (2011) Emerging metabolic targets in cancer therapy. Frontiers in bioscience (Landmark edition) , 16pp. 1844-1860 .

Zheng, H., Ying, H., Yan, H., Kimmelman, A.C., Hiller, D.J., Chen, A., Perry, S.R., Tonon, G., Chu, G.C. and Ding, Z. (2008) p53 and Pten control neural and glioma stem/progenitor cell renewal and differentiation. Nature , 455(7216), pp. 1129 .

Zhou, Y., Huang, Z., Wu, S., Zang, X., Liu, M. and Shi, J. (2014) miR-33a is up-regulated in chemoresistant osteosarcoma and promotes osteosarcoma cell resistance to cisplatin by down-regulating TWIST. Journal of experimental & clinical cancer research , 33(1), pp. 12 .

Zhou, Z., Du, D., Huang, G., Chen, A. and Zhu, L. (2018) Circular RNA Atp9b, a competing endogenous RNA, regulates the progression of osteoarthritis by targeting miR-138-5p. Gene .

Zhu, W., Krishna, S., Garcia, C., Lin, C.J., Mitchell, B.D., Scott, K.L., Mohila, C.A., Creighton, C.J., Yoo, S. and Lee, H.K. (2017) Daam2 driven degradation of VHL promotes gliomagenesis. eLife , 6pp. e31926 .

Zhuang, Y., Chan, D.K., Haugrud, A.B. and Miskimins, W.K. (2014) Mechanisms by Which Low Glucose Enhances the Cytotoxicity of Metformin to Cancer Cells Both *In vitro* and *In vivo*. PloS one , 9(9), pp. e108444 .

Zong, W.X., Ditsworth, D., Bauer, D.E., Wang, Z.Q. and Thompson, C.B. (2004) Alkylating DNA damage stimulates a regulated form of necrotic cell death. Genes & development , 18(11), pp. 1272-1282 .

Zordoky, B.N., Bark, D., Soltys, C.L., Sung, M.M. and Dyck, J.R. (2014) The anti-proliferative effect of metformin in triple-negative MDA-MB-231 breast cancer cells is highly dependent on glucose concentration: implications for cancer therapy and prevention. Biochimica et Biophysica Acta (BBA)-General Subjects , 1840(6), pp.